

Front Interactions in a Three-Component System

Peter van Heijster

The cover shows a uniformly traveling 5-front solution. For more information see Section 4.4.3.

ISBN-10: 90-6196550-0

ISBN-13: 978-90-6196550-3

Copyright © 2009, Peter van Heijster, Amsterdam, The Netherlands.

Front Interactions in a Three-Component System

ACADEMISCH PROEFSCHRIFT

ter verkrijging van de graad van doctor
aan de Universiteit van Amsterdam
op gezag van de Rector Magnificus
prof. dr. D.C. van den Boom
ten overstaan van een door het college voor promoties
ingestelde commissie,
in het openbaar te verdedigen in de Agnietenkapel
op dinsdag 26 mei 2009, te 14:00 uur

door

Petrus Johannes Adrianus van Heijster

geboren te Heerhugowaard

Promotiecommissie:

Promotor: prof. dr. A. Doelman

Overige leden: prof. dr. G.J.B. van den Berg
dr. A.J. Homburg
prof. dr. M.A. Peletier
prof. dr. R.P. Stevenson
prof. dr. J.J.O.O. Wiegerinck
dr. A. Zagaris

Faculteit der Natuurwetenschappen, Wiskunde en Informatica

This thesis was made possible by the support of



Netherlands Organisation for Scientific Research



Centrum
Wiskunde & Informatica

THOMAS STELTJES INSTITUTE
FOR MATHEMATICS



*voor papa
niet meer hier
maar altijd in mijn hart*

Contents

1	Introduction	1
1.1	Model equations	3
1.1.1	Physical background	3
1.1.2	Mathematical background	4
1.2	Basic concepts	5
1.2.1	Singular perturbations	6
1.2.2	Stability and bistability	9
1.3	More advanced concepts	11
1.3.1	Geometric singular perturbation theory	11
1.3.2	The Evans function	14
1.3.3	The renormalization group method	20
1.4	Outline	22
2	Existence	27
2.1	Introduction	27
2.1.1	Statement of the model equations	28
2.1.2	Outline of the main results	30
2.2	Stationary 1-pulse solutions	33
2.2.1	Basic observations	33
2.2.2	The construction of 1-pulse solutions $\gamma_{h,j}^-(\xi)$ homoclinic to P_ε^-	35
2.2.3	Existence theorem	41
2.2.4	The proof of Theorem 2.2.1	42
2.2.5	Explicit analysis of the number K of stationary 1-pulse solutions	46
2.3	Traveling pulse solutions	47
2.3.1	The formal construction of traveling 1-pulse solutions, $\gamma_{tr,j}^-(\xi)$	47
2.3.2	Existence theorem for traveling pulse solutions	51
2.3.3	Proof of Theorem 2.3.1	53
2.4	Bifurcation from stationary to traveling pulse solutions	55
2.4.1	Leading order analysis	55
2.4.2	Subcriticality and supercriticality of the bifurcation	56

2.5	Stationary 2-pulse solutions	62
2.5.1	The construction of $\gamma_{2p,j}^-(\xi)$ homoclinic to P_ε^-	62
2.5.2	The existence of 2-pulse solutions	66
2.5.3	Asymptotics for $D \rightarrow \infty$	67
2.6	The two-component model	70
2.7	Simulations, conclusions and discussion	71
2.7.1	Simulations	71
2.7.2	Conclusions and discussion	77
3	Stability	79
3.1	Introduction	79
3.2	Review of existence theory	84
3.2.1	Standing 1-pulse solutions	84
3.2.2	Traveling 1-pulse solutions	87
3.2.3	Standing 2-pulse solutions	90
3.3	The linearized stability problem	91
3.3.1	Linearizing around a homoclinic pulse	92
3.3.2	The essential spectrum	93
3.3.3	The construction of the Evans function	97
3.3.4	The slow-fast decomposition of $\mathcal{D}(\lambda)$	98
3.4	Stability of the standing 1-pulse solution for $\tau, \theta = \mathcal{O}(1)$	100
3.4.1	The transmission function t_1 and the fast eigenvalues	101
3.4.2	The slow basis functions $\phi_{2,3}$	104
3.4.3	The slow-fast transmission functions t_{ij}	107
3.5	1-pulse solutions for $\tau = \mathcal{O}(\varepsilon^{-2})$	113
3.5.1	Stability of the standing 1-pulse solution for $\tau, \theta = \mathcal{O}(\varepsilon^{-2})$	114
3.5.2	Bifurcations for $\tau = \mathcal{O}(\varepsilon^{-2})$ and $\theta = 1$	118
3.5.3	Stability of the traveling 1-pulse solution	125
3.5.4	Small speed c : the weakly nonlinear analysis	126
3.5.5	(In)stability of traveling pulse solutions for asymptotically large $\hat{\tau}$	128
3.6	Standing 2-pulse solutions	129
3.6.1	Proof of Theorem 3.6.1	131
3.6.2	The small eigenvalues	133
4	Interactions	139
4.1	Introduction	139
4.2	Formal derivation of N -front dynamics	145
4.3	A renormalization group method	147
4.3.1	The χ -norm	147
4.3.2	The main result	149
4.3.3	Nonlinearity and residual	153
4.3.4	Resolvent	154
4.3.5	Initializing the renormalization group method	158

4.3.6	Projecting onto the small eigenspace $X_{\Gamma^0}^C$	162
4.3.7	Projecting onto X_{Γ^0}	163
4.3.8	Iteration	166
4.3.9	Completion of the proof of Theorem 4.3.2	167
4.4	The dynamics of N -front solutions	168
4.4.1	N -front solutions with N even and N odd	169
4.4.2	The 2-front solutions	170
4.4.3	The 3-front solutions	171
4.4.4	The 4-front solutions	178
Bibliography		185
Summary		191
Samenvatting: Frontinteractie in een driecomponenten systeem		195
Dankwoord		199
Curriculum Vitae		201

Chapter 1

Introduction

Pattern formation is a very lively field of research within the nonlinear sciences, where the traditional disciplines of mathematics, physics, chemistry, and biology merge, interact, and exchange ideas. Reaction-diffusion equations (RDEs) serve as relevant, often simplified models within several branches of these fields. For instance, pulses traveling through nerve cells, as well as vegetation patterns [44] and stripes on zebras [37] are modeled by RDEs, see Figure 1.1. From a mathematical perspective, RDEs are arguably the simplest nonlinear partial differential equations (PDEs) that exhibit complex patterns observed in many natural systems such as spiral waves and spatio-temporal chaos which are observed in many natural systems, see Figure 1.1. Therefore, RDEs can be considered as the key prototype models in which one can begin to develop a fundamental understanding of complex patterns.

Localized structures form a special class of solutions to these RDEs related to the aforementioned patterns. These structures are solutions to the PDE remaining close to a trivial background state except in one or more localized spatial regions, see Figure 1.2. Fronts and pulses are the most well-known and well-studied localized structures in one spatial dimension; spots, spirals, and stripes are examples of localized structures in two dimensions. Localized patterns can be seen as the foundation for the mathematical analysis of more complex patterns.

In recent years, significant progress has been made in our mathematical understanding of the simplest localized structures. These being fronts and pulses that are stationary or move with a constant speed through a 1-dimensional domain [59]. In general, the behavior of localized structures is less well-ordered: those structures interact with each other and thus also move with different velocities, see Figure 1.2. At present, there is a well-developed theory that describes the interaction of fronts and pulses in the *weak* interaction regime [19, 20, 55]. In this regime these fronts or pulses are ‘far away’ from each other, meaning, all

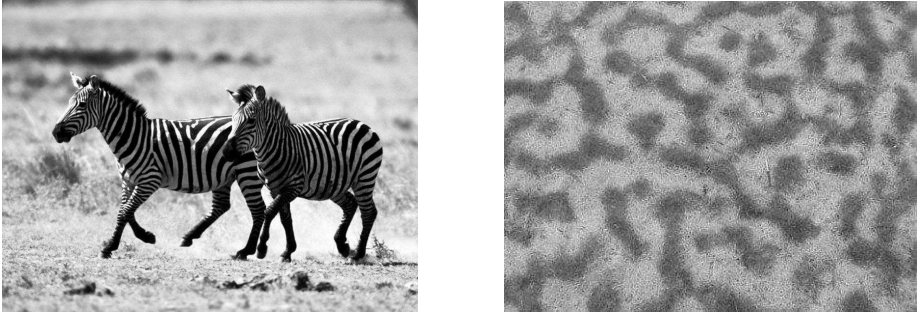


Figure 1.1: In the left frame, one sees pattern formation on the coats of two zebras [73]. In the right frame, one sees pattern formation at the edge of the Negev Desert. The dark stripes correspond to vegetation, whereas the lighter stripes correspond to sand. Note that the scale of this frame is in decimeters. Both phenomena are modeled by RDEs.

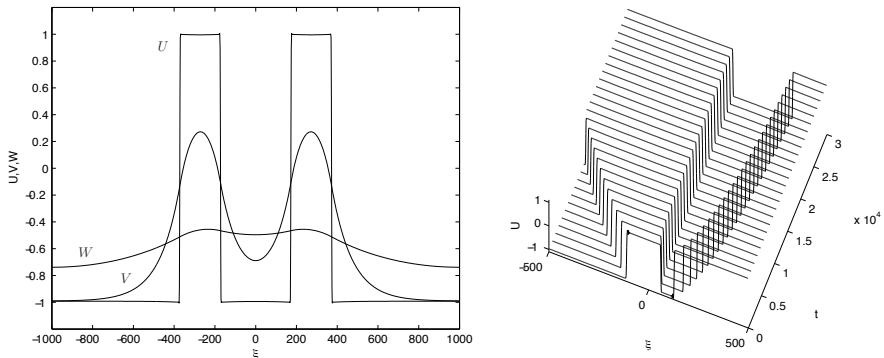


Figure 1.2: In the left frame, we plotted a localized stationary 2-pulse or 4-front solution of the three-component system under investigation in this thesis, see (1.1.3). Note that two of the components (V and W) interact strongly, while the U -component interacts only via their background states. In the right frame, we plotted an interacting 3-front solution of the same system; only the U -component is plotted. In the context of Figure 1.1: black/dark corresponds to $U = -1$, and white/light to $U = 1$.

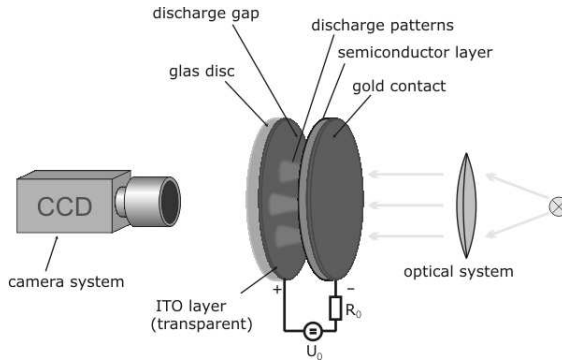


Figure 1.3: The schematically experimental setting of a planar gas-discharge system (with high-ohmic barrier) [74].

components of the structure interact only through their trivial background states mentioned above. However, there is no mathematical theory that explains the interaction of fronts and pulses in the *strong* interaction regime where the fronts and pulses are close to each other, and all solution components are far from equilibrium in the regions between the fronts and pulses. In that regime, interesting behavior such as collision, repulsion, annihilation, and self-replication of fronts and pulses can be observed; in a daily life setting, one could, for instance, think of the collision of two stern waves. In between the weak and strong interaction regimes lies a third regime, the *semi-strong* interaction regime, where certain components of the fronts or pulses interact via the background state, while the remaining components interact strongly with each other, see Figure 1.2. Understanding this regime is a fundamental next step in furthering our understanding of how localized structures interact. In this thesis, we take a first step in that direction for a specific RDE.

1.1 Model equations

1.1.1 Physical background

In the mid-nineties, the physicist H. G. Purwins studied pattern formation in gas-discharges, the effect that creates light in fluorescent tubes, see Figures 1.3 and 1.4. He mainly considered the interactions of localized states with each other and first modeled his observations by a two-component RDE

$$\begin{cases} U_t = D_U \Delta U + f(U) - \kappa_3 V + \kappa_1, \\ \tau V_t = D_V \Delta V + U - V, \end{cases} \quad (1.1.1)$$

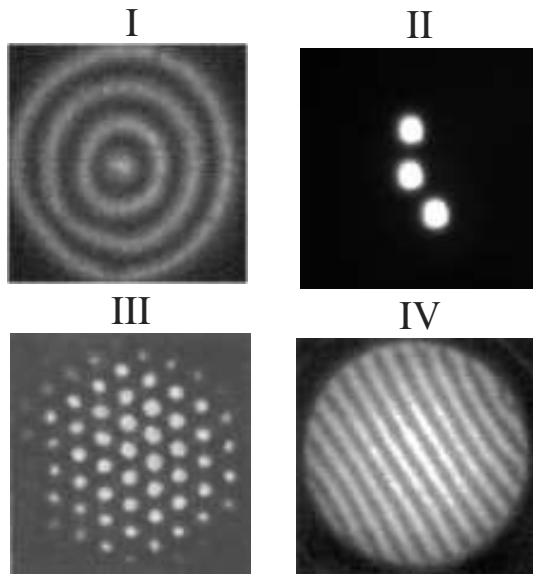


Figure 1.4: Examples of experimentally observed patterns [74].

where $f(U)$ was taken to be a cubic polynomial. Numerical simulations revealed that certain 2-dimensional structures – such as traveling spots – were unstable; they were, nevertheless, observed in experiments – an apparent contradiction. To rectify this situation, Purwins introduced a third component to his model [54, 60],

$$\begin{cases} U_t = D_U \Delta U + f(U) - \kappa_3 V - \kappa_4 W + \kappa_1, \\ \tau V_t = D_V \Delta V + U - V, \\ \theta W_t = D_W \Delta W + U - W. \end{cases} \quad (1.1.2)$$

It turned out that this extended model supports stable traveling spots and a variety of other interesting localized solutions, as well. In subsequent years, many variations of this model were studied extensively by several research groups of both physicists ([5, 32, 54, 60, 65, 70]) and mathematicians ([50–53, 71]). These studies went beyond the original gas-discharge context and established the Purwins system as a paradigm model within the field of pattern formation that can be used to investigate the interaction of fronts, pulses, and spots.

1.1.2 Mathematical background

Besides its physical background and the richness of dynamics it exhibits, exemplified by such patterns as breathing pulses, scattering pulses, and bouncing pulses,

the model (1.1.2) is also particularly interesting from a mathematical point of view. Even within the class of RDEs, the extended Purwins model has a remarkably transparent structure, especially in the scaling we consider in this thesis. In the next chapter, we will show that (1.1.2) can be rescaled, under certain circumstances, into a particularly simple form. In one spatial dimension, this rescaled version is given by

$$\begin{cases} U_t = U_{\xi\xi} + U - U^3 - \varepsilon(\alpha V + \beta W + \gamma), \\ \tau V_t = \frac{1}{\varepsilon^2} V_{\xi\xi} + U - V, \\ \theta W_t = \frac{D^2}{\varepsilon^2} W_{\xi\xi} + U - W, \end{cases} \quad (1.1.3)$$

with

$$0 < \varepsilon \ll 1; D > 1; 0 < \tau, \theta \ll \varepsilon^{-3}; (\xi, t) \in \mathbb{R} \times \mathbb{R}^+; \\ \alpha, \beta, \gamma \in \mathbb{R} \text{ and } \mathcal{O}(1) \text{ with respect to } \varepsilon.$$

This equation is the central object of study of this thesis. Note that we consider it in a single spatial dimension, since we use the dynamical systems approach of *spatial dynamics* to study it. The model is singularly perturbed (see Section 1.2.1), bistable (see Section 1.2.2), and its U -component is only weakly coupled to its V, W -components which, in turn, are linearly coupled back to U . Moreover, explicit nonlinear effects occur directly only through the U^3 term in the first PDE. As a consequence, localized states typically interact in a *semi-strong* fashion, see Figure 1.2. The combination of these properties makes this model amenable to a rigorous mathematical analysis, something which has not yet been accomplished before for three-component systems.

In this thesis, we study (1.1.3) to gain insight in the interactions of fronts and pulses in the semi-strong interaction regime.

1.2 Basic concepts

In this section, we lay down certain basic features of (1.1.3) in relatively simple terminology. We have chosen to do so by means of a number of specific examples. This way, we can solidify the introduction of these concepts by means of concrete calculations. First, we expound on the notion of a singular perturbation by looking into simple yet instructive perturbations of cubic polynomials and ordinary differential equations (ODEs). Next, we introduce the concept of bistability. In Section 1.3, we proceed in a similar fashion: we exemplify the three main mathematical tools used in this thesis by three relatively simple examples. These examples are chosen for convenience in introducing the mathematical techniques we use, and wherever possible we specify if there is a connection between the example and some part of the full model (1.1.3).

1.2.1 Singular perturbations

In simple terms, a singularly perturbed problem is a problem containing a small parameter, usually denoted by ε , with the property that one cannot obtain a valid approximation to all of its solutions by setting this small parameter to zero. This feature of singularly perturbed problems is in stark contrast with the behavior of regularly perturbed problems, where one can directly obtain such an approximation by setting the small parameter to zero. To obtain more insight what differentiates a singularly and a regularly perturbed setting, we now consider several simple examples.

A cubic algebraic equation

In the first example, we contrast the behavior of the roots of the regularly perturbed cubic equation

$$x^3 - x^2 + \varepsilon = 0, \quad 0 < \varepsilon \ll 1,$$

to that of the roots of the singularly perturbed equation

$$\varepsilon x^3 - x^2 + 1 = 0, \quad 0 < \varepsilon \ll 1. \quad (1.2.1)$$

In both cases, we consider the behavior of these roots as we let $\varepsilon \rightarrow 0$. *A priori*, one may think that approximations of the zeroes of either equation can be (formally) obtained from the reduced equation which is obtained by setting $\varepsilon \rightarrow 0$ in the original equation. However, this is only true for the regularly perturbed equation; its reduced equation has the zeroes $x_0^r = 0$, with multiplicity two, and $x_0^r = 1$. It is simple to show that these values are the limiting values of the roots for $\varepsilon \neq 0$ as we let $\varepsilon \rightarrow 0$. The reduced equation corresponding to the singularly perturbed equation has, on the contrary, only two zeroes $x_0^s = \pm 1$, since it is of degree two instead of three. The third zero of the singularly perturbed equation has ‘disappeared’ in the limit $\varepsilon \rightarrow 0$; in fact, it is $\mathcal{O}(\varepsilon^{-1})$ and thus becomes arbitrarily large for $\varepsilon \rightarrow 0$. More explicitly, for $\varepsilon = 0.01$, the zeroes of the singularly perturbed equation are approximately $x^s = 1.005$, $x^s = -0.9951$, and $x^s = 99.99$, while the zeroes of the regularly perturbed equation approximately read $x^r = 0.1057$, $x^r = -0.09554$, and $x^r = 0.9898$.

So, by naively setting $\varepsilon \rightarrow 0$, one loses information on one of the zeroes of the singularly perturbed equation, while this is not the case for the regularly perturbed one.

The asymptotic behavior of the third zero of the singularly perturbed equation can, naturally, also be determined. Indeed, by rescaling the variable $y := \varepsilon x$, (1.2.1) transforms into

$$y^3 - y^2 + \varepsilon^2 = 0.$$

The corresponding reduced equation is now of degree three, and it also yields the root $y_0^s = 1$ apart from the the double zero solution. In the original variable, this first root becomes $x_0^s = \varepsilon^{-1}$ and it corresponds to the leading order approximation of the third root (which is not captured by the reduced equation of (1.2.1)); the double zero solution, in turn, corresponds to the bounded roots $x_0^s = \pm 1$.

Ordinary differential equations

The terminology introduced above can be transplanted easily to the field of differential equations. An example of a singularly perturbed ODE is the equation for a rescaled damped oscillator,

$$\begin{aligned} \varepsilon \ddot{x} + \dot{x} + x &= 0, & 0 < \varepsilon \ll 1, \\ x(0) &= A_1, \quad \dot{x}(0) = A_2, \end{aligned} \tag{1.2.2}$$

where $\dot{} = \frac{d}{dt}$, and A_1, A_2 are arbitrary real numbers. Setting $\varepsilon \rightarrow 0$ in this equation yields the reduced equation

$$\dot{x} + x = 0.$$

The solution to this first order ODE is readily found to be $x_0(t) = Ce^{-t}$. This formula, in turn, yields that $x_0(0) = C = A_1$ and $\dot{x}_0(0) = -C = A_2$. Therefore, the reduced problem cannot satisfy both initial conditions, unless $A_1 = -A_2$.

In this particular example, the general solution to the full equation (1.2.2) can be explicitly found to be

$$x(t) = C_1 e^{-\left(\frac{1+\sqrt{1-4\varepsilon}}{2\varepsilon}\right)t} + C_2 e^{-\left(\frac{1-\sqrt{1-4\varepsilon}}{2\varepsilon}\right)t} = C_1 e^{-(\frac{1}{\varepsilon} + \mathcal{O}(1))t} + C_2 e^{-(1 + \mathcal{O}(\varepsilon))t},$$

where C_1 and C_2 are determined by the initial conditions. We see that, here also, one of the exponents is of $\mathcal{O}(\varepsilon^{-1})$ and thus becomes arbitrarily large for $\varepsilon \rightarrow 0$.

So, here again, setting $\varepsilon \rightarrow 0$ leads to the loss of crucial information. This fact is most readily evident through our observation above that the reduced ODE cannot accommodate both initial conditions. However, the reduced dynamics actually describes the long time behavior of the full system, see Figure 1.5 and Section 1.3.1 (where the reduced dynamics are termed slow dynamics). On the other hand, this is a mere coincidence: if one changes the $+\dot{x}$ into a $-\dot{x}$ in (1.2.2) the new reduced dynamics does no longer describe the asymptotic behavior of the full system, since the stability type of the fixed point at $x = 0$ changes from attractive to repulsive.

A prototype example of a regularly perturbed ODE is the first order ODE

$$\begin{aligned} \dot{x} &= -(1 - \varepsilon)x, & 0 < \varepsilon \ll 1, \\ x(0) &= A_1. \end{aligned} \tag{1.2.3}$$

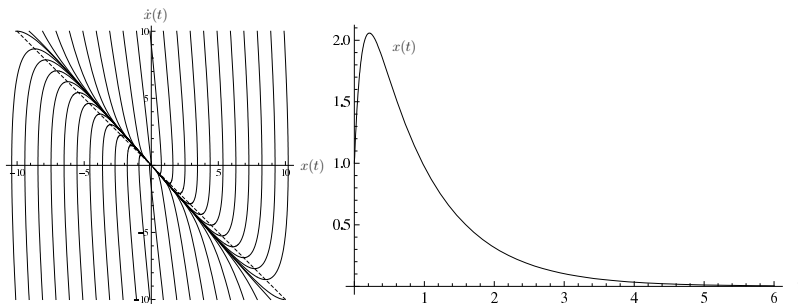


Figure 1.5: In the left frame, we plotted the phase portrait of the singularly perturbed rescaled damped oscillator (1.2.2) (solid line) and of its reduced problem (dotted line). Note that all initial conditions eventually approach 0. Observe that, to leading order, all initial conditions align with the linear subspace associated with the reduced problem. In the right frame, we plotted the time series of the specific initial condition $A_1 = 1$ and $A_2 = 14.36$. Note that we set $\varepsilon = 0.1$ in both frames.

The solution to this equation is given by

$$x(t) = A_1 e^{-(1-\varepsilon)t} = A_1 e^{-t} + \mathcal{O}(\varepsilon),$$

while the solution to the corresponding reduced equation reads $x_0(t) = A_1 e^{-t}$. In this case, then, the dynamics of the reduced equation offers a good approximation of the full dynamics for all time t , see Figure 1.6. A slightly more complicated version of this simple first order ODE will be analyzed in more detail in Section 1.3.3 in order to introduce the renormalization group (RG) method.

A second example of a regularly perturbed ODE is offered by the equation for a rescaled oscillator with small damping,

$$\begin{aligned} \ddot{x} + \varepsilon \dot{x} + x &= 0, & 0 < \varepsilon \ll 1, \\ x(0) &= A_1, \quad \dot{x}(0) = A_2. \end{aligned} \tag{1.2.4}$$

The solution to this full equation is given by

$$x(t) = C_1 e^{-\frac{1}{2}(\varepsilon + \sqrt{\varepsilon^2 - 4})t} + C_2 e^{-\frac{1}{2}(\varepsilon - \sqrt{\varepsilon^2 - 4})t} = A_2 \sin t + A_1 \cos t + \mathcal{O}(\varepsilon t), \tag{1.2.5}$$

whereas the solution to the reduced equation reads $x_0(t) = A_2 \sin t + A_1 \cos t$. After an $\mathcal{O}(\varepsilon^{-1})$ time scale the expansion of (1.2.5) is no longer well-ordered, and secular terms get a leading order influence. However, since the reduced equation misses the effect of the small damping, these secular terms do not appear in the solution to the reduced equation. Therefore, trajectories of the full problem do

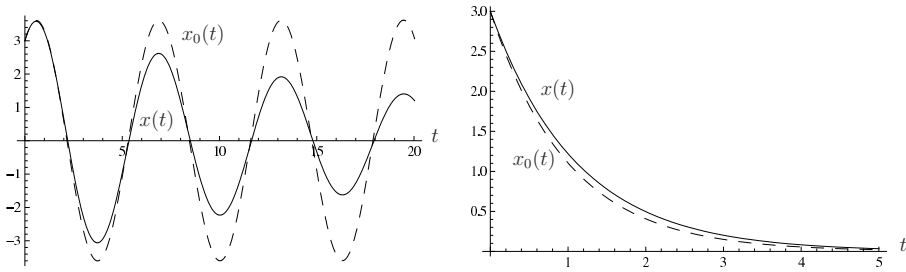


Figure 1.6: In the left frame, we plotted the solutions to the regularly perturbed equation (1.2.4) (solid line) and to the reduced equation (dotted line). The initial conditions here were $A_1 = 3$, $A_2 = 2$, and $\varepsilon = 0.1$. The trajectory corresponding to the reduced equation mimics the dynamics of the full equation, to leading order and over a bounded time interval. After some time, however, the dynamics of the reduced equation is completely different from the actual full dynamics. In the right frame, we plotted the solutions to the full and reduced equations corresponding to (1.2.3). The initial condition here was $A_1 = 3$, whereas $\varepsilon = 0.1$. Note that the trajectory of the reduced equation describes the dynamics of the full equation to leading order for all time.

indeed follow the trajectories of the reduced problem to leading order but only up to $\mathcal{O}(\varepsilon^{-1})$ time. This observation serves to highlight the important fact that the reduced equation of a regularly perturbed problem can also yield insufficient approximations, see Figure 1.6.

In conclusion, whereas one observes a radical change in the dimensionality of the dynamics of the singularly perturbed system (made explicit foremost by a reduction in the dimensionality of the system) when one sets the small parameter to zero, this is not the case for regularly perturbed problems.

1.2.2 Stability and bistability

The concept of bistability is best illustrated by Figure 1.7. Consider the double-well (two minima) potential landscape plotted in the figure. Because of friction, a marble dropped in this landscape eventually ends up in one of the two wells. For a given, sufficiently large but not too large, friction, the initial position of the marble fully determines the well in which it ends up resting. For instance, marble 1 in Figure 1.7 ends up in the first well, while marble 2 ends up in the second well. However, there is also the possibility that the marble lands exactly on the peak (maximum) in between the two wells (marble 3 in Figure 1.7). In this case, the marble does not move at all. This situation is highly unlikely of

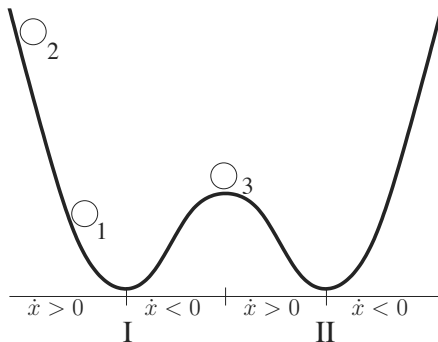


Figure 1.7: A double-well potential. Because of friction, marble 1 will end up in well I , while marble 2 will end up in well II . The third marble will not move at all.

course, since an arbitrarily small perturbation would cause the marble to move into one of the two wells. Mathematically, we call this peak location unstable, as opposed to the two wells which are termed stable. Accordingly, we say that this double-well landscape is of *bistable* nature.

Mathematically, a simple example of a bistable ODE is

$$\dot{x} = x - x^3, \quad x(0) = A_1. \quad (1.2.6)$$

This first order ODE has two attracting (stable) fixed points at $x = \pm 1$ and an unstable fixed point at $x = 0$. This unstable fixed point acts as a separatrix between the two attractors at $x = \pm 1$, that is, negative initial conditions tend to -1 and positive initial conditions go to $+1$ without trajectories originating from one region being able to cross into the other, see Figure 1.8. Moreover, note the connection between (1.2.6) and the (graph of the) potential in Figure 1.7: $x - x^3 > 0$ in the regions where $\dot{x} > 0$ and $x - x^3 < 0$ in the regions where $\dot{x} < 0$. Mathematically speaking, $x - x^3$ corresponds to minus the derivative of $-\frac{1}{2}x^2 + \frac{1}{4}x^4$, the graph of which corresponds to the potential of Figure 1.8.

Perhaps the simplest bistable PDE [26, 45] reads,

$$U_t = U_{xx} + U - U^3,$$

which is identical to the U -component of (1.1.3) with $\varepsilon = 0$. Besides the trivial fixed points at $U(x, t) \equiv \pm 1$ and at $U(x, t) \equiv 0$, this PDE also has the spatially inhomogeneous stationary solutions $U(x, t) = \pm \tanh(\frac{1}{2}\sqrt{2}x)$ that connect $x = \mp 1$ to $x = \pm 1$. In Section 1.3.2, we analyze the stability of one of these inhomogeneous

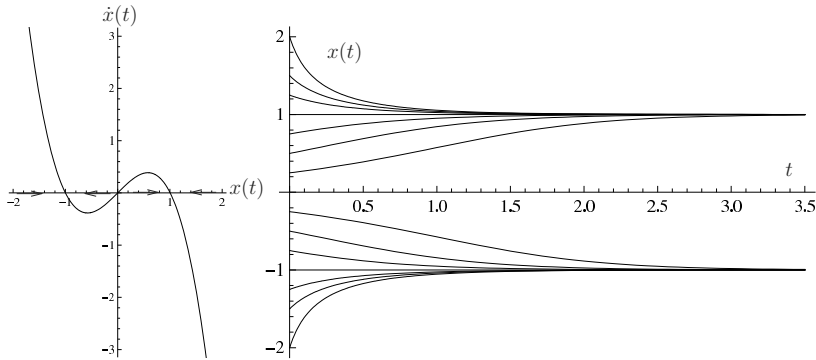


Figure 1.8: In the left frame, we plotted the phase portrait of the bistable ODE (1.2.6). The arrows indicate the direction in which a trajectory evolves. For instance, trajectories starting in $x = -0.5$ end up in $x = -1$, while trajectories starting in $x = 0.5$ end up in $x = 1$. In the right frame, we plotted the time series of several initial conditions. Positive initial conditions tend to $+1$ and negative initial conditions go to -1 . Therefore, the unstable fixed point at $x = 0$ acts as a separatrix.

solutions to introduce the concept of the Evans function, see also Sections 2.2.1 and 3.4.1.

1.3 More advanced concepts

The three main mathematical tools which we use in this thesis are geometric singular perturbation theory (Chapter 2), the Evans function (Chapter 3), and the RG method (Chapter 4). Proceeding along the lines of the previous section, we introduce and explain the basic ideas underlying these concepts by means of three simple examples.

1.3.1 Geometric singular perturbation theory

Consider the reaction kinetics of the two-component limit model of (1.1.3) (with $\tau = \varepsilon^{-1}$, $\alpha = -1$, $\beta = 0$, and $\gamma = 0$),

$$\begin{cases} \dot{u} &= u - u^3 + \varepsilon v, \\ \dot{v} &= \varepsilon(u - v), \end{cases} \quad (1.3.1)$$

where $\dot{\cdot} = \frac{d}{dt}$, $u, v \in \mathbb{R}^1$, and $0 < \varepsilon \ll 1$. This small parameter ε gives the system its singular character. With a change of time scale, $\hat{t} := \varepsilon t$, this system is

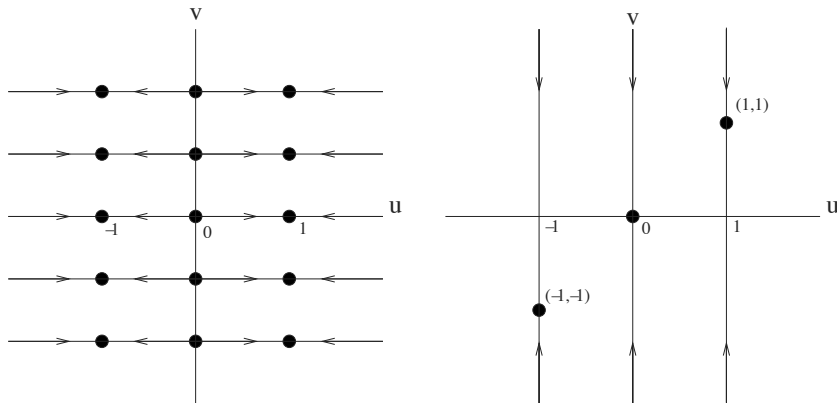


Figure 1.9: In the left frame, we plotted the dynamics of the FRS (1.3.2) and in the right frame, we plotted the dynamics of the SRS (1.3.3). The dynamics of the SRS, the slow dynamics, is only defined on the fixed points of the FRS.

transformed into

$$\begin{cases} \varepsilon u' &= u - u^3 + \varepsilon v, \\ v' &= u - v, \end{cases}$$

with $' = \frac{d}{dt}$. The time scale corresponding to t is termed the *fast* time scale, whereas the time scale corresponding to \hat{t} is called *slow*. Accordingly, the former system is called the fast system, while the latter one is called the slow system. These two systems are equivalent for $\varepsilon \neq 0$ but have very different reduced equations, *i.e.*, limit systems as $\varepsilon \rightarrow 0$. The fast reduced system (FRS) reads

$$\dot{u} = u - u^3 \quad \text{and} \quad v \equiv v_0 \in \mathbb{R}. \quad (1.3.2)$$

This is a 1-parameter family of 1-dimensional systems parametrized by $v \equiv v_0$, a constant in \mathbb{R} . The slow reduced system (SRS), on the other hand, is given by

$$\begin{cases} 0 &= u - u^3, \\ v' &= u - v, \end{cases} \quad (1.3.3)$$

which is a 1-dimensional differential-algebraic system. In fact, the SRS is only defined exactly on the fixed points of the FRS by virtue of these points coinciding with the solutions to that constraint. Both reduced systems are simpler and of lower dimension compared to the full systems and therefore easier to analyze; see Figure 1.9 for their dynamics.

The idea underlying geometric singular perturbation theory is to analyze the full system (with $\varepsilon \neq 0$ but sufficiently small) by suitably combining the dynamics of the two limiting systems, see [33, 39, 43, 64] for instance. The foundations of the theory were laid out by Fenichel [27, 28], and the theory is accordingly also called Fenichel theory. We first need to recall certain definitions before we can state Fenichel's persistence theorems.

Consider the following slow-fast system (in fast formulation)

$$\begin{cases} \dot{u} &= f(u, v; \varepsilon), \\ \dot{v} &= \varepsilon g(u, v; \varepsilon). \end{cases} \quad (1.3.4)$$

A manifold \mathcal{M}_ε is said to be *locally invariant* under the flow generated by (1.3.4) if there exists a neighborhood $V \supset \mathcal{M}$ such that no orbit can leave \mathcal{M} without leaving V .

A locally invariant manifold \mathcal{M}_0 is called *normally hyperbolic* if the eigenvalues of the linearization $D_u f(u, v; 0)$ restricted to \mathcal{M}_0 are bounded away from the imaginary axis.

The *stable manifold* $W^s(\mathcal{M})$ and *unstable manifold* $W^u(\mathcal{M})$ of a manifold \mathcal{M} which is locally invariant under a flow $\phi(\cdot; \cdot)$ are defined as follows:

$$\begin{aligned} W^s(\mathcal{M}) &:= \{y \mid d(\phi(t; y), \mathcal{M}) \rightarrow 0 \text{ as } t \rightarrow +\infty\}, \\ W^u(\mathcal{M}) &:= \{y \mid d(\phi(t; y), \mathcal{M}) \rightarrow 0 \text{ as } t \rightarrow -\infty\}, \end{aligned}$$

with $\phi(0; y) = y$ and $d(\cdot, \cdot)$ is the usual Euclidean distance.

Fenichel's first persistence theorem states that, if the FRS has a normally hyperbolic invariant manifold \mathcal{M}_0 , then, for ε small enough, the full system possesses a locally invariant slow manifold \mathcal{M}_ε that is $\mathcal{O}(\varepsilon)$ close to \mathcal{M}_0 in the C^1 topology. Moreover, Fenichel's second persistence theorem states that the full system also possesses locally invariant stable and unstable manifolds $W^{s,u}(\mathcal{M}_\varepsilon)$ which are $\mathcal{O}(\varepsilon)$ close to the stable and unstable manifolds $W^{s,u}(\mathcal{M}_0)$ of the FRS.

We are ready to apply these the two persistence theorems to the problem at hand. The three manifolds $\mathcal{M}_0^{\pm 1,0} := \{(u, v) \mid u = \pm 1, v = 0\}$ are normally hyperbolic, since each $\mathcal{M}_0^{\pm 1,0}$ is invariant with respect to the FRS (1.3.2) and

$$\left. \frac{d}{du}(u - u^3) \right|_{\mathcal{M}_0^{\pm 1,0}} = 1 - 3u^2 \Big|_{\mathcal{M}_0^{\pm 1,0}} = \{-2, 1\}.$$

Moreover,

$$\begin{aligned} W^s(\mathcal{M}_0^{\pm 1}) &= \mathbb{R}_\pm \setminus \{0\} \times \mathbb{R}, & W^u(\mathcal{M}_0^{\pm 1}) &= \mathcal{M}_0^{\pm 1}, \\ W^s(\mathcal{M}_0^0) &= \mathcal{M}_0^0, & W^u(\mathcal{M}_0^0) &= [-1, 1] \setminus \{0\} \times \mathbb{R}. \end{aligned}$$

By Fenichel's first persistence theorem, the full system (1.3.1) possesses locally invariant slow manifolds $\mathcal{M}_\varepsilon^{\pm 1,0}$ that are $\mathcal{O}(\varepsilon)$ close to $\mathcal{M}_0^{\pm 1,0}$, respectively. Note that $\mathcal{M}_0^{\pm 1,0}$ themselves are no longer (locally) invariant manifolds as $\varepsilon \neq 0$. We now (formally) determine $\mathcal{M}_\varepsilon^{\pm 1,0}$. By Fenichel theory, we know that $\mathcal{M}_\varepsilon^{\pm 1,0}$ can be expressed as a graph $u = h_\varepsilon^{\pm 1,0}(v)$; local invariance then yields

$$u = h_\varepsilon^{\pm 1,0}(v) \implies \dot{u} = \frac{dh_\varepsilon^{\pm 1,0}}{dv} \dot{v} = \varepsilon \frac{dh_\varepsilon^{\pm 1,0}}{dv} (u - v).$$

On the other hand, $\dot{u} = u - u^3 + \varepsilon v$. Combining these two expressions for \dot{u} , we obtain an equation for $h_\varepsilon^{\pm 1,0}(v)$,

$$\varepsilon \frac{dh_\varepsilon^{\pm 1,0}}{dv} (u - v) = u - u^3 + \varepsilon v.$$

Expanding $h_\varepsilon^{\pm 1,0}$ asymptotically in ε , $h_\varepsilon^{\pm 1,0}(v) = h_0^{\pm 1,0}(v) + \varepsilon h_1^{\pm 1,0}(v) + \mathcal{O}(\varepsilon^2)$, and equating $\mathcal{O}(1)$ terms of course yields the normally hyperbolic manifolds $\mathcal{M}_0^{\pm 1,0}$; $h_0^0 = 0$ and $h_0^{\pm 1} = \pm 1$. Substituting these expressions in the $\mathcal{O}(\varepsilon)$ terms of the expansion yields,

$$\begin{aligned} h_1^0 + v = 0 &\implies \mathcal{M}_\varepsilon^0 = \{(u, v) \mid u = h_\varepsilon^0(v) = -\varepsilon v + \mathcal{O}(\varepsilon^2)\}, \\ -2h_1^{\pm 1} + v = 0 &\implies \mathcal{M}_\varepsilon^{\pm 1} = \{(u, v) \mid u = h_\varepsilon^{\pm 1}(v) = \pm 1 + \frac{\varepsilon v}{2} + \mathcal{O}(\varepsilon^2)\}. \end{aligned}$$

By Fenichel's second persistence theorem, $\mathcal{M}_\varepsilon^{\pm 1}$ have local 2-dimensional stable manifolds, $W^s(\mathcal{M}_\varepsilon^{\pm 1})$, and $\mathcal{M}_\varepsilon^0$ has a local 2-dimensional unstable manifold, $W^u(\mathcal{M}_\varepsilon^0)$. Moreover, since the full problem (1.3.1) is planar, all initial conditions in between $\mathcal{M}_\varepsilon^{-1}$ and $\mathcal{M}_\varepsilon^0$ lie in both $W^u(\mathcal{M}_\varepsilon^0)$ and $W^s(\mathcal{M}_\varepsilon^{-1})$, and hence are forward asymptotic to $\mathcal{M}_\varepsilon^{-1}$. A similar statement can be made for all initial conditions between $\mathcal{M}_\varepsilon^0$ and $\mathcal{M}_\varepsilon^{+1}$. Moreover, since $\mathcal{M}_\varepsilon^{\pm 1}$ possess attracting fixed points $\pm u_f$, respectively, $\mathcal{M}_\varepsilon^0$ acts as a separatrix between $W^s(-u_f)$ and $W^s(u_f)$. In Figure 1.10, we plotted the dynamics of (1.3.1).

1.3.2 The Evans function

In this section, which can be seen as background information to the first part of Section 3.4.1, we introduce the notion of the Evans function. In particular, we use an Evans function to determine explicitly the linear stability properties of a heteroclinic stationary solution to a bistable PDE, that is, to determine the spectrum of the linearized flow corresponding to a certain time independent solution joining two distinct trivial states of the PDE. Note that, under certain rather general conditions, which apply to the specific PDE under consideration in this section, linear stability of a solution implies that the solution is also nonlinear stable [59].

For concreteness of presentation, we work with the bistable PDE introduced in

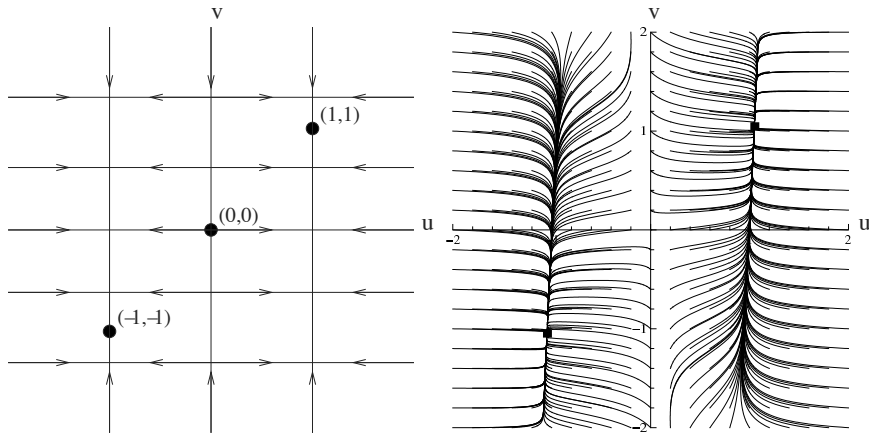


Figure 1.10: In the left frame, we plotted the dynamics of the FRS and the SRS of (1.3.1), see Figure 1.9. In the right frame, we plotted the dynamics of the full system with $\varepsilon = 0.1$. The fixed points of the system are $(0,0)$ and $\pm u_f = \pm(1.0488, 1.0488)$ (to four decimals places). The former is unstable, while the latter two are stable. Observe the locally invariant slow manifolds $\mathcal{M}_\varepsilon^{\pm 1,0}$ close to $\mathcal{M}_0^{\pm 1,0}$, respectively, whose existence are guaranteed by Fenichel's first persistence theory. The asymptotic dynamics on $\mathcal{M}_\varepsilon^{\pm 1,0}$ is given by the SRS to leading order. For the two attracting manifolds $\mathcal{M}_\varepsilon^{\pm 1}$ this can be seen in the plot. Moreover, note that $\mathcal{M}_\varepsilon^0$ acts as a separatrix between $W^s(-u_f)$ and $W^s(u_f)$.

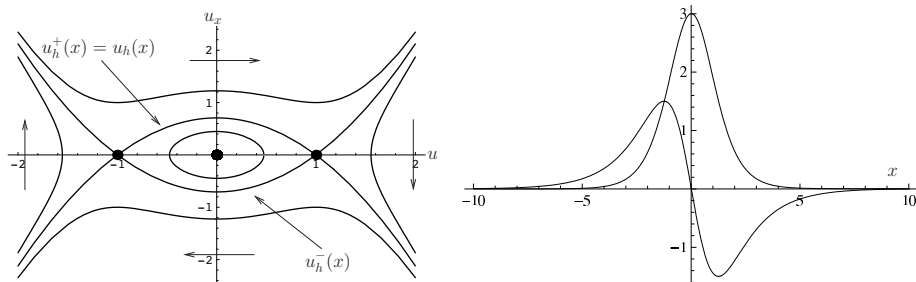


Figure 1.11: In the left frame, we plotted the phase portrait of the stationary solutions of (1.3.5). It possesses two heteroclinic stationary solutions $u_h^\pm(x)$. In the right frame, we plotted the even and odd eigenfunctions of the associated linear stability problem (1.3.7), which have been determined using an Evans function.

Section 1.2.2,

$$U_t = U_{xx} + U - U^3, \quad (1.3.5)$$

which also forms the backbone of the three-component system (1.1.3). Equation (1.3.5) possesses the heteroclinic stationary solutions $U(x, t) = u_h^\pm(x) := \pm \tanh\left(\frac{1}{2}\sqrt{2}x\right)$, see also Section 2.2.1. Here, we analyze the solution $u_h^+(x)$ connecting $U = -1$ (at $x = -\infty$) to $U = +1$ (at $x = \infty$), see Figure 1.11. Then, by symmetry considerations, we replicate our results for the remaining heteroclinic solution $u_h^-(x)$. For notational convenience, we drop the superscript ‘+’ in $u_h^+(x)$. To determine the linear stability properties of $u_h(x)$, we consider the (standard) small perturbation of $u_h(x)$

$$U(x, t) = u_h(x) + e^{\lambda t}u(x), \quad (1.3.6)$$

where $x \in \mathbb{R}$, $\lambda \in \mathbb{C}$, and u is an integrable function. Note that this is a realistic assumption: nonintegrable perturbations cannot be assumed to be small in any natural topology. Plugging this perturbation into (1.3.5), and linearizing we obtain the stability problem

$$0 = u_{xx} + (1 - 3(u_h)^2 - \lambda)u = u_{xx} + \left(3\operatorname{sech}^2\left(\frac{1}{2}\sqrt{2}x\right) - (\lambda + 2)\right)u. \quad (1.3.7)$$

Thus, the linearized operator reads

$$\mathcal{L} = \frac{d^2}{dx^2} + \left(3\operatorname{sech}^2\left(\frac{1}{2}\sqrt{2}x\right) - 2\right);$$

its spectrum is equal to the union of its point spectrum and its essential or continuous spectrum. The part of the spectrum in the left half of the complex plane

corresponds to stable eigendirections, whereas spectrum in the right half plane corresponds to unstable eigendirections, see (1.3.6).

The essential spectrum σ_{ess} covers instabilities under perturbations ‘at infinity’. Usually, it is straightforward to determine this essential spectrum for a localized solution [59, 63]; here, $\sigma_{\text{ess}} = \{\lambda \in \mathbb{R} \mid \lambda \leq -2\}$. Roughly speaking, this can be concluded as follows: for $|x|$ large, (1.3.7) is to leading order given by

$$u_{xx} - (\lambda + 2)u = 0,$$

with the general solution reading

$$u(x) = A_1 e^{\sqrt{\lambda+2}x} + A_2 e^{-\sqrt{\lambda+2}x}.$$

This solution becomes oscillatory, also in the neighborhood of infinity, for $\lambda \in (-\infty, -2] = \sigma_{\text{ess}}$. So, although these solutions $u(x)$ are bounded, they fail to be integrable for $\lambda \in \sigma_{\text{ess}}$ and thus do not belong the function space we settled on in advance.

The point spectrum, that is, the set of isolated eigenvalues corresponding to localized integrable eigenfunctions, is usually much harder to determine. It is here where the Evans function, an analytic function whose zeroes correspond to these isolated eigenvalues [1, 21–24], comes into play. Generally, and for $\lambda \notin \sigma_{\text{ess}}$, it is possible to construct two sets E_1 and E_2 of solutions to the linearized system in such a way that E_1 forms a basis for the subspace of solutions that approach zero at positive spatial infinity, while E_2 forms a basis for the subspace of solutions that approach zero at negative spatial infinity. Together E_1 and E_2 span the solution space of the linear problem. Since the eigenfunctions corresponding to isolated eigenvalues necessarily converge to zero in both spatial limits, as they are integrable, any eigenfunction is an element of both E_1 and E_2 . The Evans function \mathcal{D} is defined as the determinant of the Wronskian of the fundamental matrix solution generated by E_1 and E_2 . In general, this Evans function is nonzero, *i.e.*, E_1 and E_2 together form a basis of the solution space. However, for any specific value of λ to be in the point spectrum, E_1 and E_2 must be linearly dependent, and therefore the Wronskian must be zero. Thus, zeroes of the Evans function \mathcal{D} correspond to isolated eigenvalues in the point spectrum of the linearized operator [1, 59, 63]. Note that, an Evans function is only determined up to a scaling constant by construction. Therefore, there exists a whole 1-dimensional subspace of Evans functions rather than a unique Evans function.

We now proceed to determine the point spectrum of (1.3.7) and the corresponding eigenfunctions with the help of an Evans function. Upon rescaling y via $y := \frac{1}{2}\sqrt{2}x$, the stability problem (1.3.7) reads

$$0 = u_{yy} + (6\text{sech}^2 y - P^2) u, \tag{1.3.8}$$

where $P^2 := 2\lambda + 4$. To avoid that $\lambda \in \sigma_{\text{ess}}$, P^2 should satisfy $P^2 \in \mathbb{C} \setminus (-\infty, 0]$. It follows that we can select the square root branch in such a way that $P \in \mathbb{C}^+ = \{P \in \mathbb{C} \mid \Re(P) > 0\}$. It is hard to solve this problem straightforwardly, but this can be done via a reduction to (so-called) hypergeometric functions. To do so, we introduce the function $F(y) := u(y) \cosh^P y$ and the independent variable $z := \frac{1}{2}(1 - \tanh y)$. Since $y \in (-\infty, \infty)$, it follows that $z \in (0, 1)$ and

$$\frac{d}{dy} = \frac{d}{dz} \frac{dz}{dy} = -\frac{\text{sech}^2 y}{2} \frac{d}{dz} = -2z(1-z) \frac{d}{dz}.$$

Therefore, (1.3.8) transforms to

$$\begin{aligned} 0 &= F_{yy} - 2P \tanh(y) F_y - (P^2 + P - 6) \text{sech}^2(y) F \\ &= z(1-z) F_{zz} + (P+1)(1-2z) F_z - (P+3)(P-2) F, \end{aligned} \quad (1.3.9)$$

where in the two steps the respective factors $\text{sech}^P y$ and $4z(1-z)$ are divided out. This is a hypergeometric differential equation. The solution space of the general hypergeometric differential equation,

$$z(1-z) F_{zz} + (c - (a+b+1)z) F_z - abF = 0,$$

is spanned by the hypergeometric series

$$F(a, b|c|z) := 1 + \sum_{n=1}^{\infty} \frac{a(a+1) \dots (a+n-1) b(b+1) \dots (b+n-1)}{n! c(c+1) \dots (c+n-1)} z^n$$

and $z^{1-c} F(a-c+1, b-c+1|2-c|z)$, see [48] for example. Here, $a = P+3$, $b = P-2$, and $c = P+1$, and therefore $F(P+3, P-2|P+1|z)$ and $z^{-P} F(3, -2|1-P|z)$ are two independent solutions of (1.3.9). Note that $F(3, -2|1-P|z)$ is a quadratic polynomial in z ,

$$F(3, -2|1-P|z) = 1 - \frac{6}{1-P} z + \frac{12}{(1-P)(2-P)} z^2.$$

Next, we define a scaled version of $z^{-P} F(3, -2|1-P|z)$ which is also a solution to (1.3.9)

$$J^-(z; P) := (2z)^{-P} (1-P)(2-P) F(3, -2|1-P|z).$$

Note that the scaling factor 2^{-P} is incorporated only for our convenience. Now, $J^-(z; P)$ solves (1.3.9), has no singularities at $P = 1, 2$, and $\lim_{z \rightarrow 1} J^-(z; P)$ is bounded. Working backwards, we find then that

$$u^-(y; P) := \text{sech}^P(y) J^-(z; P), \quad \text{with } z = \frac{1}{2}(1 - \tanh y),$$

solves (1.3.8) and $\lim_{y \rightarrow -\infty} u^-(y; P) = 0$. By the reversibility symmetry of equation (1.3.8) (*i.e.*, its invariance under the change $y \rightarrow -y$)

$$u^+(y; P) := u^-(-y; P) = \text{sech}^P(y) J^-(1-z; P)$$

is also a solution of (1.3.8) and $\lim_{y \rightarrow \infty} u^+(y; P) = 0$. Hence, we have explicitly constructed two independent solutions of (1.3.8). Plainly, $u^-(y; P)$ corresponds to the set E_2 , whereas $u^+(y; P)$ corresponds to E_1 .

Using these independent solutions, we now define the Evans function

$$\tilde{\mathcal{D}}(P) := \begin{vmatrix} u^-(y; P) & u^+(y; P) \\ \frac{d}{dy}u^-(y; P) & \frac{d}{dy}u^+(y; P) \end{vmatrix}.$$

Note that the function $\tilde{\mathcal{D}}$ is independent of y by Abel's identity, see also [1]. Note also that, since u^+ has been obtained from u^- by an application of the reversibility symmetry, u^+ and u^- can only be dependent for values of P if $u^+ = \pm u^-$. This implies that the eigenfunctions are either odd or even. In general, $\mathcal{D}(P)$ cannot be computed explicitly. However, in the context of this example, a tedious yet direct computation shows that

$$\begin{aligned} \tilde{\mathcal{D}}(P) &= u^-(y; P) \frac{d}{dy}u^+(y; P) - u^+(y; P) \frac{d}{dy}u^-(y; P) \\ &= \operatorname{sech}^P(y) J^-(z; P) \left(J^-(1-z; P) \frac{d}{dy} \left(\operatorname{sech}^P y \right) \right. \\ &\quad \left. + \operatorname{sech}^P y \frac{dz}{dy} \frac{d}{dz} (J^-(1-z; P)) \right) - \operatorname{sech}^P(y) J^-(1-z; P) \\ &\quad \left(J^-(z; P) \frac{d}{dy} \left(\operatorname{sech}^P y \right) + \operatorname{sech}^P y \frac{dz}{dy} \frac{d}{dz} (J^-(z; P)) \right) \\ &= \frac{\operatorname{sech}^{2P} y}{2^{2P-1} Z^P (1-z)^P} (z(1-z) (Q(z; P) Q_z(1-z; P) - Q(1-z; P) Q_z(z; P)) \\ &\quad - P Q(z; P) Q(1-z; P)) \\ &= 2P (12z(1-z) (-12z^2 + 12z + P^2 - 4) - (144z^4 - 288z^3 \\ &\quad - 12P^2 z^2 + 192z^2 + 12P^2 z - 48z + P^4 - 5P^2 + 4P)) \\ &= -2P (P^2 - 1) (P^2 - 4). \end{aligned}$$

Recalling the definition of P , we find that the Evans function associated with the linear stability of the front solution $u_h(x)$ of (1.3.5) reads

$$\mathcal{D}(\lambda) = \tilde{\mathcal{D}}(P(\lambda)) = -8\sqrt{2}\lambda \left(\lambda + \frac{3}{2} \right) \sqrt{\lambda + 2}.$$

The zeroes of this Evans function, and thus the isolated eigenvalues of (1.3.7), are $\lambda = 0$ and $\lambda = -\frac{3}{2}$. The zero eigenvalue is due to the translation invariance of the system (see also the next paragraph), and therefore the heteroclinic solution $u_h(x)$ is linearly stable as $\lambda < 0$. Note also that the essential spectrum corresponds to $\{\lambda \in \mathbb{R} \mid \lambda \leq -2\}$, so that $\mathcal{D}(\lambda)$ is purely imaginary for $\lambda \in \sigma_{\text{ess}}$. Thus for this system also the essential spectrum can be obtained from the Evans function calculation.

Since the original problem (1.3.5) is translation invariant – that is, every translated version (in x) of a solution to (1.3.5) is also a solution to (1.3.5) – $\lambda = 0$ was expected to be an eigenvalue with corresponding eigenfunction equal to (a scaled version of) the derivative of the heteroclinic solution $u_h(x)$. A short computation shows that

$$\lambda = 0 \implies P = 2 \implies J^-(z; 2) = 3 \implies u^-(y; 2) = 3 \operatorname{sech}^2 y = u^+(x; 2).$$

Thus, $\lambda = 0$ indeed yields an even eigenfunction that is a scaled version $u'_h(x)$ – this is given by $\frac{1}{2}\sqrt{2} \operatorname{sech}^2(\frac{1}{2}\sqrt{2}x)$ – namely $3 \operatorname{sech}^2(\frac{1}{2}\sqrt{2}x)$. The other eigenvalue, $\lambda = -\frac{3}{2}$, yields

$$\begin{aligned} \lambda = -\frac{3}{2} &\implies P = 1 \implies J^-(z; 1) = -3(1 - 2z) \\ &\implies u^-(y; 1) = -3 \operatorname{sech} y \tanh y = -u^+(y; 1). \end{aligned}$$

Thus, the second (odd) eigenfunction is given by $-3 \tanh(\frac{1}{2}\sqrt{2}x) \operatorname{sech}(\frac{1}{2}\sqrt{2}x)$, see Figure 1.11.

1.3.3 The renormalization group method

There are a variety of methods which entail a form or another of renormalization, and all these methods are called RG methods. Originally, renormalization was developed in field theory and in the theory of phase transitions [42, 61, 66, 67] to cope with irregularities in critical exponents. More recently, the RG method has been adapted to deal with various perturbation and asymptotic problems arising both in ODEs and PDEs [7]. These new methods use either a continuous invariance condition [7, 10] or a discrete one [68, 69]; see also [49] for a discussion and examples of this RG method. Another type of an RG method using scaling invariance to prove rigorously that the solutions to a nonlinear parabolic PDEs have a particular asymptotic form, was developed in [6] and has originated in statistical physics. This method has also been used to prove stability of solutions, see [18].

The aforementioned RG methods also differ from the RG method we use in this thesis. Our method was developed in [55] and uses renormalization to establish the existence and nonlinear stability properties of certain special solutions to PDEs and ODEs. Moreover, it was also used in [16] to validate a formally derived system of ODEs describing the dynamics of semi-strongly interacting fronts. It is for this purpose that we employ the RG method, see Chapter 4.

We remark that in many physical problems, the dynamics of the positions of fronts are referred to as collective coordinates, see for example [3]. In [19, 20, 55], it is proved that for a certain type of weakly interacting structures, a reduction to such collective coordinates always possible is. However, in this thesis we are

dealing with semi-strongly interacting structures. For such a structures, the author is not aware of methods other than that developed in [55] (and used in this thesis) to prove rigorously the collective coordinates reduction.

To explain the basic ideas behind the RG method we use in Chapter 4 [16, 31, 47, 55], we consider the first order nonautonomous ODE,

$$\begin{aligned} \dot{x} &= -(1 - \varepsilon(t))x, & 0 < |\varepsilon(t)| \leq \varepsilon_0 < 1, \\ x(0) &= A_0, \end{aligned} \tag{1.3.10}$$

for ε_0 small enough (see below). Note that for $\varepsilon(t) \equiv \varepsilon$, (1.3.10) can be solved explicitly: $x(t) = A_0 e^{-(1-\varepsilon)t}$, see (1.2.3). It follows that there is a globally attracting fixed point at $x = 0$. This is, of course, also the case for any general $\varepsilon(t)$ satisfying $0 < |\varepsilon(t)| \leq \varepsilon_0 \ll 1$. However, for the sake of demonstration, we pretend that both the exact solution of (1.3.10) and the existence of the attracting fixed point at the origin are unavailable. Using the RG method, we identify the attracting fixed point at $x = 0$ and prove that it is, indeed, globally attracting.

The variation of constants formula applied to (1.3.10) yields

$$x(t) = e^{-t} A_0 + \int_0^t e^{-(t-s)} \varepsilon(s) x(s) ds. \tag{1.3.11}$$

Defining

$$y(t) := \sup_{0 < t' < t} e^{t'} |x(t')|$$

and multiplying both sides of (1.3.11) by e^t , we obtain the estimate

$$e^t x(t) \leq |A_0| + \varepsilon_0 \int_0^t y(s) ds \leq |A_0| + \varepsilon_0 t y(t).$$

Note that the last term is secular: it becomes arbitrarily large for increasing t . Taking the supremum over all time up to time τ yields

$$y(\tau) \leq |A_0| + \varepsilon_0 \tau y(\tau) \implies y(\tau) \leq \frac{|A_0|}{1 - \varepsilon_0 \tau}.$$

It seems that, according to this inequality, the secular term yields blow up for too large τ , see also Figure 1.12. A prototypical area of applications of the RG method concerns problems on which the estimates exhibit similar secular behavior. Problems solved by using the RG method often have this property of an uncontrollable secular term. Using these naive estimates, we have an *a priori finite* time control over the solution,

$$|x(t)| \leq 2e^{-t} |A_0|, \quad t \in \left(0, \frac{1}{2\varepsilon_0}\right). \tag{1.3.12}$$

The idea behind the RG method is to choose a specific new initial condition A_1 at time $t = \frac{1}{2\varepsilon_0}$ – the moment when (1.3.12) loses its validity – and to repeat the above procedure using this new initial condition A_1 . (Note that we can also *renormalize* at any other moment smaller than $\frac{1}{\varepsilon_0}$. This specific choice of A_1 is

$$A_1 := 2e^{-\frac{1}{2\varepsilon_0}} |A_0|,$$

namely, the upperbound of (1.3.12) at $t = \frac{1}{2\varepsilon_0}$. Using this new initial condition, we now consider the initial value problem

$$\begin{aligned} \dot{x} &= -(1 - \varepsilon(t))x, \quad 0 < |\varepsilon(t)| \leq \varepsilon_0 \ll 1, \\ x\left(\frac{1}{2\varepsilon_0}\right) &= A_1. \end{aligned}$$

The variation of constants formula combined with the above estimates yields, then,

$$|x(t)| \leq 2e^{-\left(t - \frac{1}{2\varepsilon_0}\right)} |A_1| = 4e^{-t} |A_0|, \quad t \in \left(\frac{1}{2\varepsilon_0}, \frac{1}{\varepsilon_0}\right).$$

Repeating this *renormalization procedure*, we obtain

$$|A_{n+1}| := 2e^{-\frac{1}{2\varepsilon_0}} |A_n| = 2^{(n+1)} e^{-\frac{n+1}{2\varepsilon_0}} |A_0|.$$

An easy induction shows, then, that

$$|x(t)| \leq 2e^{-\left(t - \frac{n}{2\varepsilon_0}\right)} |A_N| = 2^{(n+1)} e^{-t} |A_0|, \quad t \in \left(\frac{n}{2\varepsilon_0}, \frac{n+1}{2\varepsilon_0}\right).$$

Thus,

$$|x(t)| \leq 2|A_0| e^{-t(1-2\varepsilon_0 \log 2)} \quad \text{for all } t.$$

Since ε_0 is a small enough, which in this particular case means $\varepsilon_0 < \frac{1}{2 \log 2}$, we obtain a net contraction of the initial condition A_0 . Therefore, there is a globally attracting fixed point of (1.3.10) at $x(t) = 0$. See Figure 1.12.

In Chapter 4, we use this same method to establish the attractivity of a set spanned by N -front solutions. There, however, we do not choose a different initial condition when we renormalize; instead, we choose a different position of the fronts we linearize about.

1.4 Outline

As we already remarked, system (1.1.3) is the central object of study in this thesis. Our ultimate goal is to understand the semi-strong front and pulse interactions

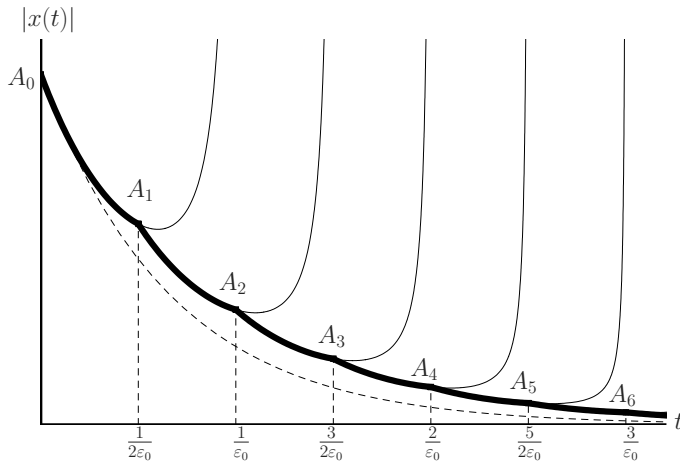


Figure 1.12: Schematic depiction of the main idea underlying the RG method. After a finite time, the secular term becomes too large (diverges) and one has to renormalize. For (1.3.10), this entails to choosing a new initial condition.

present in this system. Before we can thoroughly study those interactions, we need to first study the existence and stability properties of the ‘simple’ asymptotic states. That is, we need to analyze the existence and stability of several stationary or uniformly traveling 1- or 2-pulse solutions (2- or 4-front solutions). In all of these cases, and for both the existence and stability problems, we find that we can reduce the system of PDEs to a 6-dimensional system of first order ODEs in the spatial variable ξ , so that the analysis reduces to investigating these ODEs. Note that these ODEs turn out to be autonomous and nonlinear for the existence problem and nonautonomous but linear for the stability problem.

In Chapter 2, we consider the existence problem. This chapter was published in 2009 under the title *Pulse dynamics in a three-component system: existence analysis* in the *Journal of Dynamics and Differential Equations*, and it is joint work with A. Doelman and T.J. Kaper. The main mathematical tool we use in that chapter is geometric singular perturbation theory (see Section 1.3.1).

In Chapter 3, we consider the nonlinear stability problem. This chapter was published in 2008 under the title *Pulse dynamics in a three-component system: Stability and bifurcations* in the journal *Physica D*, and it is also joint work with A. Doelman and T.J. Kaper. The main mathematical tool used here is the Evans function (see Section 1.3.2).

It should be noted that these first two chapters are more than merely preliminary work towards the interaction analysis of the final chapter, as they deal with several other issues. For example, we analyze the way in which the second inhibitor, the W -component, alters the dynamics of the two-component limit model (1.1.1). More specifically, we map out the type of dynamics exhibited by the three-component model which is absent from the two-component limit model (1.1.1). As in the case of the original Purwins system (1.1.2), several solutions only exist or are only stable in the extended model (1.1.3). For instance, stationary 2-pulse solutions do not exist in the two-component limit model (Section 2.6) but do exist in the extended three-component model (Section 2.5.2). In a similar vein, stationary 1-pulse solutions can only emerge from a saddle-node bifurcation in the extended system; this is not the case in the limit system, see Corollary 3.4.2 and Figure 3.3. We also study the possible bifurcations of stable stationary 1-pulse solutions. Besides the aforementioned saddle-node bifurcation, a 1-pulse solution can bifurcate into a breathing 1-pulse solution (Hopf bifurcation) or into a traveling 1-pulse solution as the bifurcation parameter τ keeps increasing, see Sections 2.4 and 3.5.2. Note that the latter bifurcation can be either supercritical or subcritical, see Lemma 2.4.1 and Figure 3.11. Moreover, observe that these bifurcations only occur for large $\tau = \mathcal{O}(\varepsilon^{-2})$. This makes the bifurcation analysis much more involved compared to the existence and stability analysis of stationary 1-pulse solutions.

In the final chapter, we analyze the semi-strong front and pulse interactions. Using the RG method (see Section 1.3.3), we derive systems of ODEs describing the motion of the various fronts of an N -front solution. This derivation contains a fully nonlinear PDE analysis, in contrast to the previous chapters. Eventually, we analyze the derived ODEs to understand the semi-strong front and pulse dynamics. This chapter has been recently submitted for publication under the title *Front interactions in a three-component system*, and it is joint work with A. Doelman, T.J. Kaper, and K. Promislow.

Finally, we would like to clarify that the material in this thesis only offers a the first few glimpses into the dynamics generated by (1.1.3). One of the main ‘gaps’ in our current understanding is related to the fact that we only study interactions in the parameter regime where $\tau = \mathcal{O}(1)$, see the last chapter. In particular, we do not study the much more interesting regime $\tau = \mathcal{O}(\varepsilon^{-2})$, where uniformly traveling, breathing, and stationary 1-pulse solutions co-exist and interact, see Chapters 2 and 3. The reason behind that is quite fundamental: in that regime, the essential spectrum associated with the stability of an N -front solution lies asymptotically close to the imaginary axis. As a consequence, some of the central estimates on which the RG method is built no longer hold. Our analysis is also limited in the sense that we only consider patterns in one spatial dimension; a natural and challenging future project concerns the analysis of the planar variant of (1.1.3). This is a natural next step, for instance to make a bet-

ter comparison with the (numerical) observations obtained for the original model (1.1.2). Two *a priori* bottlenecks for this analysis concern the extensions of, first, the dynamical system-informed *spatial dynamics* approach and of the RG method to a 2-dimensional setting. To the former bottleneck there exist solutions in the literature, while the latter bottleneck is still largely unsolved.

Chapter 2

Existence

2.1 Introduction

Spatially-localized structures, such as fronts, pulses and spots, have been found to exhibit a wide variety of interesting dynamics in dissipative systems. These dynamics include repulsion, annihilation, attraction, breathing, collision, scattering, self-replication, and spontaneous generation. The richness of the observed dynamics typically increases with the complexity and the size of the system. Localized structures, that do not exist in reaction-diffusion equations (RDEs) with a small number of components, may readily exist when more components and more terms are added to the system. Likewise, solutions that are unstable in small or simple RDEs may become stable with such additions.

The aim of this chapter is to report on the mathematical analysis of a paradigm example that exhibits this increased richness. In particular, we study the three-component model introduced in [60] and studied further in [5, 51, 53, 54, 70, 71], see also the previous chapter. In one space dimension, the equations are

$$\begin{cases} U_t = D_U U_{xx} + f(U) - \kappa_3 V - \kappa_4 W + \kappa_1, \\ \tau V_t = D_V V_{xx} + U - V, \\ \theta W_t = D_W W_{xx} + U - W, \end{cases} \quad (2.1.1)$$

where we used the notation of [51], see also (1.1.2). Note that (2.1.1) has the reversibility symmetry $x \rightarrow -x$. Here, the (U, V) -subsystem is a classical, bistable two-component RDE, which exhibits dynamics similar to the classical FitzHugh-Nagumo (FHN) equations (although here $D_V \neq 0$, whereas $D_V = 0$ in FHN), and the variable W denotes an added inhibitor component. We will show that it is responsible for increasing the richness of the types of solutions the model possesses.

In (2.1.1), U, V , and W are real-valued functions of $x \in \mathbb{R}$ and $t \in \mathbb{R}^+$, and

the subscripts indicate partial derivatives. The parameters τ and θ are positive constants, and the primary interest is in using τ as the bifurcation parameter. The diffusivities of the respective components are denoted by D_U, D_V , and D_W , $f(U)$ is a bistable cubic reaction function (often taken to be $f(U) = 2U - U^3$), κ_3 and κ_4 denote reaction rates, and κ_1 denotes a constant source term.

The fundamental discovery reported in [60] is that, in this three-component model, the added component W can stabilize stationary and traveling single spot solutions and multi-spot solutions in two space dimensions, which otherwise are inherently unstable in the classical two-component (U, V) -bistable model. This stabilization was shown to occur when D_W is sufficiently large relative to D_U and D_V , because then the presence of W prevents spots from extending in the directions perpendicular to their directions of motion. In this manner, W suppresses the instability that spots undergo in two-component systems [60].

The dynamics of pulses in the 1-dimensional model (2.1.1) is also known to be richer than in the corresponding 1-dimensional version of the two-component model. Pulses collide, scatter, annihilate, among others, as has been shown in [51, 52], whereas the dynamics of pulses in the restricted two-component system is much less rich. A special class of unstable 2-pulse solutions, called scatters or separators, is identified for (2.1.1) in [51, 52]. It is shown that their stable and unstable manifolds organize the evolution in phase space of all nearby solutions. More precisely, during the course of a collision between two pulses, they converge to a separator state, and the location of the initial data relative to the stable and unstable manifolds of this separator determines how and when the pulses scatter off each other. Furthermore, in some parameter regimes, the scattering process may be directed by a combination of two separators, where the colliding pulses first approach one separator, spend a long time near it, and then approach a second separator state, and then finally repel or annihilate, see [51, 52].

Our work is inspired by the results from [54, 60] and [51, 52]. We carry out a complementary, rigorous analysis of the existence of certain pulse solutions for a scaled version of the three-component model, see (2.1.6) below. The model has a rich geometric structure that will be studied using geometric singular perturbation theory, and we note that the application of this theory is challenging due to the fact that the associated ordinary differential equations (ODEs) are 6-dimensional.

2.1.1 Statement of the model equations

In [5, 51, 53, 54, 60, 70, 71], the numerical values of the diffusivities of the three species differ by several orders of magnitude. For example, in [51], the values are $D_U = 5 \times 10^{-6}$, $D_V = 5 \times 10^{-5}$, and $D_W = 10^{-2}$. Therefore, we are motivated

to introduce a scaled spatial variable

$$\tilde{x} = \frac{x}{\sqrt{D_V}}. \quad (2.1.2)$$

For computational convenience we also scale out the factor two in the nonlinearity $f(U) = 2U - U^3$. Therefore, we introduce

$$\begin{aligned} \tilde{t} = 2t, \quad (\tilde{U}, \tilde{V}, \tilde{W}) &= \frac{1}{2}\sqrt{2}(U, V, W), \quad (\tilde{\tau}, \tilde{\theta}) = 2(\tau, \theta), \\ (\tilde{\kappa}_1, \tilde{\kappa}_3, \tilde{\kappa}_4) &= \frac{1}{2}(\frac{1}{2}\sqrt{2}\kappa_1, \kappa_3, \kappa_4). \end{aligned} \quad (2.1.3)$$

In terms of these scaled quantities, the system (2.1.1) is

$$\begin{cases} \tilde{U}_{\tilde{t}} &= \varepsilon^2 \tilde{U}_{\tilde{x}\tilde{x}} + \tilde{U} - \tilde{U}^3 - \tilde{\kappa}_3 \tilde{V} - \tilde{\kappa}_4 \tilde{W} + \tilde{\kappa}_1, \\ \tilde{\tau} \tilde{V}_{\tilde{t}} &= \tilde{V}_{\tilde{x}\tilde{x}} + \tilde{U} - \tilde{V}, \\ \tilde{\theta} \tilde{W}_{\tilde{t}} &= D^2 \tilde{W}_{\tilde{x}\tilde{x}} + \tilde{U} - \tilde{W}, \end{cases} \quad (2.1.4)$$

with the nondimensional diffusivities $\varepsilon^2 = \frac{D_U}{2D_V} \ll 1$ and $D^2 = \frac{D_W}{D_V} \gg 1$.

As to the parameters in the reaction terms, the numerical values that are used in [51] are $(\kappa_1, \kappa_3, \kappa_4) = (-7, 1, 8.5)$, and very similar values are used in [60]. While these are $\mathcal{O}(1)$ with respect to ε , it is helpful to first study the system with $\mathcal{O}(\varepsilon)$ values of these parameters; *i.e.*, to introduce scaled parameters, as follows:

$$\tilde{\kappa}_1 = -\varepsilon\gamma, \quad \tilde{\kappa}_3 = \varepsilon\alpha, \quad \tilde{\kappa}_4 = \varepsilon\beta, \quad (2.1.5)$$

where α, β , and γ are $\mathcal{O}(1)$ quantities and where we have taken κ_1 to be negative, since it is negative in all of the above cited articles.

The rationale for this choice of scalings (2.1.5) is threefold. First, this choice was made to facilitate the mathematical analysis, since in this regime the terms in the U -equation corresponding to the source and to the coupling from the inhibitor components are weak, yet not too weak. In fact, the effects of the source and the coupling terms are too weak when they are of $\mathcal{O}(\varepsilon^2)$ [14]. Second, it turns out that much of the rich pulse dynamics exhibited by system (2.1.4) exists also when the parameters have $\mathcal{O}(\varepsilon)$ values, as we will show in this chapter (see also [56]). Therefore, one might reasonably hope to understand the origins of the dynamics observed in [51] by beginning with the present analysis. Third, in the numerical simulations of [51, 60], which were done on bounded domains, the W variable stays near -0.8 , approximately. Hence, in a very approximate (and rough) sense one might argue, as follows, that there is an effective impact of the parameters in the U -equation of (2.1.4) that is of $\mathcal{O}(\varepsilon)$. Since $\tilde{\kappa}_3 = 0.5$ and $\varepsilon = \frac{1}{10}\sqrt{5} \approx 0.22$, the effect of V in this equation can indeed be considered to be $\mathcal{O}(\varepsilon)$. Moreover, by the scalings (2.1.3), $\tilde{\kappa}_4 \tilde{W} - \tilde{\kappa}_1 \approx 0.07$ for $W = -0.8$ (and $\kappa_{1,4}$ as in [51]), which is clearly also $\mathcal{O}(\varepsilon)$. Thus, it appears that the impact

of the source and coupling terms are indeed small. Of course this last argument is far from being mathematically consistent. However, this argument formed the original motivation to introduce the aforementioned rescalings.

In light of the above scalings, the model equations that we study are

$$\begin{cases} U_t = \varepsilon^2 U_{xx} + U - U^3 - \varepsilon(\alpha V + \beta W + \gamma), \\ \tau V_t = V_{xx} + U - V, \\ \theta W_t = D^2 W_{xx} + U - W, \end{cases} \quad (2.1.6)$$

where we dropped the tildes. Furthermore, we require that $0 < \varepsilon \ll 1$, $0 < \tau, \theta \ll \varepsilon^{-3}$, $D > 1$, and $\alpha, \beta, \gamma \in \mathbb{R}$, where the upper bound on τ and θ is derived in Section 2.3.1. Moreover, we assume that the solutions $(U(x, t), V(x, t), W(x, t))$ are bounded over the entire domain.

At various stages throughout the analysis, we will see that it is also useful to examine the three-component model in a stretched (or ‘fast’) spatial variable $\xi = \frac{x}{\varepsilon}$:

$$\begin{cases} U_t = U_{\xi\xi} + U - U^3 - \varepsilon(\alpha V + \beta W + \gamma), \\ \tau V_t = \frac{1}{\varepsilon^2} V_{\xi\xi} + U - V, \\ \theta W_t = \frac{D^2}{\varepsilon^2} W_{\xi\xi} + U - W. \end{cases} \quad (2.1.7)$$

We refer to this system as the fast system, and to system (2.1.6) as the slow system.

The system (2.1.6) or (2.1.7) is well-suited as a paradigm for the analysis of three-component RDEs. On the one hand, it is sufficiently nonlinear and complex so that it supports a rich variety of localized structures, and on the other hand it is sufficiently simple, with linear reaction functions in the second and third components and with linear coupling, so that much of the dynamics can be computed analytically, including certain bifurcations. In this respect, we believe that the results presented here also provide a basis to establish a theory of interacting pulses in this paradigm model.

2.1.2 Outline of the main results

We begin in Section 2.2 with examining the stationary, or standing, 1-pulse solutions. For these solutions, the U -component consists of a front, which connects the (quiescent) state $U = -1 + \mathcal{O}(\varepsilon)$ to the (active) state $U = 1 + \mathcal{O}(\varepsilon)$, and a back, which provides the opposite connection, concatenated together to form a pulse (or homoclinic orbit). Both the front and the back are sharp, so that the pulse is highly localized, due to the asymptotically small value of ε^2 in (2.1.6). The V -component of the 1-pulse solutions consists of a smooth pulse that is centered on the middle of the interval in which the U -component is in the active

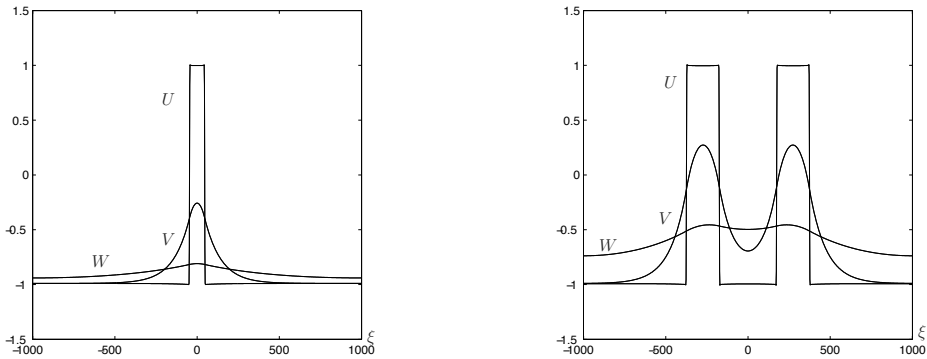


Figure 2.1: Stable stationary 1-pulse and 2-pulse solutions of system (2.1.6) obtained via numerical simulation. For the 1-pulse the system parameters are $(\alpha, \beta, \gamma, D, \tau, \theta, \varepsilon) = (3, 1, 2, 5, 1, 1, 0.01)$, and for the 2-pulse we had $(\alpha, \beta, \gamma, D, \tau, \theta, \varepsilon) = (2, -1, -0.25, 5, 1, 1, 0.01)$.

state and that varies over slightly wider interval than the U -pulse. Finally, the W -component also consists of a single, smooth pulse, but it varies on a wider interval than either of the other two components due to the fact that $D > 1$. See Figure 2.1. The standing 1-pulse solutions are formally constructed in Section 2.2.2. Then, we make this construction rigorous in Theorem 2.2.1, which states that the three-component model (2.1.6) possesses standing 1-pulse solutions whenever the system parameters satisfy (2.2.22). See Section 2.2.3 for the statement of this theorem and Section 2.2.4 for its proof.

Next, we analyze the existence of traveling 1-pulse solutions. This analysis, presented in Section 2.3, follows the same two-step procedure: we first construct solutions formally (see Section 2.3.1) and then we prove their existence rigorously (see Sections 2.3.2 and 2.3.3). The main result is Theorem 2.3.1, which states that there exist traveling pulse solutions whenever either τ or θ (or both) is $\mathcal{O}(\varepsilon^{-2})$ and the system parameters satisfy (2.3.13).

Given these results about standing and traveling 1-pulse solutions, it is of interest to investigate the bifurcation of the former into the latter. We do so in Section 2.4. The leading order results are given by (2.4.2) in Section 2.4.1, and then the rigorous, high-order asymptotics for the main bifurcation parameter τ as a function of the other parameters is summarized in Lemma 2.4.1, see Section 2.4.2. It turns out that this bifurcation can be supercritical, as well as subcritical, depending on the parameters, see Corollaries 2.4.2 and 2.4.3. This result contrasts with the

bifurcation result for the 2-dimensional version of this model, obtained in [54], where it was shown that this bifurcation is supercritical.

Having completed our analysis of the 1-pulse solutions, we next turn our attention to 2-pulse solutions of (2.1.6). The main result is Theorem 2.5.1, which guarantees the existence of 2-pulse solutions whenever the system parameters satisfy (2.5.6). These 2-pulse solutions have U -components that consist of two copies of the U -component of the single pulses, while the V - and W -components exhibit two peaks as well, but are not near equilibrium in the interval between their two peaks. See Figure 2.1. In this sense, the interaction between the pulses is semi-strong, according to the terminology of [12]. We also note that (2.5.6) is rather complex, and we present investigations of it when $D = 2$, and when D is general. Moreover, we give the asymptotics of the key quantities as $D \rightarrow \infty$. See Sections 2.5.2 and 2.5.3, respectively.

After completing the analysis of these pulse solutions, we examine in Section 2.6 the two-component (U, V) -subsystem, obtained from (2.1.6) by setting W constant at -1 . This analysis of the two-component system enables us to make observations about the differences between the two-component and the three-component systems. For instance, for the 2-pulse solutions, we observe that the inclusion of the third component is essential, because the two-component version of the model cannot possess 2-pulse solutions. Simply put, there is not enough freedom in the two-component model to permit the construction of these solutions, and our analysis reveals why the third component – which naturally makes the phase space of the associated ODE problem 6-dimensional – creates sufficient space/freedom for their existence.

In Section 2.7.1 we present the results of a series of numerical simulations of (2.1.6). These simulations confirm the various analytical existence and bifurcation results presented herein, and they also reveal the presence of rich pulse interactions, including pulse reflection and annihilation, stable breathing single and double pulses (which bifurcate from stationary pulse solutions), pulse scattering, as well as combinations of these. See Figures 2.14–2.18. The single and double pulses analyzed in this chapter are key building blocks to understand these rich pulse interactions. Finally, in Section 2.7.2, we summarize our analysis and discuss some related items.

Remark 2.1.1. The 2-pulse solutions constructed in [25, 34] for the FHN differ in several respects from those constructed here. In FHN, these are essentially copies of the 1-pulse solution, that must be very far apart, and that exhibit oscillatory behavior in the interval between the pulses. The mechanism responsible for their existence is related to the classical Shilnikov mechanism.

Remark 2.1.2. Other examples of stabilization via the inclusion of an additional component in a model are given for instance by the Gray-Scott and Gierer-

Meinhardt systems. In these, 1-pulse (homoclinic) solutions that are unstable with respect to the scalar RDE for the activator component are stabilized in certain parameter regimes by the coupling to the equation for the inhibitory component. The diffusive flux of inhibitor into the pulse domains helps to localize the activator concentration, hence stabilizing 1-pulse solutions, and we refer to [12, 13] for the mathematical analysis using the Evans function and the stability index. Moreover, it is worth noting that the converse may also arise; namely in [14] it is shown that stable fronts of a bistable, scalar RDE are *destabilized* through coupling to a second component when the parameters are chosen so that either the essential spectrum approaches the origin or an eigenvalue emerges from the essential spectrum and becomes unstable.

2.2 Stationary 1-pulse solutions

2.2.1 Basic observations

First, we look at stationary pulses of system (2.1.7), *i.e.*, we put $(U_t, V_t, W_t) = (0, 0, 0)$. By introducing $p = u_\xi, q = \frac{1}{\varepsilon}v_\xi$ and $r = \frac{D}{\varepsilon}w_\xi$, we transform system (2.1.7) into a 6-dimensional singularly perturbed ODE

$$\begin{cases} u_\xi &= p, \\ p_\xi &= -u + u^3 + \varepsilon(\alpha v + \beta w + \gamma), \\ v_\xi &= \varepsilon q, \\ q_\xi &= \varepsilon(v - u), \\ w_\xi &= \frac{\varepsilon}{D}r, \\ r_\xi &= \frac{\varepsilon}{D}(w - u). \end{cases} \quad (2.2.1)$$

Although ξ is the spatial variable, it will play the role of ‘time’ in our analysis. The system possesses two symmetries

$$\begin{aligned} (\xi, p, q, r) &\rightarrow (-\xi, -p, -q, -r) \quad \text{and} \\ (u, p, v, q, w, r, \gamma) &\rightarrow (-u, -p, -v, -q, -w, -r, -\gamma). \end{aligned} \quad (2.2.2)$$

Note that the first symmetry corresponds to the reversibility symmetry $(x, \xi) \rightarrow (-x, -\xi)$ in (2.1.6), (2.1.7), respectively. The fixed points of system (2.2.1) have $p = q = r = 0$, and $u = v = w$ with $u^3 + u(-1 + \varepsilon(\alpha + \beta)) + \varepsilon\gamma = 0$. Solving this last equation yields

$$u_\varepsilon^\pm = \pm 1 \mp \frac{1}{2}\varepsilon(\alpha + \beta \pm \gamma) + \mathcal{O}(\varepsilon^2), \quad u_\varepsilon^0 = \varepsilon\gamma + \mathcal{O}(\varepsilon^2). \quad (2.2.3)$$

Hence, there are three fixed points,

$$P_\varepsilon^\pm = (u_\varepsilon^\pm, 0, u_\varepsilon^\pm, 0, u_\varepsilon^\pm, 0), \quad P_\varepsilon^0 = (u_\varepsilon^0, 0, u_\varepsilon^0, 0, u_\varepsilon^0, 0). \quad (2.2.4)$$

It can be checked that P_ε^\pm , respectively P_ε^0 , represent stable, respectively unstable, trivial states of the partial differential equations (PDEs) (2.1.6) and (2.1.7).

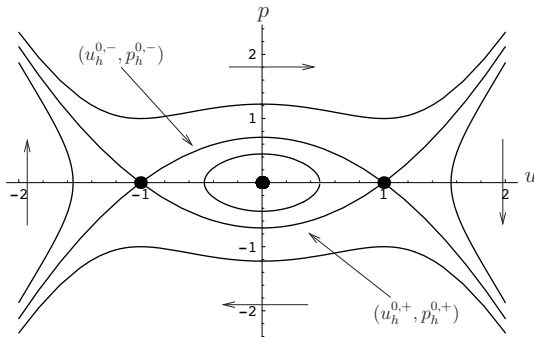


Figure 2.2: The phase portrait of the fast reduced Hamiltonian system (2.2.5).

The fast reduced system (FRS) is obtained by letting $\varepsilon \downarrow 0$ in (2.2.1),

$$\begin{cases} u_\xi &= p, \\ p_\xi &= -u + u^3, \end{cases} \quad (2.2.5)$$

as well as $(v_\xi, q_\xi, w_\xi, r_\xi) = (0, 0, 0, 0)$, *i.e.*, $(v, q, w, r) \equiv (v_*, q_*, w_*, r_*)$ with $v_*, q_*, w_*, r_* \in \mathbb{R}$ constants. The fixed points of the FRS are given by $(u, p) \in \{(\pm 1, 0), (0, 0)\}$. The former are saddles. The latter, $(0, 0)$, is a center that corresponds to P_ε^0 and thus to an unstable trivial state of (2.1.6) – we will therefore not consider it.

We define the 4-dimensional invariant manifolds \mathcal{M}_0^\pm by

$$\mathcal{M}_0^\pm := \{(u, p, v, q, r, w) \in \mathbb{R}^6 : u = \pm 1, p = 0\},$$

which are the unions of the saddle points over all possible $v_*, q_*, w_*, r_* \in \mathbb{R}$. Planar system (2.2.5) is integrable with Hamiltonian

$$H(u, p) = \frac{1}{2}(p^2 + u^2) - \frac{1}{4}(u^4 + 1), \quad (2.2.6)$$

which is chosen such that $H(u, p) = 0$ on \mathcal{M}_0^\pm . The FRS possesses heteroclinic orbits $(u_h^{0,\pm}(\xi), p_h^{0,\pm}(\xi))$ that connect the fixed points $(u, p) = (\pm 1, 0)$ to $(\mp 1, 0)$,

$$u_h^{0,\pm}(\xi) = \mp \tanh\left(\frac{1}{2}\sqrt{2}\xi\right), \quad p_h^{0,\pm}(\xi) = \mp \frac{1}{2}\sqrt{2}\operatorname{sech}^2\left(\frac{1}{2}\sqrt{2}\xi\right). \quad (2.2.7)$$

See Figure 2.2. The manifolds \mathcal{M}_0^\pm are normally hyperbolic, and they have 5-dimensional stable and unstable manifolds $W^{s,u}(\mathcal{M}_0^\pm)$ that are the unions of the

4-parameter (v_*, q_*, w_*, r_*) -families of 1-dimensional stable and unstable manifolds of the saddle points $(u, p) = (\pm 1, 0)$ in (2.2.5).

Fenichel's first persistence theorem [27, 39, 43] implies that for ε small enough, system (2.2.1) has locally invariant slow manifolds $\mathcal{M}_\varepsilon^\pm$ which are $\mathcal{O}(\varepsilon)$ C^1 -close to \mathcal{M}_0^\pm , *i.e.*, $\mathcal{M}_\varepsilon^\pm$ can be represented by

$$\mathcal{M}_\varepsilon^\pm := \{u = \pm 1 + \varepsilon u_1^\pm(v, q, w, r; \varepsilon), p = \varepsilon p_1^\pm(v, q, w, r; \varepsilon)\}, \quad (2.2.8)$$

where the graphs u_1 and p_1 can be computed by an expansion in ε ,

$$\mathcal{M}_\varepsilon^\pm = \{u = \pm 1 - \frac{1}{2}\varepsilon(\alpha v + \beta w + \gamma) + \mathcal{O}(\varepsilon^2), p = \mathcal{O}(\varepsilon^2)\}. \quad (2.2.9)$$

The application of Fenichel's second persistence theorem establishes that $\mathcal{M}_\varepsilon^\pm$ have 5-dimensional stable and unstable manifolds, $W^{s,u}(\mathcal{M}_\varepsilon^\pm)$, that are $\mathcal{O}(\varepsilon)$ C^1 -close to their $\varepsilon = 0$ counterparts $W^{s,u}(\mathcal{M}_0^\pm)$. Observe that the critical points P_ε^\pm have 3-dimensional stable and unstable manifolds $W^{s,u}(P_\varepsilon^\pm)$ which are contained in $W^{s,u}(\mathcal{M}_\varepsilon^\pm)$.

There are two slow reduced limit systems (SRS), both of which we write in terms of the fast variable ξ : one that governs the flow on $\mathcal{M}_\varepsilon^-$,

$$\begin{cases} v_{\xi\xi} &= \varepsilon^2(v + 1 + \mathcal{O}(\varepsilon)), \\ w_{\xi\xi} &= \frac{\varepsilon^2}{D^2}(w + 1 + \mathcal{O}(\varepsilon)), \end{cases} \quad (2.2.10)$$

and one that governs the flow on $\mathcal{M}_\varepsilon^+$,

$$\begin{cases} v_{\xi\xi} &= \varepsilon^2(v - 1 + \mathcal{O}(\varepsilon)), \\ w_{\xi\xi} &= \frac{\varepsilon^2}{D^2}(w - 1 + \mathcal{O}(\varepsilon)). \end{cases} \quad (2.2.11)$$

Observe that $(v, q, w, r) = (\pm 1, 0, \pm 1, 0) + \mathcal{O}(\varepsilon)$ are saddle points on $\mathcal{M}_\varepsilon^\pm$ that correspond to the fixed points P_ε^\pm (2.2.4). Also note that the v - and w -equations are to leading order decoupled, so that both ODEs can be considered separately. See also Remark 2.2.1. Hence, we have a (v, q) -subsystem and a (w, r) -subsystem, both with two saddle points. These four saddle points each have 1-dimensional stable and unstable manifolds, $l_{v,w}^{s,u,\pm}$, that are given to leading order by

$$\begin{aligned} l_v^{s,\pm} &= \{q = \pm 1 - v\}, & l_w^{s,\pm} &= \{r = \pm 1 - w\}, \\ l_v^{u,\pm} &= \{q = \mp 1 + v\}, & l_w^{u,\pm} &= \{r = \mp 1 + w\}. \end{aligned} \quad (2.2.12)$$

In Figure 2.3, we sketch some orbits on the manifolds $\mathcal{M}_\varepsilon^\pm$.

2.2.2 The construction of 1-pulse solutions $\gamma_{h,j}^-(\xi)$ homoclinic to P_ε^-

In this section, we consider symmetric stationary 1-pulse solutions $\gamma_{h,j}^-(\xi)$ that are homoclinic (denoted by the subscript 'h') to P_ε^- (denoted by the superscript

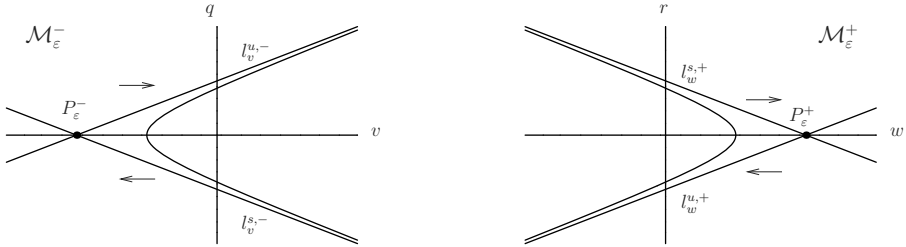


Figure 2.3: The flow generated by the (v, q) -subsystem on \mathcal{M}_ϵ^- and that of the (w, r) -subsystem on \mathcal{M}_ϵ^+ . Note that stable/unstable manifolds $l_v^{s,u,\pm}$ and $l_w^{s,u,\mp}$ have the same slopes.

‘-’). The last subscript ‘ j ’ is an index which is needed since there can be more than one pulse solution for a given set of parameters. Here, we present the formal derivation. Then, in section 2.2.3, we formulate a theorem based on this analysis – Theorem 2.2.1, and we prove this theorem in Section 2.2.4. This proof also establishes the validity of the asymptotic analysis in this section. Note that orbits homoclinic to the other fixed point P_ϵ^+ can be obtained from these orbits by application of the symmetries (2.2.2).

Before we start with the construction of $\gamma_{h,j}^-(\xi)$, we introduce some notation. From Figures 2.1 and 2.4, we notice that there are five different regions, three in which the leading order spatial evolution is given by the SRS (2.2.10) and (2.2.11), and two regions that are governed by the FRS (2.2.5). Since the PDEs are translation invariant, we may parametrize the pulse solution so that its u, v, w -components are at a local extremum at $\xi = 0$, *i.e.*, $p_{h,j}^-(0) = q_{h,j}^-(0) = r_{h,j}^-(0) = 0$ – we will find that $v_{h,j}^-(0)$ and $w_{h,j}^-(0)$ are maxima, while $u_{h,j}^-(0)$ is a (local) minimum. Moreover, we introduce ξ_* as the position of the ‘jump mid-point(s)’, more precisely ξ_* is such that $\gamma_{h,j}^-(\xi)$ is half-way between the two slow manifolds at $\xi = \xi_*$, *i.e.*, $u_{h,j}^- = 0$ at $\xi = \pm\xi_*$ (2.2.2). We will find that $\xi_* = \mathcal{O}(\frac{1}{\epsilon})$, but at this point of the analysis it is still undetermined. Next, we define the two ‘fast intervals’ I_f^\mp and the three ‘slow intervals’ I_s^\mp, I_s^0 ,

$$\begin{aligned} I_f^- &:= \left(-\xi_* - \frac{1}{\sqrt{\epsilon}}, -\xi_* + \frac{1}{\sqrt{\epsilon}}\right), I_f^+ := \left(\xi_* - \frac{1}{\sqrt{\epsilon}}, \xi_* + \frac{1}{\sqrt{\epsilon}}\right), \\ I_s^- &:= \left(-\infty, -\xi_* - \frac{1}{\sqrt{\epsilon}}\right], I_s^0 := \left[-\xi_* + \frac{1}{\sqrt{\epsilon}}, \xi_* - \frac{1}{\sqrt{\epsilon}}\right], I_s^+ := \left[\xi_* + \frac{1}{\sqrt{\epsilon}}, \infty\right). \end{aligned} \quad (2.2.13)$$

Note that the choice of the width for I_f^\pm of $\frac{2}{\sqrt{\epsilon}}$ is standard, but arbitrary. We can now give a more precise definition of the five regions mentioned above (see Figure 2.4).

- 1: The dynamics take place exponentially close to the slow manifold $\mathcal{M}_\varepsilon^-$: $\xi \in I_s^-$.
- 2: The dynamics take place in the fast field: $\xi \in I_f^-$.
- 3: The dynamics take place exponentially close to $\mathcal{M}_\varepsilon^+$: $\xi \in I_s^0$.
- 4: The dynamics take place in the fast field: $\xi \in I_f^+$.
- 5: The dynamics take place exponentially close to $\mathcal{M}_\varepsilon^-$: $\xi \in I_s^+$.

By definition,

$$\gamma_{h,j}^- = (u_{h,j}^-, p_{h,j}^-, v_{h,j}^-, q_{h,j}^-, w_{h,j}^-, r_{h,j}^-) \in W^u(P_\varepsilon^-) \cap W^s(P_\varepsilon^-) \subset W^u(\mathcal{M}_\varepsilon^-) \cap W^s(\mathcal{M}_\varepsilon^-),$$

while the jump mid-points are defined by

$$\gamma_{h,j}^-(\pm\xi_*) = (0, \mp p_*, v_*, \mp q_*, w_*, \mp r_*).$$

Furthermore, since $\gamma_{h,j}^-(\xi)$ remains exponentially close to $\mathcal{M}_\varepsilon^+$ for $\xi \in I_s^0$, $\gamma_{h,j}(\xi)$ is also exponentially close to $W^u(P_\varepsilon^-) \cap W^s(\mathcal{M}_\varepsilon^+)$ and to $W^s(P_\varepsilon^-) \cap W^u(\mathcal{M}_\varepsilon^+)$ for sufficiently long time. Note that $\gamma_{h,j}^-(\xi) \notin W^u(\mathcal{M}_\varepsilon^-) \cap W^s(\mathcal{M}_\varepsilon^+)$ or $W^s(\mathcal{M}_\varepsilon^-) \cap W^u(\mathcal{M}_\varepsilon^+)$, since it has to be able to jump back again from $\mathcal{M}_\varepsilon^+$ to $\mathcal{M}_\varepsilon^-$.

By considering possible take off and touch down points of jumps through the fast field and by studying, in fact explicitly solving, the slow flows on $\mathcal{M}_\varepsilon^-$ (2.2.10) and on $\mathcal{M}_\varepsilon^+$ (2.2.11), we obtain relations between the coordinates $(v_*, \mp q_*, w_*, \mp r_*)$ of the jump mid-points and their spatial positions $\pm\xi_*$ that uniquely determine the homoclinic orbit(s) $\gamma_{h,j}^-(\xi)$; see Remark 2.2.1.

For $\varepsilon \neq 0$, the Hamiltonian $H(u, p)$ (2.2.6) is not conserved

$$\begin{aligned} \frac{d}{d\xi} H(u(\xi), p(\xi)) &= uu_\xi + pp_\xi - u^3 u_\xi \\ &= up + p(-u + u^3 + \varepsilon(\alpha v + \beta w + \gamma)) - u^3 p \quad (2.2.14) \\ &= \varepsilon p(\alpha v + \beta w + \gamma). \end{aligned}$$

Since $(u_{h,j}^-(\xi), p_{h,j}^-(\xi))$ must be $\mathcal{O}(\varepsilon)$ close to the heteroclinic solution $(u_h^{0,-}(\xi), p_h^{0,-}(\xi))$ (2.2.7) of the FRS (2.2.5) in the fast field I_f^- , the total change in H for an orbit $\gamma_{h,j}^-(\xi)$ that jumps from $\mathcal{M}_\varepsilon^-$ to $\mathcal{M}_\varepsilon^+$ is approximated by

$$\begin{aligned} \Delta_f^- H(v_*, q_*, w_*, r_*) &= \int_{I_f^-} H_\xi d\xi \\ &= \int_{I_f^-} \varepsilon p_h^{0,-}(\xi + \xi_*)(\alpha v_* + \beta w_* + \gamma) d\xi + \mathcal{O}(\varepsilon\sqrt{\varepsilon}) \\ &= \varepsilon(\alpha v_* + \beta w_* + \gamma) \int_{-\infty}^{\infty} p_h^{0,-}(\xi) d\xi + \mathcal{O}(\varepsilon\sqrt{\varepsilon}) \\ &= 2\varepsilon(\alpha v_* + \beta w_* + \gamma) + \mathcal{O}(\varepsilon\sqrt{\varepsilon}), \end{aligned}$$

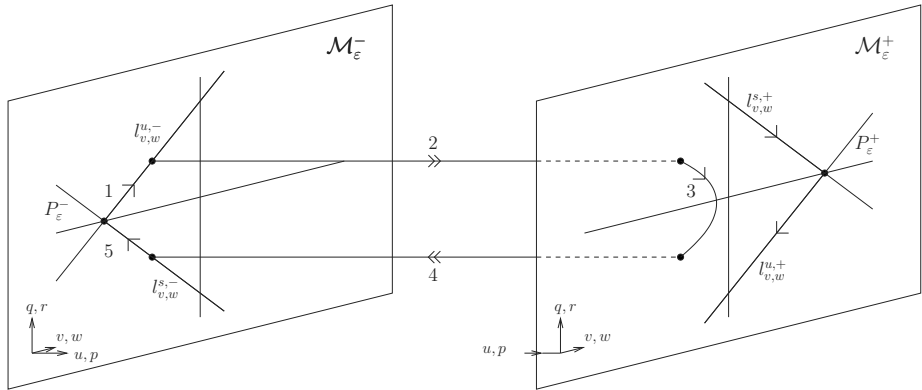


Figure 2.4: A schematic sketch of a standing pulse solution $\gamma_{h,j}^-(\xi)$ in the 6-dimensional (u, p, v, q, w, r) -phase space. In region 1, the pulse is exponentially close to $\mathcal{M}_\varepsilon^-$ for a long ‘spatial time’ and approaches P_ε^- as $\xi \rightarrow -\infty$. It ‘takes off’ from $\mathcal{M}_\varepsilon^-$ at $\xi = -\xi_* - \frac{1}{\sqrt{\varepsilon}}$ (by definition) and ‘jumps’ through the fast field ($\xi \in I_f^-$) towards $\mathcal{M}_\varepsilon^+$ – this is region 2. In region 3, $\gamma_{h,j}^-(\xi)$ touches down near $\mathcal{M}_\varepsilon^+$ at $\xi = -\xi_* + \frac{1}{\sqrt{\varepsilon}}$ and remains exponentially close to $\mathcal{M}_\varepsilon^+$ until $\xi = \xi_* - \frac{1}{\sqrt{\varepsilon}}$, from where it jumps back towards $\mathcal{M}_\varepsilon^-$, which defines region 4 ($\xi \in I_f^+$). In the final region, 5, $\gamma_{h,j}^-(\xi)$ is again exponentially close to $\mathcal{M}_\varepsilon^-$ and approaches P_ε^- as $\xi \rightarrow \infty$. See also Figure 2.1 in which $\gamma_{h,j}^-(\xi)$ exhibits the same structure.

where we have used (2.2.7), (2.2.14), and assumed that $\xi_* = \mathcal{O}(\frac{1}{\varepsilon})$. Note that $\Delta_f^- H$ in principle depends on (v_*, q_*, w_*, r_*) , the slow (v, q, w, r) -coordinates of the jump mid-points, and that these coordinates do not vary to leading order during a jump through the fast field,

$$\begin{aligned} \Delta_f^- v &= \int_{I_f^-} v_\xi d\xi = \int_{I_f^-} \varepsilon q d\xi = 2q_* \sqrt{\varepsilon} + \mathcal{O}(\varepsilon) = \mathcal{O}(\sqrt{\varepsilon}), \\ \Delta_f^- q &= \int_{I_f^-} q_\xi d\xi = \int_{I_f^-} \varepsilon(v - u) d\xi = 2v_* \sqrt{\varepsilon} + \mathcal{O}(\varepsilon) = \mathcal{O}(\sqrt{\varepsilon}), \\ \Delta_f^- w &= \int_{I_f^-} w_\xi d\xi = \int_{I_f^-} \frac{\varepsilon}{D} r d\xi = 2r_* \frac{1}{D} \sqrt{\varepsilon} + \mathcal{O}(\varepsilon) = \mathcal{O}(\sqrt{\varepsilon}), \\ \Delta_f^- r &= \int_{I_f^-} r_\xi d\xi = \int_{I_f^-} \frac{\varepsilon}{D} (w - u) d\xi = 2w_* \frac{1}{D} \sqrt{\varepsilon} + \mathcal{O}(\varepsilon) = \mathcal{O}(\sqrt{\varepsilon}). \end{aligned} \quad (2.2.15)$$

On the other hand, such an orbit $\gamma_{h,j}^-(\xi)$ cannot have a total change of more than $\mathcal{O}(\varepsilon^2)$ over a jump through the fast field I_f^- , since

$$\begin{aligned} H(u, p)|_{\mathcal{M}_\varepsilon^\pm} &= \frac{1}{2} \left((\pm 1 - \frac{1}{2}\varepsilon(\alpha v + \beta w + \gamma) + \mathcal{O}(\varepsilon^2))^2 + \mathcal{O}(\varepsilon^2)^2 \right) \\ &\quad - \frac{1}{4} \left((\pm 1 - \frac{1}{2}\varepsilon(\alpha v + \beta w + \gamma) + \mathcal{O}(\varepsilon^2))^4 + 1 \right) \\ &= \frac{1}{2} \mp \frac{1}{2}\varepsilon(\alpha v + \beta w + \gamma) - \frac{1}{4} \pm \frac{1}{2}\varepsilon(\alpha v + \beta w + \gamma) - \frac{1}{4} + \mathcal{O}(\varepsilon^2) \\ &= \mathcal{O}(\varepsilon^2), \end{aligned} \quad (2.2.16)$$

where we recall (2.2.8), (2.2.9). Thus, we conclude that for an orbit $\gamma_{h,j}^-(\xi)$ that jumps from $\mathcal{M}_\varepsilon^-$ to $\mathcal{M}_\varepsilon^+$ the following relation for the slow (v_*, q_*, w_*, r_*) -coordinates of the jump mid-point must hold to leading order

$$\alpha v_* + \beta w_* + \gamma = 0. \quad (2.2.17)$$

Note that $\Delta_f^- H(v_*, q_*, w_*, r_*)$ is in fact a Melnikov function that measures the distance between $W^u(\mathcal{M}_\varepsilon^-)$ and $W^s(\mathcal{M}_\varepsilon^+)$ as they intersect the $\{u = 0\}$ hyperplane (see [12, 14, 57]). Condition (2.2.17) determines the 3-dimensional set of initial conditions in $\{u = 0\}$ that defines the 4-dimensional intersection of the two 5-dimensional manifolds $W^u(\mathcal{M}_\varepsilon^-)$ and $W^s(\mathcal{M}_\varepsilon^+)$ (recall that the phase space is 6-dimensional and that the p -coordinates of these initial conditions are necessarily $\mathcal{O}(\varepsilon)$ close to $p_h^{0,-}(0) = \frac{1}{2}\sqrt{2}$ (2.2.7)).

By the reversibility symmetry (2.2.2), we know that (2.2.17) also must hold for the $(v_*, -q_*, w_*, -r_*)$ -coordinates, which are the coordinates of the jump mid-points of the orbits that jump from $\mathcal{M}_\varepsilon^+$ to $\mathcal{M}_\varepsilon^-$ near $\xi = \xi_*$.

Next, we study the slow flows on $\mathcal{M}_\varepsilon^\pm$. The equations (2.2.10) and (2.2.11) for these flows are linear and decoupled to leading order, thus we may solve for v and w separately. Based on the above analysis, we write down the following boundary

conditions for the solutions in regions 1, 3, and 5:

$$\begin{aligned} v_h(\pm\infty) &= -1, & v_h(-\xi_* \pm \frac{1}{\sqrt{\varepsilon}}) &= v_h(\xi_* \mp \frac{1}{\sqrt{\varepsilon}}) = v_* + \mathcal{O}(\sqrt{\varepsilon}), \\ q_h(\pm\infty) &= 0, & q_h(-\xi_* \pm \frac{1}{\sqrt{\varepsilon}}) &= -q_h(\xi_* \mp \frac{1}{\sqrt{\varepsilon}}) = q_* + \mathcal{O}(\sqrt{\varepsilon}), \\ w_h(\pm\infty) &= -1, & w_h(-\xi_* \pm \frac{1}{\sqrt{\varepsilon}}) &= w_h(\xi_* \mp \frac{1}{\sqrt{\varepsilon}}) = w_* + \mathcal{O}(\sqrt{\varepsilon}), \\ r_h(\pm\infty) &= 0, & r_h(-\xi_* \pm \frac{1}{\sqrt{\varepsilon}}) &= -r_h(\xi_* \mp \frac{1}{\sqrt{\varepsilon}}) = r_* + \mathcal{O}(\sqrt{\varepsilon}), \end{aligned} \quad (2.2.18)$$

see Figures 2.1 and 2.4. Note that there are more (boundary) conditions than free parameters in the general solutions of (2.2.10) and (2.2.11). As a consequence, we find that both v_* and q_* , as well as w_* and r_* , must be related,

$$q_* = v_* + 1, \quad r_* = w_* + 1, \quad (2.2.19)$$

which in geometrical terms is equivalent to $(v_*, q_*) \in l_v^{u,-}$, and $(w_*, r_*) \in l_w^{u,-}$ (2.2.12), see also Figure 2.3. Moreover, (2.2.18) yields additional relations between v_* and ξ_* and between w_* and ξ_* ,

$$v_* = -A^2, \quad w_* = -A^{\frac{2}{D}} \quad \text{where} \quad A = e^{-\varepsilon\xi_*}. \quad (2.2.20)$$

Observe that, since $\xi_* > 0$, $A \in (0, 1)$, so that $v_*, w_* \in (-1, 0)$. For (v_*, q_*, w_*, r_*) and ξ_* that satisfy (2.2.18), (2.2.19) and (2.2.20), we obtain the explicit (slow) solutions,

$$v_h(\xi) = \begin{cases} 2e^{\varepsilon\xi} \sinh \varepsilon\xi_* - 1, \\ -2e^{-\varepsilon\xi} \cosh \varepsilon\xi + 1, \\ 2e^{-\varepsilon\xi} \sinh \varepsilon\xi_* - 1, \end{cases} \quad w_h(\xi) = \begin{cases} 2e^{\frac{\varepsilon}{D}\xi} \sinh \frac{\varepsilon}{D}\xi_* - 1 & \text{in 1,} \\ -2e^{-\frac{\varepsilon}{D}\xi} \cosh \frac{\varepsilon}{D}\xi + 1 & \text{in 3,} \\ 2e^{-\frac{\varepsilon}{D}\xi} \sinh \frac{\varepsilon}{D}\xi_* - 1 & \text{in 5} \end{cases} \quad (2.2.21)$$

to leading order in ε . Thus, together with the Melnikov condition (2.2.17), the boundary conditions (2.2.18) imply three relations between v_* , w_* , and ξ_* . These relations combine into the following jump condition on A ,

$$\alpha A^2 + \beta A^{\frac{2}{D}} = \gamma + \mathcal{O}(\sqrt{\varepsilon}). \quad (2.2.22)$$

A solution $A \in (0, 1)$ of this equation uniquely determines the jump mid-points $(v_*, \mp q_*, w_*, \mp r_*)$ in phase space of a homoclinic solution $\gamma_{h,j}^-(\xi)$, as well as their spatial positions $\pm\xi_*$ (2.2.20).

Remark 2.2.1. We comment briefly on the coupling between the V - and W -components and on the related fact that the homoclinic orbits are isolated. In the PDE (2.1.7), the variables V and W seem to be only coupled through the equation for U . In the construction of $\gamma_{h,j}^-(\xi)$, this coupling induces the Melnikov condition (2.2.17) and gives a natural relationship between the v_* - and w_* -coordinates of the jump mid-points. However, we observe that there is an additional geometrically-induced coupling between these two components that is not directly obvious from the equations. In particular, the jump mid-points ξ_* must be the same for both the v - and w -components in (2.2.1), which implies that also the ‘time-of-flight’

along the slow manifolds must be the same for both the v - and w -components, since the parametrizations of all of the components of a homoclinic orbit $\gamma_{h,j}^-(\xi)$ are of course the same. Hence, from among the entire 1-parameter set of pairs (v_*, w_*) that satisfy the Melnikov condition (2.2.17), a unique pair, with $v_* = -(-w_*)^D$ (2.2.20), is selected by this ‘time-of-flight’ constraint. Together, the two constraints determine the values of v_* and w_* uniquely and thus establish that the homoclinic orbits are isolated.

2.2.3 Existence theorem

Based on the analysis of the previous section, we can formulate the following existence result:

Theorem 2.2.1. *Let $(\alpha, \beta, \gamma, D)$ be such that (2.2.22) has K solutions $A_j \in (0, 1)$ ($K \in \{0, 1, 2\}$), and let ε be small enough. If $K = 0$, there are no symmetric orbits homoclinic to P_ε^- in system (2.2.1). If $K > 0$, then there are K symmetric homoclinic orbits $\gamma_{h,j}^-(\xi)$, $j \in \{1, K\}$ to P_ε^- that have a structure as sketched in Figure 2.4, i.e., the orbits $\gamma_{h,j}^-(\xi)$ consist of five distinct parts, two fast parts in which it is $\mathcal{O}(\varepsilon)$ close to a fast reduced heteroclinic orbits $(u_h^{0,\mp}(\xi \mp \xi_*), p_h^{0,\pm}(\xi \mp \xi_*), v_*, \pm q_*, w_*, \pm r_*)$ (2.2.7) with (v_*, q_*, w_*, r_*) given by (2.2.19) and (2.2.20), and three slow parts in which $(u_{h,j}^-(\xi), p_{h,j}^-(\xi)) = (\pm 1, 0) + \mathcal{O}(\varepsilon)$ and $(v_{h,j}^-(\xi), q_{h,j}^-(\xi), w_{h,j}^-(\xi), r_{h,j}^-(\xi))$ are given by (2.2.21), up to $\mathcal{O}(\sqrt{\varepsilon})$ corrections, with*

$$\xi_* = \xi_{*,j} = -\frac{1}{\varepsilon} \log A_j = \mathcal{O}\left(\frac{1}{\varepsilon}\right). \quad (2.2.23)$$

The orbits $\gamma_{h,j}^-(\xi)$ correspond to stationary pulse solutions

$$(U(\xi, t), V(\xi, t), W(\xi, t)) \equiv (u_{h,j}(\xi), v_{h,j}(\xi), w_{h,j}(\xi))$$

of (2.1.7).

Moreover, if $|\alpha D| > |\beta|$ and $\text{sgn}(\alpha) \neq \text{sgn}(\beta)$, then a saddle-node bifurcation of homoclinic orbits occurs, to leading order in ε , as γ crosses through

$$\begin{aligned} \gamma_{c1}(\alpha, \beta, D) &= (-\alpha)^{-\frac{1}{D-1}} \beta^{\frac{D}{D-1}} \left(D^{-\frac{1}{D-1}} - D^{-\frac{D}{D-1}} \right) > 0 \quad \text{for } \alpha < 0 < \beta, \\ \gamma_{c2}(\alpha, \beta, D) &= \alpha^{-\frac{1}{D-1}} (-\beta)^{\frac{D}{D-1}} \left(D^{-\frac{D}{D-1}} - D^{-\frac{1}{D-1}} \right) < 0 \quad \text{for } \beta < 0 < \alpha. \end{aligned} \quad (2.2.24)$$

The explicit expressions for the values $\gamma_{c1,2}$ of the saddle-node bifurcations are based on a straightforward leading order analysis: set the partial derivative of (2.2.22) with respect to A equal to zero to obtain

$$A_c = A_1(\alpha, \beta, D) = \left(-\frac{\alpha D}{\beta} \right)^{-\frac{1}{2} \frac{D}{D-1}} \in (0, 1), \quad (2.2.25)$$

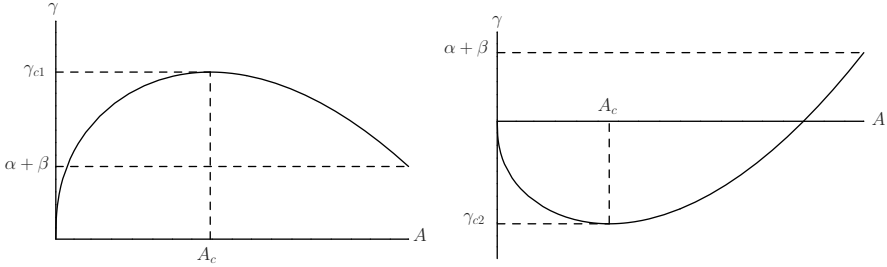


Figure 2.5: A graphical representation of the jump condition (2.2.22) and the associated saddle-node bifurcations as described by Theorem 2.2.1 for $\alpha < 0 < \beta$ (with $\alpha + \beta > 0$) and for $\beta < 0 < \alpha$ (also with $\alpha + \beta > 0$). Note that $A_K \in (0, 1)$ for all parameter combinations.

and then insert this expression back into formula (2.2.22) to obtain $\gamma_{c1,2}$ (2.2.24).

In Figure 2.5, the relations between A_j and γ as solutions of (2.2.22) have been plotted. The two saddle-node cases at A_c described by the theorem are also clearly visible. Two other bifurcations occur: one at $\gamma = A = 0$, which corresponds to $\xi_* = \infty$ (2.2.23), *i.e.*, the plateau at which the U -component of the 1-pulse solution is near 1 becomes infinitely long; the other at $\gamma = \alpha + \beta$, $A = 1$, where the pulse becomes infinitely thin – see also Lemma 2.2.2 below.

2.2.4 The proof of Theorem 2.2.1

The existence of the homoclinic orbit $\gamma_{h,j}^-(\xi) \subset W^u(P_\varepsilon^-) \cap W^s(P_\varepsilon^-)$ will be established by studying $W^u(\mathcal{M}_\varepsilon^-)$ and $W^u(P_\varepsilon^-)$ as they pass along $\mathcal{M}_\varepsilon^+$. The reversibility symmetry (2.2.2) plays a crucial role in the proof.

The manifold $W^u(P_\varepsilon^-)$ is 3-dimensional, so that all orbits $\gamma_{\bar{P}}^-(\xi) \subset W^u(P_\varepsilon^-)$ can be represented by a 2-parameter family, $\gamma_{\bar{P}}^-(\xi) = \gamma_{\bar{P}}^-(\xi; v_*, w_*)$, where (v_*, w_*) represents the jump mid-point. Of course, we only consider the part of $W^u(P_\varepsilon^-)$ that is spanned by orbits $\gamma_{\bar{P}}^-(\xi)$ that are $\mathcal{O}(\varepsilon)$ close to a heteroclinic solution of the FRS (2.2.5) away from $\mathcal{M}_\varepsilon^-$ and $\mathcal{M}_\varepsilon^+$, *i.e.*, we do not pay attention to the other ‘half’ of $W^u(P_\varepsilon^-)$ that is spanned by solutions with a monotonically decreasing u -coordinate – see Figure 2.2. More precisely, $\gamma_{\bar{P}}^-(\xi)$ is exponentially close to $\mathcal{M}_\varepsilon^-$ for asymptotically large, negative values of ξ , jumps away as ξ increases, and crosses through the $\{u = 0\}$ hyperplane at

$$\gamma_{\bar{P}}^-(-\xi_{P,*}) = \gamma_{\bar{P}}^-(-\xi_{P,*}(v_*, w_*)) = (0, p_*, v_*, q_*, w_*, r_*). \quad (2.2.26)$$

Note that $\gamma_{\bar{P}}^-(\xi; v_*, w_*)$ must be exponentially close to the slow unstable manifold $W_{\text{slow}}^u(P_\varepsilon^-) \subset \mathcal{M}_\varepsilon^-$ that is spanned by $l_v^{u,-}$ and $l_w^{u,-}$ (2.2.12), so that $q_* = v_* + 1$, $r_* = w_* + 1$ as in (2.2.19). Moreover, we note that this family of orbits $\gamma_{\bar{P}}^-(\xi; v_*, w_*)$ with finite pairs (v_*, w_*) has as its natural geometric completion the slow unstable manifold $W_{\text{slow}}^u(P_\varepsilon^-) \subset \mathcal{M}_\varepsilon^-$ in the limit that $|v_*| \rightarrow \infty$ and $|w_*| \rightarrow \infty$ such that their ratio remains fixed.

Within $W^u(P_\varepsilon^-)$, there is *a priori* a 1-parameter family of orbits that is forward asymptotic to $\mathcal{M}_\varepsilon^+$, because $W^u(P_\varepsilon^-) \cap W^s(\mathcal{M}_\varepsilon^+)$ is the intersection of a 3- and a 5-dimensional manifold in a 6-dimensional space, *i.e.*, $W^u(P_\varepsilon^-) \cap W^s(\mathcal{M}_\varepsilon^+)$ is expected to be 2-dimensional. The Melnikov calculus [12, 14, 57] of the previous section implies that $\gamma_{\bar{P}}^-(\xi; v_*, w_*) \subset W^u(P_\varepsilon^-) \cap W^s(\mathcal{M}_\varepsilon^+)$ if v_* and w_* are related by (2.2.17). By construction, $W^u(P_\varepsilon^-) \cap W^s(\mathcal{M}_\varepsilon^+)$ is spanned by $\gamma_{\text{het}}^-(\xi; v_*) = \gamma_{\bar{P}}^-(\xi; v_*, w_*(v_*))$ with $w_*(v_*)$ given by (2.2.17).

The evolution of $\gamma_{\text{het}}^-(\xi; v_*)$ near $\mathcal{M}_\varepsilon^+$ is governed by the linear SRS (2.2.11). If $v_*, w_* \in (-1, 0)$, then $\gamma_{\text{het}}^-(\xi)$ intersects the $\{q = 0\}$ -hyperplane (Figure 2.3). We may assume that the intersection $\gamma_{\text{het}}^-(\xi; v_*) \cap \{q = 0\}$ takes place at $\xi = 0$. This assumption determines the jump mid-point $\xi_{\text{het},*}(v_*) = \xi_{P,*}(v_*, w_*(v_*))$. Moreover, it follows that $\xi_{\text{het},*}(v_*) > 0$ (2.2.26). For $\xi > -\xi_{\text{het},*}(v_*) + \mathcal{O}(\varepsilon^{-1/2})$, *i.e.*, if $\gamma_{\text{het}}^-(\xi; v_*)$ is exponentially close to $\mathcal{M}_\varepsilon^+$, the evolution of the r -coordinate $r_{\text{het}}^-(\xi; v_*)$ of $\gamma_{\text{het}}^-(\xi; v_*)$ can be computed explicitly. For general v_* , $r_{\text{het}}^-(0; v_*) \neq 0$, but there are special values of v_* such that $r_{\text{het}}^-(0; v_*) = 0$. In fact, $r_{\text{het}}^-(0; v_*) = 0$ if and only if $v_* = -A_{0,*}^2$, where $A_{0,*}$ solves an algebraic equation that is to leading order given by (2.2.22). Note that this is in essence how (2.2.22) has been obtained. However, also note that the relation (2.2.22) has been deduced for the so far only formally constructed homoclinic orbit $\gamma_{h,j}^-(\xi) \subset W^u(P_\varepsilon^-) \cap W^s(P_\varepsilon^-)$, while $A_{0,*}$ corresponds to the heteroclinic orbit $\gamma_{\text{het}}^-(\xi; v_*) \subset W^u(P_\varepsilon^-) \cap W^s(\mathcal{M}_\varepsilon^+)$. This is explained by the fact that $\xi_{j,*}$, the position of the jump mid-point of $\gamma_{h,j}^-(\xi)$, is of $\mathcal{O}(\varepsilon^{-1})$ (2.2.23). Thus $\gamma_{h,j}^-(\xi)$ must be exponentially close to $\mathcal{M}_\varepsilon^+$ for an asymptotically long ‘time’. Hence, it must be exponentially close to $W^s(\mathcal{M}_\varepsilon^+)$. We define the (rigorously constructed) critical heteroclinic orbit $\gamma_{0,*}^-(\xi)$ by $\gamma_{0,*}^-(\xi) = \gamma_{\text{het}}^-(\xi; v_*)$ with v_* determined by $A_{0,*}$. Moreover, we observe that $\gamma_{0,*}^-(\xi)$ is such that $\|\gamma_{h,j}^-(\xi) - \gamma_{0,*}^-(\xi)\|$ is exponentially small for $\xi < 0$; and $|A_j - A_{0,*}|$ is also exponentially small, but nonzero. Note that $\gamma_{0,*}^-(\xi)$ cannot be symmetric, since it remains exponentially close to $\mathcal{M}_\varepsilon^+$ for $\xi > 0$; this necessarily implies that $p_{0,*}^-(0) \neq 0$.

Now assume that $K \neq 0$, *i.e.*, that there exists at least one solution $A = A_j \in (0, 1)$ of (2.2.22), and that $(\alpha, \beta, \gamma, D)$ are such that $W^u(\mathcal{M}_\varepsilon^-)$ and $W^s(\mathcal{M}_\varepsilon^+)$ intersect transversely, *i.e.*, that γ is not asymptotically close to $\gamma_{c1,c2}(\alpha, \beta, D)$, the values at which the saddle-node bifurcations occur (2.2.24). The above arguments imply that the heteroclinic orbit $\gamma_{0,*}^-(\xi) \subset W^u(P_\varepsilon^-) \cap W^s(\mathcal{M}_\varepsilon^+)$ with $A_{0,*} = A_j$ to

leading order, exists and, by construction, that $\gamma_{0,*}^-(0) \in \{q = r = 0\}$.

By definition, the orbit $\gamma_{0,*}^-(\xi)$ for $\xi \in (a, b)$ spans a curve $\Gamma_{0,*}^-(a, b) \subset \mathbb{R}^6$, and there is a 3-dimensional tube $\mathcal{T}_{0,*}^- \subset W^u(P_\varepsilon^-)$ around $\Gamma_{0,*}^-(a, b)$ (for any $-\infty < a < b \leq \infty$) which consists of all orbits $\gamma^-(\xi; v_*, w_*) \subset W^u(P_\varepsilon^-)$ with $(v_*; w_*)$ so close to $(-A_{0,*}^2, w_*(-A_{0,*}^2))$ that

$$\sup_{\xi \leq -\frac{1}{2}\xi_{0,*}} \|\gamma^-(\xi; v_*, w_*) - \gamma_{0,*}^-(\xi)\| < e^{-\frac{1}{\sqrt{\varepsilon}}},$$

where $-\xi_{0,*} = -\xi_{\text{het},*}(v_*)$, the position of the jump mid-point of $\gamma_{0,*}^-(\xi)$. The existence of $\mathcal{T}_{0,*}^-$ follows from the continuous dependence on the initial conditions of solutions of smooth ODEs (as (2.2.1) clearly is); $\mathcal{T}_{0,*}^-$ defines an open neighborhood of $\Gamma_{0,*}^-(a, b)$ for any $-\infty < a < b \leq \infty$ in the relative topology of $W^u(P_\varepsilon^-)$. Note that $\mathcal{T}_{0,*}^-$ contains both orbits that jump away from $\mathcal{M}_\varepsilon^+$ $\mathcal{O}(\sqrt{\varepsilon})$ close to $\gamma_{0,*}^-(-\frac{1}{2}\xi_{0,*})$ – these are the orbits close to $\partial\mathcal{T}_{0,*}^-$ that only remain close to $\mathcal{M}_\varepsilon^+$ up to $\xi = -\frac{1}{2}\xi_{0,*} + \mathcal{O}(\varepsilon^{-1/2})$ – and orbits that are exponentially close to $\mathcal{M}_\varepsilon^+$ for arbitrarily long ‘time’ – the orbits that are close enough to $\gamma_{0,*}^-(\xi)$. Note also that the ‘secondary’ jump mid-points, *i.e.*, the points at which the orbits $\gamma^-(\xi; v_*, w_*)$ take off again from $\mathcal{M}_\varepsilon^+$, of all orbits in $\mathcal{T}_{0,*}^-$ must be exponentially close to the curve $\Gamma_{0,*}^-(-\frac{1}{2}\xi_{0,*}, \infty)$, that is itself exponentially close to $\mathcal{M}_\varepsilon^+$ and is approximated, or represented, by a part of a solution curve of (2.2.11) – compare to region 3 in Figure 2.4 in which the curve $\Gamma_{0,*}^-(-\xi_*, \xi_*)$ is approximated.

The tube $\mathcal{T}_{0,*}^-$ is stretched by the fast dynamics near $\mathcal{M}_\varepsilon^+$ into a 3-dimensional manifold that is no longer exponentially small in the direction of the fast unstable eigenvalue of $\mathcal{M}_\varepsilon^+$ – see Remark 2.2.2. In fact, $\mathcal{T}_{0,*}^-$ is exponentially close and parallel to $W^u(\mathcal{M}_\varepsilon^+)$. Since $W^u(\mathcal{M}_\varepsilon^+)$ intersects $W^s(\mathcal{M}_\varepsilon^-)$ transversely – which can be shown by the same Melnikov-type arguments that established the intersection of $W^u(\mathcal{M}_\varepsilon^-)$ and $W^s(\mathcal{M}_\varepsilon^+)$ – it follows that $\mathcal{T}_{0,*}^- \cap W^s(\mathcal{M}_\varepsilon^-)$ exists as a 2-dimensional submanifold of $\mathcal{T}_{0,*}^-$. We label this manifold as $\mathcal{S}_{0,*}^-$; it consists of a 1-parameter family of orbits $\gamma^-(\xi; v_*, w_*) \subset W^u(P_\varepsilon^-) \cap W^s(\mathcal{M}_\varepsilon^-)$, *i.e.*, orbits in $W^u(P_\varepsilon^-)$ that are homoclinic to $\mathcal{M}_\varepsilon^-$. Since $\mathcal{T}_{0,*}^-$ is exponentially close to $\gamma_{0,*}^-(\xi)$ for $\xi \leq -\frac{1}{2}\xi_{0,*}$, and since $\gamma_{0,*}^-(\xi)$ takes off from $\mathcal{M}_\varepsilon^-$ at $W_{\text{slow}}^u(P_\varepsilon^-)$, it follows by the reversibility symmetry (2.2.2) that the orbits in $\mathcal{S}_{0,*}^-$ touch down on $\mathcal{M}_\varepsilon^-$ close to $W_{\text{slow}}^s(P_\varepsilon^-)$, the slow stable manifold of P_ε^- in $\mathcal{M}_\varepsilon^-$ that is spanned by $l_{v,w}^{s,-}$.

The existence of the homoclinic orbit $\gamma_{h,j}^-(\xi)$ is established if it can be shown that there is an orbit $\gamma^-(\xi; v_*, w_*) \subset \mathcal{S}_{0,*}^-$ that indeed touches down exactly on $W_{\text{slow}}^s(P_\varepsilon^-)$. This result will follow from another application of the reversibility symmetry. The above construction of the 2-dimensional manifold $\mathcal{S}_{0,*}^- \subset W^u(P_\varepsilon^-) \cap W^s(\mathcal{M}_\varepsilon^-)$, that is based on the heteroclinic orbit $\gamma_{0,*}^-(\xi) \subset W^u(P_\varepsilon^-) \cap$

$W^s(\mathcal{M}_\varepsilon^+)$ and on the tube $\mathcal{T}_{0,*}^-$, has a symmetric counterpart in the 2-dimensional manifold $\mathcal{S}_{0,*}^+ \subset W^s(P_\varepsilon^-) \cap W^u(\mathcal{M}_\varepsilon^-)$, that is based on the heteroclinic orbit $\gamma_{0,*}^+(\xi) \subset W^s(P_\varepsilon^-) \cap W^u(\mathcal{M}_\varepsilon^+)$ and on the tube $\mathcal{T}_{0,*}^+$. Note that by construction all orbits in $\mathcal{S}_{0,*}^+$ touch down (or: take off in backward ‘time’) on $W_{\text{slow}}^s(P_\varepsilon^-) \subset \mathcal{M}_\varepsilon^-$. Thus, $\gamma_{h,j}^-(\xi)$ exists if it can be shown that $\mathcal{S}_{0,*}^-$ and $\mathcal{S}_{0,*}^+$ intersect.

To show this, we first note that

$$\mathcal{S}_{0,*}^- \cap \mathcal{S}_{0,*}^+ = \mathcal{T}_{0,*}^- \cap \mathcal{T}_{0,*}^+ \subset W^u(P_\varepsilon^-) \cap W^s(P_\varepsilon^-),$$

since orbits in $\mathcal{T}_{0,*}^-$ that are also in $\mathcal{T}_{0,*}^+ \subset W^s(P_\varepsilon^-) \subset W^s(\mathcal{M}_\varepsilon^-)$ must, by definition, lie inside $\mathcal{S}_{0,*}^-$. Moreover,

$$\dim(\mathcal{S}_{0,*}^- \cap \mathcal{S}_{0,*}^+) = \dim(\mathcal{T}_{0,*}^- \cap \mathcal{T}_{0,*}^+) = 1.$$

Since both $\mathcal{S}_{0,*}^\pm$ consist of solutions of (2.2.1), the dimension of $\mathcal{S}_{0,*}^- \cap \mathcal{S}_{0,*}^+$ cannot be zero, *i.e.*, $\mathcal{S}_{0,*}^- \cap \mathcal{S}_{0,*}^+$ cannot be a point. It also cannot be two, which would imply that the 2-dimensional sets $\mathcal{S}_{0,*}^\pm$ coincide. This is not the case, since $\mathcal{S}_{0,*}^\pm$ are, as subsets of $\mathcal{T}_{0,*}^\pm$, stretched like $\mathcal{T}_{0,*}^\pm$, thus $\mathcal{S}_{0,*}^-$ is parallel to $W^u(\mathcal{M}_\varepsilon^+)$ and $\mathcal{S}_{0,*}^+$ to $W^s(\mathcal{M}_\varepsilon^+)$. Hence, we may conclude that we have proved the existence of the (locally) uniquely determined homoclinic orbit $\gamma_{h,j}(\xi) \subset W^u(P_\varepsilon^-) \cap W^s(P_\varepsilon^-)$, if we have shown that $\mathcal{T}_{0,*}^-$ and $\mathcal{T}_{0,*}^+$ intersect.

This follows from the local stretching of the tubes $\mathcal{T}_{0,*}^-$ and $\mathcal{T}_{0,*}^+$ near $\mathcal{M}_\varepsilon^+$. To see this, we consider the curves $\Gamma_{0,*}^-(-\frac{1}{2}\xi_{0,*}, \frac{1}{2}\xi_{0,*})$ and $\Gamma_{0,*}^+(-\frac{1}{2}\xi_{0,*}, \frac{1}{2}\xi_{0,*})$ that are associated to $\gamma_{0,*}^-(\xi)$ and $\gamma_{0,*}^+(\xi)$ (note that $\gamma_{0,*}^+(\xi)$ jumps at $+\xi_{0,*}$ by (2.2.2)). By construction, $\Gamma_{0,*}^-(-\frac{1}{2}\xi_{0,*}, \frac{1}{2}\xi_{0,*})$ and $\Gamma_{0,*}^+(-\frac{1}{2}\xi_{0,*}, \frac{1}{2}\xi_{0,*})$ are exponentially close to each other and exponentially close to $\mathcal{M}_\varepsilon^+$. The tube $\mathcal{T}_{0,*}^-$ is stretched in the direction of the fast unstable eigenvalue of $\mathcal{M}_\varepsilon^+$ near $\Gamma_{0,*}^\pm(-\frac{1}{2}\xi_{0,*}, \frac{1}{2}\xi_{0,*})$ and is exponentially close to $W^u(\mathcal{M}_\varepsilon^+)$, while $\mathcal{T}_{0,*}^+$ is stretched in the direction of the fast stable eigenvalue of $\mathcal{M}_\varepsilon^+$ near $\Gamma_{0,*}^\pm(-\frac{1}{2}\xi_{0,*}, \frac{1}{2}\xi_{0,*})$ and is exponentially close to $W^s(\mathcal{M}_\varepsilon^+)$. Moreover, both 3-dimensional manifolds $\mathcal{T}_{0,*}^\pm$ extend to two sides – $\{u < 1\}$ and $\{u > 1\}$ – of $\mathcal{M}_\varepsilon^+$ near $\Gamma_{0,*}^\pm(-\frac{1}{2}\xi_{0,*}, \frac{1}{2}\xi_{0,*})$, since they both contain orbits that are asymptotic to $\mathcal{M}_\varepsilon^+$. Thus, $\mathcal{T}_{0,*}^-$ and $\mathcal{T}_{0,*}^+$ must have a nontrivial intersection. This completes the proof for $K > 0$.

Observe that the left hand side of (2.2.22) has at most one extremum for $A \in (0, 1)$, namely

$$A = \left(-\frac{\alpha D}{\beta} \right)^{-\frac{1}{2} \frac{D}{D-1}},$$

see (2.2.25). Therefore, K cannot be more than two.

Finally, we briefly consider the situation in which $K = 0$, *i.e.* in which there is no solution $A \in (0, 1)$ of (2.2.22). In this case, the critical heteroclinic orbits $\gamma_{0,*}^{\mp}(\xi)$ cannot be constructed, and it follows immediately that $W^u(P_{\varepsilon}^{-}) \cap W^s(P_{\varepsilon}^{-}) = \emptyset$. The saddle-node bifurcations occur at the transition from $K = 2$ to $K = 0$ and must be locally unique by the C^1 -smoothness with respect to ε of the stable and unstable manifolds of $\mathcal{M}_{\varepsilon}^{\pm}$ and P_{ε}^{\pm} [27, 28]. \square

Remark 2.2.2. In [40, 41], the stretching and squeezing associated to the passage of an invariant manifold along a slow manifold are described by the Exchange Lemma. This lemma can be used to study the deformation of $W^u(P_{\varepsilon}^{-})$ as it passes along $\mathcal{M}_{\varepsilon}^{+}$. Indeed, one may verify explicitly that the sets of touch down points of the tracked manifold on the slow manifolds are transverse to the flows on those manifolds. However, we have chosen for a somewhat more direct approach here.

2.2.5 Explicit analysis of the number K of stationary 1-pulse solutions

Theorem 2.2.1 above establishes that $K \leq 2$. In this section, we carry out a straightforward analysis of the jump condition (2.2.22) to derive explicit results for the number (K) of stationary 1-pulse solutions in (2.1.6) for a given set of parameters. The following lemma is an example; it is stated without proof.

Lemma 2.2.2. *Let (α, β, D) be such that $|\alpha D| > |\beta|$. Then, for $\varepsilon > 0$ small enough, and $\gamma_{c1, c2}$ as given in (2.2.24), we have*

- (a1) if $\text{sgn}(\alpha) = \text{sgn}(\beta)$, $\text{sgn}(\gamma) = \text{sgn}(\alpha)$, and $|\gamma| < |\alpha + \beta|$, then $K = 1$.
- (a2) if $\text{sgn}(\alpha) = \text{sgn}(\beta)$, $\text{sgn}(\gamma) = \text{sgn}(\alpha)$, and $|\gamma| > |\alpha + \beta|$, then $K = 0$.
- (a3) if $\text{sgn}(\alpha) = \text{sgn}(\beta)$ and $\text{sgn}(\gamma) \neq \text{sgn}(\alpha)$, then $K = 0$.
- (b1) if $\text{sgn}(\alpha) = -1 = -\text{sgn}(\beta)$, $\alpha + \beta > 0$, and $\text{sgn}(\gamma) = -1$, then $K = 0$.
- (b2) if $\text{sgn}(\alpha) = -1 = -\text{sgn}(\beta)$, $\alpha + \beta > 0$, and $0 < \gamma < \alpha + \beta$, then $K = 1$.
- (b3) if $\text{sgn}(\alpha) = -1 = -\text{sgn}(\beta)$, $\alpha + \beta > 0$, and $\alpha + \beta < \gamma < \gamma_{c1}$, then $K = 2$.
- (b4) if $\text{sgn}(\alpha) = -1 = -\text{sgn}(\beta)$, $\alpha + \beta > 0$, and $\gamma > \gamma_{c1}$, then $K = 0$.
- (c1) if $\text{sgn}(\alpha) = -1 = -\text{sgn}(\beta)$, $\alpha + \beta < 0$, and $\gamma < \alpha + \beta$, then $K = 0$.
- (c2) if $\text{sgn}(\alpha) = -1 = -\text{sgn}(\beta)$, $\alpha + \beta < 0$, and $\alpha + \beta < \gamma < 0$, then $K = 1$.
- (c3) if $\text{sgn}(\alpha) = -1 = -\text{sgn}(\beta)$, $\alpha + \beta < 0$, and $0 < \gamma < \gamma_{c1}$, then $K = 2$.
- (c4) if $\text{sgn}(\alpha) = -1 = -\text{sgn}(\beta)$, $\alpha + \beta < 0$, and $\gamma > \gamma_{c1}$, then $K = 0$.
- (d1) if $\text{sgn}(\alpha) = 1 = -\text{sgn}(\beta)$, $\alpha + \beta > 0$, and $\gamma < \gamma_{c2}$, then $K = 0$.
- (d2) if $\text{sgn}(\alpha) = 1 = -\text{sgn}(\beta)$, $\alpha + \beta > 0$, and $\gamma_{c2} < \gamma < 0$, then $K = 2$.
- (d3) if $\text{sgn}(\alpha) = 1 = -\text{sgn}(\beta)$, $\alpha + \beta > 0$, and $0 < \gamma < \alpha + \beta$, then $K = 1$.
- (d4) if $\text{sgn}(\alpha) = 1 = -\text{sgn}(\beta)$, $\alpha + \beta > 0$, and $\gamma > \alpha + \beta$, then $K = 0$.

- (e1) if $\text{sgn}(\alpha) = 1 = -\text{sgn}(\beta)$, $\alpha + \beta < 0$, and $\gamma < \gamma_{c2}$, then $K = 0$.
(e2) if $\text{sgn}(\alpha) = 1 = -\text{sgn}(\beta)$, $\alpha + \beta < 0$, and $\gamma_{c2} < \gamma < \alpha + \beta$, then $K = 2$.
(e3) if $\text{sgn}(\alpha) = 1 = -\text{sgn}(\beta)$, $\alpha + \beta < 0$, and $\alpha + \beta < \gamma < 0$, then $K = 1$.
(e4) if $\text{sgn}(\alpha) = 1 = -\text{sgn}(\beta)$, $\alpha + \beta < 0$, and $\gamma > 0$, then $K = 0$.

See also Figure 2.5, where we plotted (2.2.22) for certain parameter combinations. The left frame represents the cases (b1) – (b4), the right frame (d1) – (d4).

2.3 Traveling pulse solutions

In this section, we establish the existence of localized 1-pulse solutions to (2.1.6) that travel with a fixed, well-determined, speed. As in the previous section, we will construct these pulses as homoclinic orbits $\gamma_{tr,j}^-(\xi)$ to the critical point P_ε^- .

2.3.1 The formal construction of traveling 1-pulse solutions,

$$\gamma_{tr,j}^-(\xi)$$

We introduce the moving coordinates $\eta = x - \varepsilon^2 ct$ and, with a slight abuse of notation, set $\xi = \frac{\eta}{\varepsilon}$, so that (2.1.6) reduces to the 6-dimensional dynamical system,

$$\begin{cases} u_\xi &= p, \\ p_\xi &= -u + u^3 + \varepsilon(\alpha v + \beta w + \gamma - cp), \\ v_\xi &= \varepsilon q, \\ q_\xi &= \varepsilon(v - u) - \varepsilon^3 c\tau q, \\ w_\xi &= \frac{\varepsilon}{D} r, \\ r_\xi &= \frac{\varepsilon}{D}(w - u) - \frac{\varepsilon^3}{D^2} c\theta r, \end{cases} \quad (2.3.1)$$

with an additional parameter c for the speed of the traveling pulse. The structure of this equation justifies our choice for the magnitude of c ($= \mathcal{O}(\varepsilon^2)$). With this scaling, the perturbation of the fast (u, p) -subsystem induced by c is of the same order as the perturbations induced by the V, W -components in the U -equation of (2.1.6). Note that, unlike (2.2.1), (2.3.1) depends explicitly on the parameters τ and θ . However, the critical points of (2.3.1) are identical to those of (2.2.1) and, thus, given by (2.2.4).

The fast reduced system is identical to (2.2.5), as long as $\tau, \theta \ll \frac{1}{\varepsilon^3}$, and is thus again governed by the Hamiltonian $H(u, p)$ (2.2.6). For any c of $\mathcal{O}(1)$, system (2.3.1) possesses two invariant slow manifolds and their associated stable and unstable manifolds, which we denote, with a slight abuse of notation, by $\mathcal{M}_\varepsilon^\pm$ and $W^{s,u}(\mathcal{M}_\varepsilon^\pm)$. Although $\mathcal{M}_\varepsilon^\pm$ depend on c , the leading and first order approximations of $\mathcal{M}_\varepsilon^\pm$ are still given by (2.2.8) and (2.2.9), so that it again follows that $H(u, p)|_{\mathcal{M}_\varepsilon^\pm} = \mathcal{O}(\varepsilon^2)$ (2.2.16).

However, there are two significant differences between (2.3.1) and (2.2.1). First, (2.3.1) does not have the reversibility symmetry of (2.2.1) for $c \neq 0$. As a consequence, we cannot expect to find symmetric pulses and, more importantly, we cannot exploit the symmetry in the construction of the pulse and in the associated validity proof. However, system (2.3.1) does inherit the symmetry,

$$(\xi, p, q, r, c) \rightarrow (-\xi, -p, -q, -r, -c), \quad (2.3.2)$$

which implies that the traveling pulses do not have a preferred direction, *i.e.*, to any pulse traveling with speed $c > 0$, there is a symmetrical counterpart that travels with speed $c < 0$. Second,

$$\frac{d}{d\xi} H(u(\xi), p(\xi)) = \varepsilon p(\alpha v + \beta w + \gamma - cp), \quad (2.3.3)$$

instead of (2.2.14), which implies that the Melnikov conditions will depend in an $\mathcal{O}(1)$ fashion on c – which also further validates our scaling of the magnitude of the speed of the pulses.

As in section 2.2.2, we define the position of the jump mid-points of $\gamma_{tr,j}^-(\xi)$ to be $\mp\xi_*$, *i.e.*, $\gamma_{tr,j}^-(\xi)$ crosses the hyperplane $\{u = 0\}$ at $\xi = \mp\xi_*$ ($\xi_* > 0$). The coordinates of the jump mid-points are defined by

$$\gamma_{tr,j}^-(\mp\xi_*) = (0, p_*^\mp, v_*^\mp, q_*^\mp, w_*^\mp, r_*^\mp). \quad (2.3.4)$$

Unlike the symmetric stationary case, the coordinates of the jump through the fast field from $\mathcal{M}_\varepsilon^-$ to $\mathcal{M}_\varepsilon^+$, denoted by $(p_*^-, v_*^-, q_*^-, w_*^-, r_*^-)$, will differ from those of the jump back from $\mathcal{M}_\varepsilon^+$ to $\mathcal{M}_\varepsilon^-$, denoted by $(p_*^+, v_*^+, q_*^+, w_*^+, r_*^+)$. Moreover, the middle of the pulse, $\gamma_{tr,j}^-(0)$, has become slightly artificial by this definition, in the sense that $\xi = 0$ does not in general correspond to an extremum of any of the U -, V - or W -components in (2.1.6). Nevertheless, with this definition we can use the same partition of the homoclinic orbit $\gamma_{tr,j}^-(\xi)$ into five regions – see Section 2.2.2 – with $I_{f,s}^\mp$ and I_s^0 as in (2.2.13).

We again use the Melnikov function to measure the distance between $W^u(\mathcal{M}_\varepsilon^-)$ and $W^s(\mathcal{M}_\varepsilon^+)$. We find, assuming that $\xi_* = \mathcal{O}(\frac{1}{\varepsilon})$,

$$\begin{aligned} \Delta_f^- H(v_*^-, q_*^-, w_*^-, r_*^-) &= \int_{I_f^-} H_\xi d\xi \\ &= \int_{I_f^-} \varepsilon p_h^{0,-}(\xi + \xi_*) \left(\alpha v_*^- + \beta w_*^- + \gamma \right. \\ &\quad \left. - c p_h^{0,-}(\xi + \xi_*) \right) d\xi + \mathcal{O}(\varepsilon\sqrt{\varepsilon}) \\ &= 2\varepsilon \left(\alpha v_*^- + \beta w_*^- + \gamma - \frac{1}{3}\sqrt{2}c \right) + \mathcal{O}(\varepsilon\sqrt{\varepsilon}), \end{aligned}$$

where we have implicitly used that the slow coordinates (v, p, w, r) do not vary to leading order during a jump through the fast field, *i.e.*, that

$$\Delta_f^\mp v, \Delta_f^\mp p, \Delta_f^\mp w, \Delta_f^\mp r = \mathcal{O}(\sqrt{\varepsilon}) \quad (2.3.5)$$

(see 2.2.15)). Since $H(u, p)|_{\mathcal{M}_\varepsilon^\mp} = \mathcal{O}(\varepsilon^2)$, we find as the first Melnikov condition,

$$\alpha v_*^- + \beta w_*^- + \gamma = \frac{1}{3}\sqrt{2}c. \quad (2.3.6)$$

Since there is no reversibility symmetry, the second Melnikov condition for the jump from $\mathcal{M}_\varepsilon^+$ to $\mathcal{M}_\varepsilon^-$ is slightly different,

$$\alpha v_*^+ + \beta w_*^+ + \gamma = -\frac{1}{3}\sqrt{2}c, \quad (2.3.7)$$

which follows from

$$\begin{aligned} \Delta_f^+ H(v_*^+, q_*^+, w_*^+, r_*^+) &= \int_{I_f^+} H_\xi d\xi \\ &= \int_{I_f^+} \varepsilon p_h^{0,+}(\xi - \xi_*) \left(\alpha v_*^+ + \beta w_*^+ + \gamma \right. \\ &\quad \left. - c p_h^{0,+}(\xi - \xi_*) \right) d\xi + \mathcal{O}(\varepsilon\sqrt{\varepsilon}) \\ &= 2\varepsilon \left(\alpha v_*^+ + \beta w_*^+ + \gamma + \frac{1}{3}\sqrt{2}c \right) + \mathcal{O}(\varepsilon\sqrt{\varepsilon}) \end{aligned}$$

(compare $p_h^{0,+}(\xi)$ to $p_h^{0,-}(\xi) - (2.2.7)$). Note that the jump conditions are consistent with the symmetry (2.3.2).

We can proceed (formally) as in the stationary case. We solve the (linear) slow subsystems explicitly, imposing boundary conditions like those in (2.2.18) at the boundaries of the three slow regions (1, 3, and 5) and also imposing the Melnikov conditions (2.3.6) and (2.3.7). Here, we present this analysis for the critical case $\tau, \theta = \mathcal{O}(\frac{1}{\varepsilon^2})$, since traveling pulses can only exist for these values of τ and θ . More precisely, if both $\tau, \theta \ll \frac{1}{\varepsilon^2}$, then the flows on $\mathcal{M}_\varepsilon^\pm$ are symmetric to leading order and the only asymmetries in the construction of $\gamma_{tr,j}^\pm(\xi)$ are introduced by the c 's in the Melnikov conditions (2.3.6) and (2.3.7). From this, it follows that $c = 0$, *i.e.*, that $\gamma_{tr,j}^-(\xi) = \gamma_{h,j}^-(\xi)$, the stationary pulse – see Remark 2.3.1.

Thus, we introduce $\hat{\tau}$ and $\hat{\theta}$ by

$$\hat{\tau} = \varepsilon^2 \tau \ll \frac{1}{\varepsilon}, \quad \hat{\theta} = \varepsilon^2 \theta \ll \frac{1}{\varepsilon}.$$

The flows on $\mathcal{M}_\varepsilon^-$ and $\mathcal{M}_\varepsilon^+$ are, up to correction terms of $\mathcal{O}(\varepsilon^3)$, given by

$$\begin{cases} v_{\xi\xi} = -\varepsilon c \hat{\tau} v_\xi + \varepsilon^2(v+1), \\ w_{\xi\xi} = -\varepsilon c \frac{\hat{\theta}}{D^2} w_\xi + \frac{\varepsilon^2}{D^2}(w+1), \end{cases} \quad \text{and} \quad \begin{cases} v_{\xi\xi} = -\varepsilon c \hat{\tau} v_\xi + \varepsilon^2(v-1), \\ w_{\xi\xi} = -\varepsilon c \frac{\hat{\theta}}{D^2} w_\xi + \frac{\varepsilon^2}{D^2}(w-1), \end{cases}$$

see Figure 2.6. The eigenvalues $\lambda_{v,w}^\pm$ of the to leading order decoupled (v, q) - and (w, r) -subsystems are given by

$$\lambda_v^\pm = \frac{1}{2}(-c\hat{\tau} \pm \sqrt{c^2\hat{\tau}^2 + 4}), \quad \lambda_w^\pm = \frac{1}{2} \frac{1}{D} \left(-\frac{c\hat{\theta}}{D} \pm \sqrt{\frac{c^2\hat{\theta}^2}{D^2} + 4} \right), \quad (2.3.8)$$

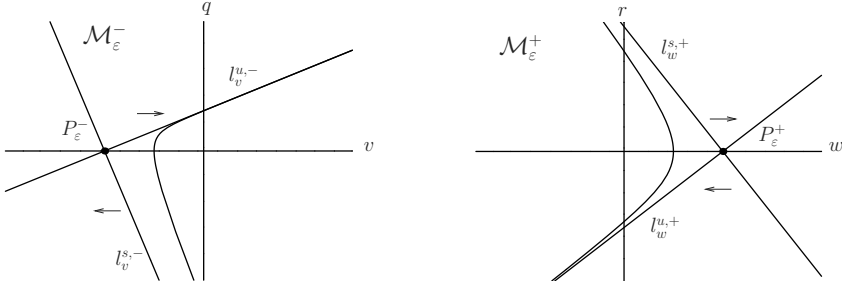


Figure 2.6: The asymmetric slow flows for the (v, q) -subsystem on $\mathcal{M}_\varepsilon^-$ (left) and the (w, r) -subsystem on $\mathcal{M}_\varepsilon^+$ (right) for c positive.

which clearly establishes the asymmetric character of the flows on $\mathcal{M}_\varepsilon^\pm$ (for $\hat{\tau}, \hat{\theta} \neq 0$). The stable and unstable manifolds of P_ε^\pm restricted to $\mathcal{M}_\varepsilon^\pm$ are spanned by

$$\begin{aligned} l_v^{s,\pm} &= \{q = \lambda_v^\mp(\mp 1 + v)\}, & l_w^{s,\pm} &= \{r = D\lambda_w^\mp(\mp 1 + w)\}, \\ l_v^{u,\pm} &= \{q = \lambda_v^\pm(\mp 1 + v)\}, & l_w^{u,\pm} &= \{r = D\lambda_w^\pm(\mp 1 + w)\}, \end{aligned} \quad (2.3.9)$$

(compare with (2.2.12)).

Since the slow (v, q, w, r) -coordinates do not vary to leading order during a jump through the fast field (2.3.5), we can ‘match’ the solutions in the slow regions 1, 3, and 5 by imposing boundary conditions as in (2.2.18). As in the stationary case, there are more boundary conditions than free parameters. Hence, there are relations between the coordinates of the jump mid-points,

$$(v_*^-, q_*^-) \in l_v^{u,-}, (w_*^-, r_*^-) \in l_w^{u,-}, (v_*^+, q_*^+) \in l_v^{s,-}, (w_*^+, r_*^+) \in l_w^{s,-}, \quad (2.3.10)$$

as may be seen from the system geometry (see Figure 2.7). Furthermore,

$$v_*^\pm = s_v^\pm \left(e^{\pm 2\varepsilon \lambda_v^\mp \xi_*} - 1 \right) - 1, \quad w_*^\pm = s_w^\pm \left(e^{\pm 2\varepsilon \lambda_w^\mp \xi_*} - 1 \right) - 1, \quad (2.3.11)$$

with

$$s_v^\pm = -\frac{2\lambda_v^\pm}{\lambda_v^\pm - \lambda_v^\mp} < 0, \quad s_w^\pm = -\frac{2\lambda_w^\pm}{\lambda_w^\pm - \lambda_w^\mp} < 0. \quad (2.3.12)$$

(Note that (2.3.10) and (2.3.11) reduce to their stationary equivalents (2.2.19) and (2.2.20) if either $c = 0$ or $\hat{\tau} = \hat{\theta} = 0$ – see Remark 2.3.1.) We conclude that for any given pair (c, ξ_*) , the (slow) coordinates $(v_*^\mp, q_*^\mp, w_*^\mp, r_*^\mp)$ of the jump mid-points are uniquely determined by the above conditions combined with the matching conditions (2.3.5). Moreover, we have the following leading order approximations

of the v - and w -components of $\gamma_{tr,j}^-(\xi)$ in the slow regions (1, 3, 5),

$$v_{tr} = \begin{cases} -2s_v^- e^{\varepsilon\lambda_v^+ \xi} \sinh \varepsilon\lambda_v^+ \xi_* - 1 & \text{in 1,} \\ s_v^- e^{\varepsilon\lambda_v^+ (\xi - \xi_*)} + s_v^+ e^{\varepsilon\lambda_v^- (\xi + \xi_*)} + 1 & \text{in 3,} \\ 2s_v^+ e^{\varepsilon\lambda_v^- \xi} \sinh \varepsilon\lambda_v^- \xi_* - 1 & \text{in 5,} \end{cases}$$

$$w_{tr} = \begin{cases} -2s_w^- e^{\varepsilon\lambda_w^+ \xi} \sinh \varepsilon\lambda_w^+ \xi_* - 1 & \text{in 1,} \\ s_w^- e^{\varepsilon\lambda_w^+ (\xi - \xi_*)} + s_w^+ e^{\varepsilon\lambda_w^- (\xi + \xi_*)} + 1 & \text{in 3,} \\ 2s_w^+ e^{\varepsilon\lambda_w^- \xi} \sinh \varepsilon\lambda_w^- \xi_* - 1 & \text{in 5,} \end{cases}$$

see Figure 2.7. The Melnikov conditions (2.3.6) and (2.3.7) impose two relations between c and ξ_* ,

$$\begin{cases} \frac{1}{3}\sqrt{2}c = \alpha \left(s_v^- \left(e^{-2\varepsilon\lambda_v^+ \xi_*} - 1 \right) - 1 \right) + \beta \left(s_w^- \left(e^{-2\varepsilon\lambda_w^+ \xi_*} - 1 \right) - 1 \right) + \gamma, \\ -\frac{1}{3}\sqrt{2}c = \alpha \left(s_v^+ \left(e^{2\varepsilon\lambda_v^- \xi_*} - 1 \right) - 1 \right) + \beta \left(s_w^+ \left(e^{2\varepsilon\lambda_w^- \xi_*} - 1 \right) - 1 \right) + \gamma. \end{cases} \quad (2.3.13)$$

A pair of solutions (c, ξ_*) to (2.3.13) with $c \neq 0$ corresponds formally to a homoclinic solution $\gamma_{tr,j}^-(\xi)$ of (2.3.1) and thus to a pulse solution of (2.1.6) that travels with speed $\varepsilon^2 c$.

Remark 2.3.1. If $\tau, \theta \ll \frac{1}{\varepsilon^2}$, *i.e.*, if $\hat{\tau}, \hat{\theta} = 0$ to leading order, then $\lambda_v^\pm = \pm 1$, $\lambda_w^\pm = \pm \frac{1}{D}$, and $s_v^\pm = s_w^\pm = -1$, so that (2.3.13) reduces to

$$-\frac{1}{3}\sqrt{2}c = \alpha A^2 + \beta A^{\frac{2}{D}} - \gamma = \frac{1}{3}\sqrt{2}c,$$

to leading order, with A as in (2.2.20). Hence, $c = 0$ and $\gamma_{tr,j}^-(\xi) = \gamma_{h,j}^-(\xi)$ (2.2.22).

2.3.2 Existence theorem for traveling pulse solutions

Theorem 2.3.1. *Let $(\alpha, \beta, \gamma, D, \tau, \theta)$ be such that $\tau = \frac{\hat{\tau}}{\varepsilon^2}$, $\theta = \frac{\hat{\theta}}{\varepsilon^2}$, and assume that (2.3.13) has K solution pairs $(c_j, (\xi_*)_j)$ with $c_j \neq 0$. Let $\varepsilon > 0$ be small enough. If $K = 0$, then there are no homoclinic orbits to P_ε^- in (2.3.1) with $c \neq 0$. If $K > 0$, there are K homoclinic orbits $\gamma_{tr,j}^-(\xi)$, $j \in \{1, \dots, K\}$, to P_ε^- in (2.3.1) that have a structure as sketched in Figure 2.7 and that correspond to traveling 1-pulse solutions of (2.1.6) which travel with speed $\varepsilon^2 c_j^* \neq 0$, where $c_j^* = c_j^*(\varepsilon) = c_j + \mathcal{O}(\varepsilon)$.*

The proof of Theorem 2.3.1 is similar to that of Theorem 2.2.1 in Section 2.2.4. Nevertheless, there are differences, especially since the proof of Theorem 2.2.1 strongly depended on the reversibility symmetry in (2.2.1). The proof is given in Section 2.3.3.

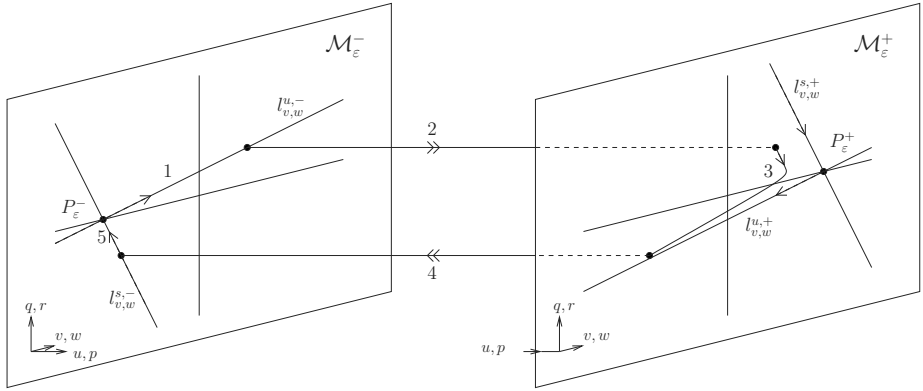


Figure 2.7: A schematic sketch of a traveling pulse $\gamma_{tr,j}^-(\xi)$ homoclinic to P_ϵ^- .

Generically, K can be expected to be positive for open regions in the $(\alpha, \beta, \gamma, D, \hat{\tau}, \hat{\theta})$ -parameter space. However, *a priori*, it is not clear whether parameter combinations exist for which K can be nonzero. In fact, though (2.3.13) is a relatively simple expression, it can – of course – not be solved explicitly. Nevertheless, it can be evaluated, and the (open) region in parameter space in which $K \neq 0$ can be determined with a simple and reliable numerical procedure. Moreover, (2.3.13) can be approximated asymptotically in various limit settings. As an example, we consider the case

$$\hat{\tau} = \frac{1}{\delta} \gg 1, \quad \hat{\theta} = h\delta \ll 1,$$

i.e., we assume that $\hat{\tau}$ is large and $\hat{\theta}$ is small, but both still $\mathcal{O}(1)$ with respect to ϵ . We thus introduce an artificial second asymptotic parameter δ that is independent of ϵ such that $0 < \epsilon \ll \delta \ll 1$. We further assume that all other parameters, including h , are $\mathcal{O}(1)$ with respect to δ . We search for solutions (c, ξ_*) of (2.3.13) such that

$$c > 0, \quad c = \mathcal{O}(1), \quad X_* = \epsilon\delta\xi_* = \mathcal{O}(1),$$

with respect to δ . Note that this implies that we look for homoclinic orbits that spend a long ‘time’ ($\mathcal{O}(\frac{1}{\epsilon\delta})$) near \mathcal{M}_ϵ^+ . It follows by a straightforward computation from (2.3.11) that,

$$\begin{aligned} v_*^- &= -2e^{2\frac{X_*}{c}(1+\mathcal{O}(\delta))} + 1 + \mathcal{O}(\delta), & v_*^+ &= -1 + \mathcal{O}(\delta), \\ w_*^- &= \mathcal{O}(\delta), & w_*^+ &= \mathcal{O}(\delta), \end{aligned} \quad (2.3.14)$$

so that (2.3.13) reduces to

$$\frac{1}{3}\sqrt{2}c = \alpha v_*^- + \gamma + \mathcal{O}(\delta), \quad -\frac{1}{3}\sqrt{2}c = -\alpha + \gamma + \mathcal{O}(\delta).$$

Hence, there exists a homoclinic orbit $\gamma_{tr,1}^-(\xi)$ to P_ε^- in (2.3.1) for $\alpha > \gamma$ with

$$c = c_1 = \frac{3}{2}\sqrt{2}(\alpha - \gamma) + \mathcal{O}(\delta, \varepsilon). \quad (2.3.15)$$

Moreover, $X_{*,1}$, and thus $(\xi_*)_1$, can be determined through v_*^- and (2.3.14). By the symmetry (2.3.2), we conclude that $K = 2$ for $\hat{\tau} \gg 1$, $\hat{\theta} \ll 1$ and $\alpha > \gamma$.

2.3.3 Proof of Theorem 2.3.1

The construction of

$$\gamma_{tr,j}^-(\xi) \subset W^u(P_\varepsilon^-) \cap W^s(P_\varepsilon^-) \subset W^u(P_\varepsilon^-) \cap W^s(\mathcal{M}_\varepsilon^-)$$

is again based on a special heteroclinic orbit $\gamma_{*,*}^-(\xi) \subset W^u(P_\varepsilon^-) \cap W^s(\mathcal{M}_\varepsilon^+)$, a tube $\mathcal{T}_{*,*}^- \subset W^u(P_\varepsilon^-)$ around it, their counterparts in backwards ‘time’ $\gamma_{*,*}^+(\xi) \subset W^s(P_\varepsilon^-) \cap W^u(\mathcal{M}_\varepsilon^+)$ and $\mathcal{T}_{*,*}^+ \subset W^s(P_\varepsilon^-)$, so that $\gamma_{tr,j}^-(\xi) \subset \mathcal{T}_{*,*}^- \cap \mathcal{T}_{*,*}^+$.

For any $c > 0$ (fixed), $W^u(P_\varepsilon^-)$ is represented by the 2-parameter family of orbits $\gamma_{\bar{P}}^-(\xi; v_*^-, w_*^-) \subset W^u(P_\varepsilon^-)$. We know by the Melnikov analysis that there is a 1-parameter subfamily of orbits $\gamma_{\text{het}}^-(\xi; v_*^-) = \gamma_{\bar{P}}^-(\xi; v_*^-; w_*^-(v_*^-)) \subset W^u(P_\varepsilon^-) \cap W^s(\mathcal{M}_\varepsilon^+)$, with $w_*^-(v_*^-)$ determined by (2.3.6). The orbits $\gamma_{\text{het}}^-(\xi; v_*^-)$ follow the slow flow on $\mathcal{M}_\varepsilon^+$, and it can be checked that those with $v_*^- \in (-1, S_v^-)$ again cross the $\{q = 0\}$ -hyperplane. Here, S_v^- is determined by the observation that $(v_*^-, q_*^-) \in l_{v_*^-}^{u,-}$ in the (v, q) -subsystem on $\mathcal{M}_\varepsilon^-$ (2.3.10), while (v_*^-, q_*^-) must be to the left of $l_{v_*^-}^{s,+}$ in the (v, q) -subsystem on $\mathcal{M}_\varepsilon^+$ so that $\gamma_{\text{het}}^-(\xi; v_*^-)$ may cross through $\{q = 0\}$; a similar condition must hold for $(w_*^-(v_*^-), r_*^-)$ in the (w, r) -subflows on $\mathcal{M}_\varepsilon^\mp$ – see Figure 2.7. For each $v_*^- \in (-1, S_v^-)$ the intersection of $\gamma_{\text{het}}^-(\xi; v_*^-)$ with $\{q = 0\}$ occurs by definition at $\xi = \xi_{\text{het}}^-(v_*^-) \in (-\xi_*, \xi_*)$, and these intersections define a 1-dimensional curve denoted by

$$\begin{aligned} Z^- &= \{(u^-(v_*^-), p^-(v_*^-), v^-(v_*^-), 0, w^-(v_*^-), r^-(v_*^-)) \\ &= \gamma_{\text{het}}^-(\xi_{\text{het}}^-; v_*^-) : v_*^- \in (-1, S_v^-)\}, \end{aligned} \quad (2.3.16)$$

see Figure 2.8, where one point on Z^- is illustrated, since v_*^- is fixed in the figure. The curve Z^- is by construction exponentially close to $\mathcal{M}_\varepsilon^+$, and its projection on $\mathcal{M}_\varepsilon^+$ is given by

$$Z_{\text{slow}}^- = \{(1 + \varepsilon u_1^+(v^-, 0, w^-, r^-), p_1^+(v^-, 0, w^-, r^-), v^-, 0, w^-, r^-) : v_*^- \in (-1, S_v^-)\},$$

see (2.2.8).

We perform the same construction in backwards (spatial) time and define the 1-parameter family of orbits $\gamma_{\text{het}}^+(\xi; v_*^+) \in W^s(P_\varepsilon^-) \cap W^u(\mathcal{M}_\varepsilon^+)$ by (2.3.7), the 1-dimensional curve $Z^+ = \{(u^+(v_*^+), p^+(v_*^+), v^+(v_*^+), 0, w^+(v_*^+), r^+(v_*^+))\} \subset \{q = 0\}$, and its projection Z_{slow}^+ on $\mathcal{M}_\varepsilon^+$. The (w, r) -components of Z_{slow}^\pm define two

curves, that typically intersect, *i.e.*, the condition $(w^-(v_*^-), r^-(v_*^-)) = (w^+(v_*^+), r^+(v_*^+))$ determines for each given c a discrete number of critical values $(v_{*,*}^-(c), v_{*,*}^+(c))$. However, for general c , the 1-dimensional curves Z_{slow}^- and Z_{slow}^+ do not intersect within the 3-dimensional manifold $\mathcal{M}_\varepsilon^+$, *i.e.*, $v^-(v_{*,*}^-(c)) \neq v^+(v_{*,*}^+(c))$ in general. Nevertheless, the combined condition,

$$(v^-(v_*^-(c)), w^-(v_*^-(c)), r^-(v_*^-(c))) = (v^+(v_*^+(c)), w^+(v_*^+(c)), r^+(v_*^+(c))), \quad (2.3.17)$$

in principle determines discrete critical values c_j of c for which Z_{slow}^- and Z_{slow}^+ intersect (transversely) in $\mathcal{M}_\varepsilon^+$. It is a matter of straightforward calculations to show that (2.3.17) is equivalent to (2.3.13).

The present construction is computationally more cumbersome than that of section 2.3.1, but its character is more geometrical and it can thus be more easily extended into a validity proof. To do so, we define (for any c) the special heteroclinic orbits $\gamma_{*,*}^-(\xi; c) = \gamma_{\text{het}}^-(\xi; v_{*,*}^-) \subset W^u(P_\varepsilon^-) \cap W^s(\mathcal{M}_\varepsilon^+)$ and $\gamma_{*,*}^+(\xi; c) = \gamma_{\text{het}}^+(\xi; v_{*,*}^+) \subset W^s(P_\varepsilon^-) \cap W^u(\mathcal{M}_\varepsilon^+)$. The tube $\mathcal{T}_{*,*}^-(c) \subset W^u(P_\varepsilon^-)$ is spanned by those orbits $\gamma_P^-(\xi; v_*^-, w_*^-) \subset W^u(P_\varepsilon^-)$ that are exponentially close to $\gamma_{*,*}^-(\xi; c)$ for $\xi < \frac{1}{2}(-\xi_* + \xi_{\text{het}}^-(v_{*,*}^-))$. Likewise, the tube $\mathcal{T}_{*,*}^+(c) \subset W^s(P_\varepsilon^-)$ is spanned by those orbits $\gamma_P^+(\xi; v_*^-, w_*^-) \subset W^s(P_\varepsilon^-)$ that are exponentially close to $\gamma_{*,*}^+(\xi; c)$ for $\xi > \frac{1}{2}(\xi_* + \xi_{\text{het}}^+(v_{*,*}^+))$. In forwards ‘time’, $\mathcal{T}_{*,*}^-(c)$ is stretched along $W^u(\mathcal{M}_\varepsilon^+)$, while $\mathcal{T}_{*,*}^+(c)$ is stretched along $W^s(\mathcal{M}_\varepsilon^+)$ in backwards ‘time’. By construction, the (stretched) tubes intersect the 5-dimensional hyperplane $\{q = 0\}$ in 2-dimensional manifolds, $Z_{\mathcal{T}}^\pm(c)$ (by definition).

The theorem is proved if it can be established that there are nonzero values of c for which $Z_{\mathcal{T}}^-(c) \cap Z_{\mathcal{T}}^+(c) \neq \emptyset$, since each point in this intersection determines a point in $W^u(P_\varepsilon^-) \cap W^s(P_\varepsilon^-) \cap \{q = 0\}$.

To show this, we extend $\{q = 0\}$ to a 6-dimensional space, denoted by $\{\{q = 0\}, c\}$, by adding c as an independent variable. This space contains the extended manifolds $\{Z_{\mathcal{T}}^-(c), c\}$ and $\{Z_{\mathcal{T}}^+(c), c\}$ as 3-dimensional subsets. Since $\gamma_{*,*}^-(\xi; c)$ and $\gamma_{*,*}^+(\xi; c)$ are exponentially close to $\mathcal{M}_\varepsilon^+$ as they intersect $\{q = 0\}$, and since the projections Z_{slow}^- and Z_{slow}^+ intersect by construction near $c = c_j$ determined by (2.3.13), it follows that $\{Z_{\mathcal{T}}^-(c), c\}$ and $\{Z_{\mathcal{T}}^+(c), c\}$ are exponentially close for c near c_j . As in the proof of Theorem 2.2.1, it now follows from the fact that $\mathcal{T}_{*,*}^-(c)$ is stretched along $W^u(\mathcal{M}_\varepsilon^+)$ and $\mathcal{T}_{*,*}^+(c)$ along $W^s(\mathcal{M}_\varepsilon^+)$, that – in the 6-dimensional space $\{\{q = 0\}, c\}$ – the 3-dimensional manifolds $\{Z_{\mathcal{T}}^-(c), c\}$ and $\{Z_{\mathcal{T}}^+(c), c\}$ must intersect transversely in discrete points that have c -coordinates $c_j^*(\varepsilon)$, which are to leading order determined by (2.3.13) or (2.3.17). Hence, $Z_{\mathcal{T}}^-(c) \cap Z_{\mathcal{T}}^+(c) = \gamma_{\text{tr},j}^-(\xi) \cap \{q = 0\} \neq \emptyset$ at $c_j^*(\varepsilon) = c_j + \mathcal{O}(\varepsilon)$. \square

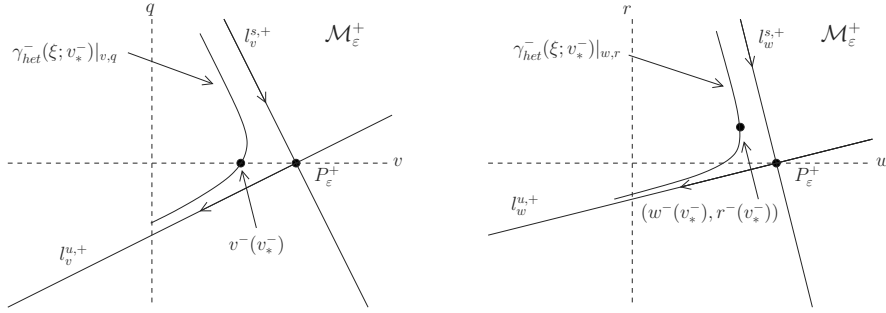


Figure 2.8: Example of the construction of $v^-(v_*^-)$, $w^-(v_*^-)$, and $r^-(v_*^-)$.

2.4 Bifurcation from stationary to traveling pulse solutions

2.4.1 Leading order analysis

To investigate the nature of the bifurcation from stationary 1-pulse solutions to traveling 1-pulse solutions, we start by considering the traveling pulse just after ‘creation’, that is, we set

$$c = \delta, \quad (2.4.1)$$

with $0 < \varepsilon \ll \delta \ll 1$ (so c is no longer an unknown anymore). We expand the three unknowns, $\hat{\tau} = \hat{\tau}_{*,0} + \mathcal{O}(\delta)$, $\hat{\theta} = \hat{\theta}_{*,0} + \mathcal{O}(\delta)$, $\xi_* = \xi_{*,0} + \delta\xi_{*,1} + \mathcal{O}(\delta^2)$. Notice that $\hat{\tau}_{*,0}$ and $\hat{\theta}_{*,0}$ determine the bifurcation values of $\hat{\tau}$ and $\hat{\theta}$ at which the bifurcation occurs, since the speed of the bifurcating traveling pulse reduces to zero at $\hat{\tau} = \hat{\tau}_{*,0}$ and $\hat{\theta} = \hat{\theta}_{*,0}$. Since the bifurcation is co-dimension one we expect to find a relation between $\hat{\tau}_{*,0}$ and $\hat{\theta}_{*,0}$.

The eigenvalues (2.3.8) and (2.3.12) become

$$\begin{aligned} \lambda_v^\pm &= \pm 1 - \frac{1}{2}\hat{\tau}_{*,0}\delta + \mathcal{O}(\delta^2), & \lambda_w^\pm &= \pm \frac{1}{D} - \frac{1}{2}\frac{\hat{\theta}_{*,0}}{D^2}\delta + \mathcal{O}(\delta^2), \\ s_v^\pm &= -1 \pm \frac{1}{2}\hat{\tau}_{*,0}\delta + \mathcal{O}(\delta^2), & s_w^\pm &= -1 \pm \frac{1}{2}\frac{\hat{\theta}_{*,0}}{D}\delta + \mathcal{O}(\delta^2). \end{aligned}$$

We also expand the four equalities in (2.3.11), using $A_0 := e^{-\varepsilon\xi_{*,0}}$,

$$\begin{aligned} v_*^\pm &= -A_0^2 \mp \hat{\tau}_{*,0}\delta \left(\frac{1}{2} - \frac{1}{2}A_0^2 + A_0^2 \log A_0 \right) + 2\varepsilon\xi_{*,1}A_0^2\delta + \mathcal{O}(\delta^2), \\ w_*^\pm &= -A_0^{\frac{2}{D}} \mp \frac{\hat{\theta}_{*,0}}{D}\delta \left(\frac{1}{2} - \frac{1}{2}A_0^{\frac{2}{D}} + \frac{1}{D}A_0^{\frac{2}{D}} \log A_0 \right) + 2\frac{\varepsilon}{D}\xi_{*,1}A_0^{\frac{2}{D}}\delta + \mathcal{O}(\delta^2). \end{aligned}$$

Next, we substitute the above expansions into the jump condition (2.3.13), and we recall that $c = \delta$, to obtain

$$\begin{cases} \gamma = \alpha A_0^2 + \beta A_0^{\frac{2}{D}} & (\text{twice}), \\ 0 = 4\varepsilon \xi_{*,1} \left(\alpha A_0^2 + \frac{\beta}{D} A_0^{\frac{2}{D}} \right), \\ \frac{1}{3}\sqrt{2} = \alpha \hat{\tau}_{*,0} \left(\frac{1}{2} - \frac{1}{2} A_0^2 + A_0^2 \log A_0 \right) + \frac{\beta \hat{\theta}_{*,0}}{D} \left(\frac{1}{2} - \frac{1}{2} A_0^{\frac{2}{D}} + \frac{1}{D} A_0^{\frac{2}{D}} \log A_0 \right), \end{cases} \quad (2.4.2)$$

where we equated coefficients on $\mathcal{O}(1)$ and $\mathcal{O}(\delta)$ terms, respectively, and added and subtracted the two $\mathcal{O}(\delta)$ equations. Note that the equation for A_0 is identical to that of the stationary 1-pulse orbit (2.2.22): near the bifurcation the width of the traveling pulse is to leading order equal to that of the stationary pulse. Equations (2.4.2) determine the three unknowns A_0 (which gives $\xi_{*,0}$), $\hat{\tau}_{*,0}$ as function of $\hat{\theta}_{*,0}$, and $\xi_{*,1} = 0$. The solution $\hat{\tau}_{*,0}$ as function of $\hat{\theta}_{*,0}$, is plotted in Figure 2.9 for several values of D .

Remark 2.4.1. We briefly consider the case of D large, *i.e.*, $D = \mathcal{O}(\frac{1}{\delta})$. It immediately follows from (2.4.2) that $\xi_{*,0} = -\frac{1}{2} \frac{1}{\varepsilon} \log \left(\frac{\gamma - \beta}{\alpha} \right)$. (Here, we also have to assume that $\gamma > \beta, \alpha > 0$ or that $\gamma < \beta, \alpha < 0$). Moreover,

$$\hat{\tau}_{*,0}(\hat{\theta}) = \frac{2}{3} \sqrt{2} \left(\alpha - (\gamma - \beta) + (\gamma - \beta) \log \left(\frac{\gamma - \beta}{\alpha} \right) \right)^{-1} + \mathcal{O}(\delta).$$

This $\hat{\tau}_{*,0}$ is analogous to the $(\hat{\tau}_2)_{*,0}$ we find in the analysis for traveling pulses of the reduced two-component system (2.6.1) – see Section 2.6.

2.4.2 Subcriticality and supercriticality of the bifurcation

To determine the nature (supercritical versus subcritical) of the bifurcation, see Figure 2.11, and also for the stability analysis of the next chapter, we actually need the correction terms up to and including third order in δ in the above calculations. To keep the calculations within reasonable limits, we set the bifurcation parameter θ equal to one, such that in the above analysis the w -component is symmetric and has no higher order corrections, *i.e.*, $\hat{\theta} = 0$ in (2.3.8), etc. Note that θ has also been set to $\theta = 1$ in [53, 70, 71]. Moreover, most of the numerical results presented in [5, 51, 54, 60] are for $\theta = 1$. We also assume that $\alpha A_0^2 + \frac{\beta}{D} A_0^{2/D} > 0$, which implies that the stationary 1-pulse limit is not near a saddle-node bifurcation and that it is stable, see Theorem 3.4.1.

Lemma 2.4.1. *Let $(\alpha, \beta, \gamma, D, \tau, \theta, \varepsilon)$ be such that $\tau = \mathcal{O}(\frac{1}{\varepsilon^2}), \theta = 1, \alpha > 0$, (2.2.22) holds, and $\alpha A_0^2 + \frac{\beta}{D} A_0^{2/D} > 0$, where $A_0 = e^{-\varepsilon \xi_{*,0}}$ and $0 < \varepsilon \ll 1$. For $c = \delta$, with $\varepsilon \ll \delta \ll 1$, a traveling pulse exists for $\tau = \frac{1}{\varepsilon^2} (\hat{\tau}_{*,0} + \delta^2 \hat{\tau}_{*,2} + \mathcal{O}(\delta^3))$,*

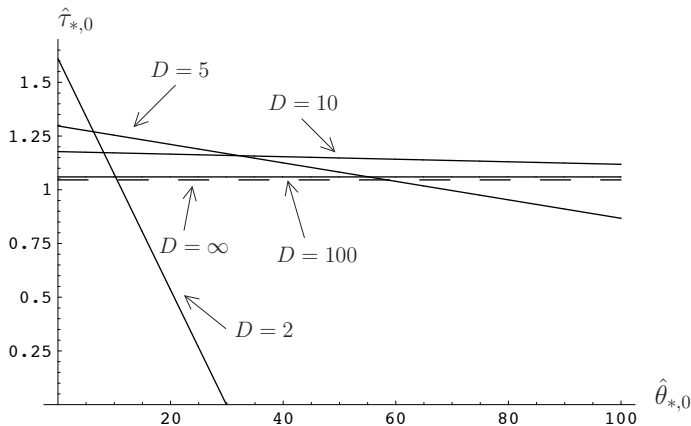


Figure 2.9: For $(\alpha, \beta, \gamma, \varepsilon) = (3, 1, 2, 0.01)$, the bifurcation point $\hat{\tau}_{*,0}(\hat{\theta}_{*,0})$ is plotted for $D = 2, 5, 10, 100$. The value of the jump mid-point $\xi_{*,0}$ is, respectively, 40.547, 47.018, 50.356, 54.393 and is computed through (2.4.2). When $D = \infty$, we have $\xi_{*,0} = 54.931$ and $\hat{\tau}_{*,0}(\hat{\theta}_{*,0}) = \hat{\tau}_{*,0} = 1.0460$. This is the dotted line in the figure.

with

$$\begin{aligned} \hat{\tau}_{*,0} &= \frac{2}{3} \sqrt{2} \frac{1}{\alpha(1-A_0^2 + A_0^2 \log A_0^2)} > 0, \\ \hat{\tau}_{*,2} &= \frac{3}{32} \sqrt{2} \alpha (\hat{\tau}_{*,0})^4 \left[1 - A_0^2 + A_0^2 \log A_0^2 - \frac{1}{3} A_0^2 \log^3 A_0^2 \right. \\ &\quad \left. + \frac{\alpha A_0^4 \log^2 A_0^2 (\log A_0^2 - 1)}{\alpha A_0^2 + \frac{\beta}{D} A_0^{2/D}} \right]. \end{aligned} \quad (2.4.3)$$

Note that the sign of $\hat{\tau}_{*,2}$ determines the nature of the bifurcation: a negative $\hat{\tau}_{*,2}$ yields a subcritical bifurcation, while a positive $\hat{\tau}_{*,2}$ yields a supercritical bifurcation. For given system parameters, we can evaluate (2.4.3) to determine the sign of $\hat{\tau}_{*,2}$. Moreover, we observe that it is possible for the same (α, β, D) for $\hat{\tau}_{*,2}$ to take on positive, as well as negative, values, depending on γ (via A_0), as is illustrated in Figure 2.10.

Proof. The proof consists of an elaborate – but straightforward – asymptotic analysis of the jump conditions (2.3.13). Plugging in v_*^\pm, w_*^\pm with $\theta = 1$ yields, to leading order in ε ,

$$\alpha (s_v^\pm (e^{\pm 2\varepsilon \lambda_v^\mp \xi_*} - 1) - 1) - \beta e^{-2\frac{\varepsilon}{D} \xi_*} + \gamma = \mp \frac{1}{3} \sqrt{2} c.$$

After expanding the two unknown variables $\hat{\tau}$ and ξ_* ,

$$\hat{\tau} = \hat{\tau}_{*,0} + \delta \hat{\tau}_{*,1} + \delta^2 \hat{\tau}_{*,2} + \delta^3 \hat{\tau}_{*,3} + \mathcal{O}(\delta^4), \quad \xi_* = \xi_{*,0} + \delta \xi_{*,1} + \delta^2 \xi_{*,2} + \delta^3 \xi_{*,3} + \mathcal{O}(\delta^4),$$

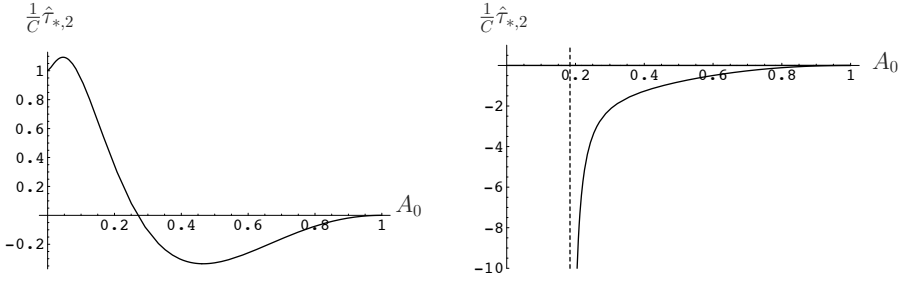


Figure 2.10: Left frame: $(\alpha, \beta, D) = (3, 1, 5)$. Right frame: $(\alpha, \beta, D) = (3, -1, 5)$. Note that we did not plot $\hat{\tau}_{*,2}$ but a ‘scaled’ version $\frac{1}{C}\hat{\tau}_{*,2}$. To be more precise, $C = \frac{3}{32}\sqrt{2}\alpha(\hat{\tau}_{*,0})^4$, and the scaling therefore depends on A_0 . However, $C > 0$ for $A_0 \in (0, 1)$. Thus, the scaling does not change the sign of $\hat{\tau}_{*,2}$. Moreover, note that the vertical asymptote (for $\beta < 0$) is exactly where $\alpha A_0^2 + \frac{\beta}{D}A_0^{\frac{2}{D}} = 0$ ($A_0 = A_c$, see (2.2.25)). The last free parameter, γ , actually determines the value of A_0 via (2.4.7). Thus for $(\alpha, \beta, D) = (3, 1, 5)$ it is possible to have a negative, as well as a positive $\hat{\tau}_{*,2}$.

we obtain the leading order approximations of (2.3.8) and (2.3.12),

$$\begin{aligned} \lambda_v^\pm &= \pm 1 - \frac{1}{2}\hat{\tau}_{*,0}\delta + \left(\pm\frac{1}{8}\hat{\tau}_{*,0}^2 - \frac{1}{2}\hat{\tau}_{*,1}\right)\delta^2 + \left(\pm\frac{1}{4}\hat{\tau}_{*,0}\hat{\tau}_{*,1} - \frac{1}{2}\hat{\tau}_{*,2}\right)\delta^3 + \mathcal{O}(\delta^4), \\ s_v^\pm &= -1 \pm \frac{1}{2}\hat{\tau}_{*,0}\delta \pm \frac{1}{2}\hat{\tau}_{*,1}\delta^2 \mp \left(\frac{1}{16}\hat{\tau}_{*,0}^3 - \frac{1}{2}\hat{\tau}_{*,2}\right)\delta^3 + \mathcal{O}(\delta^4). \end{aligned} \quad (2.4.4)$$

With these expressions we deduce

$$\begin{aligned} e^{\pm 2\varepsilon\lambda_v^\mp \xi_*} &= e^{-2\varepsilon\xi_{*,0}} + e^{-2\varepsilon\xi_{*,0}}(\mp\varepsilon\hat{\tau}_0\xi_{*,0} - 2\varepsilon\xi_{*,1})\delta + e^{-2\varepsilon\xi_{*,0}} \\ &\quad \left[-\frac{1}{4}\varepsilon(\hat{\tau}_{*,0})^2\xi_{*,0} \mp \varepsilon\hat{\tau}_{*,1}\xi_{*,0} \mp \varepsilon\hat{\tau}_{*,0}\xi_{*,1} \pm 2\varepsilon^2\hat{\tau}_{*,0}\xi_{*,0}\xi_{*,1}\right. \\ &\quad \left. + \frac{1}{2}\varepsilon^2(\hat{\tau}_{*,0})^2(\xi_{*,0})^2 + 2\varepsilon^2(\xi_{*,1})^2 - 2\varepsilon\xi_{*,2}\right]\delta^2 + e^{-2\varepsilon\xi_{*,0}} \\ &\quad \left[-\frac{1}{2}\varepsilon\hat{\tau}_{*,0}\hat{\tau}_{*,1}\xi_{*,0} \mp \varepsilon\hat{\tau}_2\xi_{*,0} \pm \frac{1}{4}\varepsilon^2(\hat{\tau}_{*,0})^3(\xi_{*,0})^2\right. \\ &\quad \left. + \varepsilon^2\hat{\tau}_{*,0}\hat{\tau}_{*,1}(\xi_{*,0})^2 \mp \frac{1}{6}\varepsilon^3(\hat{\tau}_{*,0})^3(\xi_{*,0})^3 - \frac{1}{4}\varepsilon(\hat{\tau}_{*,0})^2\xi_{*,1}\right. \\ &\quad \left. \mp \varepsilon\hat{\tau}_{*,1}\xi_{*,1} + \frac{3}{2}\varepsilon^2(\hat{\tau}_{*,0})^2\xi_{*,0}\xi_{*,1} \pm 2\varepsilon^2\hat{\tau}_{*,1}\xi_{*,0}\xi_{*,1}\right. \\ &\quad \left. - \varepsilon^3(\hat{\tau}_{*,0})^2(\xi_{*,0})^2\xi_{*,1} \pm 2\varepsilon^2\hat{\tau}_{*,0}(\xi_{*,1})^2 \mp 2\varepsilon^3\hat{\tau}_{*,0}\xi_{*,0}(\xi_{*,1})^2\right. \\ &\quad \left. - \frac{4}{3}\varepsilon^3(\xi_{*,1})^3 \mp \varepsilon\hat{\tau}_{*,0}\xi_{*,2} \pm 2\varepsilon^2\hat{\tau}_{*,0}\xi_{*,0}\xi_{*,2} + 4\varepsilon^2\xi_{*,1}\xi_{*,2}\right. \\ &\quad \left. - 2\varepsilon\xi_{*,3}\right]\delta^3 + \mathcal{O}(\delta^4), \end{aligned} \quad (2.4.5)$$

and

$$\begin{aligned} e^{-2\frac{\varepsilon}{D}\xi_*} &= e^{-2\frac{\varepsilon}{D}\xi_{*,0}} - \frac{2}{D}\varepsilon\xi_{*,1}e^{-2\frac{\varepsilon}{D}\xi_{*,0}}\delta + e^{-2\frac{\varepsilon}{D}\xi_{*,0}}\left[\frac{2}{D^2}\varepsilon^2(\xi_{*,1})^2\right. \\ &\quad \left. - \frac{2}{D}\varepsilon\xi_{*,2}\right]\delta^2 + e^{-2\frac{\varepsilon}{D}\xi_{*,0}}\left[-\frac{4}{3D^3}\varepsilon^3(\xi_{*,1})^3 + \frac{4}{D^2}\varepsilon^2\xi_{*,1}\xi_{*,2}\right. \\ &\quad \left. - \frac{2}{D}\varepsilon\xi_{*,3}\right]\delta^3 + \mathcal{O}(\delta^4). \end{aligned} \quad (2.4.6)$$

(Recall that $\varepsilon\xi_{*,j} = \mathcal{O}(1)$.)

Combining (2.4.4), (2.4.5), and (2.4.6), we find to leading order (twice)

$$\alpha A_0^2 + \beta A_0^{\frac{2}{D}} = \gamma, \quad (2.4.7)$$

which agrees with the first equation in (2.4.2).

The $\mathcal{O}(\delta)$ corrections read

$$\pm\frac{1}{2}\alpha\hat{\tau}_{*,0}(1 - A_0^2 + A_0^2 \log A_0^2) + 2\varepsilon\xi_{*,1}(\alpha A_0^2 + \frac{\beta}{D}A_0^{\frac{2}{D}}) = \pm\frac{1}{3}\sqrt{2}.$$

By adding and subtracting the above two equations, we obtain

$$\xi_{*,1} = 0, \quad \hat{\tau}_{*,0} = \frac{2}{3}\sqrt{2}\frac{1}{\alpha(1 - A_0^2 + A_0^2 \log A_0^2)},$$

which agrees with (2.4.2), since $\hat{\theta}_{*,0} = 0$. Note that the function $1 - A_0^2 + A_0^2 \log A_0^2$ is positive for all $A_0 \in (0, 1)$ – it decreases monotonically from one to zero as A_0 increases from zero to one. Since $\alpha > 0$ it follows that $\hat{\tau}_{*,0} > 0$.

At $\mathcal{O}(\delta^2)$, we find

$$\begin{aligned} 0 &= \pm\frac{1}{2}\alpha\hat{\tau}_{*,1}(A_0^2 - 1) - \alpha A_0^2\left[-\frac{1}{4}\varepsilon(\hat{\tau}_{*,0})^2\xi_{*,0} \mp \varepsilon\hat{\tau}_{*,1}\xi_{*,0} + \frac{1}{2}\varepsilon^2(\hat{\tau}_{*,0})^2(\xi_{*,0})^2\right. \\ &\quad \left. - 2\varepsilon\xi_{*,2}\right] - \frac{1}{2}\varepsilon\alpha(\hat{\tau}_{*,0})^2\xi_{*,0}A_0^2 + 2\frac{\beta}{D}\varepsilon\xi_{*,2}A_0^{\frac{2}{D}} \end{aligned}$$

(since $\xi_{*,1} = 0$). Subtracting the two equalities implies

$$\alpha\hat{\tau}_{*,1}(1 - A_0^2 + A_0^2 \log A_0^2) = 0 \quad \Rightarrow \quad \hat{\tau}_{*,1} = 0.$$

Adding both terms yields

$$\xi_{*,2} = \frac{1}{16}\frac{1}{\varepsilon}\frac{\alpha A_0^2(\hat{\tau}_{*,0})^2 \log A_0^2(\log A_0^2 - 1)}{\alpha A_0^2 + \frac{\beta}{D}A_0^{2/D}}.$$

We note that $\log A_0^2 - 1 < \log A_0^2 < 0$ and $\alpha A_0^2 + \frac{\beta}{D}A_0^{2/D} > 0$, therefore, $\text{sgn}(\xi_{*,2}) = \text{sgn}(\alpha) = +1$. Thus, the width of the pulse ($2\xi_*$) is larger than the leading order width ($2\xi_{*,0}$), *i.e.*, the width of the traveling pulse is larger than

the width of the standing pulse.

The $\mathcal{O}(\delta^3)$ term is given by

$$\begin{aligned} 0 &= \pm\alpha\left(\frac{1}{16}(\hat{\tau}_{*,0})^3 - \frac{1}{2}\hat{\tau}_{*,2}\right)(A_0^2 - 1) \mp \frac{1}{2}\alpha\hat{\tau}_{*,0}A_0^2\left[-\frac{1}{4}\varepsilon(\hat{\tau}_{*,0})^2\xi_{*,0}\right. \\ &\quad \left. + \frac{1}{2}\varepsilon^2(\hat{\tau}_{*,0})^2(\xi_{*,0})^2 - 2\varepsilon\xi_{*,2}\right] \mp \alpha A_0^2[\varepsilon\hat{\tau}_{*,2}\xi_{*,0} - \frac{1}{4}\varepsilon^2(\hat{\tau}_{*,0})^3(\xi_{*,0})^2 \\ &\quad \left. + \frac{1}{6}\varepsilon^3(\hat{\tau}_{*,0})^3(\xi_{*,0})^3 + \varepsilon\hat{\tau}_{*,0}\xi_{*,2} - 2\varepsilon^2\hat{\tau}_{*,0}\xi_{*,0}\xi_{*,2} \mp 2\varepsilon\xi_{*,3}\right] + 2\frac{\beta}{D}\varepsilon\xi_{*,3}A_0^{\frac{2}{D}}. \end{aligned}$$

Adding both terms implies $\xi_{*,3} = 0$, subtracting yields,

$$\begin{aligned} 0 &= \alpha\left(\frac{1}{16}(\hat{\tau}_{*,0})^3 - \frac{1}{2}\hat{\tau}_{*,2}\right)(A_0^2 - 1) - \frac{1}{2}\alpha\hat{\tau}_{*,0}A_0^2\left[-\frac{1}{4}\varepsilon(\hat{\tau}_{*,0})^2\xi_{*,0}\right. \\ &\quad \left. + \frac{1}{2}\varepsilon^2(\hat{\tau}_{*,0})^2(\xi_{*,0})^2 - 2\varepsilon\xi_{*,2}\right] - \alpha A_0^2[\varepsilon\hat{\tau}_{*,2}\xi_{*,0} - \frac{1}{4}\varepsilon^2(\hat{\tau}_{*,0})^3(\xi_{*,0})^2 \\ &\quad \left. + \frac{1}{6}\varepsilon^3(\hat{\tau}_{*,0})^3(\xi_{*,0})^3 + \varepsilon\hat{\tau}_{*,0}\xi_{*,2} - 2\varepsilon^2\hat{\tau}_{*,0}\xi_{*,0}\xi_{*,2}\right], \end{aligned}$$

which can be rewritten as

$$\begin{aligned} 0 &= -\alpha A_0^2\hat{\tau}_{*,0}\varepsilon\xi_{*,2}\log A_0^2 + \frac{1}{48}\alpha A_0^2(\hat{\tau}_{*,0})^3\log^3 A_0^2 - \frac{1}{16}\alpha(\hat{\tau}_{*,0})^3(1 - A_0^2 \\ &\quad + A_0^2\log A_0^2) + \frac{1}{2}\alpha\hat{\tau}_{*,2}(1 - A_0^2 + A_0^2\log A_0^2). \end{aligned}$$

Then, using the expression for $\hat{\tau}_{*,0}$ and $\xi_{*,2}$, we obtain

$$\begin{aligned} \hat{\tau}_{*,2} &= \frac{1}{8}(\hat{\tau}_{*,0})^3 - \frac{1}{32}\sqrt{2}\alpha A_0^2(\hat{\tau}_{*,0})^4\log^3 A_0^2 \\ &\quad + \frac{3}{32}\sqrt{2}\frac{\alpha^2 A_0^4(\hat{\tau}_{*,0})^4\log^2 A_0^2(\log A_0^2 - 1)}{\alpha A_0^2 + \frac{\beta}{D}A_0^{2/D}}, \end{aligned} \tag{2.4.8}$$

which can be rewritten as in (2.4.3). \square

For D large, we can analytically determine the sign of $\hat{\tau}_{*,2}$ in (2.4.3), as we now show.

Corollary 2.4.2. *Let $(\alpha, \beta, \gamma, D, \tau, \theta, \varepsilon)$ and A_0 be as in Lemma 2.4.1 and assume that $D = \frac{1}{\delta}$ with $0 < \varepsilon \ll \delta \ll 1$. Define $A_0^Z \in (0, 1)$ as the (unique) solution of*

$$1 - A_0^2 + A_0^2\log A_0^2 + \frac{2}{3}A_0^2\log^3 A_0^2 - A_0^2\log^2 A_0^2 = 0 \tag{2.4.9}$$

($A_0^Z = 0.11063\dots$). Then, $\hat{\tau}_{*,2} > 0$ for parameter combinations such that $0 < A_0 < A_0^Z + \mathcal{O}(\delta)$ and $\hat{\tau}_{*,2} < 0$ for $1 > A_0 > A_0^Z + \mathcal{O}(\delta)$.

Proof. It follows from (2.4.3) that, to leading order in δ ,

$$\begin{aligned} \hat{\tau}_{*,2}|_{D=\mathcal{O}(\delta^{-1})} &= \frac{3}{32}\sqrt{2}\alpha(\hat{\tau}_{*,0})^4\left[1 - A_0^2 + A_0^2\log A_0^2 - \frac{1}{3}A_0^2\log^3 A_0^2\right. \\ &\quad \left. + A_0^2\log^2 A_0^2(\log A_0^2 - 1)\right] \\ &= \frac{3}{32}\sqrt{2}\alpha(\hat{\tau}_{*,0})^4\left[1 - A_0^2 + A_0^2\log A_0^2 + \frac{2}{3}A_0^2\log^3 A_0^2 - A_0^2\log^2 A_0^2\right] \\ &=: C\hat{\tau}_{*,2}', \end{aligned}$$

with $C = \frac{3}{32}\sqrt{2}\alpha(\hat{\tau}_{*,0})^4 > 0$ and $\hat{\tau}'_{*,2} = 1 - A_0^2 + A_0^2 \log A_0^2 + \frac{2}{3}A_0^2 \log^3 A_0^2 - A_0^2 \log^2 A_0^2$. Thus $\text{sgn}(\hat{\tau}_{*,2}) = \text{sgn}(\hat{\tau}'_{*,2})$. We notice that $\hat{\tau}'_{*,2}(0) = 1$ and $\hat{\tau}'_{*,2}(1) = 0$. We now show that $\hat{\tau}'_{*,2}(s)$, with $s := A_0^2$, has a negative minimum by differentiating,

$$\frac{d}{ds} \hat{\tau}'_{*,2} = (\log s) \left(\frac{2}{3} \log^2 s + \log s - 1 \right).$$

Thus, with $z := \log s$ (so that $z \in (-\infty, 0)$), we see that $\hat{\tau}'_{*,2}(z)$ has a unique extremum if $\frac{2}{3}z^2 + z - 1 = 0$, *i.e.*, $z = z^M = -\frac{3}{4} - \frac{1}{4}\sqrt{33}$. This implies that $A_0^M = e^{-\frac{1}{8}(3+\sqrt{33})} \in (0, 1)$, so that

$$\hat{\tau}'_{*,2}(A_0^M) = 1 - e^{-\frac{1}{4}(3+\sqrt{33})} \left(\frac{31}{4} + \frac{5}{4}\sqrt{33} \right) < 0.$$

Hence, A_0^M determines a negative minimum of $\hat{\tau}'_{*,2}$, which implies $\hat{\tau}'_{*,2}$ must change sign once for $A = A_0^Z \in (0, A_0^M)$, where A_0^Z is determined by (2.4.9). \square

An additional consequence of Lemma 2.4.1, that holds for more general values of D , is

Corollary 2.4.3. *Let $(\alpha, \beta, \gamma, D, \tau, \theta, \varepsilon)$ and A_0 be as in Lemma 2.4.1. Furthermore, assume that $\beta < 0$, $\alpha D > -\beta$, $A_0 > A_c > A_0^Z$ (with A_c, A_0^Z as in (2.2.25), (2.4.9), respectively), then the bifurcation is subcritical, *i.e.*, $\hat{\tau}_{*,2} < 0$.*

Proof. Observe that in this case

$$\frac{\alpha A_0^4 \log^2 A_0^2 (\log A_0^2 - 1)}{\alpha A_0^2 + \frac{\beta}{D} A_0^{2/D}} < A_0^2 \log^2 A_0^2 (\log A_0^2 - 1) < 0.$$

Therefore, $\hat{\tau}_{*,2}(A_0) < C\hat{\tau}'_{*,2}(A_0)$, with $\hat{\tau}'_{*,2}(A_0)$ as defined above, and $C\hat{\tau}'_{*,2}(A_0)$ is negative for $A_0 > A_0^Z$. \square

Remark 2.4.2. If, in addition to the conditions in Corollary 2.4.3, it is also assumed that $\alpha > \gamma$, then it follows from our analysis in Section 2.3.2 that there is a traveling pulse with speed $c = \frac{3}{2}\sqrt{2}(\alpha - \gamma) + \mathcal{O}(\delta, \varepsilon) > 0$ for $\hat{\tau} \gg 1$ (2.3.15). This indicates that the curve $c = c(\hat{\tau})$ has a fold structure, *i.e.*, for increasing $\hat{\tau}$ (and all other parameters fixed) there is a saddle-node bifurcation of traveling pulses at $\hat{\tau} = \hat{\tau}_{SN} < \hat{\tau}_{*,0}$ at which two traveling pulses bifurcate with speeds $c_{\pm}(\hat{\tau}) > 0$ and $c_{\pm}(\hat{\tau}_{SN}) = c_{SN} > 0$; the pulse associated to $c_{-}(\hat{\tau})$ merges with the stationary pulse at $\hat{\tau} = \hat{\tau}_{*,0}$, while the other pulse exists for all $\hat{\tau} > \hat{\tau}_{SN}$, so that $c_{+}(\hat{\tau}) \rightarrow \frac{3}{2}\sqrt{2}(\alpha - \gamma)$ as $\hat{\tau} \rightarrow \infty$. This can be checked by using a continuation method for the solutions of (2.3.13), see Figure 2.11. Hence, there exist parameter combinations for which two types of traveling pulses coexist with the stationary pulse (for $\hat{\tau}_{SN} < \hat{\tau} < \hat{\tau}_{*,0}$). Both the stationary pulse and the traveling pulse associated to $c_{+}(\hat{\tau})$ may be stable, see Figure 3.11 of Chapter 3.

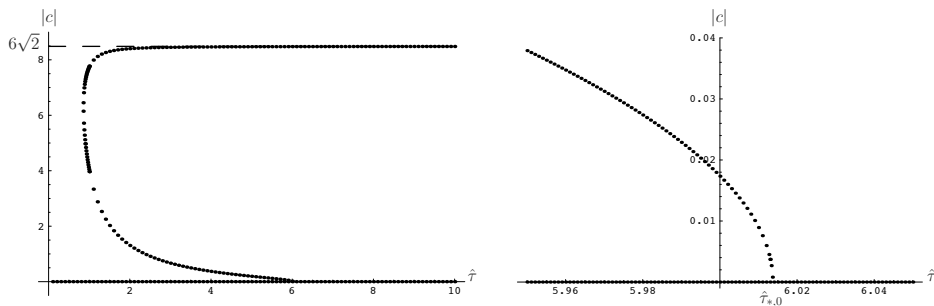


Figure 2.11: The solution curve of equation (2.3.13) in the $(\hat{\tau}, c)$ plane for the parameter values $(\alpha, \beta, \gamma, D, \theta, \varepsilon) = (5, -3, 1, 4, 1, 0.01)$. We have chosen the parameters in such a fashion that they satisfy the conditions in Remark 2.4.2. In the left frame we observe a subcritical bifurcation at $\hat{\tau} = \hat{\tau}_{*,0} = 6.01363$. Moreover, we observe that as $\hat{\tau}$ goes to infinity the upperbranch, $c_+(\hat{\tau})$, goes to the theoretically-predicted, leading order value, $\frac{3}{2}\sqrt{2}(\alpha - \gamma) = 6\sqrt{2}$, see (2.3.15). Finally, from this numerical continuation we observe that the two branches merge at a saddle-node bifurcation at $\hat{\tau}_{SN}^{num} = 0.84917$ and $c_{SN}^{num} = 6.3027$. In the right frame, the region near $\hat{\tau} = \hat{\tau}_{*,0}$ is magnified.

2.5 Stationary 2-pulse solutions

In this section, we establish the existence of localized, symmetric, standing, 2-pulse solutions of (2.1.6). We construct these pulses as homoclinic orbits $\gamma_{2p,j}^-(\xi)$ to the critical point P_ε^- .

2.5.1 The construction of $\gamma_{2p,j}^-(\xi)$ homoclinic to P_ε^-

We search for stationary pulse-like solutions. Therefore, the PDE (2.1.7) again reduces to (2.2.1), and the basic observations (on the fixed points, the reduced limits, the slow manifolds, etc.) are the same as in Section 2.2.1. However, for symmetric standing 2-pulse solutions, we have to distinguish nine different regions instead of the five regions as we did for the 1-pulse solutions – see Section 2.2.2. We again parametrize the 2-pulse solutions so that its u, v, w -components are at a local extremum at $\xi = 0$. However, there are three local extrema, see Figure 2.1, and for symmetry considerations we choose to put the zero of the ξ -axis at the second location, the one exponentially close to $\mathcal{M}_\varepsilon^-$. It turns out that $v_{2p,j}^-(0)$ and $w_{2p,j}^-(0)$ are local minima, while $u_{2p,j}^-(0)$ is a local maximum, see Figure 2.1 and Figure 2.12. We define the four ‘jump mid-points’ of $\gamma_{2p,j}^-$ by $\pm\xi_*^{1,2}$ (not to be confused with the $\xi_{*,1}, \xi_{*,2}$ of the previous section). Where the last ‘back’ (*i.e.*, the final jump of $\mathcal{M}_\varepsilon^+$ back to $\mathcal{M}_\varepsilon^-$) of $\gamma_{2p,j}^-(\xi)$ crosses the $\{u = 0\}$ -hyperplane at

$\xi = \xi_*^1$, and the last front of $\gamma_{2p,j}^-(\xi)$ crosses the same hyperplane at $\xi = \xi_*^2$. Note that by construction $0 < \xi_*^2 < \xi_*^1$. The reversibility symmetry implies that $-\xi_*^1$ is the jump mid-point of the first front and $-\xi_*^2$ is the jump mid-point of the first back. Thus,

$$\begin{aligned}\gamma_{2p,j}^-(\pm\xi_*^1) &= (0, \mp p_*^1, v_*^1, \mp q_*^1, w_*^1, \mp r_*^1), \\ \gamma_{2p,j}^-(\pm\xi_*^2) &= (0, \pm p_*^2, v_*^2, \pm q_*^2, w_*^2, \pm r_*^2).\end{aligned}\tag{2.5.1}$$

We assume that ξ_*^1, ξ_*^2 , as well as $\xi_*^1 - \xi_*^2$, are large, *i.e.*, $\xi_*^{1,2}$ and $\xi_*^1 - \xi_*^2$ are $\mathcal{O}(\frac{1}{\varepsilon})$. We now define the four fast intervals $I_f^{2,4,6,8}$ and the five slow intervals $I_s^{1,3,5,7,9}$

$$\begin{aligned}I_f^{2,4} &:= \left(-\xi_*^{1,2} - \frac{1}{\sqrt{\varepsilon}}, -\xi_*^{1,2} + \frac{1}{\sqrt{\varepsilon}}\right), I_f^{6,8} := \left(\xi_*^{2,1} - \frac{1}{\sqrt{\varepsilon}}, \xi_*^{2,1} + \frac{1}{\sqrt{\varepsilon}}\right), \\ I_s^1 &:= \left(-\infty, -\xi_*^1 - \frac{1}{\sqrt{\varepsilon}}\right], I_s^{3,7} := \left[\mp\xi_*^{1,2} + \frac{1}{\sqrt{\varepsilon}}, \mp\xi_*^{2,1} - \frac{1}{\sqrt{\varepsilon}}\right], \\ I_s^5 &:= \left[-\xi_*^2 + \frac{1}{\sqrt{\varepsilon}}, \xi_*^2 - \frac{1}{\sqrt{\varepsilon}}\right], I_s^9 := \left[\xi_*^1 + \frac{1}{\sqrt{\varepsilon}}, \infty\right).\end{aligned}$$

The nine different regions are then

- 1: The dynamics take place exponentially close to the slow manifold $\mathcal{M}_\varepsilon^-$: $\xi \in I_s^1$.
- 2: The dynamics take place in the fast field: $\xi \in I_f^2$.
- 3: The dynamics take place exponentially close to $\mathcal{M}_\varepsilon^+$: $\xi \in I_s^3$.
- 4: The dynamics take place in the fast field: $\xi \in I_f^4$.
- 5: The dynamics take place exponentially close to $\mathcal{M}_\varepsilon^-$: $\xi \in I_s^5$.
- 6: The dynamics take place in the fast field: $\xi \in I_f^6$.
- 7: The dynamics take place exponentially close to $\mathcal{M}_\varepsilon^+$: $\xi \in I_s^7$.
- 8: The dynamics take place in the fast field: $\xi \in I_f^8$.
- 9: The dynamics take place exponentially close to $\mathcal{M}_\varepsilon^-$: $\xi \in I_s^9$.

The analysis of the formal construction is now nearly the same as for the standing 1-pulse case (Section 2.2.2); the only difference is that it involves a bit more bookkeeping. However, qualitatively, nothing changes; for example we still have $\Delta_f^{2,4,6,8}(v, w, q, r) = \mathcal{O}(\sqrt{\varepsilon})$, the equivalent of (2.2.15). The homoclinic v, w -component on the slow manifolds are still governed by (2.2.10) and (2.2.11). Together with the usual boundary conditions, of which there are in total forty, we

get

$$v_{2p}(\xi) = \begin{cases} 2e^{\varepsilon\xi} (\sinh(\varepsilon\xi_*^1) - \sinh(\varepsilon\xi_*^2)) - 1 & \text{in 1,} \\ -e^{-\varepsilon(\xi+\xi_*^1)} - e^{\varepsilon(\xi-\xi_*^1)} - 2e^{\varepsilon\xi}(\sinh(\varepsilon\xi_*^2)) + 1 & \text{in 3,} \\ -e^{-\varepsilon(\xi+\xi_*^1)} + e^{-\varepsilon(\xi+\xi_*^2)} + e^{\varepsilon(\xi-\xi_*^2)} - e^{\varepsilon(\xi-\xi_*^1)} - 1 & \text{in 5,} \\ -e^{-\varepsilon(\xi+\xi_*^1)} - e^{\varepsilon(\xi-\xi_*^1)} - 2e^{-\varepsilon\xi}(\sinh(\varepsilon\xi_*^2)) + 1 & \text{in 7,} \\ 2e^{-\varepsilon\xi} (\sinh(\varepsilon\xi_*^1) - \sinh(\varepsilon\xi_*^2)) - 1 & \text{in 9,} \end{cases} \quad (2.5.2)$$

and likewise

$$w_{2p}(\xi) = \begin{cases} 2e^{\frac{\varepsilon}{D}\xi} (\sinh(\frac{\varepsilon}{D}\xi_*^1) - \sinh(\frac{\varepsilon}{D}\xi_*^2)) - 1 & \text{in 1,} \\ -e^{-\frac{\varepsilon}{D}(\xi+\xi_*^1)} - e^{\frac{\varepsilon}{D}(\xi-\xi_*^1)} - 2e^{\frac{\varepsilon}{D}\xi}(\sinh(\frac{\varepsilon}{D}\xi_*^2)) + 1 & \text{in 3,} \\ -e^{-\frac{\varepsilon}{D}(\xi+\xi_*^1)} + e^{-\frac{\varepsilon}{D}(\xi+\xi_*^2)} + e^{\frac{\varepsilon}{D}(\xi-\xi_*^2)} - e^{\frac{\varepsilon}{D}(\xi-\xi_*^1)} - 1 & \text{in 5,} \\ -e^{-\frac{\varepsilon}{D}(\xi+\xi_*^1)} - e^{\frac{\varepsilon}{D}(\xi-\xi_*^1)} - 2e^{-\frac{\varepsilon}{D}\xi}(\sinh(\frac{\varepsilon}{D}\xi_*^2)) + 1 & \text{in 7,} \\ 2e^{-\frac{\varepsilon}{D}\xi} (\sinh(\frac{\varepsilon}{D}\xi_*^1) - \sinh(\frac{\varepsilon}{D}\xi_*^2)) - 1 & \text{in 9.} \end{cases} \quad (2.5.3)$$

By the reversibility symmetry (2.2.2), there are two Melnikov conditions (instead of the expected four), which are analogous to (2.2.17),

$$\alpha v_*^{1,2} + \beta w_*^{1,2} + \gamma = 0, \quad (2.5.4)$$

with $v_*^{1,2}$ and $w_*^{1,2}$ defined in (2.5.1). When we define $A_1 := e^{-\varepsilon\xi_*^1}$ and $A_2 := e^{-\varepsilon\xi_*^2}$ ($0 < A_1 < A_2 < 1$), and combine this with the above results (2.5.2), (2.5.3), and (2.5.4), we obtain

$$\begin{cases} -\alpha A_1^2 + \alpha A_1 A_2 - \alpha A_1 A_2^{-1} - \beta A_1^{\frac{2}{D}} + \beta A_1^{\frac{1}{D}} A_2^{\frac{1}{D}} - \beta A_1^{\frac{1}{D}} A_2^{-\frac{1}{D}} + \gamma = 0, \\ +\alpha A_2^2 - \alpha A_1 A_2 - \alpha A_1 A_2^{-1} + \beta A_2^{\frac{2}{D}} - \beta A_1^{\frac{1}{D}} A_2^{\frac{1}{D}} - \beta A_1^{\frac{1}{D}} A_2^{-\frac{1}{D}} + \gamma = 0. \end{cases} \quad (2.5.5)$$

By adding and subtracting, this system can be transformed into

$$\begin{cases} G_1(A_1, A_2) := \alpha(A_1 - A_2)^2 + \beta(A_1^{\frac{1}{D}} - A_2^{\frac{1}{D}})^2 = 0, \\ G_2(A_1, A_2) := \alpha(A_2^2 - A_1^2) - 2\alpha A_1 A_2^{-1} + \beta(A_2^{\frac{2}{D}} - A_1^{\frac{2}{D}}) \\ \quad - 2\beta A_1^{\frac{1}{D}} A_2^{-\frac{1}{D}} = -2\gamma. \end{cases} \quad (2.5.6)$$

The above formal analysis gives rise to the following theorem.

Theorem 2.5.1. *Let $(\alpha, \beta, \gamma, D)$ be such that (2.5.6) has K solution pairs (A_1, A_2) with $0 < A_1 < A_2 < 1$, and let $\varepsilon > 0$ be small enough. If $K = 0$, then there are no homoclinic orbits to P_ε^- in (2.2.1) that have a structure as sketched in Figure 2.12. If $K > 0$, there are K homoclinic orbits $\gamma_{2p,j}(\xi)$, $j \in \{1, \dots, K\}$, to P_ε^- in (2.2.1) (with structure as in Figure 2.12). These correspond to symmetric standing 2-pulse solutions of (2.1.6).*

Given the form of equations (2.5.6), it is natural to solve A_1 and γ as functions of A_2 and the system parameters α, β and D . In Figure 2.13, both A_1 and γ are plotted. Note also that $G_1(A_1, A_2)$ cannot vanish in (2.5.6) if $\text{sgn}(\alpha) = \text{sgn}(\beta)$. Thus, there only exist homoclinic 2-pulse solutions if $\text{sgn}(\alpha) \neq \text{sgn}(\beta)$ – see section 2.6.

Proof of Theorem 2.5.1. A symmetric standing 2-pulse $\gamma_{2p,j}^-(\xi)$ is reversible (2.2.2) and we can therefore argue along the same lines as in the proof of Theorem 2.2.1. In fact, the proof of this theorem goes in essence very similar to that of Theorem 2.2.1. Therefore, we will omit most details. By the first Melnikov condition in (2.5.4), there exists a 1-parameter family of orbits $\gamma_{het}^{1,-}(\xi; v_*^1; w_*^1(v_*^1)) \in W^u(P_\varepsilon^-) \cap W^s(\mathcal{M}_\varepsilon^+)$. We define the tube $\mathcal{T}_{1,*}^- \subset W^u(P_\varepsilon^-)$ as the collection of orbits in $W^u(P_\varepsilon^-)$ that are exponentially close to $\gamma_{het}^{1,-}(\xi; v_*^1; w_*^1(v_*^1))$ for $\xi < -\xi_*^1$. All orbits in $\mathcal{T}_{1,*}^-$ approach $\mathcal{M}_\varepsilon^+$ and follow the slow flow on $\mathcal{M}_\varepsilon^+$ for some ‘time’ (which may be infinite), after which they take off parallel (and exponentially close to) $W^u(\mathcal{M}_\varepsilon^+)$. In other words, near $\mathcal{M}_\varepsilon^+$ $\mathcal{T}_{1,*}^-$ is strongly stretched along the direction of $W^u(\mathcal{M}_\varepsilon^+)$. It thus follows by the application of the second Melnikov condition in (2.5.4) that $\mathcal{T}_{1,*}^-$ intersects $W^s(\mathcal{M}_\varepsilon^-)$; the intersection $\mathcal{T}_{1,*}^- \cap W^s(\mathcal{M}_\varepsilon^-)$ is again 2-dimensional, *i.e.*, it consists of a 1-parameter family of orbits $\subset W^u(P_\varepsilon^-) \cap W^s(\mathcal{M}_\varepsilon^-)$. As in the proof of Theorem 2.2.1, it can now be shown that there is a unique orbit $\gamma_{0,*}^{2,-}(\xi) \subset \mathcal{T}_{1,*}^- \cap W^s(\mathcal{M}_\varepsilon^-)$ that is homoclinic to $\mathcal{M}_\varepsilon^-$ such that $\gamma_{0,*}^{2,-}(0) \in \{q = r = 0\}$ – note that this also determines the position of the symmetry point $\xi = 0$. Again, the algebra leading to the construction of $\gamma_{0,*}^{2,-}(\xi)$ is equivalent to the above analysis and yields at leading order (2.5.6). The existence of the 2-pulse homoclinic orbits $\gamma_{2p,j}^-(\xi)$ now follows by arguments that are identical to those in Theorem 2.2.1. It is based on the construction of the sub-tube $\mathcal{T}_{2,*}^- \subset \mathcal{T}_{1,*}^-$ around $\gamma_{0,*}^{2,-}(\xi)$, its symmetrical counterpart $\mathcal{T}_{2,*}^+$ around the orbit $\gamma_{0,*}^{2,+}(\xi)$ and the application of the reversibility symmetry. \square

Remark 2.5.1. In the proof presented above we have used that the jump mid-points $v_*^{1,2}$ and $w_*^{1,2}$ satisfy certain constraints. In particular, $v_*^1 \in (-1, 0)$, $w_*^1 = -\frac{1}{\beta}(\alpha v_*^1 + \gamma)$, $v_*^2 \in (v_*^1, V)$ and $w_*^2 = -\frac{1}{\beta}(\alpha v_*^2 + \gamma)$, where $V = -\frac{\xi_*^1 + \xi_*^2}{2} - \frac{1}{2\varepsilon} \log\left(1 - e^{-2\varepsilon\xi_*^2} + e^{-\varepsilon(\xi_*^1 + \xi_*^2)}\right)$. These constraints arise naturally from the requirement that the tracked orbits lie on the correct side of the stable and unstable manifolds of the slow manifold, so that they can have a second pulse.

Remark 2.5.2. In our analysis we have focused on the existence of localized one- and 2-pulse patterns. As for instance in [17], the same geometrical approach as in the proofs of Theorems 2.2.1, 2.3.1 and 2.5.1 can be applied to establish the existence of many other kinds of stationary or traveling patterns, such as N -pulse solutions and various kinds of spatially-periodic wave trains. We refrain from going into the details here. However, we do notice that these patterns can be stable and do play an important role in the dynamics of (2.1.7) – see section 2.7.1

When we implement this into formula (2.5.7) for $H_2(A_1, A_2)$ we find, after some manipulation, a unique γ :

$$\gamma = \alpha - 2\alpha(1 + A_2^2)\sqrt{-\frac{\beta}{\alpha A_2}} - \beta \left(1 + 3A_2 + \frac{1}{A_2} - \sqrt{-\frac{A_2\beta}{\alpha}} - \sqrt{-\frac{\beta}{\alpha A_2}} \right) \quad (2.5.9)$$

However, there are also restrictions on the choice of A_2 . We need $0 < A_1 < A_2 < 1$. Therefore,

$$-\frac{1}{4} \frac{\beta}{\alpha} < A_2 < \min \left\{ -\frac{\beta}{\alpha}, 1 \right\}. \quad (2.5.10)$$

We conclude that if A_2 satisfies (2.5.10), there is a (α, β, γ) -parameter combination such that (2.5.7) is satisfied, *i.e.*, such that a 2-pulse solution exists. However, if (2.5.10) cannot be satisfied – which is the case when $|\alpha| < |\beta|$, there are no such 2-pulse solutions.

This nonexistence result can be generalized to all $D > 1$:

Corollary 2.5.2. *Let $\text{sgn}(\alpha) \neq \text{sgn}(\beta)$. There is an open region in $(\alpha, \beta, \gamma, D)$ -space for which homoclinic 2-pulse solutions as described in Theorem 2.5.1 exist. However, if $|\alpha|D^2 < |\beta|$, then there are no such 2-pulse solutions.*

Proof. We start again by observing that $G_1(A_1, A_2) = 0$ does not depend on γ , and that the γ in $G_2(A_1, A_2) = -2\gamma$ only shifts $G_2(A_1, A_2)$ up or down. So, again instead of solving A_1 and A_2 in terms of α, β and γ via (2.5.6), we solve this equation for given α, β and A_2 with the unknown parameters A_1 and γ .

The condition $0 < A_1 < A_2 < 1$ yields the following generalization of (2.5.10)

$$\left(-\frac{\beta}{\alpha D^2} \right)^{\frac{1}{2} \frac{D}{D-1}} < A_2 < \min \left\{ \left(-\frac{\beta}{\alpha} \right)^{\frac{1}{2} \frac{D}{D-1}}, 1 \right\}. \quad (2.5.11)$$

Here, the latter inequality ensures $A_2 \in (0, 1)$, and the former implies $A_1 < A_2$. This interval is empty when $|\alpha|D^2 < |\beta|$. \square

2.5.3 Asymptotics for $D \rightarrow \infty$

In this section, we analyze the large D asymptotics of solutions of equation (2.5.6). From Figure 2.13, we observe that, over a large portion of the interval $A_2 \in (0, 1)$, the solution curves for A_1 lie near the axis, and the solution curves for γ lie near the lower dashed curve. Moreover, these curves approach their respective asymptotes as D increases. We establish this result precisely in the following lemma:

Lemma 2.5.3. *Assume that $\alpha > 0 > \gamma > \beta$. Then, for strictly $\mathcal{O}(1)$ values of $A_2 \in \left(0, \sqrt{-\frac{\beta}{\alpha}} \right)$, as measured with respect to the asymptotically small parameter*

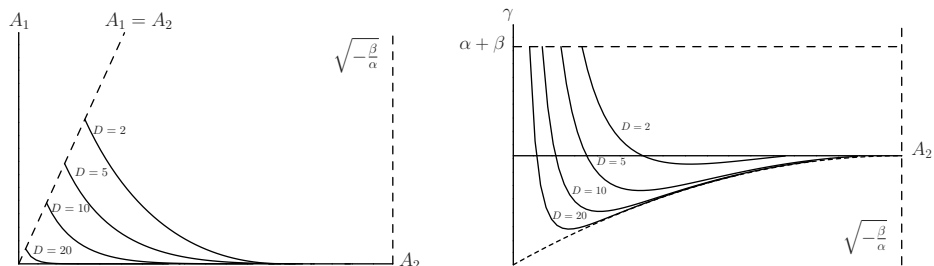


Figure 2.13: In the left frame, A_1 is plotted as function of A_2 for several values of D . In the right frame, γ is plotted as function of A_2 for the same values for D . The dashed curve represents the asymptotic behavior for D large and is given by (2.5.12). The 2-pulse orbits are typically created or annihilated in a saddle-node bifurcation – see Section 2.7, Figure 2.15.

$\frac{1}{D}$, the solutions $A_1 = A_1(\alpha, \beta, A_2, D)$ and $\gamma = \gamma(\alpha, \beta, A_2, D)$ of equation (2.5.6) satisfy, to leading order,

$$A_1 = \left(1 - \sqrt{-\frac{\alpha}{\beta}} A_2\right)^D, \quad \gamma = -\alpha \left(\sqrt{-\frac{\beta}{\alpha}} - A_2\right)^2 \quad \text{as } D \rightarrow \infty. \quad (2.5.12)$$

The lower dashed curve in the right frame of Figure 2.13 is this parabola of γ as function of A_2 . It is also useful to combine the results of (2.5.12) of this lemma into expressions for A_1 and A_2 in terms of the given system parameters. The result is, to leading order,

$$A_1 = \left(\frac{\gamma}{\beta}\right)^{\frac{D}{2}}, \quad A_2 = \sqrt{-\frac{\beta}{\alpha}} - \sqrt{-\frac{\gamma}{\alpha}}.$$

We also remark that in both frames there is a boundary layer at $A_2 = A_1$, which is why we require A_2 to be strictly of $\mathcal{O}(1)$ for this result and we recall that the existence construction requires that $A_1 < A_2$. In the boundary layer, the graph of A_1 limits on the diagonal, with a slope of -1 , while the graph of γ is nearly vertical. Although the asymptotic analysis is not too involved, we refrain from going into the details here. Nevertheless, we notice that, by (2.5.6), $\gamma = \alpha + \beta$ in the limit $A_2 \downarrow A_1$, see Figure 2.13.

Proof of Lemma 2.5.3. We observe that, for A_2 strictly of $\mathcal{O}(1)$ in $(0,1)$, we may assume that

$$A_1 = C^D, \quad (2.5.13)$$

to leading order, for some $C \in (0,1)$. Indeed, if one instead assumed that $A_1 = a\delta^\sigma$ to leading order, for $\delta = \frac{1}{D}$ and for some $\sigma > 0$, then from the first equation

in (2.5.6) one would find that $A_2 = 0$ to leading order, which is a contradiction. Hence, with the assumption (2.5.13), the first equation in (2.5.6) becomes

$$\alpha A_2^2 + \beta(C - 1)^2 = 0,$$

to leading order, where we used that $A_2^{1/D} = 1 + \mathcal{O}(D^{-1})$ for $A_2 \in (0, 1)$, and that $\frac{1}{7}D \log(A_2) \ll C$. Solving, one finds, to leading order,

$$A_1 = \left(1 - \sqrt{-\frac{\alpha}{\beta}} A_2\right)^D, \quad (2.5.14)$$

which is precisely the first formula of (2.5.12).

With the asymptotics for A_1 in hand, one may use the second formula in (2.5.6) to find the asymptotics for γ . To leading order,

$$\gamma = -\frac{1}{2} \left[\alpha A_2^2 + \beta \left(1 - \left(1 - \sqrt{-\frac{\alpha}{\beta}} A_2\right)^2\right) - 2\beta \left(1 - \sqrt{-\frac{\alpha}{\beta}} A_2\right) \right].$$

Simplifying the right member, we find precisely the asymptotic result (2.5.12) for γ . \square

To conclude this section on the large D asymptotics, we comment briefly on the form of the W profile for stationary 2-pulse solutions in the interval between the two pulses. From the above asymptotics, we find, to leading order,

$$\begin{aligned} \varepsilon \xi &= \mathcal{O}(1), & \varepsilon \xi_*^2 &= -\log A_2 = \mathcal{O}(1), \\ \varepsilon \xi_*^1 &= -D \log \left(1 - \sqrt{-\frac{\alpha}{\beta}} A_2\right) = \mathcal{O}(D). \end{aligned} \quad (2.5.15)$$

Hence, from (2.5.3), we find in region 5, to leading order,

$$\begin{aligned} w_{2p}(\xi) &= -e^{-\frac{\varepsilon}{D}(\xi + \xi_*^1)} + e^{-\frac{\varepsilon}{D}(\xi + \xi_*^2)} + e^{\frac{\varepsilon}{D}(\xi - \xi_*^2)} - e^{\frac{\varepsilon}{D}(\xi - \xi_*^1)} - 1 \\ &= 2\sqrt{-\frac{\alpha}{\beta}} A_2 - 1 \\ &= 1 - 2\sqrt{\frac{\gamma}{\beta}}. \end{aligned} \quad (2.5.16)$$

Therefore, for each $A_2 \in \left(0, \sqrt{-\frac{\beta}{\alpha}}\right)$, the W -component is constant to leading order, where the constant is given by (2.5.16). Moreover, we observe that W takes on all of the values in the interval $(-1, 1)$, since the above analysis applies for all $A_2 \in \left(0, \sqrt{-\frac{\beta}{\alpha}}\right)$.

A stability analysis similar to that presented in the next Chapter shows that the 2-pulse solutions are stable for parameter combinations in the ‘boundary layer’. However, they are unstable for parameter values near the dashed curve in the asymptotic regime studied in Lemma 2.5.3.

2.6 The two-component model

In this section, we investigate the two-component (U, V) -subsystem of the three-component model, that is, we send D to infinity and assume that the W -component is constant at $W = -1$ everywhere in the PDE (2.1.6). The PDE model reduces to

$$\begin{cases} U_t &= \varepsilon^2 U_{xx} + U - U^3 - \varepsilon(\alpha_2 V + \gamma_2), \\ \tau_2 V_t &= V_{xx} + U - V, \end{cases} \quad (2.6.1)$$

with the same assumptions as before, $0 < \varepsilon \ll 1, 0 < \tau_2 \ll \varepsilon^{-3}$ and $\alpha_2, \gamma_2 \in \mathbb{R}$. Note that the notation for the parameters has the following correspondence with the parameters of the three-component model: $\alpha_2 = \alpha, \tau_2 = \tau$ and $\gamma_2 = \gamma - \beta$.

It can be shown with the same techniques used in this chapter that for $\tau_2 = \mathcal{O}(1)$ the two-component system has standing 1-pulse solutions homoclinic to $P_{2,\varepsilon}^- = (u_{2,\varepsilon}^-, 0, u_{2,\varepsilon}^-, 0)$ with $u_{2,\varepsilon}^- = -1 + \frac{1}{2}\varepsilon(\alpha_2 - \gamma_2) + \mathcal{O}(\varepsilon^2)$ if there exists an $A \in (0, 1)$ satisfying

$$\alpha_2 A^2 = \gamma_2 + \mathcal{O}(\sqrt{\varepsilon}),$$

recall (2.2.22). Hence, we immediately observe that necessary conditions for a standing pulse homoclinic to $P_{2,\varepsilon}^-$ to exist are that $\text{sgn}(\alpha_2) = \text{sgn}(\gamma_2)$ and $0 < |\gamma_2| < |\alpha_2|$. Also, the existence of traveling pulse solutions to $P_{2,\varepsilon}^-$ for large τ_2 can be proved, and in the end it boils down to solving a system of equations which is a simplification of (2.3.13). Moreover, when we increase τ_2 from an $\mathcal{O}(1)$ parameter to an $\mathcal{O}(\varepsilon^{-2})$ parameter a traveling pulse solution bifurcates from a standing pulse solution at $(\tau_2)_{0,*} = \frac{1}{\varepsilon^2}(\hat{\tau}_2)_{0,*} = \frac{1}{\varepsilon^2} \frac{2}{3} \sqrt{2} \left(\alpha_2 - \gamma_2 + \gamma_2 \log \left(\frac{\gamma_2}{\alpha_2} \right) \right)$. This bifurcation can be supercritical, as well as subcritical. See also Section 2.4 and especially the proof of Lemma 2.4.2.

Finally, the two-component system possesses no symmetric standing 2-pulse solutions to $P_{2,\varepsilon}^-$. Physically, this can be explained by the fact that the model has too few free constants (too few dimensions). The absence of 2-pulse solutions is also plausible when we look at Theorem 2.5.1. There only exists a standing 2-pulse solution if at least $\text{sgn}(\alpha) \neq \text{sgn}(\beta)$ and for the two-component system this condition cannot be fulfilled because there is no equivalent parameter for β in the two-component system.

To summarize, we have shown that the two-component model also possesses stationary and traveling pulse solutions. However, it does not support 2-pulse solutions.

Remark 2.6.1. There are two ways in which the three-component system (2.1.6) may limit on a two-component system, either by considering $W \rightarrow V$, associated to $D \downarrow 1$, or by $W \rightarrow W_0$, a constant when $D \rightarrow \infty$. In the former case one has

to make the additional assumption that $\tau = \theta$. Since in most studies of systems like (2.1.1)/(2.1.6) $D \gg 1$ and $\tau \gg \theta$, we do not consider this limit here.

If one considers the limit $D \rightarrow \infty$ in Theorems 2.2.1 and 2.3.1 for 1-pulse solutions, then it immediately follows that $W \rightarrow -1$ uniformly on \mathbb{R} – see for instance (2.2.21). However, since the two-component limit cannot have standing 2-pulse solutions, taking the limit $D \rightarrow \infty$ in Theorem 2.5.1 is less straightforward. In fact, this limit has already been discussed in section 2.5.3 (under the assumption that $A_2 = \mathcal{O}(1)$). It follows from (2.5.15) that the width of the pulses in the 2-pulse solution increases linearly with D , while the distance between the pulses approaches a finite limit. Thus, on bounded intervals, the 2-pulse solution of the three-component system limits on a 1-pulse solution of a two-component (U, V) -system that is homoclinic to $(U, V) = (+1, +1)$ (with $W \rightarrow 1 - 2\sqrt{\frac{\gamma}{\beta}}$, the constant value given in (2.5.16)).

2.7 Simulations, conclusions and discussion

2.7.1 Simulations

In this section, we show the results of some numerical simulations to further illustrate the theory presented in this chapter and also to illustrate some of the basic pulse interactions and instabilities. These simulations are carried out using the numerical software presented in [4].

We already illustrated a stationary 1-pulse solution in the left frame of Figure 2.1. Therefore, we begin here with some traveling pulses of the type constructed in Section 2.3. The pulses shown in Figure 2.14 exist for values of τ greater than the theoretically-predicted value $\hat{\tau}_{*,0} = 0.59$ for the bifurcation in which traveling pulses are created (which translates into an unscaled $\tau_{*,0} = 59$). In the left frame, the traveling pulse collides with its mirror image pulse at the boundary, since the boundary conditions are of homogeneous Neumann type, and afterwards they repel each other. By contrast, in the right frame, the pulse and its mirror image collide and then annihilate. The changeover from repulsion to annihilation after the collision occurs at $\tau_{ann}^{num} = 112$. Finally, we observe that the numerically-observed value of the bifurcation to traveling waves is $\tau_*^{num} = 103$, which is within the relative error of magnitude $\mathcal{O}(\varepsilon^{-1}) = \mathcal{O}(10)$ of the leading order theoretical value $\tau_{*,0} = 59$. Of course, in these simulations ε is not yet really small, and hence we checked that the value of τ_*^{num} decreases toward the value predicted by the leading order theory as ε is decreased. For example, for $\varepsilon = 0.01$, we find $\tau_*^{num} = 5.95 \times 10^3$ (compared to 5.9×10^3 theoretically).

Next, we illustrate the theoretical results for stationary 2-pulse solutions of (2.1.6), as derived in Section 2.5. For each of the four values of $\gamma = 0.8, 0.75, -0.25, -0.3$,

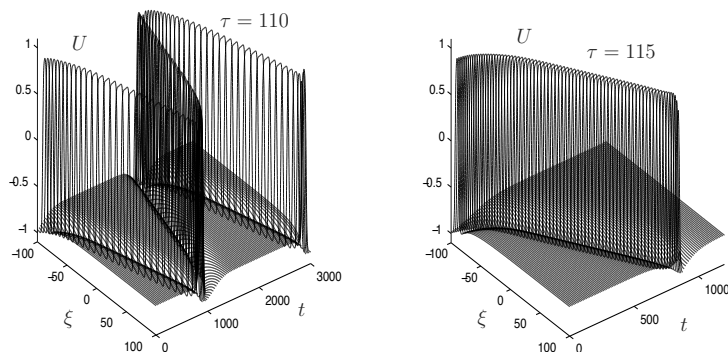


Figure 2.14: Stable traveling pulses. The parameter values are $(\alpha, \beta, \gamma, D, \theta, \varepsilon) = (6, 3, 4, 2, 1, 0.1)$, and τ is the bifurcation parameter. Here, we plotted a bouncing traveling pulse solution for $\tau = 110$ and an annihilation of a traveling pulse for $\tau = 115$.

Figure 2.15 shows the corresponding stationary solution. Based on the simulations for these parameter values, we find that the homogeneous background state $U = -1$ undergoes a subcritical bifurcation into a 2-pulse solution at $\gamma^{num} = 0.78$. Likewise, due to the reversibility symmetry, the homogeneous state $U = +1$ bifurcates supercritically into a 2-pulse solution at $\gamma^{num} = -0.78$, though we do not show this. In addition, we observe that, as we decrease γ from 0.78, the width of the pulses increases, until there is a bifurcation at $\gamma^{num} = -0.27$ at which the pulses coalesce, and the solution is $U = +1$ everywhere, except inside an interior layer and inside the layers at the boundaries of the computational interval. This solution is a spatially-periodic solution. Moreover, the observed value for this coalescence of the pulses agrees well with the theoretically-predicted value of $\gamma = -0.31$ for the saddle-node bifurcation, which occurs at the minimum in the curve shown in the right frame of Figure 2.13.

One of the most commonly-encountered bifurcations that the pulse solutions undergo is a supercritical Hopf bifurcation in which the widths, and heights, of the pulses oscillate periodically in time. In Figure 2.16, we show a breathing 1-pulse in the left frame, and a breathing 2-pulse in the right frame. For the 1-pulse solution (with $\varepsilon = 0.1$), the Hopf bifurcation occurs at $\tau_H^{num} = 47$. Moreover, we find that the breather dies out for $\tau = 49.8$. For the 2-pulse solution (with $\varepsilon = 0.01$), the Hopf bifurcation takes place at $\tau_{H,2p}^{num} = 4590$. Moreover, at $\tau = 5060$, the

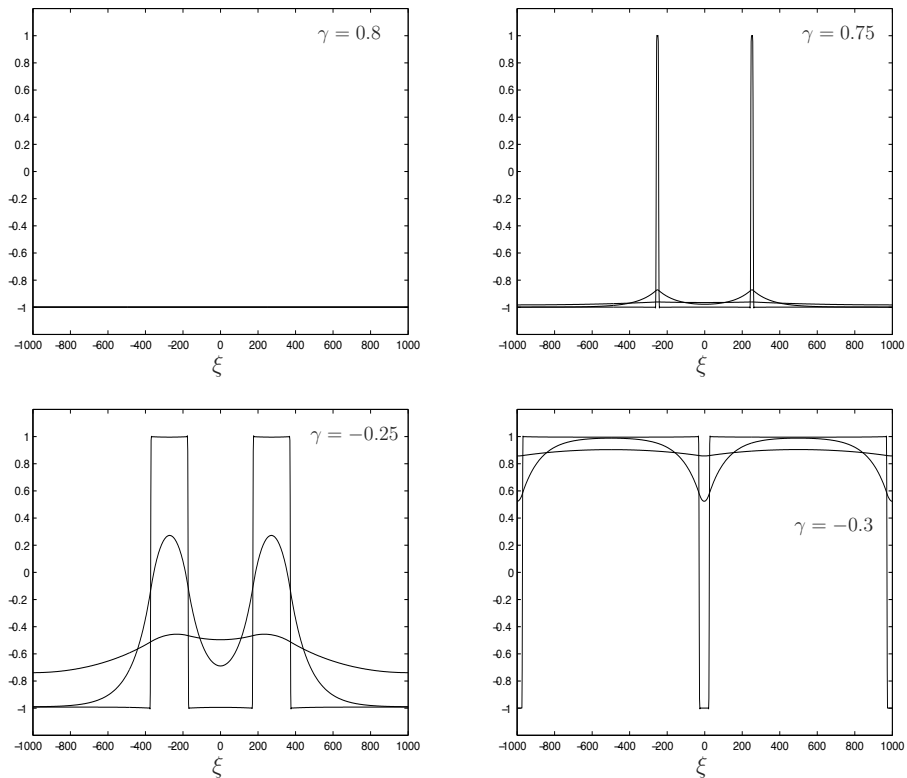


Figure 2.15: Plots of the stationary solutions of the three-component model (2.1.6) for four values of γ : $\gamma = 0.8, 0.75, -0.25, -0.3$. The values of the other parameters are $(\alpha, \beta, D, \tau, \theta, \varepsilon) = (2, -1, 5, 1, 1, 0.01)$.

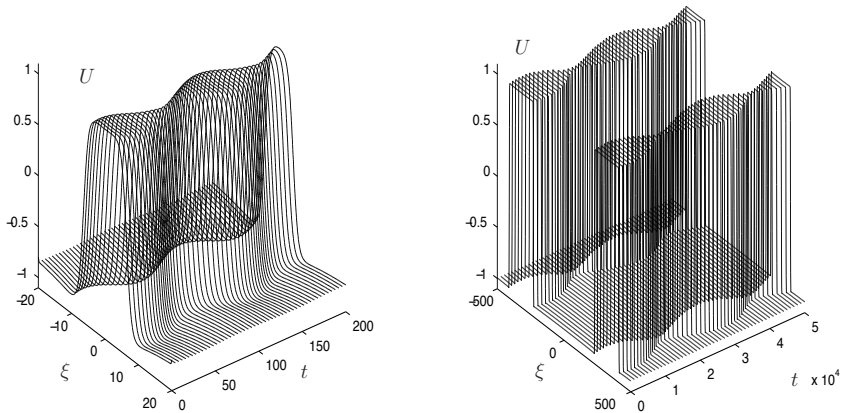


Figure 2.16: Stable breathing 1-pulse and 2-pulse solutions. For the simulation shown in the left frame, $\tau = 49.7$, and the other parameters are $(\alpha, \beta, \gamma, D, \theta, \varepsilon) = (6, 3, 4, 10, 1, 0.1)$. Also, we note that the interval used in the simulation is $\xi \in [-100, 100]$, however we have displayed only a subinterval to better display the breathing behavior. For the simulation shown in the right frame, $\tau = 5000$, and the other parameters are $(\alpha, \beta, \gamma, D, \theta, \varepsilon) = (2.2, -1, 0, 10, 1, 0.01)$. Also, we note that the interval used in the simulation is $\xi \in [-1000, 1000]$.

breathing 2-pulse solution becomes unstable and dies out. We note that we have observed breathing 2-pulse solutions for which the pulse widths breath in an antisymmetric manner.

Scattering of pulses is also observed in the three-component model (2.1.7). In the left frame of Figure 2.17, we show the V -component of a 2-pulse solution in which the pulses initially approach each other, spend a substantial amount of time at a nearly constant distance from each other with a significantly-decreased amplitude, and then regain their original amplitudes and repel each other. The pulses continue to repel each other until they reflect off the boundary, and the process repeats. A similar phenomenon has been observed in [51, 52]. There the unstable, stationary 2-pulse, which the 2-pulse data approaches, is called a ‘scattor’ (or ‘separator’). The importance of a scattor stems from the observation made in [51, 52] that the forward evolution of 2-pulse data that approaches it is determined by where that data lies with respect to the stable and unstable manifolds of the scattor or separator solution. The relation between scatters and the 2-pulse solutions constructed in this chapter is the subject of future investigation.

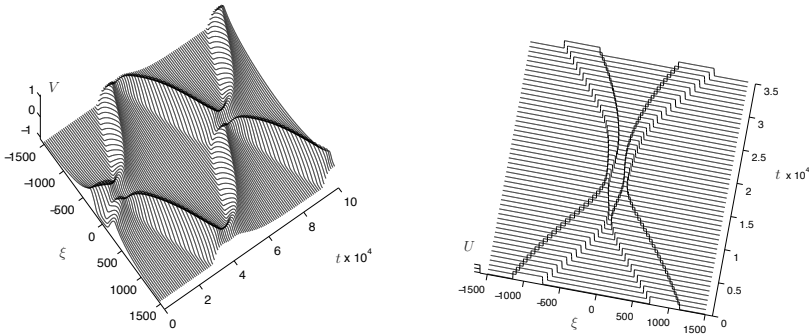


Figure 2.17: Scattering of two pulses. In the left frame, we show the V -component over a long time interval, and in the right frame we show the U -component during the third central scattering event (not shown for the V -component). The parameter values are $(\alpha, \beta, \gamma, D, \tau, \theta, \varepsilon) = (6, 3, 2, 2, 6500, 1, 0.01)$.

We emphasize that the time interval shown in Figure 2.17 is long and that the length of time where the two pulses are near to each other is also long in comparison to the time interval over which the pulses move an $\mathcal{O}(1)$ distance. Moreover, we found that the duration of this time interval can be changed by varying the parameter values. Finally, it is worth noting that, during the time that the two pulses are near the boundaries, they are also near their counterparts across the boundary, in what also appears to be a scatter state.

To conclude this brief section illustrating some of the pulse dynamics, we show the spatio-temporal evolution of 4-pulse initial data in Figure 2.18. Initially, the four pulses approach each other. Then, they start to breath in a time-periodic manner, until finally the middle two pulses die out and the two remaining pulses become stationary. In the right frame, we have zoomed in on the time interval containing the last few breathing periods, and here the destabilization process is visible in detail. The maximal widths per period of the inner two pulses increase as the time of annihilation gets closer and closer, while the minimal widths decrease. One can see that during the final oscillation the maximal pulse widths exceed the lengths of the gaps between the pulses. Finally, stepping back out to the time scale shown in the left frame, one sees that the time asymptotic state is a stable 2-pulse solution of the type constructed in Section 2.3, with pulse centers well inside $\xi = -1000$ and $\xi = 1000$ on the domain $\xi \in [-2000, 2000]$.

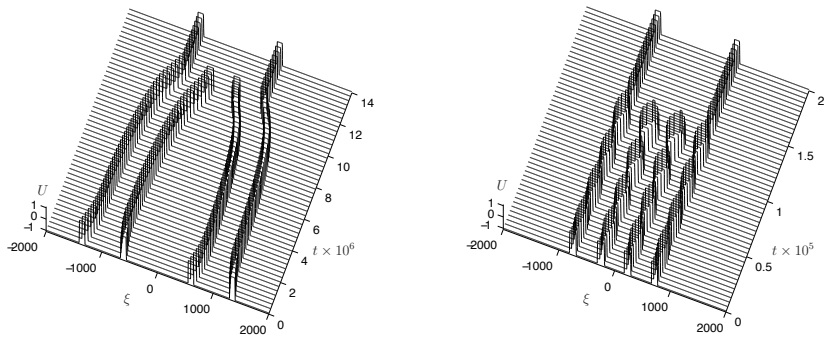


Figure 2.18: The spatio-temporal dynamics of a solution with symmetric 4-pulse initial data. The parameter values are $(\alpha, \beta, \gamma, D, \tau, \theta, \varepsilon) = (2.1, -1, 0, 5, 3900, 1, 0.01)$. Note that we actually give an asymmetric 2-pulse as initial condition and just ‘mirrored’ the domain, this can be done because of the Neumann boundary conditions. Note that the time interval shown in the left frame is so long that the breathing is not visible. Therefore, in the right frame, we zoomed in on the time interval $[11.2 \times 10^6, 11.4 \times 10^6]$ for the same solution, so that the breathing is clearly visible.

2.7.2 Conclusions and discussion

In this chapter, we established the existence of stationary and traveling 1-pulse solutions of the three-component model (2.1.6), as well as the existence of stationary 2-pulse solutions. The main results are presented in Theorem 2.2.1, Lemma 2.2.2, and Theorem 2.3.1 for the 1-pulse solutions, and in Theorem 2.5.1 for the 2-pulse solutions. Moreover, we studied various bifurcations of these solutions, including the saddle-node bifurcation in which the stationary 1-pulse solutions are created (see Theorem 2.2.1), the bifurcation from stationary to traveling 1-pulses (showing that this may be either subcritical or supercritical depending on the system parameters, see Lemma 2.4.1 and Corollary 2.4.2), and the saddle-node bifurcation of 2-pulse solutions, see Figure 2.13.

In the course of this analysis, we also showed that this three-component system constitutes an ideal system on which to study pulse dynamics. On one hand, it is sufficiently simple for analysis using geometric singular perturbation theory, with all of the reaction terms, except for one, being linear. On the other hand, it is sufficiently nonlinear to support rich pulse dynamics. Indeed, the extent of this richness was first demonstrated in [51, 52, 54, 60], and these interacting pulse solutions exist also for the scaled equations (2.1.6) studied here. We think that the analysis presented in this chapter offers a useful starting point for the analysis of these various pulse interaction scenarios.

Finally, we considered the limit in which the three-component system (2.1.6) reduces to the more classical two-component system (2.6.1). This two-component system is almost the same as the FHN, except that the second species (inhibitor) also diffuses here. It is shown that the two-component system possesses only the 1-pulse solutions, and not the 2-pulse solutions of the type studied here. Hence, the addition of the third component, as introduced in [60], is essential for the existence of 2-pulse solutions.

Stability of the solutions studied here is an important topic, as is demonstrated for instance by the bifurcations to breathing pulses shown in Figure 2.16. This is the topic of the next chapter, in which we use the Evans function and the Non-Local Eigenvalue Problem method [12] to carry out this analysis.

The methods and analysis of this chapter can be extended to carry out the analysis of pulse solutions in the three-component model with heterogeneity that is studied in [71]. There, heterogeneity is introduced in (2.1.1) by making the constant term in the U -component vary in space according to a smoothed out step function. The heterogeneity induces interesting new pulse dynamics, such as rebounding off defects, pinning by defects, and penetration of defects, as observed in numerical simulations. The invariant manifold theory from the field of geometric singular perturbation theory that we have used in this chapter, as well as the Melnikov

conditions that we used, can also be applied to these types of heterogeneous systems, so that the pulse solutions may be constructed. In conjunction with these observations, we point to an earlier example in which geometric singular perturbation theory was used to establish the existence of standing wave solutions in a RDE of the Fabry-Perot interferometer, which involves spatially-dependent coefficients. See [58].

Chapter 3

Stability

3.1 Introduction

The analysis of the dynamics and interactions of spatially-localized structures, such as pulses or fronts, consists of a hierarchy of problems. As a first step, the existence of stationary, or uniformly traveling, localized solutions must be considered. If the dynamics are governed by a partial differential equation (PDE) in which the space variable is 1-dimensional, this is equivalent to constructing a homoclinic orbit (for a pulse) or a heteroclinic orbit (for a front) in an ordinary differential equation (ODE) reduction. As a next step, it is necessary to obtain information about the stability of these homoclinic or heteroclinic orbits as solutions of the PDE. A full mathematical understanding of the dynamics and interactions of the localized structures can only be developed if these first two issues, existence and stability, are in some way settled.

From this point of view, this work may be considered as the natural next step following the existence analysis of Chapter 2. In that chapter, the existence of various types of localized structures of (multi-)pulse type (or of multi-front type, see Figure 3.1) is established for a three-component reaction-diffusion equation (RDE) that was originally introduced in [60]. By the scalings introduced in the previous chapter, this equation can be written (in one space dimension) as

$$\begin{cases} U_t = U_{\xi\xi} + U - U^3 - \varepsilon(\alpha V + \beta W + \gamma), \\ \tau V_t = \frac{1}{\varepsilon^2} V_{\xi\xi} + U - V, \\ \theta W_t = \frac{D^2}{\varepsilon^2} W_{\xi\xi} + U - W, \end{cases} \quad (3.1.1)$$

with $0 < \varepsilon \ll 1$, $D > 1$, $0 < \tau, \theta \ll \varepsilon^{-3}$, $\alpha, \beta, \gamma \in \mathbb{R}$ and $\mathcal{O}(1)$ with respect to ε , and $(\xi, t) \in \mathbb{R} \times \mathbb{R}^+$ (see Remark 3.1.1). In this chapter, the stability of the pulse solutions to (3.1.1) that were constructed in the previous chapter is considered.

In recent years, system (3.1.1) has been studied, mostly by numerical simulations, as a paradigm model in three components, see [5, 32, 50, 51, 53, 54, 60, 65]. The dynamics exhibited by the localized solutions to equation (3.1.1) are remarkably rich. This phenomenon may perhaps be related to the intuition that three-component RDEs may have more ‘freedom’ to generate complex dynamics than one- or two-component equations. This intuition can be considered as a mathematical fact if one compares two-component systems to scalar, one-component, systems (for instance since scalar RDEs in one (unbounded) spatial dimension cannot have stable localized solutions of pulse type, whereas two-component systems can, as for example in the Gray-Scott and Gierer-Meinhardt equations). However, there is no decisive mathematical evidence that three-component RDEs indeed may generate behavior that cannot be observed in two-component systems (see also Remark 3.1.3). In fact, the mathematical literature on pattern formation in RDEs is almost completely devoted to the study of scalar and two-component systems (see however [29], in which a three-component model with two fast and one slow component is studied).

This latter observation provides a second – and, from the mathematical point of view perhaps, more important – motivation for the analysis in this chapter. We develop an approach by which the stability of (multi-)front or (multi-)pulse patterns of a three-component system can be established. Although we focus the attention on the explicit model (3.1.1), the ideas can readily be extended to the stability analysis of localized structures in other singularly perturbed N -component systems. However, as in previous work on two-component systems [12–14], the assumption that the system is singularly perturbed, *i.e.*, that $0 < \varepsilon \ll 1$ in (3.1.1), is essential.

Apart from the richness of its dynamics, equation (3.1.1) is remarkable in the sense that the methods allow us to determine the spectra associated with the stability of the (multi-)pulse solutions in terms of explicit expressions (Remark 3.1.1). Thus, although (3.1.1) has three components, we will for instance show, for the stationary 1-pulse solution plotted in Figure 3.1, that it is possible to explicitly determine whether it bifurcates into a traveling pulse solution, see Chapter 2 and [50], or into a breathing pulse solution (by a Hopf bifurcation). Moreover, both types of bifurcations are induced by a preceding edge bifurcation, *i.e.*, the creation of a ‘new’ eigenvalue from the essential spectrum, that can also be investigated in full analytical detail – see Section 3.5. We also obtain analytical expressions for the four eigenvalues associated to the stability of the 2-pulse solution of Figure 3.1, based on which we can formulate general results (in terms of the parameters in (3.1.1)) on the stability and instability of these 2-pulse solutions (Section 3.6). This combination of being accessible for detailed mathematical analysis and of exhibiting rich and complex dynamics indeed makes system (3.1.1) a paradigm for the study of pulse dynamics in three-component RDEs.

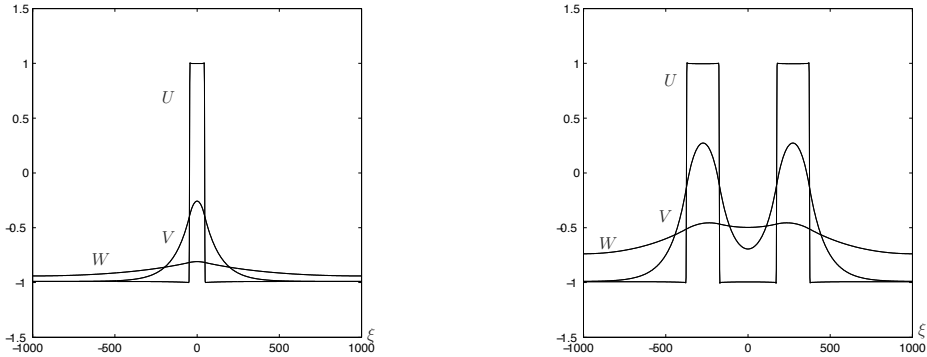


Figure 3.1: Stable stationary 1-pulse and 2-pulse solutions of system (3.1.1) obtained via numerical simulation. For the 1-pulse the parameters were $(\alpha, \beta, \gamma, D, \tau, \theta, \varepsilon) = (3, 1, 2, 5, 1, 1, 0.01)$, and for the 2-pulse we had $(\alpha, \beta, \gamma, D, \tau, \theta, \varepsilon) = (2, -1, -0.25, 5, 1, 1, 0.01)$.

The approach to the stability of localized patterns in (3.1.1) is based on the Evans function $\mathcal{D}(\lambda)$, of which the zeroes correspond to the eigenvalues of the linearized operator associated to the stability of a localized solution. The Evans function is analytic as function of λ outside the essential spectrum σ_{ess} of this linearized operator [1, 59]. It has already been shown in [1] that $\mathcal{D}(\lambda)$ can be decomposed into the product of a fast and a slow Evans function, $\mathcal{D}_{\text{fast}}(\lambda)$ and $\mathcal{D}_{\text{slow}}(\lambda)$, if the governing RDE is singularly perturbed. In [11–13], a method, called the NLEP method, was developed in the context of two-component RDEs by which both components, and their zeroes, can be determined explicitly. In fact, it was shown that $\mathcal{D}(\lambda)$ could be written, up to a nonzero constant, as the product of two transmission functions $t_1(\lambda)$ and $t_2(\lambda)$, where $t_1(\lambda)$ is analytic and corresponds to $\mathcal{D}_{\text{fast}}(\lambda)$, while $t_2(\lambda)$ is meromorphic and corresponds to $\mathcal{D}_{\text{slow}}(\lambda)$. Equation (3.1.1) has two slow components ($V(\xi, t)$ and $W(\xi, t)$) so that one expects, by the ideas of [12, 13], that there again is one fast transmission function $t_1(\lambda)$ and four slow-fast transmission functions $t_{ij}(\lambda)$, $i, j = 2, 3$ – see Section 3.3. One of the main results of this chapter is the following explicit decomposition of $\mathcal{D}(\lambda)$,

$$\mathcal{D}(\lambda) = d(\lambda)\mathcal{D}_{\text{fast}}(\lambda)\mathcal{D}_{\text{slow}}(\lambda) = d(\lambda)t_1(\lambda)[t_{22}(\lambda)t_{33}(\lambda) - t_{23}(\lambda)t_{32}(\lambda)],$$

where $d(\lambda)$ is nonzero and smooth (outside σ_{ess}) – see also Remark 3.1.2. Moreover, all transmission functions can be determined (to leading order in the asymptotically small parameter ε) by an extension of the NLEP method to three-component systems. In fact, another extension of the NLEP method is necessary: the 1-pulse solutions to (3.1.1) are of 2-front type – Figure 3.1 – so that the con-

cept of ‘intermediate transmission functions’ has to be introduced, see Section 3.4. As a consequence, all slow-fast transmission functions $t_{ij}(\lambda)$ have second order poles, that are cancelled by the zeroes of $t_1(\lambda)$ – this phenomenon was called the NLEP paradox in [12, 13] (in which only simple poles appeared).

The major part of this chapter is devoted to analytically computing the zeroes of the slow Evans function $\mathcal{D}_{\text{slow}}(\lambda)$. In Section 3.4, it is shown for $\tau, \theta = \mathcal{O}(1)$ with respect to ε , that, to leading order, $\mathcal{D}_{\text{slow}}(\lambda) = t_{22}(\lambda)t_{33}(\lambda) - t_{23}(\lambda)t_{32}(\lambda)$ has a zero at

$$\lambda = \varepsilon^2 \hat{\lambda}^- = -3\sqrt{2}\varepsilon^2 \left(\alpha A^2 + \frac{\beta}{D} A^{\frac{2}{D}} \right), \text{ with } A \in (0, 1) \text{ such that } \alpha A^2 + \beta A^{\frac{2}{D}} = \gamma,$$

a result that determines the stability of the 1-pulse solution represented in Figure 3.1 – see Theorem 3.4.1. This 1-pulse solution may lose its stability when τ, θ become $\mathcal{O}(\frac{1}{\varepsilon^2})$. The stability/bifurcation analysis of the standing 1-pulse solution, and the associated traveling pulse solution derived in the previous chapter is the main topic of Section 3.5. Although the expressions that determine the eigenvalues, which now include new eigenvalues that have appeared from σ_{ess} , have become more involved than in the case $\tau, \theta = \mathcal{O}(1)$, the ‘NLEP-machinery’ enables us to explicitly determine the co-dimension 1 regions in parameter space at which the pulse undergoes a Hopf, saddle-node, or drift (*i.e.*, a bifurcation into a traveling pulse) bifurcation. In the final section, Section 3.6, the stability of the 2-pulse (or 4-front) pattern is established, where, for simplicity, we restricted ourselves to the case $\tau, \theta = \mathcal{O}(1)$.

Combined with Chapter 2, the results of this chapter provide a foundation for a mathematical analysis of the pulse dynamics generated by (3.1.1) – see [5, 32, 50, 51, 53, 54, 60, 65] and Remark 3.1.1. Due to the singularly perturbed nature of (3.1.1), it exhibits pulse- and/or front-interactions of a semi-strong nature [15, 16, 47]. Unlike the situation of weak pulse interactions [19, 20, 55, 59], in which the pulses are assumed to be ‘sufficiently far apart’, so that the pulses to leading order can be considered as ‘particles’, pulses that undergo semi-strong interactions typically change shape and even may bifurcate, see also [38, 62]. Note that such an analysis of semi-strong pulse interactions differs from, and is complementary to, the analysis of [20, 50], in which the pulse interactions are of a weak nature, but in which it is assumed that the parameters in the system are such that the pulses are close to a bifurcation (sometimes of co-dimension ≥ 1). The semi-strong approach of [15, 16, 47] allows one to study nontrivial pulse dynamics (including the bifurcations induced by the interactions [15]), for parameters that are not necessarily close to a bifurcation value of the limiting isolated pulses. However, unlike the approach of [20, 50], it is necessary for the semi-strong analysis to have full control over the existence and stability of the interacting structures. Therefore, the semi-strong analysis must be preceded by results such as those in the previous chapter and in the present chapter, while

the approach of [20, 50] may for a large part be based on assumptions on the properties of the linearized system associated to the stability of the pulses.

Finally, it should be noted that the multi-front nature of the pulse solutions to (3.1.1) – Figure 3.1 – imply that instead of for instance considering the semi-strong interactions of two pulse solutions, one should study the (semi-strong) interactions of four localized heteroclinic fronts – see for instance the simulations represented in Figures 2.17 and 2.18 of the previous chapter. A stable 2-pulse solution of the type depicted in Figure 3.1 is expected to appear as an attracting fixed point in the system of ODEs that governs the interaction between these four fronts. This is the subject of Chapter 4.

Remark 3.1.1. Equation (3.1.1) has a particularly simple structure. The slow components V and W only have linear reaction terms, while the coupling between the fast component U to the slow components in the fast (U -)equation is only $\mathcal{O}(\varepsilon)$ weak. This form of the equation has been proposed in Chapter 2. Certainly not all versions of (3.1.1) considered in the literature [5, 32, 50, 51, 53, 54, 60] are of the type considered here. Especially the assumption that the coupling term ‘ $\varepsilon(\alpha V + \beta W + \gamma)$ ’ in the U -equation is $\mathcal{O}(\varepsilon)$ small, may *a priori* seem to be too restrictive. However, it is argued in Chapter 2 that this is not the case. Moreover, it is shown that the richness of dynamics of the system with weak coupling is comparable to those studied in the literature. We refer to Chapter 2 for more details on the choices of the parameters.

Remark 3.1.2. The fact that the four slow-fast transmission functions $t_{ij}(\lambda)$, $i, j = 2, 3$, appear as a determinant of a 2×2 -matrix in the expression for the slow Evans function $\mathcal{D}_{\text{slow}}(\lambda)$ follows by an orthogonalization procedure of Gram-Schmidt type in a 2-dimensional manifold of slowly growing solutions to the linearized stability problem (see Section 3.3). A similar argument applied to the linear system associated to the stability of a pulse (or front) solution to an N -component system with $N - 1$ slow components, yields that $\mathcal{D}_{\text{slow}}(\lambda)$ will be given by the determinant of an $(N - 1) \times (N - 1)$ matrix of $(N - 1)^2$ slow-fast transmission functions. Moreover, it is shown in Remark 3.4.3 that the 2×2 -determinant of our three-component system reduces to one transmission function $t_2(\lambda) = t_{22}(\lambda)$ in the situation in which (3.1.1) approaches a two-component limit (Remark 3.1.3).

Remark 3.1.3. At several places in the text, see especially Remark 3.4.3, Remark 3.5.1, and Lemma 3.6.3, we consider the limit $D \gg 1$. This case may be seen as a two-component limit of (3.1.1), since the W -component of a 1-pulse solution converges uniformly to $W \equiv -1$, see (3.2.10) (and the previous chapter). The results for this two-component limit can be seen as ‘regular limits’ of the results for the full system. However, it was shown in the previous chapter that the 2-pulse solutions cannot exist in the two-component model. This is confirmed by Lemma 3.6.3, in which it is shown that the parameter region of stable 2-pulse solutions shrinks to zero as $D \rightarrow \infty$.

3.2 Review of existence theory

The existence analysis for various types of pulse solutions was presented in Chapter 2. Here, we summarize the results. Moreover, we also derive some integral relations, (3.2.18), (3.2.28), and (3.2.35), for the higher order correction terms of the constructed homoclinic pulses. This information will be needed for the stability analysis.

3.2.1 Standing 1-pulse solutions

We start with the existence results for standing 1-pulse solutions. For standing pulse solutions, system (3.1.1) transforms into a 6-dimensional ODE

$$\begin{cases} u_\xi &= p, \\ p_\xi &= -u + u^3 + \varepsilon(\alpha v + \beta w + \gamma), \\ v_\xi &= \varepsilon q, \\ q_\xi &= \varepsilon(v - u), \\ w_\xi &= \frac{\varepsilon}{D} r, \\ r_\xi &= \frac{\varepsilon}{D}(w - u). \end{cases} \quad (3.2.1)$$

This system has three fixed points

$$P_\varepsilon^\pm = (u_\varepsilon^\pm, 0, u_\varepsilon^\pm, 0, u_\varepsilon^\pm, 0), \quad P_\varepsilon^0 = (u_\varepsilon^0, 0, u_\varepsilon^0, 0, u_\varepsilon^0, 0), \quad (3.2.2)$$

where u_ε^\pm and u_ε^0 are given by

$$u_\varepsilon^\pm = \pm 1 \mp \frac{1}{2}\varepsilon(\alpha + \beta \pm \gamma) + \mathcal{O}(\varepsilon^2), \quad u_\varepsilon^0 = \varepsilon\gamma + \mathcal{O}(\varepsilon^2). \quad (3.2.3)$$

Moreover, for 1-pulse solutions, we can divide the spatial domain into five intervals, three slow intervals and two fast intervals. The fast intervals are given by

$$I_f^- := \left(-\xi_* - \frac{1}{\sqrt{\varepsilon}}, -\xi_* + \frac{1}{\sqrt{\varepsilon}} \right) \quad \text{and} \quad I_f^+ := \left(\xi_* - \frac{1}{\sqrt{\varepsilon}}, \xi_* + \frac{1}{\sqrt{\varepsilon}} \right), \quad (3.2.4)$$

where ξ_* is the so-called jumping point. In physical terms this is the half-width of the pulse under investigation, see Figure 3.1. More mathematically, $\xi_* > 0$ is the point where $u_h(\xi_*) = 0$, given that $(u_h)_\xi(0) = 0$, with $u_h(\xi)$ the u -component of the homoclinic pulse solution of (3.2.1). The three slow intervals $I_s^{\pm,0}$ are

$$\begin{aligned} I_s^- &:= \left(-\infty, -\xi_* - \frac{1}{\sqrt{\varepsilon}} \right], & I_s^0 &:= \left[-\xi_* + \frac{1}{\sqrt{\varepsilon}}, \xi_* - \frac{1}{\sqrt{\varepsilon}} \right], \\ I_s^+ &:= \left[\xi_* + \frac{1}{\sqrt{\varepsilon}}, \infty \right), \end{aligned} \quad (3.2.5)$$

and they are the complements of the two fast intervals.

The existence theorem for the standing 1-pulse solutions reads

Theorem 3.2.1. *Let $\varepsilon > 0$ be small, and let $(\alpha, \beta, \gamma, D)$ be such that*

$$\alpha A^2 + \beta A^{\frac{2}{D}} = \gamma + \mathcal{O}(\sqrt{\varepsilon}). \quad (3.2.6)$$

has K solutions $A \in (0, 1)$ ($K \in \{0, 1, 2\}$). If $K = 0$, there are no symmetric orbits homoclinic to P_ε^- in system (3.2.1). If $K > 0$, then, for ε small enough, there are K symmetric homoclinic orbits $\gamma_h(\xi)$ to P_ε^- , that is, there are orbits $\gamma_h(\xi)$ that consist of five distinct parts, two fast parts where $\xi \in I_f^\pm$, in which it is $\mathcal{O}(\varepsilon)$ close to a fast reduced heteroclinic orbit $(u_{\text{fast}}^\mp(\xi \pm \xi_), p_{\text{fast}}^\mp(\xi \pm \xi_*), v_*, \pm q_*, w_*, \pm r_*)$, with*

$$u_{\text{fast}}^\pm(\xi) = \mp \tanh\left(\frac{1}{2}\sqrt{2}\xi\right), \quad p_{\text{fast}}^\pm(\xi) = \mp \frac{1}{2}\sqrt{2}\operatorname{sech}^2\left(\frac{1}{2}\sqrt{2}\xi\right), \quad (3.2.7)$$

$$v_* = -A^2, \quad w_* = -A^{\frac{2}{D}}, \quad q_* = v_* + 1, \quad r_* = w_* + 1 \quad \text{and} \quad A := e^{-\varepsilon\xi_*}, \quad (3.2.8)$$

and three slow parts where $\xi \in I_s^{\pm,0}$, in which $(u_h(\xi), p_h(\xi)) = (\pm 1, 0) + \mathcal{O}(\varepsilon)$ and $(v_h(\xi), q_h(\xi), w_h(\xi), r_h(\xi))$ are given by

$$v_h(\xi) = \begin{cases} 2e^{\varepsilon\xi} \sinh \varepsilon\xi_* - 1 & \text{in } I_s^-, \\ -2e^{-\varepsilon\xi} \cosh \varepsilon\xi + 1 & \text{in } I_s^0, \\ 2e^{-\varepsilon\xi} \sinh \varepsilon\xi_* - 1 & \text{in } I_s^+, \end{cases} \quad (3.2.9)$$

and

$$w_h(\xi) = \begin{cases} 2e^{\frac{\varepsilon}{D}\xi} \sinh \frac{\varepsilon}{D}\xi_* - 1 & \text{in } I_s^-, \\ -2e^{-\frac{\varepsilon}{D}\xi} \cosh \frac{\varepsilon}{D}\xi + 1 & \text{in } I_s^0, \\ 2e^{-\frac{\varepsilon}{D}\xi} \sinh \frac{\varepsilon}{D}\xi_* - 1 & \text{in } I_s^+, \end{cases} \quad (3.2.10)$$

up to $\mathcal{O}(\sqrt{\varepsilon})$ corrections. The orbits $\gamma_h(\xi)$ correspond to stationary 1-pulse solutions

$$(U(\xi, t), V(\xi, t), W(\xi, t)) \equiv (u_h(\xi), v_h(\xi), w_h(\xi))$$

of (3.1.1).

Moreover, if $|\alpha D| > |\beta|$ and $\operatorname{sgn}(\alpha) \neq \operatorname{sgn}(\beta)$, then a saddle-node bifurcation of homoclinic orbits occurs as γ crosses through

$$\begin{aligned} \gamma_{c1}(\alpha, \beta, D) &= (-\alpha)^{-\frac{1}{D-1}} \beta^{\frac{D}{D-1}} \left(D^{-\frac{1}{D-1}} - D^{-\frac{D}{D-1}} \right) > 0 \quad \text{for } \alpha < 0 < \beta, \\ \gamma_{c2}(\alpha, \beta, D) &= \alpha^{-\frac{1}{D-1}} (-\beta)^{\frac{D}{D-1}} \left(D^{-\frac{D}{D-1}} - D^{-\frac{1}{D-1}} \right) < 0 \quad \text{for } \beta < 0 < \alpha. \end{aligned} \quad (3.2.11)$$

Finally,

$$A_c(\alpha, \beta, \gamma_{c1, c2}, D) = \left(-\frac{\alpha D}{\beta} \right)^{-\frac{1}{2} \frac{D}{D-1}} \in (0, 1). \quad (3.2.12)$$

The PDE (3.1.1) is translation invariant, yielding that the derivative of the pulse is a solution to the linearized stability problem with eigenvalue $\lambda = 0$ [59]. It is useful to label the derivatives of the u -components in the fast fields. Note that these derivatives are by definition $p_{\text{fast}}^{\pm}(\xi)$, thus

$$\psi^{-}(\xi) := \frac{1}{2}\sqrt{2}\operatorname{sech}^2\left(\frac{1}{2}\sqrt{2}(\xi + \xi_*)\right), \quad \psi^{+}(\xi) := \frac{1}{2}\sqrt{2}\operatorname{sech}^2\left(\frac{1}{2}\sqrt{2}(\xi - \xi_*)\right). \quad (3.2.13)$$

Observe that $\psi^{+}(\xi)$ is actually $-\frac{d}{d\xi}(u_{\text{fast}}^{+}(\xi - \xi_*))$. However, with this choice of $\psi^{+}(\xi)$, we have that $\psi^{+}(\xi)$, as well as $\psi^{-}(\xi)$, are strictly positive, and for both functions we have to leading order

$$\int_{I_f^{\pm}} \psi^{\pm}(\xi) d\xi = 2 \quad \text{and} \quad \int_{I_f^{\pm}} (\psi^{\pm}(\xi))^2 d\xi = \frac{2}{3}\sqrt{2}. \quad (3.2.14)$$

This completes the review of the existence theory for standing 1-pulse solutions, as presented in the previous chapter.

For the stability theory, we will also need some information about the second order correction term of the u -component, $u_{h,2}^{\pm}(\xi)$, of the standing 1-pulse in the fast regions I_f^{\pm} . In particular, we need an integral relation involving these terms. We differentiate (3.2.1) once with respect to ξ . Also, we scale $(v_h)_{\xi}(\xi) = \varepsilon(\tilde{v}_h)_{\xi}(\xi)$ and $(w_h)_{\xi}(\xi) = \varepsilon(\tilde{w}_h)_{\xi}(\xi)$, since these components vary slowly in ξ (and since one can show that these components cannot be larger than $\mathcal{O}(\varepsilon)$ – see Section 3.4 and especially Remark 3.4.2, where a similar property is deduced for the slow components of basis functions associated to small eigenvalues). We obtain

$$\begin{cases} ((u_h)_{\xi})_{\xi\xi} + (u_h)_{\xi}(1 - 3u_h^2) &= \varepsilon^2(\alpha(\tilde{v}_h)_{\xi} + \beta(\tilde{w}_h)_{\xi}), \\ ((\tilde{v}_h)_{\xi})_{\xi\xi} &= -\varepsilon(u_h)_{\xi} + \varepsilon^2(\tilde{v}_h)_{\xi}, \\ ((\tilde{w}_h)_{\xi})_{\xi\xi} &= -\frac{\varepsilon}{D^2}(u_h)_{\xi} + \frac{\varepsilon^2}{D^2}(\tilde{w}_h)_{\xi}. \end{cases} \quad (3.2.15)$$

For the fast u -component, we may assume a perturbation expansion of the form

$$u_h^{\pm}(\xi) = u_{h,0}^{\pm}(\xi) + \varepsilon^2 u_{h,2}^{\pm}(\xi) + \mathcal{O}(\varepsilon^3),$$

where $u_{h,0}^{\pm}(\xi)$ are given in Theorem 3.2.1, in particular, they are translations of $u_{\text{fast}}^{\pm}(\xi)$ (3.2.7).

At second order in the fast regions I_f^{\pm} , we find

$$\begin{aligned} \mathcal{L}^{-} \left(u_{h,2}^{-} \right)_{\xi} &= \alpha \left((\tilde{v}_h^{-})_{\xi}(-\xi_*) \right) + \beta \left((\tilde{w}_h^{-})_{\xi}(-\xi_*) \right) + 6u_{h,0}^{-} u_{h,2}^{-} (u_{h,0}^{-})_{\xi}, \\ \mathcal{L}^{+} \left(u_{h,2}^{+} \right)_{\xi} &= \alpha \left((\tilde{v}_h^{+})_{\xi}(\xi_*) \right) + \beta \left((\tilde{w}_h^{+})_{\xi}(\xi_*) \right) + 6u_{h,0}^{+} u_{h,2}^{+} (u_{h,0}^{+})_{\xi}. \end{aligned} \quad (3.2.16)$$

Here, \mathcal{L}^{\pm} are given by

$$\mathcal{L}^{\pm} u := u_{\xi\xi} + (1 - 3(u_{h,0}^{\pm})^2)u, \quad (3.2.17)$$

and, up to $\mathcal{O}(\sqrt{\varepsilon})$ corrections,

$$\begin{aligned} (\tilde{v}_h^-)_\xi(-\xi_*) &= 1 - e^{-2\varepsilon\xi_*}, & (\tilde{v}_h^+)_\xi(\xi_*) &= e^{-2\varepsilon\xi_*} - 1, \\ (\tilde{w}_h^-)_\xi(-\xi_*) &= \frac{1}{D}(1 - e^{-2\frac{\varepsilon}{D}\xi_*}), & (\tilde{w}_h^+)_\xi(\xi_*) &= \frac{1}{D}(e^{-2\frac{\varepsilon}{D}\xi_*} - 1), \end{aligned}$$

where we used (3.2.9) and (3.2.10). Since $\mathcal{L}^\pm\psi^\pm = 0$, we deduce for (3.2.16) by the Fredholm Alternative or Solvability condition that

$$\int_{I_f^\pm} u_{h,0}^\pm u_{h,2}^\pm (\psi^\pm)^2 d\xi = -\frac{1}{3} \left(\alpha(1 - e^{-2\varepsilon\xi_*}) + \frac{\beta}{D}(1 - e^{-2\frac{\varepsilon}{D}\xi_*}) \right). \quad (3.2.18)$$

3.2.2 Traveling 1-pulse solutions

For traveling 1-pulse solutions of (3.1.1), we introduce the co-moving variable $\xi_{tp} = \xi - \varepsilon ct$. In this co-moving frame we analyze stationary solutions, that is, we investigate the following system

$$\begin{cases} u_\xi &= p, \\ p_\xi &= -u + u^3 + \varepsilon(\alpha v + \beta w + \gamma - cp), \\ v_\xi &= \varepsilon q, \\ q_\xi &= \varepsilon(v - u) - \varepsilon^3 c\tau q, \\ w_\xi &= \frac{\varepsilon}{D}r, \\ r_\xi &= \frac{\varepsilon}{D}(w - u) - \frac{\varepsilon^3}{D^2}c\theta r, \end{cases} \quad (3.2.19)$$

where we dropped the underscore tp in ξ_{tp} . Also, for the dynamics of a traveling 1-pulse solution, we need to distinguish five different regions. They are still given by I_f^\pm , $I_s^{\pm,0}$ (3.2.4), (3.2.5). However, the point $\xi = 0$ is now a bit artificial. For standing pulse solutions we have, by the reversibility symmetry, that $(p(0), q(0), r(0)) = (0, 0, 0)$, this is not longer true for traveling pulse solutions, see Chapter 2.

It follows from the existence analysis that we need to rescale τ and θ . More precisely, $\tau := \frac{1}{\varepsilon^2}\hat{\tau}$, $\theta := \frac{1}{\varepsilon^2}\hat{\theta}$ with, $\hat{\tau}, \hat{\theta} = \mathcal{O}(1)$, see the previous chapter. The existence theorem (Theorem 2.3.1 from Chapter 2) for the traveling pulse reads

Theorem 3.2.2. *Let $\varepsilon > 0$ be small enough, and let $(\alpha, \beta, \gamma, D, \tau, \theta, \varepsilon)$ be such that $\tau = \frac{\hat{\tau}}{\varepsilon^2}$, $\theta = \frac{\hat{\theta}}{\varepsilon^2}$. Moreover, assume that*

$$\begin{cases} \frac{1}{3}\sqrt{2}c = \alpha \left(s_w^- \left(e^{-2\varepsilon\lambda_v^+\xi_*} - 1 \right) - 1 \right) + \beta \left(s_w^- \left(e^{-2\varepsilon\lambda_w^+\xi_*} - 1 \right) - 1 \right) + \gamma, \\ -\frac{1}{3}\sqrt{2}c = \alpha \left(s_v^+ \left(e^{2\varepsilon\lambda_v^-\xi_*} - 1 \right) - 1 \right) + \beta \left(s_w^+ \left(e^{2\varepsilon\lambda_w^-\xi_*} - 1 \right) - 1 \right) + \gamma \end{cases} \quad (3.2.20)$$

has K solution pairs $(c_j, (\xi_*)_j)$ with $c_j \neq 0$, where $\lambda_{v,w}^\pm$ are defined by

$$\lambda_v^\pm = \frac{1}{2}(-c\hat{\tau} \pm \sqrt{c^2\hat{\tau}^2 + 4}), \quad \lambda_w^\pm = \frac{1}{2}\frac{1}{D} \left(-\frac{c\hat{\theta}}{D} \pm \sqrt{\frac{c^2\hat{\theta}^2}{D^2} + 4} \right), \quad (3.2.21)$$

and $s_{v,w}^\pm$ are defined by

$$s_v^\pm = -\frac{2\lambda_v^\pm}{\lambda_v^\pm - \lambda_v^\mp} < 0, \quad s_w^\pm = -\frac{2\lambda_w^\pm}{\lambda_w^\pm - \lambda_w^\mp} < 0. \quad (3.2.22)$$

If $K = 0$, then there are no homoclinic orbits to P_ε^- in (3.2.19) with $c \neq 0$. If $K > 0$, there are K homoclinic orbits $\gamma_{tp}(\xi)$ to P_ε^- in (3.2.19) that correspond to traveling 1-pulse solutions of (3.1.1) which travel with speed $\varepsilon c_j^* \neq 0$, where $c_j^* = c_j^*(\varepsilon) = c_j + \mathcal{O}(\varepsilon)$.

The homoclinic orbits $\gamma_{tp}(\xi)$ consist of five distinct parts, two fast parts in which they are $\mathcal{O}(\varepsilon)$ close to a fast reduced heteroclinic orbits ($u_{\text{fast}}^\pm(\xi \mp \xi_*)$, $p_{\text{fast}}^\pm(\xi \mp \xi_*)$, v_*^\pm , q_*^\pm , w_*^\pm , r_*^\pm) (3.2.7), with $(v_*^\pm, q_*^\pm, w_*^\pm, r_*^\pm)$ given by

$$\begin{aligned} v_*^\pm &= s_v^\pm \left(e^{\pm 2\varepsilon \lambda_v^\mp \xi_*} - 1 \right) - 1, & q_*^\pm &= \lambda_v^\mp (v_*^\pm + 1), \\ w_*^\pm &= s_w^\pm \left(e^{\pm 2\varepsilon \lambda_w^\mp \xi_*} - 1 \right) - 1, & r_*^\pm &= \lambda_w^\mp (w_*^\pm + 1), \end{aligned} \quad (3.2.23)$$

and three slow parts in which $(u_{tp}(\xi), p_{tp}(\xi)) = (\pm 1, 0) + \mathcal{O}(\varepsilon)$ and $(v_{tp}(\xi), q_{tp}(\xi), w_{tp}(\xi), r_{tp}(\xi))$ are given by

$$v_{tp}(\xi) = \begin{cases} -2s_v^- e^{\varepsilon \lambda_v^+ \xi} \sinh(\varepsilon \lambda_v^+ \xi_*) & -1 & \text{in } I_s^-, \\ s_v^- e^{\varepsilon \lambda_v^+(\xi - \xi_*)} + s_v^+ e^{\varepsilon \lambda_v^-(\xi + \xi_*)} & +1 & \text{in } I_s^0, \\ 2s_v^+ e^{\varepsilon \lambda_v^- \xi} \sinh(\varepsilon \lambda_v^- \xi_*) & -1 & \text{in } I_s^+, \end{cases} \quad (3.2.24)$$

and

$$w_{tp}(\xi) = \begin{cases} -2s_w^- e^{\varepsilon \lambda_w^+ \xi} \sinh(\varepsilon \lambda_w^+ \xi_*) & -1 & \text{in } I_s^-, \\ s_w^- e^{\varepsilon \lambda_w^+(\xi - \xi_*)} + s_w^+ e^{\varepsilon \lambda_w^-(\xi + \xi_*)} & +1 & \text{in } I_s^0, \\ 2s_w^+ e^{\varepsilon \lambda_w^- \xi} \sinh(\varepsilon \lambda_w^- \xi_*) & -1 & \text{in } I_s^+, \end{cases} \quad (3.2.25)$$

up to $\mathcal{O}(\sqrt{\varepsilon})$ corrections.

For small speed c , that is, $c = \delta$ with $0 < \varepsilon \ll \delta \ll 1$, the bifurcation parameter $\hat{\tau}$ as function of $\hat{\theta}$ is given to leading order by

$$\hat{\tau}_{tp}(\hat{\theta}) = \frac{1}{\alpha(1-A^2+A^2 \log A^2)} \left(\frac{2}{3}\sqrt{2} - \beta \frac{\hat{\theta}}{D} \left(1 - A^{\frac{2}{D}} + A^{\frac{2}{D}} \log A^{\frac{2}{D}} \right) \right), \quad (3.2.26)$$

where A solves (3.2.6). Note that $\hat{\tau}_{tp}$ determines the value at which the traveling pulses bifurcate from the standing pulses, see Section 2.4 and note that we used a slightly different notation in this Chapter, $\hat{\tau}_{tp}$ instead of $\hat{\tau}_{*,0}$.

For the stability theory of traveling 1-pulse solutions (Section 3.5.3) we also need some information about the first and second order correction terms of the u -components in the fast fields I_f^\pm . Unlike for the standing pulse solutions, we now

have $\mathcal{O}(\varepsilon)$ terms. In the fast fields I_f^\pm , the V - and W -components of the pulses are to leading order constant and determined by the jump conditions (3.2.20). These jump conditions combined with (3.2.19) yield that in the fast fields I_f^\pm the u -components are given by

$$(u_{tp}^\pm)_{\xi\xi} = -u_{tp}^\pm + (u_{tp}^\pm)^3 + \varepsilon \left(\mp \frac{1}{3} \sqrt{2} c - c(u_{tp}^\pm)_\xi \right) + \mathcal{O}(\varepsilon^2).$$

Next, we expand $u_{tp}^\pm(\xi)$:

$$u_{tp}^\pm(\xi) = u_{tp,0}^\pm(\xi) + \varepsilon u_{tp,1}^\pm(\xi) + \varepsilon^2 u_{tp,2}^\pm(\xi) + \mathcal{O}(\varepsilon^3).$$

To leading order, the ODE is the same as in the case of standing 1-pulse solutions, and we have

$$u_{tp,0}^\pm(\xi) = \mp \tanh\left(\frac{1}{2}\sqrt{2}(\xi \mp \xi_*)\right).$$

The $\mathcal{O}(\varepsilon)$ terms read

$$\mathcal{L}^\pm u_{tp,1}^\pm = \mp c \left(\frac{1}{3} \sqrt{2} - \psi^\pm \right), \quad (3.2.27)$$

with \mathcal{L}^\pm and $\psi^\pm(\xi)$ defined as before (3.2.17), (3.2.13).

Lemma 3.2.3. *The first order correction terms $u_{tp,1}^\pm(\xi)$ of (part of) the homoclinic orbit $u_{tp}(\xi)$ are even functions around $\pm\xi_*$.*

Proof. First notice that the right hand side of (3.2.27) is an even functions around $\pm\xi_*$. Also, observe that \mathcal{L}^\pm conserves the parity of a function, *i.e.*, if $u(\xi)$ is odd/even with respect to $\xi \pm \xi_*$, so is $\mathcal{L}^\pm u$. Altogether, when we split the first order correction terms of the u -component in the fast fields up into an even part and an odd part, *i.e.*, $u_{tp,1}^\pm(\xi) := u_{tp,1}^{\pm,\text{even}}(\xi) + u_{tp,1}^{\pm,\text{odd}}(\xi)$, we get

$$\begin{cases} \mathcal{L}^\pm \left(u_{tp,1}^{\pm,\text{even}} \right) &= \mp c \left(\frac{1}{3} \sqrt{2} - \psi^\pm \right), \\ \mathcal{L}^\pm \left(u_{tp,1}^{\pm,\text{odd}} \right) &= 0. \end{cases}$$

Recall that we look for bounded solutions at infinity. Therefore, we obtain from the last equation $u_{tp,1}^{\pm,\text{odd}}(\xi) = K^\pm \psi^\pm(\xi)$, but $\psi^\pm(\xi)$ is an even function around $\pm\xi_*$, so $K^\pm = 0$. Thus $u_{tp,1}^\pm(\xi) := u_{tp,1}^{\pm,\text{even}}(\xi) + u_{tp,1}^{\pm,\text{odd}}(\xi) = u_{tp,1}^{\pm,\text{even}}(\xi)$. \square

Notice that, by (3.2.14), the solvability condition is fulfilled for $u_{tp,1}^\pm(\xi)$, and it gives us no extra information.

Lemma 3.2.3 provides all the information on $u_{tp,1}^\pm(\xi)$ that we need. Thus, we now investigate the second order correction term of the u -component, $u_{tp,2}^\pm(\xi)$. As in the last section, by looking at the derivative and by using the solvability condition, we obtain

$$\begin{aligned} 0 &= \mp 6 \int_{I_f^\pm} u_{tp,0}^\pm u_{tp,2}^\pm (\psi^\pm)^2 d\xi \mp 3 \int_{I_f^\pm} (u_{tp,1}^\pm)^2 (\psi^\pm)^2 d\xi \\ &\quad + 6 \int_{I_f^\pm} u_{tp,0}^\pm u_{tp,1}^\pm (u_{tp,1}^\pm)_\xi \psi^\pm d\xi - c_0 \int_{I_f^\pm} (u_{tp,1}^\pm)_{\xi\xi} \psi^\pm d\xi \\ &\quad + 2\alpha(w_{tp})_\xi(\pm\xi_*) + 2\beta(w_{tp})_\xi(\pm\xi_*). \end{aligned} \quad (3.2.28)$$

3.2.3 Standing 2-pulse solutions

The three-component model (3.1.1) also supports standing, symmetric 2-pulse solutions. We find them as solutions of (3.2.1). However, we now have to distinguish nine different intervals instead of five. We have four fast intervals $I_f^{2,4,6,8}$ and five slow intervals $I_s^{1,3,5,7,9}$. The fast intervals read

$$I_f^{2,4} := \left(-\xi_*^{1,2} - \frac{1}{\sqrt{\varepsilon}}, -\xi_*^{1,2} + \frac{1}{\sqrt{\varepsilon}} \right), I_f^{6,8} := \left(\xi_*^{2,1} - \frac{1}{\sqrt{\varepsilon}}, \xi_*^{2,1} + \frac{1}{\sqrt{\varepsilon}} \right), \quad (3.2.29)$$

where ξ_*^1 is the jumping point of the last ‘back’ and ξ_*^2 is the jumping point of the last ‘front’, so $0 < \xi_*^2 < \xi_*^1$ and $u_{2p}(\xi_*^{1,2}) = 0$. The five slow intervals are again the complement of the four fast intervals. For notational convenience, we introduce $A_{1,2} := e^{-\varepsilon \xi_*^{1,2}}$ such that $0 < A_1 < A_2 < 1$.

In the existence analysis of Section 2.5, we established the following theorem:

Theorem 3.2.4. *Let $\varepsilon > 0$ be small enough, and let $(\alpha, \beta, \gamma, D)$ be such that*

$$\begin{cases} G_1(A_1, A_2) := \alpha(A_1 - A_2)^2 + \beta(A_1^{\frac{1}{D}} - A_2^{\frac{1}{D}})^2 = 0, \\ G_2(A_1, A_2) := \alpha(A_2^2 - A_1^2) - 2\alpha A_1 A_2^{-1} + \beta(A_2^{\frac{2}{D}} - A_1^{\frac{2}{D}}) - 2\beta A_1^{\frac{1}{D}} A_2^{-\frac{1}{D}} = -2\gamma, \end{cases} \quad (3.2.30)$$

has K solution pairs (A_1, A_2) with $0 < A_1 < A_2 < 1$. Then there are K homoclinic orbits $\gamma_{2p}(\xi)$ to P_ε^- in (3.2.1) that correspond to symmetric standing 2-pulse solutions of (3.1.1).

The homoclinic orbits $\gamma_{2p}(\xi)$ consist of nine distinct parts, four fast parts and five slow parts. In the fast parts, the orbits $\gamma_{2p}(\xi)$ are $\mathcal{O}(\varepsilon)$ close to the fast reduced heteroclinic orbits

$$\begin{aligned} & (u_{\text{fast}}^-(\xi + \xi_*^1), p_{\text{fast}}^-(\xi + \xi_*^1), v_*^2, q_*^2, w_*^2, r_*^2), \\ & (u_{\text{fast}}^+(\xi + \xi_*^2), p_{\text{fast}}^+(\xi + \xi_*^2), v_*^4, q_*^4, w_*^4, r_*^4), \\ & (u_{\text{fast}}^-(\xi - \xi_*^2), p_{\text{fast}}^-(\xi - \xi_*^2), v_*^6, q_*^6, w_*^6, r_*^6), \\ & (u_{\text{fast}}^+(\xi - \xi_*^1), p_{\text{fast}}^+(\xi - \xi_*^1), v_*^8, q_*^8, w_*^8, r_*^8), \end{aligned}$$

respectively, where $u_{\text{fast}}^\pm(\xi), p_{\text{fast}}^\pm(\xi)$ are given by (3.2.7) and $(v_*^i, q_*^i, w_*^i, r_*^i), i \in \{2, 4, 6, 8\}$ are given by

$$\begin{aligned} v_*^2 &= -A_1^2 - A_1 A_2^{-1} + A_1 A_2, & q_*^2 &= v_*^2 + 1, \\ w_*^2 &= -A_1^{\frac{2}{D}} - A_1^{\frac{1}{D}} A_2^{-\frac{1}{D}} + A_1^{\frac{1}{D}} A_2^{\frac{1}{D}}, & r_*^2 &= w_*^2 + 1, \\ v_*^4 &= A_2^2 - A_1 A_2^{-1} - A_1 A_2, & q_*^4 &= v_*^4 - 1 + 2A_1 A_2^{-1}, \\ w_*^4 &= A_2^{\frac{2}{D}} - A_1^{\frac{1}{D}} A_2^{-\frac{1}{D}} - A_1^{\frac{1}{D}} A_2^{\frac{1}{D}}, & r_*^4 &= w_*^4 - 1 + 2A_1^{\frac{1}{D}} A_2^{-\frac{1}{D}}, \\ v_*^{6,8} &= v_*^{4,2}, q_*^{6,8} = -q_*^{4,2}, & w_*^{6,8} &= w_*^{4,2}, r_*^{6,8} = -r_*^{4,2}. \end{aligned} \quad (3.2.31)$$

In the five slow parts, the orbits $\gamma_{2p}(\xi)$ are given by $(u_{2p}(\xi), p_{2p}(\xi)) = (\pm 1, 0) + \mathcal{O}(\varepsilon)$ and

$(v_{2p}(\xi), q_{2p}(\xi), w_{2p}(\xi), r_{2p}(\xi))$ are given by

$$v_{2p}(\xi) = \begin{cases} 2e^{\varepsilon\xi} (\sinh(\varepsilon\xi_*^1) - \sinh(\varepsilon\xi_*^2)) - 1 & \text{in } I_s^1, \\ -e^{-\varepsilon(\xi+\xi_*^1)} - e^{\varepsilon(\xi-\xi_*^1)} - 2e^{\varepsilon\xi} (\sinh(\varepsilon\xi_*^2)) + 1 & \text{in } I_s^3, \\ -e^{-\varepsilon(\xi+\xi_*^1)} + e^{-\varepsilon(\xi+\xi_*^2)} + e^{\varepsilon(\xi-\xi_*^2)} - e^{\varepsilon(\xi-\xi_*^1)} - 1 & \text{in } I_s^5, \\ -e^{-\varepsilon(\xi+\xi_*^1)} - e^{\varepsilon(\xi-\xi_*^1)} - 2e^{-\varepsilon\xi} (\sinh(\varepsilon\xi_*^2)) + 1 & \text{in } I_s^7, \\ 2e^{-\varepsilon\xi} (\sinh(\varepsilon\xi_*^1) - \sinh(\varepsilon\xi_*^2)) - 1 & \text{in } I_s^9, \end{cases} \quad (3.2.32)$$

and

$$w_{2p}(\xi) = \begin{cases} 2e^{\frac{\varepsilon}{D}\xi} (\sinh(\frac{\varepsilon}{D}\xi_*^1) - \sinh(\frac{\varepsilon}{D}\xi_*^2)) - 1 & \text{in } I_s^1, \\ -e^{-\frac{\varepsilon}{D}(\xi+\xi_*^1)} - e^{\frac{\varepsilon}{D}(\xi-\xi_*^1)} - 2e^{\frac{\varepsilon}{D}\xi} (\sinh(\frac{\varepsilon}{D}\xi_*^2)) + 1 & \text{in } I_s^3, \\ -e^{-\frac{\varepsilon}{D}(\xi+\xi_*^1)} + e^{-\frac{\varepsilon}{D}(\xi+\xi_*^2)} + e^{\frac{\varepsilon}{D}(\xi-\xi_*^2)} - e^{\frac{\varepsilon}{D}(\xi-\xi_*^1)} - 1 & \text{in } I_s^5, \\ -e^{-\frac{\varepsilon}{D}(\xi+\xi_*^1)} - e^{\frac{\varepsilon}{D}(\xi-\xi_*^1)} - 2e^{-\frac{\varepsilon}{D}\xi} (\sinh(\frac{\varepsilon}{D}\xi_*^2)) + 1 & \text{in } I_s^7, \\ 2e^{-\frac{\varepsilon}{D}\xi} (\sinh(\frac{\varepsilon}{D}\xi_*^1) - \sinh(\frac{\varepsilon}{D}\xi_*^2)) - 1 & \text{in } I_s^9. \end{cases} \quad (3.2.33)$$

up to $\mathcal{O}(\sqrt{\varepsilon})$ corrections.

The orbits $\gamma_{2p}(\xi)$ correspond to standing 2-pulse solutions

$$(U(\xi, t), V(\xi, t), W(\xi, t)) \equiv (u_{2p}(\xi), v_{2p}(\xi), w_{2p}(\xi))$$

of (3.1.1). Note that a sufficient condition for K to be zero in the above theorem is $\text{sgn}(\alpha) = \text{sgn}(\beta)$, because then $G_1(A_1, A_2) \neq 0$ (3.2.30).

Just as for the 1-pulse case (see (3.2.13) and (3.2.18)), we introduce

$$\begin{aligned} \psi_{2,4}(\xi) &:= \frac{1}{2}\sqrt{2}\text{sech}^2\left(\frac{1}{2}\sqrt{2}(\xi + \xi_*^{1,2})\right), \\ \psi_{6,8}(\xi) &:= \frac{1}{2}\sqrt{2}\text{sech}^2\left(\frac{1}{2}\sqrt{2}(\xi - \xi_*^{2,1})\right). \end{aligned} \quad (3.2.34)$$

Using the solvability conditions, we find the following integral relations for $u_{2p,2}^j(\xi)$, the second order term of $u_{2p}(\xi)$ in the j -th fast interval

$$\begin{aligned} \int_{I_f^2} u_{2p,0}^2 u_{2p,2}^2 (\psi_2)^2 d\xi &= -\frac{1}{3} \left(\alpha (\tilde{v}_{2p})_\xi(-\xi_*^1) + \beta (\tilde{w}_{2p})_\xi(-\xi_*^1) \right), \\ \int_{I_f^4} u_{2p,0}^4 u_{2p,2}^4 (\psi_4)^2 d\xi &= \frac{1}{3} \left(\alpha (\tilde{v}_{2p})_\xi(-\xi_*^2) + \beta (\tilde{w}_{2p})_\xi(-\xi_*^2) \right), \\ \int_{I_f^6} u_{2p,0}^6 u_{2p,2}^6 (\psi_6)^2 d\xi &= -\frac{1}{3} \left(\alpha (\tilde{v}_{2p})_\xi(\xi_*^2) + \beta (\tilde{w}_{2p})_\xi(\xi_*^2) \right), \\ \int_{I_f^8} u_{2p,0}^8 u_{2p,2}^8 (\psi_8)^2 d\xi &= \frac{1}{3} \left(\alpha (\tilde{v}_{2p})_\xi(\xi_*^1) + \beta (\tilde{w}_{2p})_\xi(\xi_*^1) \right). \end{aligned} \quad (3.2.35)$$

3.3 The linearized stability problem

In this section, we develop a general approach to the stability of pulse solutions in the three-component system (3.1.1) with two slow components. In the subsequent

sections, Sections 3.4, 3.5, and 3.6, we will apply this theory on the constructed pulse solutions of Section 3.2.

In Section 3.3.1, we linearize the PDE around a homoclinic pulse solution. Next, in Section 3.3.2, we calculate the essential spectrum associated to the various pulse solutions. Then, in Section 3.3.3, we determine expressions for the point spectrum, using the Evans function [1, 59]. Finally, in Section 3.3.4, we exploit the slow-fast structure of the PDE to further decompose the Evans function into a fast (analytic) part and a slow (meromorphic) part.

Remark 3.3.1. From linear stability we can immediately conclude nonlinear stability since the operator associated to the linear problem is sectorial (away from bifurcations). See [35, 59].

3.3.1 Linearizing around a homoclinic pulse

We start by linearizing the PDE (3.1.1) around a homoclinic pulse solution. We introduce small perturbations $u(\xi)$, $v(\xi)$, and $w(\xi)$ of the pulse solution

$$\begin{aligned} U(\xi, t) &= u_h(\xi, \varepsilon) + u(\xi)e^{\lambda t}, & V(\xi, t) &= v_h(\xi, \varepsilon) + v(\xi)e^{\lambda t}, \\ W(\xi, t) &= w_h(\xi, \varepsilon) + w(\xi)e^{\lambda t}, \end{aligned} \quad (3.3.1)$$

where $(u_h(\xi), v_h(\xi), w_h(\xi))$ are the homoclinic pulse solutions of the existence analysis. In this section, we linearize around the standing 1-pulse solutions, see Theorem 3.2.1. The linearization around the 2-pulse solutions $(u_{2p}(\xi), v_{2p}(\xi), w_{2p}(\xi))$ is essentially the same, it has the same behavior ‘at infinity’. The linearization around the traveling pulse solution $(u_{tp}(\xi), v_{tp}(\xi), w_{tp}(\xi))$ induces a slightly different linear operator, see (3.5.18). The results for the linear operator can be modified easily for the linear operator obtained in the case of traveling pulse solutions, see Section 3.5.3.

We substitute (3.3.1) into (3.1.1) and linearize to obtain

$$\begin{cases} u_{\xi\xi} + (1 - 3u_h^2 - \lambda)u &= \varepsilon(\alpha v + \beta w), \\ v_{\xi\xi} &= \varepsilon^2((1 + \tau\lambda)v - u), \\ w_{\xi\xi} &= \frac{\varepsilon^2}{D^2}((1 + \theta\lambda)w - u). \end{cases} \quad (3.3.2)$$

We rewrite this system as a linear system in \mathbb{C}^6 ,

$$\phi_\xi(\xi) = \mathcal{M}(\xi; \lambda, \varepsilon)\phi(\xi) \text{ with } \phi(\xi) = (u(\xi), p(\xi), v(\xi), q(\xi), w(\xi), r(\xi))^t, \quad (3.3.3)$$

where $\mathcal{M}(\xi; \lambda, \varepsilon)$ is a 6×6 matrix with $Tr(\mathcal{M}) \equiv 0$, and $u_\xi(\xi) = p(\xi)$, $v_\xi(\xi) = \varepsilon q(\xi)$ and $w_\xi(\xi) = \frac{\varepsilon}{D} r(\xi)$.

In order to analyze system (3.3.3), we first examine the matrix $\mathcal{M}(\xi; \lambda, \varepsilon)$ in

the limit that $\xi \rightarrow \pm\infty$, where we observe that these limits are equal, since the pulse is homoclinic. We obtain the matrix $\mathcal{M}_\infty(\lambda, \varepsilon)$:

$$\mathcal{M}_\infty(\lambda, \varepsilon) = \begin{pmatrix} 0 & 1 & 0 & 0 & 0 & 0 \\ \lambda + 2 + 3\varepsilon(\gamma - \alpha - \beta) + \mathcal{O}(\varepsilon^2) & 0 & \varepsilon\alpha & 0 & \varepsilon\beta & 0 \\ 0 & 0 & 0 & \varepsilon & 0 & 0 \\ -\varepsilon & 0 & \varepsilon(1 + \tau\lambda) & 0 & 0 & 0 \\ 0 & 0 & 0 & 0 & 0 & \frac{\varepsilon}{D} \\ -\frac{\varepsilon}{D} & 0 & 0 & 0 & \frac{\varepsilon}{D}(1 + \theta\lambda) & 0 \end{pmatrix}. \quad (3.3.4)$$

The squares of the six eigenvalues, Λ_i^2 , are given to leading order by

$$\Lambda_{1,6}^2 = \lambda + 2 + 3\varepsilon(\gamma - \alpha - \beta), \quad \Lambda_{2,5}^2 = \varepsilon^2(1 + \tau\lambda), \quad \Lambda_{3,4}^2 = \frac{\varepsilon^2}{D^2}(1 + \theta\lambda). \quad (3.3.5)$$

Here, and in the remainder of this chapter, the first subscript denotes the square root with positive real part. The eigenvectors E_i of the matrix \mathcal{M}_∞ associated to Λ_i are given to leading order by

$$\begin{aligned} E_{1,6} &= \left(1, \pm\sqrt{\lambda + 2}, -\varepsilon^2 \frac{1}{\lambda + 2}, \mp\varepsilon \frac{1}{\sqrt{\lambda + 2}}, -\frac{\varepsilon^2}{D^2} \frac{1}{\lambda + 2}, \mp\frac{\varepsilon}{D} \frac{1}{\sqrt{\lambda + 2}} \right)^t, \\ E_{2,5} &= \left(-\frac{\alpha}{\lambda + 2}\varepsilon, \mp\frac{\alpha\varepsilon^2}{\lambda + 2}\sqrt{1 + \tau\lambda}, 1, \pm\sqrt{1 + \tau\lambda}, \mathcal{O}(\varepsilon), \mathcal{O}(\varepsilon) \right)^t, \\ E_{3,4} &= \left(-\frac{\beta}{\lambda + 2}\varepsilon, \mp\frac{\beta\varepsilon^2}{D\lambda + 2}\sqrt{1 + \theta\lambda}, \mathcal{O}(\varepsilon), \mathcal{O}(\varepsilon), 1, \pm\sqrt{1 + \theta\lambda} \right)^t. \end{aligned} \quad (3.3.6)$$

Remark 3.3.2. In the above eigenvectors, as well as the eigenvectors showing up in the forthcoming analysis, see (3.4.12), (3.5.3), (3.5.21), we do not state all components of the eigenvectors explicitly, since for some we only need to know their asymptotic magnitude.

3.3.2 The essential spectrum

By general theory [35], the essential spectrum associated to the stability of pulse solutions is equivalent to the spectrum of the stability problem of the background states u_ε^- (3.2.3) under spatially-periodic perturbations. This is equivalent to

$$\sigma_{\text{ess}} := \{\lambda \in \mathbb{C} : \exists j \text{ such that } \Lambda_j \in i\mathbb{R}\}, \quad (3.3.7)$$

where Λ_j are the eigenvalues of the matrix \mathcal{M}_∞ , see (3.3.5). It is computationally more convenient to determine σ_{ess} by introducing $k \in \mathbb{R}$ and $u, v, w, \omega \in \mathbb{C}$ by

$$(U, V, W) = (u_\varepsilon^-, u_\varepsilon^-, u_\varepsilon^-) + (u, v, w)e^{i\varepsilon k\xi + \omega t}. \quad (3.3.8)$$

Substituting the above in (3.1.1), we find to leading order

$$M_1 \begin{pmatrix} u \\ v \\ w \end{pmatrix} = \begin{pmatrix} 0 \\ 0 \\ 0 \end{pmatrix},$$

with

$$M_1 = \begin{pmatrix} -\varepsilon^2 k^2 - 2 - \omega + 3\varepsilon(\alpha + \beta - \gamma) & -\varepsilon\alpha & -\varepsilon\beta \\ 1 & -\tau\omega - k^2 - 1 & 0 \\ 1 & 0 & -\theta\omega - D^2 k^2 - 1 \end{pmatrix}. \quad (3.3.9)$$

Lemma 3.3.1. *Let $\tau, \theta = \mathcal{O}(1)$. Then, for ε sufficiently small, the essential spectrum of the standing pulse solutions homoclinic to P_ε^- , lies in the half plane*

$$\Sigma := \{\omega : \Re(\omega) < \chi\},$$

where $\max\{-2, -\frac{1}{\tau}, -\frac{1}{\theta}\} < \chi < 0$ to leading order.

Proof. The characteristic polynomial associated to (3.3.9) is given by

$$Q(\omega, k^2) = \begin{pmatrix} -\varepsilon^2 k^2 - 2 - \omega + 3\varepsilon(\alpha + \beta - \gamma) \\ (\theta\omega + D^2 k^2 + 1) - \varepsilon\alpha (\theta\omega + D^2 k^2 + 1) \\ -\varepsilon\beta (\tau\omega + k^2 + 1) \end{pmatrix} (\tau\omega + k^2 + 1) \quad (3.3.10)$$

We analyze to leading order the zeroes of this cubic polynomial in k^2 . They are

$$\omega_0^{(1)} = -2 - \varepsilon^2 k^2 \leq -2, \omega_0^{(2)} = -\frac{1+k^2}{\tau} \leq -\frac{1}{\tau}, \omega_0^{(3)} = -\frac{1+D^2 k^2}{\theta} \leq -\frac{1}{\theta}. \quad (3.3.11)$$

For the first correction terms of the zeroes, we need to distinguish two cases. After a long and tedious calculation one finds that, if the three zeroes are simple to leading order, the first correction terms are $\mathcal{O}(\varepsilon)$. If two or three of the zeroes coincide, then the first correction terms are at most $\mathcal{O}(\sqrt{\varepsilon})$. Therefore, in both cases the zeroes lie in the half plane Σ for ε sufficiently small. \square

It is also of interest to observe that, if two of the eigenvalues coincide to leading order, they can form a complex pair, and the maximum of the imaginary part can be computed explicitly. For example, if $\omega_0^{(1)} = \omega_0^{(2)}$ to leading order and if $\alpha > 0$, then it can be computed that

$$\Im(\omega_1^{1,2}) = \sqrt{-\frac{\alpha}{\tau}} \sqrt{\varepsilon}$$

at its maximum. This agrees with the data shown in Figure 3.2 I.

Stationary 1-pulse solutions may undergo bifurcations if τ and θ are $\mathcal{O}(\varepsilon^{-2})$. Although it, *a priori*, may seem that the correction term may become of leading order when two or more zeroes coincide, a more detailed analysis yields that this is not the case. In particular, in this regime, we have the following lemma:

Lemma 3.3.2. *Let $\tau, \theta = \mathcal{O}(\varepsilon^{-2})$. Then, for ε sufficiently small, the essential spectrum of the standing pulse solutions homoclinic to P_ε^- , lies in the half plane Σ , with Σ as given in Lemma 3.3.1.*

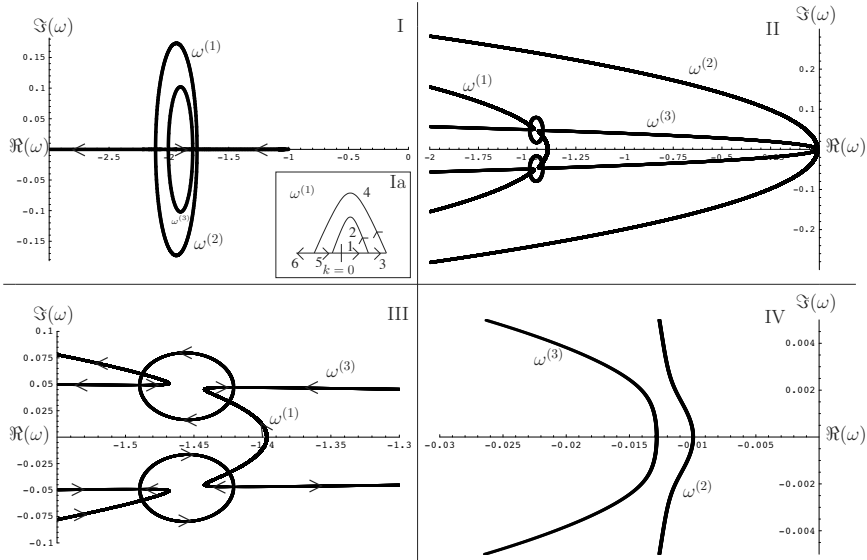


Figure 3.2: In frame I, the essential spectrum for the standing pulse with $\mathcal{O}(1)$ parameters is depicted, where $(\alpha, \beta, \gamma, D, \tau, \theta, \varepsilon) = (3, 1, \alpha A^2 + \beta A^{\frac{2}{D}}, 5, 1, 1, 0.01)$, with $A = e^{-1/2}$. This picture is typical for all $\tau, \theta = \mathcal{O}(1)$. Note that the heights of the loops are to leading order $\sqrt{-\frac{\alpha}{\tau}}\sqrt{\varepsilon}$, $\sqrt{-\frac{\beta}{\theta}}\sqrt{\varepsilon}$, respectively, as predicted by the analysis. In frame Ia, the branch $\omega^{(1)}$ is drawn schematically, the arrows and the numbering indicate the flow for increasing k . In frame II, the essential spectrum for a traveling pulse is plotted for $(\alpha, \beta, \gamma, D, \hat{\tau}, \hat{\theta}, \varepsilon, c) = (3, 1, 2, 5, 1, 1, 0.1, 2)$. In frames III, and IV we zoomed in around the interesting regions of II. The arrows in III indicate the flow of the zeroes for increasing k . From frame IV we observe that there is a spectral gap. Hence, we can still conclude nonlinear stability from the linear stability analysis. See Remark 3.3.1.

Proof. We introduce $\hat{\tau} = \varepsilon^2\tau$ and $\hat{\theta} = \varepsilon^2\theta$, so that the characteristic polynomial reads

$$\begin{aligned} \varepsilon^4 Q(\omega, k^2) &= (-\varepsilon^2 k^2 - 2 - \omega + 3\varepsilon(\alpha + \beta - \gamma)) (\hat{\tau}\omega + \varepsilon^2(k^2 + 1)) \\ &\quad \left(\hat{\theta}\omega + \varepsilon^2(D^2 k^2 + 1) \right) - \varepsilon^3 \alpha \left(\hat{\theta}\omega + \varepsilon^2(D^2 k^2 + 1) \right) \\ &\quad - \varepsilon^3 \beta (\hat{\tau}\omega + \varepsilon^2(k^2 + 1)). \end{aligned}$$

To leading order, the zeroes are given by

$$\begin{aligned} \omega_0^{(1)} &= -2 - \varepsilon^2 k^2 \leq -2, \quad \omega_0^{(2)} = -\frac{\varepsilon^2}{\hat{\tau}}(1 + k^2) \leq -\frac{1}{\hat{\tau}}, \\ \omega_0^{(3)} &= -\frac{\varepsilon^2}{\hat{\theta}}(1 + D^2 k^2) \leq -\frac{1}{\hat{\theta}}. \end{aligned} \tag{3.3.12}$$

When the zeroes are simple, the first correction terms of $\omega_0^{(2,3)}$ are of $\mathcal{O}(\varepsilon^3)$ with respect to the scaled variables. If two or more of the zeroes coincide, the first correction term may be of $\mathcal{O}(\varepsilon\sqrt{\varepsilon})$ size. However, a detailed analysis shows that this only occurs for $|k| \gg 1$. For small k it is found that (3.3.12) is correct up to $\mathcal{O}(\varepsilon^3)$ terms. Therefore, in all cases the zeroes lie in the half plane Σ for ε sufficiently small. \square

Finally, we investigate the essential spectrum of the traveling pulse solutions. Because we work in a co-moving frame, the matrix M_1 (3.3.9) possesses some extra diagonal terms. However, given the asymptotic magnitude of c , these diagonal terms have no leading order influence on the stability result. Therefore, we find

Lemma 3.3.3. *Let $\tau, \theta = \mathcal{O}(\varepsilon^{-2})$. Then, for ε sufficiently small, the essential spectrum of the traveling pulse solutions homoclinic to P_ε^- , with speed εc , lies in the half plane Σ , with Σ as given in Lemma 3.3.1.*

See also Figure 3.2, in which the essential spectrum is plotted for several parameter combinations.

In conclusion, we have shown that, in all three cases the essential spectrum is completely contained in the left half plane. Therefore, small perturbations do not lead to instabilities of the background states. The stability of the pulse solutions is determined by the discrete eigenvalues.

Remark 3.3.3. The essential spectrum associated to pulse solutions homoclinic to P_ε^+ , *i.e.*, linearization around the other background state $(u_\varepsilon^+, u_\varepsilon^+, u_\varepsilon^+)$, is effectively the same. That is, the eigenvalues are the same to leading order, and the differences at $\mathcal{O}(\varepsilon)$ do not structurally affect the main results. This also implies that we do not have to determine the possible absolute spectrum associated to the intermediate state $u_h(\xi) = +1$ ($\xi \in I_s^0$) for the pulse solution homoclinic to P_ε^- , because this absolute spectrum is contained in the essential spectrum and it is thus contained in the left half plane [59].

3.3.3 The construction of the Evans function

To determine the point spectrum of the linearized operator or, equivalently, of the matrix $\mathcal{M}(\xi; \lambda, \varepsilon)$ (3.3.3) [59], we construct an Evans function.

The matrix $\mathcal{M}(\xi; \lambda, \varepsilon)$ converges exponentially to the constant coefficient matrix $\mathcal{M}_\infty(\lambda, \varepsilon)$ as $|\xi| \rightarrow \infty$, see (3.3.4). This matrix \mathcal{M}_∞ has six eigenvalues $\Lambda_i(\lambda, \varepsilon)$ (3.3.5). If we assume that these eigenvalues $\Lambda_i(\lambda, \varepsilon)$ are simple and that λ lies outside a small δ -neighborhood of σ_{ess} , say

$$\lambda \in \mathcal{C}_\delta := \mathbb{C} \setminus B(\sigma_{\text{ess}}, \delta), \quad (3.3.13)$$

for some $0 < \delta \ll 1$, then the eigenvectors $E_i(\lambda, \varepsilon)$ are analytic functions in λ . For simplicity we furthermore assume that the $\Lambda_i(\lambda, \varepsilon)$ can be ordered:

$$\Re(\Lambda_i) > \Re(\Lambda_j) \quad \text{for } i < j. \quad (3.3.14)$$

Note that this is not a restriction for $\lambda \in \mathcal{C}_\delta$, since we can always relabel the eigenvalues in such a fashion that the above holds. See also Section 3.4 in which $\Re(\Lambda_i) > \Re(\Lambda_j)$ for all $i < j$ (3.4.11), and Section 3.5 in which $\Re(\Lambda_2)$ and $\Re(\Lambda_3)$ can change order.

The set $\{E_i(\lambda, \varepsilon)e^{\Lambda_i(\lambda, \varepsilon)\xi}, i \in \{1, 2, \dots, 6\}\}$ is a basis for the solution space of the asymptotic equation

$$\phi_\xi(\xi) = \mathcal{M}_\infty(\lambda, \varepsilon)\phi(\xi).$$

The first, respectively last, three basis-elements span the space of solutions that go to zero as $\xi \rightarrow -\infty$, respectively as $\xi \rightarrow \infty$.

We know that we can find six solutions $\phi_i^-(\xi)$ of (3.3.3) which have the asymptotic behavior

$$\phi_i^-(\xi, \lambda; \varepsilon) = E_i e^{\Lambda_i \xi}, \quad \text{as } \xi \rightarrow -\infty, \quad (3.3.15)$$

for $i \in \{1, 2, \dots, 6\}$, and six (different) solutions $\phi_i^+(\xi)$ such that

$$\phi_i^+(\xi, \lambda; \varepsilon) = E_i e^{\Lambda_i \xi}, \quad \text{as } \xi \rightarrow \infty, \quad (3.3.16)$$

for $i \in \{1, 2, \dots, 6\}$ [8]. Note that only $\phi_1^-(\xi)$ and $\phi_6^+(\xi)$ are determined uniquely, and that $\phi_i^-(\xi)$ is bounded at $-\infty$ for $i = 1, 2, 3$. We define the space $\Phi^-(\xi)$ by

$$\Phi^-(\xi; \lambda, \varepsilon) := \text{span}\{\phi_1^-(\xi), \phi_2^-(\xi), \phi_3^-(\xi)\}. \quad (3.3.17)$$

Likewise, we define the space of bounded solutions at $+\infty$ by

$$\Phi^+(\xi; \lambda, \varepsilon) := \text{span}\{\phi_4^+(\xi), \phi_5^+(\xi), \phi_6^+(\xi)\}, \quad (3.3.18)$$

If λ is not an eigenvalue, the space $\Phi^-(\xi) \cup \Phi^+(\xi)$ spans all bounded solutions of (3.3.3). Therefore, the Evans function is defined by

$$\mathcal{D}(\lambda, \varepsilon) = e^{-\int_0^\xi \text{Tr} \mathcal{M}(s; \lambda, \varepsilon) ds} \det [\phi_1^-(\xi, \lambda; \varepsilon), \dots, \phi_3^-(\xi, \lambda; \varepsilon), \phi_4^+(\xi, \lambda; \varepsilon), \dots, \phi_6^+(\xi, \lambda; \varepsilon)]. \quad (3.3.19)$$

One can prove using Abel's identity that the Evans function $\mathcal{D}(\lambda, \varepsilon)$ is indeed independent of ξ . Note that $\text{Tr} \mathcal{M}(s; \lambda, \varepsilon) \equiv 0$ in the case of stationary pulse solutions. The next theorem follows from the general theory developed in [1].

Theorem 3.3.4. *The Evans function $\mathcal{D}(\lambda; \varepsilon)$ is an analytic function on \mathcal{C}_δ ; and $\mathcal{D}(\lambda, \varepsilon) = 0$ if and only if λ is an eigenvalue of (3.3.3). Moreover, the order of a zero is equal to the algebraic multiplicity of the eigenvalue.*

3.3.4 The slow-fast decomposition of $\mathcal{D}(\lambda)$

For simplicity, we focus in this section on the stationary 1-pulse solutions. The theory developed here can be extended directly to the traveling pulse solutions and the 2-pulse solutions. 1-pulse solutions make two excursions through the fast fields I_f^\pm , with a slow field I_s^0 in between. In this section, we consider this whole interval, that is, $I_f^- \cup I_s^0 \cup I_f^+$, to be the 'domain of transition' – in between the behavior as $\xi \rightarrow -\infty$ and that as $\xi \rightarrow \infty$. In Section 3.4.2, we will address the dynamics inside I_s^0 .

By the slow-fast nature of (3.1.1), we expect to be able to decouple the Evans function into a slow and a fast component $\mathcal{D}(\lambda, \varepsilon) = \mathcal{D}_{\text{fast}}(\lambda, \varepsilon) \mathcal{D}_{\text{slow}}(\lambda, \varepsilon)$ [1, 12, 13, 30].

Lemma 3.3.5. *Let $\lambda \in \mathcal{C}_\delta$, then there exists a uniquely determined transmission function $t_1(\lambda, \varepsilon)$ that is analytic in λ such that*

$$\lim_{\xi \rightarrow \infty} \phi_1^-(\xi; \lambda, \varepsilon) e^{-\Lambda_1(\lambda, \varepsilon)\xi} = t_1(\lambda, \varepsilon) E_1(\lambda, \varepsilon). \quad (3.3.20)$$

Lemma 3.3.6. *Let $\lambda \in \mathcal{C}_\delta$ be such that $t_1(\lambda, \varepsilon) \neq 0$. There is a 2-dimensional manifold $\Phi_s^-(\xi; \lambda, \varepsilon) = \text{span}\{\phi_{s,2}^-(\xi; \lambda, \varepsilon), \phi_{s,3}^-(\xi; \lambda, \varepsilon)\}$ in which $\phi_{s,2}^-(\xi; \lambda, \varepsilon)$ is uniquely determined, such that*

$$\lim_{\xi \rightarrow -\infty} \phi_{s,i}^-(\xi; \lambda, \varepsilon) e^{-\Lambda_i(\lambda, \varepsilon)\xi} = E_i(\lambda, \varepsilon), \quad i \in \{2, 3\}, \quad (3.3.21)$$

and

$$\lim_{\xi \rightarrow \infty} \phi_{s,i}^-(\xi; \lambda, \varepsilon) e^{-\Lambda_1(\lambda, \varepsilon)\xi} = (0, 0, 0, 0, 0, 0)^t, \quad i \in \{2, 3\}. \quad (3.3.22)$$

The proof of Lemma 3.3.5 is standard, see [1]. The proof of Lemma 3.3.6 is similar to the proof of Lemma 3.7 in [12], however, here the system is 6-dimensional whereas it is only 4-dimensional in [12].

Proof. By (3.3.15) we only need to prove (3.3.22) and the uniqueness. Define the 5-dimensional space $\Phi_s^+(\xi)$ of solutions $\phi(\xi)$ of (3.3.3) by

$$\lim_{\xi \rightarrow \infty} \phi(\xi) e^{-\Lambda_1(\lambda, \varepsilon)\xi} = (0, 0, 0, 0, 0, 0)^t.$$

The dimension of $\Phi_s^+(\xi) \cap \Phi^-(\xi; \lambda, \varepsilon)$ is at least two (and at most three). However, since $\phi_1^-(\xi; \lambda, \varepsilon)$ is an element of $\Phi^-(\xi; \lambda, \varepsilon)$, but, by assumption, not of $\Phi_s^+(\xi)$, the intersection must be transversal, and its dimension is thus two. Moreover, $\phi_{s,2}^-(\xi) \in \Phi_s^-(\xi) \cap \Phi^-(\xi)$ is determined uniquely by (3.3.21) and (3.3.22). \square .

We can now introduce the four ‘slow-fast’ transmission functions $t_{ij}(\lambda, \varepsilon)$, $i, j = 2, 3$ by

$$\lim_{\xi \rightarrow \infty} \phi_{s,i}^-(\xi) e^{-\Lambda_2(\lambda, \varepsilon)\xi} = t_{i2}(\lambda, \varepsilon) E_2(\lambda, \varepsilon), \quad i = 2, 3, \quad (3.3.23)$$

and

$$\lim_{\xi \rightarrow \infty} \left(\phi_{s,i}^-(\xi) - t_{i2}(\lambda, \varepsilon) E_2(\lambda, \varepsilon) e^{\Lambda_2(\lambda, \varepsilon)\xi} \right) e^{-\Lambda_3(\lambda, \varepsilon)\xi} = t_{i3}(\lambda, \varepsilon) E_3(\lambda, \varepsilon). \quad (3.3.24)$$

Note that $t_{2j}(\lambda, \varepsilon)$ are determined uniquely, while $t_{3j}(\lambda, \varepsilon)$ depend on the choice of $\phi_{s,3}^-(\xi)$. However, if $t_{22}(\lambda, \varepsilon) \neq 0$, $\phi_{s,3}^-(\xi)$ can be chosen uniquely by $\tilde{\phi}_{s,3}^-(\xi) := \phi_{s,3}^-(\xi) - \frac{t_{32}}{t_{22}} \phi_{s,2}^-(\xi)$, so that

$$\begin{aligned} \lim_{\xi \rightarrow \infty} \tilde{\phi}_{s,3}^-(\xi) e^{-\Lambda_2\xi} &= (0, 0, 0, 0, 0, 0)^t, \\ \lim_{\xi \rightarrow \infty} \tilde{\phi}_{s,3}^-(\xi) e^{-\Lambda_3\xi} &= \left(t_{33} - \frac{t_{23}t_{32}}{t_{22}} \right) E_3. \end{aligned} \quad (3.3.25)$$

Hence, since $\mathcal{D}(\lambda, \varepsilon)$ does not depend on ξ ,

$$\begin{aligned} \mathcal{D}(\lambda, \varepsilon) &= \det \left[\phi_1^-(\xi), \phi_{s,2}^-(\xi), \tilde{\phi}_{s,3}^-(\xi), \phi_4^+(\xi), \phi_5^+(\xi), \phi_6^+(\xi) \right] \\ &= \lim_{\xi \rightarrow \infty} \det \left[\phi_1^- e^{-\Lambda_1\xi}, \phi_{s,2}^- e^{-\Lambda_2\xi}, \tilde{\phi}_{s,3}^- e^{-\Lambda_3\xi}, \right. \\ &\quad \left. \phi_4^+ e^{-\Lambda_4\xi}, \phi_5^+ e^{-\Lambda_5\xi}, \phi_6^+ e^{-\Lambda_6\xi} \right] \\ &= \det \left[t_1 E_1, t_{22} E_2, \left(t_{33} - \frac{t_{23}t_{32}}{t_{22}} \right) E_3, E_4, E_5, E_6 \right] \\ &= t_1 (t_{22}t_{33} - t_{23}t_{32}) \det [E_1, E_2, E_3, E_4, E_5, E_6]. \end{aligned} \quad (3.3.26)$$

This yields the following corollary:

Corollary 3.3.7. *The Evans function can be decomposed into $\mathcal{D}(\lambda, \varepsilon) = d(\lambda, \varepsilon) \mathcal{D}_{\text{fast}}(\lambda, \varepsilon) \mathcal{D}_{\text{slow}}(\lambda, \varepsilon)$, where $d(\lambda, \varepsilon) \neq 0$, $\mathcal{D}_{\text{fast}} = t_1$, and $\mathcal{D}_{\text{slow}} = t_{22}t_{33} - t_{23}t_{32}$. The zeroes of $\mathcal{D}(\lambda, \varepsilon)$ are therefore given by the solutions of $t_1(t_{22}t_{33} - t_{23}t_{32}) = 0$.*

Combining this corollary with Theorem 3.3.4 yields that the eigenvalues of (3.3.3) coincide with the zeroes of the fast transmission function t_1 and of the determinant $t_{22}t_{33} - t_{23}t_{32}$ of the slow-fast transmission functions.

Proof. The statement of the corollary holds true in the case $t_{22} \neq 0$ by the above calculations. Hence, here, we need only to consider the case $t_{22} = 0$, since the rescaling of $\phi_{s,3}^-(\xi)$ is undefined for $t_{22} = 0$. However, after interchanging the role of $\phi_{s,2}^-(\xi)$ with $\phi_{s,3}^-(\xi)$, no rescaling is necessary anymore and the zeroes of the Evans function are determined by the zeroes of $t_1 t_{23} t_{32}$. This agrees with (3.3.26). \square

3.4 Stability of the standing 1-pulse solution for $\tau, \theta = \mathcal{O}(1)$

In this section, we analyze the linear stability of standing 1-pulse solutions in the regime in which the bifurcation parameters τ and θ are $\mathcal{O}(1)$. We determine the zeroes of the fast transmission function t_1 explicitly. Next, we use the 2-front structure of the pulse to deduce expressions for the slow-fast transmission functions t_{ij} . Although our analysis is restricted to the problem at hand, our methods can be directly extended to the stability analysis of multi-pulse, or multi-front patterns in singularly perturbed N -component systems, see also Section 3.6.

The main stability result reads

Theorem 3.4.1. *For any $\tau, \theta = \mathcal{O}(1)$, the standing 1-pulse solutions of (3.1.1), determined by the solution(s) A of (3.2.6) and given by the homoclinic orbits $\gamma_h(\xi)$ (see Theorem 3.2.1) are stable if and only if*

$$\alpha A^2 + \frac{\beta}{D} A^{\frac{2}{D}} > 0. \quad (3.4.1)$$

Note that $\alpha A^2 + \frac{\beta}{D} A^{\frac{2}{D}} = 0$ and $A \in (0, 1)$ if and only if $A = A_c$ (3.2.12), i.e., $\alpha A^2 + \frac{\beta}{D} A^{\frac{2}{D}} = 0$ is associated to the saddle-node bifurcation of homoclinic orbits (Theorem 3.2.1).

Theorem 3.4.1 is proved in the following three subsections. A direct consequence of this theorem and Lemma 2.2.2 is the following corollary, which lists for given values of the parameters α, β , and γ , the number K of standing 1-pulse solutions, as well as the stability type of these solutions. In this manner, the corollary is a convenient user's guide to the theorem.

Corollary 3.4.2. *Let (α, β, D) be such that $|\alpha D| > |\beta|$. Then, for $\varepsilon > 0$ small enough, and $\gamma_{c1, c2}, A_c$ as given in (3.2.11) and (3.2.12), respectively, we have*

- (a1a) if $\text{sgn}(\alpha) = \text{sgn}(\beta) = \text{sgn}(\gamma) = 1$, and $\gamma < \alpha + \beta$, then $K = 1$ and $\gamma_{h,1}^-(\xi)$ is stable.
- (a1b) if $\text{sgn}(\alpha) = \text{sgn}(\beta) = \text{sgn}(\gamma) = -1$, and $\gamma > \alpha + \beta$, then $K = 1$ and $\gamma_{h,1}^-(\xi)$ is unstable.
- (b2) if $\text{sgn}(\alpha) = -1 = -\text{sgn}(\beta)$, $\alpha + \beta > 0$, and $0 < \gamma < \alpha + \beta$, then $K = 1$ and $\gamma_{h,1}^-(\xi)$ is stable (see Figure 3.3).
- (b3) if $\text{sgn}(\alpha) = -1 = -\text{sgn}(\beta)$, $\alpha + \beta > 0$, and $\alpha + \beta < \gamma < \gamma_{c1}$, then $K = 2$ and $\gamma_{h,1}^-(\xi)$ ($0 < A < A_c$) is stable, while $\gamma_{h,2}^-(\xi)$ ($A_c < A < 1$) is unstable (see Figure 3.3).
- (c2) if $\text{sgn}(\alpha) = -1 = -\text{sgn}(\beta)$, $\alpha + \beta < 0$, and $\alpha + \beta < \gamma < 0$, then $K = 1$ and $\gamma_{h,1}^-(\xi)$ is unstable.
- (c3) if $\text{sgn}(\alpha) = -1 = -\text{sgn}(\beta)$, $\alpha + \beta < 0$, and $0 < \gamma < \gamma_{c1}$, then $K = 2$ and $\gamma_{h,1}^-(\xi)$ ($0 < A < A_c$) is stable, while $\gamma_{h,2}^-(\xi)$ ($A_c < A < 1$) is unstable.
- (d2) if $\text{sgn}(\alpha) = 1 = -\text{sgn}(\beta)$, $\alpha + \beta > 0$, and $\gamma_{c2} < \gamma < 0$, then $K = 2$ and $\gamma_{h,1}^-(\xi)$ ($0 < A < A_c$) is unstable, while $\gamma_{h,2}^-(\xi)$ ($A_c < A < 1$) is stable.
- (d3) if $\text{sgn}(\alpha) = 1 = -\text{sgn}(\beta)$, $\alpha + \beta > 0$, and $0 < \gamma < \alpha + \beta$, then $K = 1$ and $\gamma_{h,1}^-(\xi)$ is stable.
- (e2) if $\text{sgn}(\alpha) = 1 = -\text{sgn}(\beta)$, $\alpha + \beta < 0$, and $\gamma_{c2} < \gamma < \alpha + \beta$, then $K = 2$ and $\gamma_{h,1}^-(\xi)$ ($0 < A < A_c$) is unstable, while $\gamma_{h,2}^-(\xi)$ ($A_c < A < 1$) is stable.
- (e3) if $\text{sgn}(\alpha) = 1 = -\text{sgn}(\beta)$, $\alpha + \beta < 0$, and $\alpha + \beta < \gamma < 0$, then $K = 1$ and $\gamma_{h,1}^-(\xi)$ is unstable.

In the remaining cases we have $K = 0$.

Note that the labelling of the different cases corresponds to the labelling of the same cases in Lemma 2.2.2. Observe that in the cases that $K = 2$ sometimes the ‘wide’ pulse solutions are stable ((b3),(c3)), while in the other cases ((d2),(e2)) the ‘narrow’ pulse solutions are stable.

3.4.1 The transmission function t_1 and the fast eigenvalues

In this section, we determine the zeroes of the fast transmission function $t_1(\lambda, \varepsilon)$. For this purpose, we need to examine the linearized stability problem of the scalar fast reduced system;

$$\mathcal{L}u - \lambda_h u := u_{\xi\xi} + (1 - 3(u_h)^2 - \lambda_h)u = 0, \quad (3.4.2)$$

with $u_h(\xi)$ the constructed homoclinic pulse solution, see Theorem 3.2.1. Observe that this eigenvalue problem, and thus its eigenvalues, still depends on ε .

In Lemma 3.4.3 below we prove that the spectrum of the above problem is to

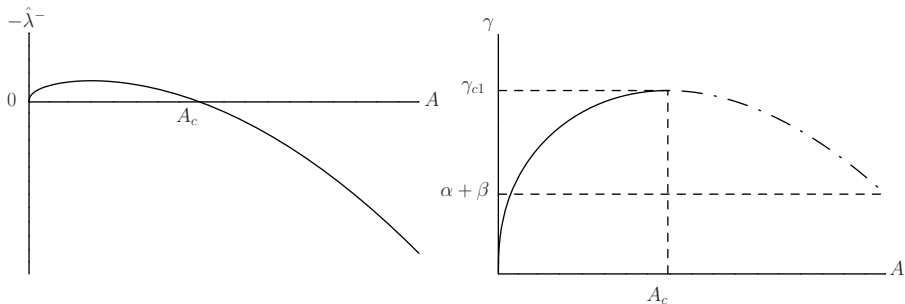


Figure 3.3: Corollary 3.4.2 cases b2) and b3). The left figure shows $-\hat{\lambda}^-$, the dominant eigenvalue, as function of A , see (3.4.20). The right figure shows the stability of the standing pulse as function of γ . The solid line corresponds to a stable standing 1-pulse, the dashed-dotted line corresponds to an unstable standing 1-pulse. Note that at $\gamma = \gamma_{c1}$ the system undergoes a saddle-node bifurcation, in which a stable and unstable standing pulse merge and disappear.

leading order determined by the spectra of the following problems

$$\mathcal{L}^\pm u - \lambda_{\text{fast}} u := u_{\xi\xi} + (1 - 3(u_{\text{fast}}^\pm(\xi \mp \xi_*))^2 - \lambda_{\text{fast}})u = 0. \quad (3.4.3)$$

The point spectra coincide, are independent of ε , and consist of the points $(\lambda_{\text{fast}})_2 = -\frac{3}{2}$ and $(\lambda_{\text{fast}})_1 = 0$, and the essential spectrum consists of the real values of λ_{fast} satisfying $\lambda_{\text{fast}} \leq -2$. This may be seen by rescaling ξ via the independent variable $\eta^\pm := \mp \frac{1}{2}\sqrt{2}(\xi \mp \xi_*)$, so that equation (3.4.3) becomes

$$u_{(\eta^\pm \mp \eta^\pm)} + \left(\frac{6}{\cosh^2 \eta^\pm} - (2\lambda_{\text{fast}} + 4) \right) u = 0. \quad (3.4.4)$$

This is a Schrödinger or Sturm-Liouville equation, which has a well-known spectrum, see Section 1.3.2 or [12, 14].

Lemma 3.4.3. *If $\max\{\tau, \theta\} > \frac{2}{3}$, then the linearized stability problem (3.3.2) has eigenvalues $\mathcal{O}(\varepsilon)$ close to the two eigenvalues $(\lambda_{\text{fast}})_{1,2} = 0, -\frac{3}{2}$ of the linearized stability problem associated to the fast reduced system (3.4.3). If $\max\{\tau, \theta\} < \frac{2}{3}$, then the linearized stability problem (3.3.2) has only eigenvalues that are $\mathcal{O}(\varepsilon)$ close to the eigenvalue $(\lambda_{\text{fast}})_1 = 0$.*

The difference between the two cases comes from the location of the essential spectrum. If one of the two bifurcation parameters is too small, that is, less than $\frac{2}{3}$, then the stable fast reduced eigenvalue $(\lambda_{\text{fast}})_2 = -\frac{3}{2}$ lies ‘inside’ the essential spectrum, see Lemma 3.3.1. Note that we do not consider the case where $\max\{\tau, \theta\}$ is asymptotically close to $\frac{2}{3}$ in which the eigenvalue near $-\frac{3}{2}$ disappears into σ_{ess} .

Proof. Without loss of generality, we can assume that $u(\xi) = \mathcal{O}(1)$ strictly in (3.3.2). Furthermore, we can assume that $v(\xi), w(\xi) = \mathcal{O}(1)$ or smaller, because when $\|v(\xi)\| \gg 1$ or $\|w(\xi)\| \gg 1$, it follows from the equations for $v(\xi)$ and $w(\xi)$ in (3.3.2) that the only solutions that are bounded as ξ goes to $\pm\infty$ are $v(\xi), w(\xi) \equiv 0$. We can solve the first equation of (3.3.2), formally we obtain

$$u(\xi) = \varepsilon(\mathcal{L} - \lambda)^{-1}(\alpha v(\xi) + \beta w(\xi)).$$

If we now assume that $|\lambda - (\lambda_{\text{fast}})_{1,2}| = \mathcal{O}(1)$, then $\|(\mathcal{L} - \lambda)^{-1}\| = \mathcal{O}(1)$ and therefore $\|u(\xi)\| = \varepsilon\|(\mathcal{L} - \lambda)^{-1}\|(\|\alpha v(\xi) + \beta w(\xi)\|) = \mathcal{O}(\varepsilon)$. However, we assumed $u(\xi) = \mathcal{O}(1)$. Therefore, we must have $|\lambda - (\lambda_{\text{fast}})_{1,2}| = \mathcal{O}(\varepsilon)$. \square

From this proposition, we conclude that also the possible zeroes of the transmission function $t_1(\lambda)$ are asymptotically close to 0 or $-\frac{3}{2}$. Specifically, we have

Lemma 3.4.4. *The zeroes of the transmission function $t_1(\lambda)$ are determined up to $\mathcal{O}(\varepsilon^3)$ corrections by the eigenvalues of (3.4.3).*

Since the details of are essentially the same as that of similar statements in [12, 13], see especially Section 6 of [12], we only state the main arguments.

Proof. It follows from the definition (3.3.20) of $t_1(\lambda)$ and the slow-fast structure of (3.3.2) that $t_1(\lambda)$ can only be zero if the v, w -components of $\phi_1^-(\xi)$ are $\mathcal{O}(\varepsilon^2)$ for all $\xi \in \mathbb{R}$. (Recall that the v, w -components of E_1 are $\mathcal{O}(\varepsilon^2)$ (3.3.6)). Thus the zeroes of $t_1(\hat{\lambda})$ are determined by the scalar equation (3.4.2) up to $\mathcal{O}(\varepsilon^3)$ corrections. \square

The zeroes of $t_1(\lambda)$ near $-\frac{3}{2}$ correspond to stable eigenvalues. However, we cannot yet conclude anything about (the signs of) the zeroes near 0. Therefore, we zoom in around $\lambda = 0$. That is, we rescale λ by $\lambda = \varepsilon^2 \hat{\lambda}$. Note that if we rescale λ with a power of ε less than 2, then it follows by the application of a solvability condition that the rescaled λ must be zero to leading order.

Lemma 3.4.5. *Transmission function $t_1(\lambda)$ has two zeroes $\lambda = \varepsilon^2 \hat{\lambda}_f^\pm$ near the origin that coincide to leading order and are given by*

$$\hat{\lambda}_f^\pm = \hat{\lambda}_f + \mathcal{O}(\varepsilon) := \frac{3}{2}\sqrt{2} \left(\alpha(1 - A^2) + \frac{\beta}{D}(1 - A^{2/D}) \right) + \mathcal{O}(\varepsilon). \quad (3.4.5)$$

Proof. After the rescaling of λ , the stability problem for the fast transmission function reads

$$u_{\varepsilon\xi} + (1 - 3u_n^2)u = \varepsilon^2 \hat{\lambda}u,$$

see (3.4.2).

We expand $u(\xi) = u_0(\xi) + \varepsilon^2 u_2(\xi) + \mathcal{O}(\varepsilon^3)$, and $u_h(\xi) = u_{h,0}(\xi) + \varepsilon^2 u_{h,2}(\xi) + \mathcal{O}(\varepsilon^3)$. To leading order, we obtain in the fast fields

$$\mathcal{L}^\pm u_0^\pm := (u_0^\pm)_{\xi\xi} + \left(1 - 3(u_{h,0}^\pm)^2\right) u_0^\pm = 0, \quad (3.4.6)$$

where $u_0^\pm(\xi)$, respectively $u_{h,0}^\pm(\xi)$, are the leading order terms of $u(\xi)$, respectively $u_h(\xi)$, in the fast fields I_f^\pm . It follows by the translation invariance of (3.1.1) that the solutions of (3.4.6) are given by

$$u_0^\pm(\xi) = \mp C^\pm \psi^\pm(\xi), \quad (3.4.7)$$

where $C^\pm \in \mathbb{R}$ denote two, as yet unknown, constants, and $\psi^\pm(\xi)$ denote the derivatives of $u_{h,0}^\pm(\xi)$ (3.2.13). In the fast fields I_f^\pm the $\mathcal{O}(\varepsilon^2)$ terms read

$$\mathcal{L}^\pm u_2^\pm = \hat{\lambda} u_0^\pm + 6u_{h,0}^\pm u_{h,2}^\pm u_0^\pm. \quad (3.4.8)$$

Next, we substitute (3.4.7) into (3.4.8), and impose the solvability condition on the resulting inhomogeneous equation, to derive that

$$\mp \hat{\lambda} C^\pm \int_{I_f^\pm} (\psi^\pm)^2 d\xi \mp 6C^\pm \int_{I_f^\pm} u_{h,0}^\pm u_{h,2}^\pm (\psi^\pm)^2 d\xi = 0.$$

Finally, we use (3.2.14) and the solvability condition of the derivative of the pulse solution (3.2.18) to obtain to leading order

$$\hat{\lambda}_f^\pm = \hat{\lambda}_f = \frac{-6 \int_{I_f^\pm} u_{h,0}^\pm u_{h,2}^\pm (\psi^\pm)^2 d\xi}{\int_{I_f^\pm} (\psi^\pm)^2 d\xi} = \frac{3}{2} \sqrt{2} \left(\alpha(1 - A^2) + \frac{\beta}{D}(1 - A^{2/D}) \right). \quad (3.4.9)$$

This completes the proof. \square

3.4.2 The slow basis functions $\phi_{2,3}$

In this section, we first return to the linearized stability problem (3.3.2). Based on the above insights, we introduce $\lambda = \varepsilon^2 \hat{\lambda}$, where $\hat{\lambda} = \mathcal{O}(1)$ with respect to ε . Also, it will be clear from the analysis that the v - and w -components of the associated eigenvalues must be $\mathcal{O}(\varepsilon)$. Hence, we scale these as $v(\xi) = \varepsilon \tilde{v}(\xi)$ and $w(\xi) = \varepsilon \tilde{w}(\xi)$ (see also Remark 3.4.2). The linear stability problem now reads

$$\begin{cases} u_{\xi\xi} + (1 - 3u_h^2)u &= \varepsilon^2(\hat{\lambda}u + \alpha\tilde{v} + \beta\tilde{w}), \\ \tilde{v}_{\xi\xi} &= -\varepsilon u + \varepsilon^2\tilde{v} + \varepsilon^4\tau\hat{\lambda}\tilde{v}, \\ \tilde{w}_{\xi\xi} &= -\frac{\varepsilon}{D^2}u + \frac{\varepsilon^2}{D^2}\tilde{w} + \frac{\varepsilon^4}{D^2}\theta\hat{\lambda}\tilde{w}. \end{cases} \quad (3.4.10)$$

The matrix \mathcal{M}_∞ for this problem differs from that in (3.3.4). Therefore, the leading order terms of the eigenvalues Λ_i and of the associated eigenvectors E_i of \mathcal{M}_∞ have changed. The squares of the eigenvalues are given by

$$\Lambda_{1,6}^2 = 2 + \mathcal{O}(\varepsilon), \quad \Lambda_{2,5}^2 = \varepsilon^2 + \mathcal{O}(\varepsilon^3), \quad \Lambda_{3,4}^2 = \frac{\varepsilon^2}{D^2} + \mathcal{O}(\varepsilon^3), \quad (3.4.11)$$

and the associated eigenvectors by

$$E_{1,6} = \begin{pmatrix} 1 \\ \pm\sqrt{2} \\ -\frac{1}{2}\varepsilon \\ \mp\frac{1}{2}\sqrt{2} \\ -\frac{1}{2}\frac{1}{D^2}\varepsilon \\ \mp\frac{1}{2}\sqrt{2}\frac{1}{D} \end{pmatrix}, \quad E_{2,5} = \begin{pmatrix} -\frac{\alpha}{2}\varepsilon^2 \\ \mathcal{O}(\varepsilon^3) \\ 1 \\ \pm 1 \\ \mathcal{O}(\varepsilon) \\ \mathcal{O}(\varepsilon) \end{pmatrix}, \quad E_{3,4} = \begin{pmatrix} -\frac{\beta}{2}\varepsilon^2 \\ \mathcal{O}(\varepsilon^3) \\ \mathcal{O}(\varepsilon) \\ \mathcal{O}(\varepsilon) \\ 1 \\ \pm 1 \end{pmatrix}. \quad (3.4.12)$$

Despite the changes in the eigenvalues and eigenvectors, the analysis of the previous sections, which is a leading order analysis, remains valid. For example, in the fast fields I_f^\pm the leading order behavior of the u -component remains given by $u_0^\pm(\xi) = \mp C^\pm \psi^\pm(\xi)$, see (3.4.7).

Now, we derive explicit expressions (see (3.4.15) and (3.4.16) below) for the slow basis functions $\phi_{s,j}^-$ ($j = 2, 3$) in the slow regimes I_s^-, I_s^0 , and I_s^+ , where we also recall Lemma 3.3.6. The main step in the analysis we present is to show that the slow basis functions $\phi_{s,2}^-$ and $\phi_{s,3}^-$ do not exhibit fast growth in the intermediate regime $I_f^- \cup I_s^0 \cup I_f^+$, and hence in particular not in I_s^0 .

A priori, these basis functions could have fast growth in this intermediate regime. In particular, there exist intermediate transmission functions s_{ji} such that, in this regime, the basis functions are in principle, to leading order, given by

$$\phi_{s,j}^-(\xi) = \sum_{i=1}^6 s_{ji} E_i e^{\Lambda_i(\xi+\xi_*)} \quad \text{for } j \in \{2, 3\},$$

However, as we now show, the fast components ($i = 1$ and $i = 6$) are actually absent. This demonstration is carried out in two steps. First, we study a closely related problem with a modified u_h and show that in the modified system the fast growing $i = 1$ component is not present. Then, we use this to show that neither of the fast components ($i = 1, 6$) are present in the original problem.

In particular, we modify $u_h(\xi)$ in $\mathcal{M}(\xi)$ (3.3.3) in such a fashion that the solutions are identical to the original solutions for $\xi \leq \xi_* - \frac{1}{\sqrt{\varepsilon}}$, and that the u -components of the solutions do not jump back to $u = -1$ (to leading order). The fact that $\hat{u}_h(\xi) \rightarrow 1$ as $\xi \rightarrow \infty$ while $u_h(\xi) \rightarrow -1$ does not have a leading order effect on the eigenvalues $\hat{\Lambda}_i$ and eigenvectors \hat{E}_i of $\hat{\mathcal{M}}_\infty$, *i.e.*, to leading order $\hat{\Lambda}_i = \Lambda_i$ (3.4.11), and $\hat{E}_i = E_i$ (3.4.12). The analysis of the preceding section is still applicable to the linear system governed by the modified matrix $\hat{\mathcal{M}}$, so that, by the equivalent of Lemma 3.3.6, we obtain

$$\hat{\phi}_j^-(\xi) = \sum_{i=2}^6 \hat{s}_{ji} E_i e^{\Lambda_i(\xi+\xi_*)} \quad \text{for } j \in \{2, 3\},$$

with $\hat{\phi}_j^-(\xi)$ the slow basis functions of the modified system. Thus, the modified system does not have a fast growing component ($i = 1$).

Since $\Lambda_{1,6} = \mathcal{O}(1)$ (and $\Lambda_{2,3,4,5} = \mathcal{O}(\varepsilon)$), $E_6 e^{\Lambda_6(\xi+\xi_*)}$ is exponentially small for $\xi \in I_s^0$ and $\xi = \mathcal{O}(1)$. So, to leading order we have

$$\begin{aligned}\hat{\phi}_{s,j}^-(\xi) &= s_{j1} E_1 e^{\Lambda_1(\xi+\xi_*)} + \sum_{i=2}^5 s_{ji} E_i e^{\Lambda_i(\xi+\xi_*)} \quad \text{for } j \in \{2, 3\}, \\ \hat{\phi}_j^-(\xi) &= \sum_{i=2}^5 \hat{s}_{ji} E_i e^{\Lambda_i(\xi+\xi_*)} \quad \text{for } j \in \{2, 3\}.\end{aligned}$$

By construction, we also have that $\hat{\phi}_{2,3}^-(\xi) = \phi_{s,2,3}^-(\xi)$ for $\xi \leq \xi_* - \frac{1}{\sqrt{\varepsilon}}$, so that we deduce that s_{j1} is exponentially small, and $s_{ji} = \hat{s}_{ji}$ for $i \in \{2, 3, 4, 5\}$ to leading order. We conclude that the slow functions $\phi_{s,2}^-(\xi)$ and $\phi_{s,3}^-(\xi)$ do not exhibit fast growth in the intermediate slow regime I_s^0 .

Thus, we may now express the leading order behavior of the \tilde{v} - and \tilde{w} -components of the slow functions $\phi_{s,2}^-(\xi)$ and $\phi_{s,3}^-(\xi)$ (Lemma 3.3.6) – which we for simplicity denote by ϕ_2 and ϕ_3 – in the slow fields in terms of the transmission functions $s_{ij}(\lambda)$ and $t_{ij}(\lambda)$. Based on the above conclusion regarding the absence of fast growth in the slow regime, we have

$$\phi_2(\xi) = \begin{cases} E_2 e^{\Lambda_2(\xi+\xi_*)} & \text{in } I_s^-, \\ s_{22} E_2 e^{\Lambda_2 \xi} + s_{23} E_3 e^{\Lambda_3 \xi} + s_{24} E_4 e^{\Lambda_4 \xi} + s_{25} E_5 e^{\Lambda_5 \xi} & \text{in } I_s^0, \\ t_{22} E_2 e^{\Lambda_2(\xi-\xi_*)} + t_{23} E_3 e^{\Lambda_3(\xi-\xi_*)} + t_{24} E_4 e^{\Lambda_4(\xi-\xi_*)} \\ \quad + t_{25} E_5 e^{\Lambda_5(\xi-\xi_*)} & \text{in } I_s^+, \end{cases} \quad (3.4.13)$$

and

$$\phi_3(\xi) = \begin{cases} E_3 e^{\Lambda_3(\xi+\xi_*)} & \text{in } I_s^-, \\ s_{32} E_2 e^{\Lambda_2 \xi} + s_{33} E_3 e^{\Lambda_3 \xi} + s_{34} E_4 e^{\Lambda_4 \xi} + s_{35} E_5 e^{\Lambda_5 \xi} & \text{in } I_s^0, \\ t_{32} E_2 e^{\Lambda_2(\xi-\xi_*)} + t_{33} E_3 e^{\Lambda_3(\xi-\xi_*)} + t_{34} E_4 e^{\Lambda_4(\xi-\xi_*)} \\ \quad + t_{35} E_5 e^{\Lambda_5(\xi-\xi_*)} & \text{in } I_s^+. \end{cases} \quad (3.4.14)$$

Note that $\phi_2(\xi) = \phi_{s,2}^-(\xi)$ is determined uniquely (Lemma 3.3.6); and $\phi_3(\xi)$ has been chosen such that it does not have a component that decays as $e^{\Lambda_2 \xi}$ for $\xi \in I_s^-$, see Figure 3.4. Finally, we substitute the eigenvalues Λ_i (3.4.11), and the components of the eigenvectors E_i (3.4.12) into the \tilde{v} - and \tilde{w} -components of $\phi_{2,3}(\xi)$. To leading order, we get

$$\begin{aligned}\phi_2^{\tilde{v}}(\xi) &= \begin{cases} e^{\varepsilon(\xi+\xi_*)} & \text{in } I_s^-, \\ s_{22} e^{\varepsilon \xi} + s_{25} e^{-\varepsilon \xi} & \text{in } I_s^0, \\ t_{22} e^{\varepsilon(\xi-\xi_*)} + t_{24} E_4^{\tilde{v}} e^{-\frac{\varepsilon}{D}(\xi-\xi_*)} + t_{25} e^{-\varepsilon(\xi-\xi_*)} & \text{in } I_s^+, \\ 0 & \text{in } I_s^-, \end{cases} \\ \phi_2^{\tilde{w}}(\xi) &= \begin{cases} s_{23} e^{\frac{\varepsilon}{D} \xi} + s_{24} e^{-\frac{\varepsilon}{D} \xi} & \text{in } I_s^0, \\ t_{22} E_2^{\tilde{w}} e^{\varepsilon(\xi-\xi_*)} + t_{23} e^{\frac{\varepsilon}{D}(\xi-\xi_*)} + t_{24} e^{-\frac{\varepsilon}{D}(\xi-\xi_*)} & \text{in } I_s^+, \end{cases} \end{aligned} \quad (3.4.15)$$

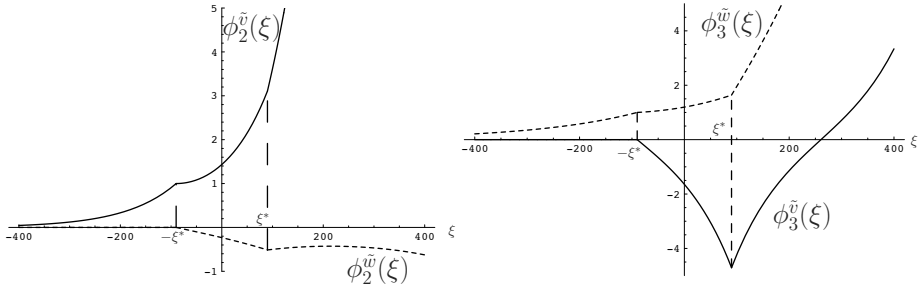


Figure 3.4: Examples of the two solutions $\phi_{2,3}(\xi)$. We have chosen the parameters in such a fashion that $\xi_* = 90$. Moreover, $\varepsilon = 0.01$ and $D = 2$. The jumps in the derivatives, produced by the change of the u -component during the jumps through the fast fields, are chosen as follows $(C_2^-, C_2^+, C_3^-, C_3^+) = (0.5, 1, 0.8, 5)$. Note that by this choice, we have $t_{22} = 4.02, t_{23} = -0.11, t_{32} = 0.16$, and $t_{33} = 3.98$.

and

$$\begin{aligned} \phi_3^{\bar{v}}(\xi) &= \begin{cases} 0 & \text{in } I_s^-, \\ s_{32}e^{\varepsilon\xi} + s_{35}e^{-\varepsilon\xi} & \text{in } I_s^0, \\ t_{32}e^{\varepsilon(\xi-\xi_*)} + t_{34}E_4^{\bar{v}}e^{-\frac{\varepsilon}{D}(\xi-\xi_*)} + t_{35}e^{-\varepsilon(\xi-\xi_*)} & \text{in } I_s^+, \\ e^{\frac{\varepsilon}{D}(\xi+\xi_*)} & \text{in } I_s^-, \end{cases} \\ \phi_3^{\bar{w}}(\xi) &= \begin{cases} s_{33}e^{\frac{\varepsilon}{D}\xi} + s_{34}e^{-\frac{\varepsilon}{D}\xi} & \text{in } I_s^0, \\ t_{32}E_2^{\bar{w}}e^{\varepsilon(\xi-\xi_*)} + t_{33}e^{\frac{\varepsilon}{D}(\xi-\xi_*)} + t_{34}e^{-\frac{\varepsilon}{D}(\xi-\xi_*)} & \text{in } I_s^+. \end{cases} \end{aligned} \quad (3.4.16)$$

These explicit expressions will be used in the next section to calculate the transmission functions s_{ij} and t_{ij} .

Remark 3.4.1. Note that although $E_4^{\bar{v}} = \mathcal{O}(\varepsilon)$, the term with t_{24} in $\phi_2^{\bar{v}}(\xi)$ in (3.4.15) may dominate the other decaying term (the one with t_{25}) in I_s^+ since $\Lambda_4 = -\frac{\varepsilon}{D} + \mathcal{O}(\varepsilon^2) > \Lambda_5 = -\varepsilon + \mathcal{O}(\varepsilon^2)$. Hence, this term has to be taken into account. By the same ordering argument it follows that the term with $t_{23}E_3^{\bar{v}}$ is always of higher order compared to the t_{22} term and thus cannot have a leading order effect. Likewise, $t_{22}E_2^{\bar{w}} = \mathcal{O}(\varepsilon)$ appears in $\phi_2^{\bar{w}}(\xi)$, while $t_{25}E_5^{\bar{w}}$ does not. The same argument can be applied to $\phi_3(\xi)$ (3.4.16).

3.4.3 The slow-fast transmission functions t_{ij}

In this section, we complete the proof of Theorem 3.4.1. In particular, we first calculate the slow-fast transmission functions $t_{ij}(\hat{\lambda})$, showing that they are meromorphic, and then compute the zeroes and poles of $\mathcal{D}_{\text{slow}}(\hat{\lambda})$ (Corollary 3.3.7), showing that the double eigenvalue $\hat{\lambda}_f$ (3.4.5) is exactly a pole of order two of

$\mathcal{D}_{\text{slow}}(\hat{\lambda})$. These results are given in Lemma 3.4.6 below, and then Theorem 3.4.1 follows directly from it.

Lemma 3.4.6. *The slow-fast transmission functions $t_{ij}(\hat{\lambda})$ are to leading order given by*

$$\begin{aligned} t_{22} &= \frac{1}{R^2} (A^{-2}R^2 - 2\alpha A^{-2}R - \alpha S), \\ t_{23} &= -\frac{\alpha}{DR^2} ((A^{-2} + A^{-2/D})R + S), \\ t_{32} &= -\frac{\beta}{R^2} ((A^{-2} + A^{-2/D})R + S), \\ t_{33} &= \frac{1}{DR^2} (DA^{-2/D}R^2 - 2\beta A^{-2/D}R - \beta S), \end{aligned} \quad (3.4.17)$$

where

$$\begin{aligned} S &= \alpha(A^2 - A^{-2}) + \frac{\beta}{D} (A^{2/D} - A^{-2/D}), \\ R &= R(\hat{\lambda}) = \alpha(1 - A^2) + \frac{\beta}{D}(1 - A^{2/D}) - \frac{1}{3}\sqrt{2}\hat{\lambda}. \end{aligned} \quad (3.4.18)$$

Moreover,

$$\begin{aligned} \mathcal{D}_{\text{slow}}(\hat{\lambda}) &= t_{22}t_{33} - t_{23}t_{32} = \\ &= A^{-2}A^{-2/D} \frac{\hat{\lambda}(\hat{\lambda} + 3\sqrt{2}(\alpha A^2 + \frac{\beta}{D}A^{2/D}))}{(\hat{\lambda} + \frac{3}{2}\sqrt{2}(\alpha(A^2 - 1) + \frac{\beta}{D}(A^{2/D} - 1)))^2}. \end{aligned} \quad (3.4.19)$$

Note that $R(\hat{\lambda}_f) = 0$, so that all $t_{ij}(\hat{\lambda})$'s have (to leading order) a pole of order 2 at the double zero $\hat{\lambda} = \hat{\lambda}_f$ of $t_1(\hat{\lambda})$ (Lemma 3.4.5). Hence, one would *a priori* expect that the determinant $\mathcal{D}_{\text{slow}}(\hat{\lambda})$ has a pole of order 4 at $\hat{\lambda}_f$. Nevertheless, it follows from a careful analysis that $\mathcal{D}_{\text{slow}}(\hat{\lambda})$ only has a pole of order 2. Of course this is necessary since the product $\mathcal{D}_{\text{fast}}\mathcal{D}_{\text{slow}}$ must be smooth (Corollary 3.3.7, [1]).

Proof of Theorem 3.4.1. It follows from Lemma 3.4.6 that the zeroes of $\mathcal{D}_{\text{slow}}(\hat{\lambda})$ are given to leading order by

$$\hat{\lambda}^+ = 0, \quad \hat{\lambda}^- = -3\sqrt{2} \left(\alpha A^2 + \frac{\beta}{D} A^{2/D} \right), \quad (3.4.20)$$

where $\hat{\lambda}^+$ corresponds to $\lambda \equiv 0$, the eigenvalue associated to the translational invariance. The sign of the dominant eigenvalue $\hat{\lambda}^-$ is determined by the sign of $\alpha A^2 + \frac{\beta}{D} A^{2/D}$. \square

The basic strategy for the proof of Lemma 3.4.6 consists of several steps. First, we impose continuity of $\tilde{v}(\xi)$ and $\tilde{w}(\xi)$ to leading order at the boundaries of the slow fields, as one crosses the fast fields, since $\tilde{v}(\xi)$ and $\tilde{w}(\xi)$ do not change to leading order in I_f^+ (3.3.2). In addition, we impose that the derivatives of these functions have jump discontinuities at the edges of the slow fields, which are determined by the accumulated change in these derivatives as the functions $\phi_{2,3}(\xi)$ pass through

the fast field. This method of matching the jump discontinuities as measured in the slow and fast fields lies at the heart of the NLEP procedure for singularly perturbed eigenvalue problems [11–13]. Finally, we consider $\phi_{2,3}(\xi)$ in the fast fields I_f^\pm and obtain explicit expressions for the slow-fast transmission functions t_{ij} by imposing the solvability conditions.

Proof of Lemma 3.4.6. We start with the construction of $\phi_2^{\tilde{v}}(\xi)$. Since $\tilde{v}(\xi)$ remains constant (to leading order) over I_f^- , we have

$$\begin{aligned} \phi_2^{\tilde{v}}(-\xi_* - \frac{1}{\sqrt{\varepsilon}}) &= \phi_2^{\tilde{v}}(-\xi_* + \frac{1}{\sqrt{\varepsilon}}) + \mathcal{O}(\sqrt{\varepsilon}) \implies \\ e^{\varepsilon(-\frac{1}{\sqrt{\varepsilon}})} &= s_{22}e^{\varepsilon(-\xi_* + \frac{1}{\sqrt{\varepsilon}})} + s_{25}e^{\varepsilon(\xi_* - \frac{1}{\sqrt{\varepsilon}})} + \mathcal{O}(\sqrt{\varepsilon}) \implies (3.4.21) \\ 1 &= s_{22}e^{-\varepsilon\xi_*} + s_{25}e^{\varepsilon\xi_*} + \mathcal{O}(\sqrt{\varepsilon}), \end{aligned}$$

where we used (3.4.15). Next, we turn to the derivative. Individually, the derivatives of $\phi_2^{\tilde{v}}(\xi)$ at the left and right boundaries of I_f^- are given by

$$\begin{aligned} (\phi_2^{\tilde{v}})_\xi(-\xi_* - \frac{1}{\sqrt{\varepsilon}}) &= \varepsilon + \mathcal{O}(\varepsilon\sqrt{\varepsilon}), \\ (\phi_2^{\tilde{v}})_\xi(-\xi_* + \frac{1}{\sqrt{\varepsilon}}) &= \varepsilon (s_{22}e^{-\varepsilon\xi_*} - s_{25}e^{\varepsilon\xi_*}) + \mathcal{O}(\varepsilon\sqrt{\varepsilon}) \\ &= \varepsilon (2s_{22}e^{-\varepsilon\xi_*} - 1) + \mathcal{O}(\varepsilon\sqrt{\varepsilon}), \end{aligned}$$

where we used (3.4.21). Thus, the change of the derivative of $\phi_2^{\tilde{v}}(\xi)$ over I_f^- is

$$\begin{aligned} \Delta_s^-(\phi_2^{\tilde{v}})_\xi &= (\phi_2^{\tilde{v}})_\xi(-\xi_* + \frac{1}{\sqrt{\varepsilon}}) - (\phi_2^{\tilde{v}})_\xi(-\xi_* - \frac{1}{\sqrt{\varepsilon}}) \\ &= 2\varepsilon (s_{22}e^{-\varepsilon\xi_*} - 1) + \mathcal{O}(\varepsilon\sqrt{\varepsilon}). \end{aligned} \quad (3.4.22)$$

This change is due to the accumulated change of the derivative of $\phi_2^{\tilde{v}}(\xi)$ over the fast field I_f^- ,

$$\Delta_f^-(\phi_2^{\tilde{v}})_\xi = \int_{I_f^-} \tilde{v}_{\xi\xi} d\xi = -\varepsilon \int_{I_f^-} u_0^- d\xi + \mathcal{O}(\varepsilon\sqrt{\varepsilon}) = -2\varepsilon C_2^- + \mathcal{O}(\varepsilon\sqrt{\varepsilon}), \quad (3.4.23)$$

where we used (3.4.10) and (3.4.7) with constant C_2^- instead of C^- , and (3.2.14). Matching the slow and fast jumps, $\Delta_s^-(\phi_2^{\tilde{v}})_\xi$ and $\Delta_f^-(\phi_2^{\tilde{v}})_\xi$, and recalling (3.4.21), we obtain

$$s_{22} = (1 - C_2^-) e^{\varepsilon\xi_*} + \mathcal{O}(\sqrt{\varepsilon}), \quad s_{25} = C_2^- e^{-\varepsilon\xi_*} + \mathcal{O}(\sqrt{\varepsilon}). \quad (3.4.24)$$

Next, we impose leading order continuity of $\phi_2^{\tilde{v}}(\xi)$ over the second fast field I_f^+ . This yields

$$\begin{aligned} \phi_2^{\tilde{v}}(\xi_* - \frac{1}{\sqrt{\varepsilon}}) &= \phi_2^{\tilde{v}}(\xi_* + \frac{1}{\sqrt{\varepsilon}}) + \mathcal{O}(\sqrt{\varepsilon}) \implies \\ (1 - C_2^-)e^{2\varepsilon\xi_*} + C_2^- e^{-2\varepsilon\xi_*} &= t_{22} + t_{25} + \mathcal{O}(\sqrt{\varepsilon}). \end{aligned} \quad (3.4.25)$$

The jump discontinuity in the derivative of the \tilde{v} -component over I_f^+ is given by

$$\begin{aligned}\Delta_s^+(\phi_2^{\tilde{v}})_\xi &= (\phi_2^{\tilde{v}})_\xi(\xi_* + \frac{1}{\sqrt{\varepsilon}}) - (\phi_2^{\tilde{v}})_\xi(\xi_* - \frac{1}{\sqrt{\varepsilon}}) \\ &= \varepsilon(t_{22} - t_{25}) - \varepsilon((1 - C_2^-)e^{2\varepsilon\xi_*} - C_2^-e^{-2\varepsilon\xi_*}) + \mathcal{O}(\varepsilon\sqrt{\varepsilon}) \\ &= 2\varepsilon(t_{22} - (1 - C_2^-)e^{2\varepsilon\xi_*}) + \mathcal{O}(\varepsilon\sqrt{\varepsilon}),\end{aligned}$$

where we used (3.4.24) and (3.4.25). The same jump is given in the fast field by

$$\Delta_f^+(\phi_2^{\tilde{v}})_\xi = \int_{I_f^+} v_{\xi\xi} d\xi = -\varepsilon \int_{I_f^+} u_0^+ d\xi + \mathcal{O}(\varepsilon\sqrt{\varepsilon}) = 2\varepsilon C_2^+ + \mathcal{O}(\varepsilon\sqrt{\varepsilon}), \quad (3.4.26)$$

where C_2^+ is a second unknown constant. Matching $\Delta_f^+(\phi_2^{\tilde{v}})_\xi$ with $\Delta_s^+(\phi_2^{\tilde{v}})_\xi$ and using (3.4.25), we find

$$t_{22} = C_2^+ + (1 - C_2^-)e^{2\varepsilon\xi_*} + \mathcal{O}(\sqrt{\varepsilon}), \quad t_{25} = C_2^-e^{-2\varepsilon\xi_*} - C_2^+ + \mathcal{O}(\sqrt{\varepsilon}). \quad (3.4.27)$$

In a similar manner, by imposing leading order continuity of $\phi_2^{\tilde{w}}(\xi)$, $\phi_3^{\tilde{v}}(\xi)$, and $\phi_3^{\tilde{w}}(\xi)$ at I_f^\pm , as well as the jump discontinuities in their derivatives, we determine the twelve other slow-fast transmission functions s_{23}, s_{24}, t_{23} , and t_{24} via $\phi_2^{\tilde{w}}(\xi)$; s_{32}, s_{35}, t_{32} , and t_{35} via $\phi_3^{\tilde{v}}(\xi)$, and s_{33}, s_{34}, t_{33} , and t_{34} via $\phi_3^{\tilde{w}}(\xi)$. To leading order they read,

$$\begin{aligned}s_{23} &= -\frac{1}{D}C_2^-e^{\frac{\varepsilon}{D}\xi_*}, & s_{24} &= \frac{1}{D}C_2^-e^{-\frac{\varepsilon}{D}\xi_*}, \\ t_{23} &= \frac{1}{D}(C_2^+ - C_2^-e^{2\frac{\varepsilon}{D}\xi_*}), & t_{24} &= \frac{1}{D}(C_2^-e^{-2\frac{\varepsilon}{D}\xi_*} - C_2^+), \\ s_{32} &= -C_3^-e^{\varepsilon\xi_*}, & s_{35} &= C_3^-e^{-\varepsilon\xi_*}, \\ t_{32} &= C_3^+ - C_3^-e^{2\varepsilon\xi_*}, & t_{35} &= C_3^-e^{-2\varepsilon\xi_*} - C_3^+, \\ s_{33} &= \frac{1}{D}(D - C_3^-)e^{\frac{\varepsilon}{D}\xi_*}, & s_{34} &= \frac{1}{D}C_3^-e^{-\frac{\varepsilon}{D}\xi_*}, \\ t_{33} &= \frac{1}{D}(C_3^+ + (D - C_3^-)e^{2\frac{\varepsilon}{D}\xi_*}), & t_{34} &= \frac{1}{D}(C_3^-e^{-2\frac{\varepsilon}{D}\xi_*} - C_3^+).\end{aligned} \quad (3.4.28)$$

Here, all the higher order corrections are of $\mathcal{O}(\sqrt{\varepsilon})$, and C_3^\pm are the, so far unknown, constants of the u -component (3.4.7) for $\phi_3(\xi)$. Substituting these quantities into (3.4.15) and (3.4.16) we find $\phi_{2,3}(\xi)$, to leading order,

$$\begin{aligned}\phi_2^{\tilde{v}}(\xi) &= \begin{cases} e^{\varepsilon(\xi+\xi_*)} & \text{in } I_s^-, \\ (1 - C_2^-)e^{\varepsilon(\xi+\xi_*)} + C_2^-e^{-\varepsilon(\xi+\xi_*)} & \text{in } I_s^0, \\ (C_2^+ + (1 - C_2^-)e^{2\varepsilon\xi_*})e^{\varepsilon(\xi-\xi_*)} \\ + (C_2^-e^{-2\varepsilon\xi_*} - C_2^+)e^{-\varepsilon(\xi-\xi_*)} \\ + \frac{1}{D}(C_2^-e^{-2\frac{\varepsilon}{D}\xi_*} - C_2^+)E_4^{\tilde{v}}e^{-\frac{\varepsilon}{D}(\xi-\xi_*)} & \text{in } I_s^+, \\ 0 & \text{in } I_s^-, \end{cases} \\ \phi_2^{\tilde{w}}(\xi) &= \begin{cases} -\frac{1}{D}C_2^-e^{\frac{\varepsilon}{D}(\xi+\xi_*)} + \frac{1}{D}C_2^-e^{-\frac{\varepsilon}{D}(\xi+\xi_*)} & \text{in } I_s^0, \\ \frac{1}{D}(C_2^+ - C_2^-e^{2\frac{\varepsilon}{D}\xi_*})e^{\frac{\varepsilon}{D}(\xi-\xi_*)} \\ + \frac{1}{D}(C_2^-e^{-2\frac{\varepsilon}{D}\xi_*} - C_2^+)e^{-\frac{\varepsilon}{D}(\xi-\xi_*)} \\ + (C_2^+ + (1 - C_2^-)e^{2\varepsilon\xi_*})E_2^{\tilde{w}}e^{\varepsilon(\xi-\xi_*)} & \text{in } I_s^+, \end{cases}\end{aligned} \quad (3.4.29)$$

and

$$\phi_3^{\tilde{v}}(\xi) = \begin{cases} 0 & \text{in } I_s^-, \\ -C_3^- e^{\varepsilon(\xi+\xi_*)} + C_3^- e^{-\varepsilon(\xi+\xi_*)} & \text{in } I_s^0, \\ (C_3^+ - C_3^- e^{2\varepsilon\xi_*}) e^{\varepsilon(\xi-\xi_*)} \\ + (C_3^- e^{-2\varepsilon\xi_*} - C_3^+) e^{-\varepsilon(\xi-\xi_*)} \\ + \frac{1}{D} (C_3^- e^{-2\frac{\varepsilon}{D}\xi_*} - C_3^+) E_4^{\tilde{v}} e^{-\frac{\varepsilon}{D}(\xi-\xi_*)} & \text{in } I_s^+, \\ e^{\frac{\varepsilon}{D}(\xi+\xi_*)} & \text{in } I_s^-, \end{cases} \quad (3.4.30)$$

$$\phi_3^{\tilde{w}}(\xi) = \begin{cases} \frac{1}{D} (D - C_3^-) e^{\frac{\varepsilon}{D}(\xi+\xi_*)} + \frac{1}{D} C_3^- e^{-\frac{\varepsilon}{D}(\xi+\xi_*)} & \text{in } I_s^0, \\ (C_3^+ - C_3^- e^{2\varepsilon\xi_*}) E_2^{\tilde{w}} e^{\varepsilon(\xi-\xi_*)} \\ + \frac{1}{D} (C_3^+ + (D - C_3^-) e^{2\frac{\varepsilon}{D}\xi_*}) e^{\frac{\varepsilon}{D}(\xi-\xi_*)} \\ + \frac{1}{D} (C_3^- e^{-2\frac{\varepsilon}{D}\xi_*} - C_3^+) e^{-\frac{\varepsilon}{D}(\xi-\xi_*)} & \text{in } I_s^+. \end{cases}$$

To determine the constants $C_{2,3}^{\pm}$ we use the solvability condition (3.2.18). The u -equation in the fast fields I_f^{\pm} (3.4.10) reads

$$u_{\xi\xi} + (1 - 3u_h^2)u = \varepsilon^2(\hat{\lambda}u + \alpha\tilde{v} + \beta\tilde{w}).$$

Observe that, by construction, the leading order term $u_0^{\pm}(\xi)$ and the first order correction term $u_1^{\pm}(\xi)$ fulfill the solvability condition. However, the second order correction term, $\mathcal{O}(\varepsilon^2)$, does not fulfill the solvability condition yet, and it is this condition which will enable us to calculate the four unknowns $C_{2,3}^{\pm}$.

In the fast fields I_f^{\pm} , the \tilde{v}, \tilde{w} -components of the basis functions $\phi_{2,3}(\xi)$ (3.4.29, 3.4.30) are constant and given to leading order by (see Remark 3.4.1)

$$\begin{aligned} \phi_2^{\tilde{v}}(-\xi_*) &= 1, & \phi_2^{\tilde{v}}(\xi_*) &= (1 - C_2^-)e^{2\varepsilon\xi_*} + C_2^- e^{-2\varepsilon\xi_*}, \\ \phi_2^{\tilde{w}}(-\xi_*) &= 0, & \phi_2^{\tilde{w}}(\xi_*) &= -\frac{1}{D}C_2^- e^{2\frac{\varepsilon}{D}\xi_*} + \frac{1}{D}C_2^- e^{-2\frac{\varepsilon}{D}\xi_*}, \\ \phi_3^{\tilde{v}}(-\xi_*) &= 0, & \phi_3^{\tilde{v}}(\xi_*) &= -C_3^- e^{2\varepsilon\xi_*} + C_3^- e^{-2\varepsilon\xi_*}, \\ \phi_3^{\tilde{w}}(-\xi_*) &= 1, & \phi_3^{\tilde{w}}(\xi_*) &= \frac{1}{D}(D - C_3^-) e^{2\frac{\varepsilon}{D}\xi_*} + \frac{1}{D}C_3^- e^{-2\frac{\varepsilon}{D}\xi_*}. \end{aligned}$$

Therefore, at $\mathcal{O}(\varepsilon^2)$, the terms of the u -equation in the fast fields I_f^{\pm} for $\phi_2(\xi)$ reduce to

$$\begin{aligned} \mathcal{L}^- u_2^- &= \hat{\lambda}u_0^- + \alpha + 6u_{h,0}^- u_{h,2}^- u_0^-, \\ \mathcal{L}^+ u_2^+ &= \hat{\lambda}u_0^+ + \alpha \left((1 - C_2^-) e^{2\varepsilon\xi_*} + C_2^- e^{-2\varepsilon\xi_*} \right) \\ &\quad + \frac{\beta}{D} C_2^- \left(-e^{2\frac{\varepsilon}{D}\xi_*} + e^{-2\frac{\varepsilon}{D}\xi_*} \right) + 6u_{h,0}^+ u_{h,2}^+ u_0^+. \end{aligned} \quad (3.4.31)$$

For $\phi_3^u(\xi)$ in the fast fields I_f^{\pm} we obtain

$$\begin{aligned} \mathcal{L}^- u_2^- &= \hat{\lambda}u_0^- + \beta + 6u_{h,0}^- u_{h,2}^- u_0^-, \\ \mathcal{L}^+ u_2^+ &= \hat{\lambda}u_0^+ + \alpha C_3^- \left(-e^{2\varepsilon\xi_*} + e^{-2\varepsilon\xi_*} \right) \\ &\quad + \frac{\beta}{D} \left((D - C_3^-) e^{2\frac{\varepsilon}{D}\xi_*} + C_3^- e^{-2\frac{\varepsilon}{D}\xi_*} \right) + 6u_{h,0}^+ u_{h,2}^+ u_0^+. \end{aligned} \quad (3.4.32)$$

Next, recalling (3.4.7) and (3.2.14), we obtain from the solvability condition

$$\begin{aligned}
0 &= \frac{2}{3}\sqrt{2}\hat{\lambda}C_2^- + 2\alpha + 6C_2^- \int_{I_f^-} u_{h,0}^- u_{h,2}^- (\psi^-)^2 d\xi, \\
0 &= -\frac{2}{3}\sqrt{2}\hat{\lambda}C_2^+ + 2\alpha \left((1 - C_2^-) e^{2\varepsilon\xi_*} + C_2^- e^{-2\varepsilon\xi_*} \right) \\
&\quad + 2\frac{\beta}{D}C_2^- \left(-e^{2\frac{\varepsilon}{D}\xi_*} + e^{-2\frac{\varepsilon}{D}\xi_*} \right) - 6C_2^+ \int_{I_f^+} u_{h,0}^+ u_{h,2}^+ (\psi^+)^2 d\xi, \\
0 &= \frac{2}{3}\sqrt{2}\hat{\lambda}C_3^- + 2\beta + 6C_3^- \int_{I_f^-} u_{h,0}^- u_{h,2}^- (\psi^-)^2 d\xi, \\
0 &= -\frac{2}{3}\sqrt{2}\hat{\lambda}C_3^+ + 2\alpha C_3^- \left(-e^{2\varepsilon\xi_*} + e^{-2\varepsilon\xi_*} \right) \\
&\quad + 2\frac{\beta}{D} \left((D - C_3^-) e^{2\frac{\varepsilon}{D}\xi_*} + C_3^- e^{-2\frac{\varepsilon}{D}\xi_*} \right) - 6C_3^+ \int_{I_f^+} u_{h,0}^+ u_{h,2}^+ (\psi^+)^2 d\xi.
\end{aligned}$$

Now, using the integral relations (3.2.18), and recalling (3.2.8), the above yields

$$\begin{aligned}
C_2^- &= \frac{\alpha}{R}, & C_2^+ &= \frac{-\alpha A^{-2} - SC_2^-}{R} = \frac{-\alpha(A^{-2}R+S)}{R^2}, \\
C_3^- &= \frac{\beta}{R}, & C_3^+ &= \frac{-\beta A^{-2/D} - SC_3^-}{R} = \frac{-\beta(A^{-2/D}R+S)}{R^2},
\end{aligned} \tag{3.4.33}$$

where S and $R = R(\hat{\lambda})$ are defined in (3.4.18). Substituting these four constants into (3.4.27) and (3.4.28) yields the explicit expressions for the four slow-fast transmission functions t_{22}, t_{23}, t_{32} , and t_{33} (3.4.17). The leading order approximation (3.4.19) of the slow component $\mathcal{D}_{\text{slow}}(\hat{\lambda})$ of the Evans function $\mathcal{D}(\hat{\lambda})$ (Corollary 3.3.7) now follows by a tedious, but straightforward, calculation. \square

It is also of interest to observe that away from $\alpha A^2 + \frac{\beta}{D}A^{\frac{2}{D}} = 0$, we can determine the eigenfunctions $\Psi^\pm(\xi)$ associated to the small eigenvalues $\hat{\lambda}^\pm$. A general nontrivial function $\phi(\xi)$ is a superposition of $\phi_2(\xi)$ and $\phi_3(\xi)$, that is, $\phi(\xi) = \mu_2\phi_2(\xi) + \mu_3\phi_3(\xi)$. For the eigenfunction $\Psi^+(\xi)$ associated to $\hat{\lambda}^+ = 0$, we have $\mu_2 = 1 - A^2$ and $\mu_3 = \frac{1}{D}(1 - A^{2/D})$. For the other eigenfunction, $\Psi^-(\xi)$, we have $\mu_2 = 1 + A^2$ and $\mu_3 = \frac{1}{D}(1 + A^{2/D})$. Note that, when we define $C^\pm := \mu_2 C_2^\pm + \mu_3 C_3^\pm$, the first eigenfunction, $\Psi^+(\xi)$, yields $C^- = C^+ = 1$, while the second eigenfunction, $\Psi^-(\xi)$, yields $C^- = -C^+ = 1$. The u -components of these eigenfunctions are zero to leading order outside the fast fields I_f^\pm , and inside these fields they are given by

$$\Psi^{+,u}(\xi) = \begin{cases} \psi^-(\xi) & \text{in } I_f^-, \\ -\psi^+(\xi) & \text{in } I_f^+, \end{cases} \quad \Psi^{-,u}(\xi) = \begin{cases} \psi^-(\xi) & \text{in } I_f^-, \\ \psi^+(\xi) & \text{in } I_f^+. \end{cases}$$

Observe that $\Psi^{+,u}(\xi)$ is an odd eigenfunction, while $\Psi^{-,u}(\xi)$ is an even function. Moreover, also the \tilde{v} - and \tilde{w} -components are odd, respectively, even, see Figure 3.5. This suggests that the bifurcation to a traveling pulse, a symmetry breaking bifurcation, is related to the asymmetric eigenfunction $\Psi^+(\xi)$, while a Hopf bifurcation, which is a symmetry preserving bifurcation, should be related to the symmetric eigenfunction $\Psi^-(\xi)$. This is confirmed in Section 3.5.2.

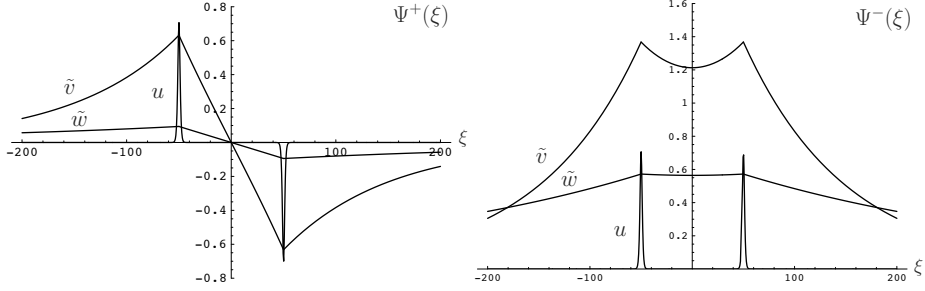


Figure 3.5: The odd eigenfunction $\Psi^+(\xi)$ associated to $\hat{\lambda}^+ = 0$, and the even eigenfunction $\Psi^-(\xi)$ associated to $\hat{\lambda}^-$.

Remark 3.4.2. The leading order terms in the integrals (3.4.23) and (3.4.26) justify the asymptotic magnitude of the rescaling of v and w . That is, it is not possible to find nontrivial bounded basis functions associated to small eigenvalues for which the v - and w -components are larger than $\mathcal{O}(\varepsilon)$, since in that scaling one finds that the slow-fast transmission functions cannot vanish.

Remark 3.4.3. For D asymptotically large, *i.e.*, in the case in which (3.1.1) approaches a two-component system (see Remark 3.1.3), the slow-fast transmission functions t_{ij} , $i, j = 2, 3$ (3.4.17) reduce, to leading order, to

$$\begin{aligned} t_{22} &= \frac{1}{R_D^2} (A_D^{-2} R_D^2 - 2\alpha A_D^{-2} - \alpha S_D), \quad t_{23} = 0, \\ t_{32} &= -\frac{\beta}{R_D^2} ((A_D^{-2} + 1)R_D + S_D), \quad t_{33} = 1, \end{aligned}$$

where $R_D = \alpha(1 - A_D^2) - \frac{1}{3}\sqrt{2}\hat{\lambda}$, $S_D = \alpha(A_D^2 - A_D^{-2})$, and $A_D = \sqrt{\frac{\gamma - \beta}{\alpha}}$. Thus, $\mathcal{D}_{\text{slow}}$ reduces to t_{22} as expected for a two-component system [12, 13]. Moreover, the zeroes of $\mathcal{D}_{\text{slow}}$ are given by $\hat{\lambda}^+ = 0$ and $\hat{\lambda}^- = -3\sqrt{2}(\gamma - \beta)$, and $\mathcal{D}_{\text{slow}}$ has a pole of order 2 at $\frac{3}{2}\sqrt{2}(\alpha - \gamma + \beta)$.

3.5 1-pulse solutions for $\tau = \mathcal{O}(\varepsilon^{-2})$

In the preceding stability analysis of standing 1-pulse solutions, the bifurcation parameters τ and θ did not play a leading order role. However, we know from the existence analysis of traveling pulse solutions that for large values of these bifurcation parameters τ, θ a traveling pulse solution can bifurcate from a standing 1-pulse solution, see Chapter 2 and Theorem 3.2.2. In this section, we therefore analyze the stability of standing pulse solutions (Section 3.5.1), as well as the stability of traveling pulse solutions (Sections 3.5.3, 3.5.4, and 3.5.5), for large

bifurcation parameters τ and θ . Moreover, in Section 3.5.2 we analyze the possible bifurcations of a standing pulse solution. It turns out that, besides a bifurcation to a traveling pulse solution, we may also encounter a Hopf bifurcation. In the latter case, the standing pulse solution bifurcates into a so-called breathing solution, see the right frame of Figure 3.7.

3.5.1 Stability of the standing 1-pulse solution for $\tau, \theta = \mathcal{O}(\varepsilon^{-2})$

We set $\hat{\tau} = \varepsilon^2 \tau$ and $\hat{\theta} = \varepsilon^2 \theta$. By arguments similar to those for the case $\tau, \theta = \mathcal{O}(1)$, we conclude that Lemma 3.4.3 is still valid. Moreover, we also conclude that we once again need to consider small $v(\xi), w(\xi)$, and λ , *i.e.*, as in Section 3.4 we rescale $v(\xi) = \varepsilon \tilde{v}(\xi), w(\xi) = \varepsilon \tilde{w}(\xi)$, and $\lambda = \varepsilon^2 \hat{\lambda}$. Therefore, the linearized stability problem reads

$$\begin{cases} u_{\xi\xi} + (1 - 3u_h^2)u &= \varepsilon^2(\hat{\lambda}u + \alpha\tilde{v} + \beta\tilde{w}), \\ \tilde{v}_{\xi\xi} &= -\varepsilon u + \varepsilon^2(\hat{\lambda}\hat{\tau} + 1)\tilde{v}, \\ \tilde{w}_{\xi\xi} &= -\frac{\varepsilon}{D^2}u + \frac{\varepsilon^2}{D^2}(\hat{\lambda}\hat{\theta} + 1)\tilde{w}. \end{cases} \quad (3.5.1)$$

We determine \mathcal{M}_∞ and compute its eigenvalues Λ_i and its eigenvectors E_i (see section 3.3.1). To leading order, we find

$$\Lambda_{1,6}^2 = 2, \quad \Lambda_{2,5}^2 = \varepsilon^2(1 + \hat{\tau}\hat{\lambda}) =: \varepsilon^2 L_2^2, \quad \Lambda_{3,4}^2 = \frac{\varepsilon^2}{D^2}(1 + \hat{\theta}\hat{\lambda}) =: \frac{\varepsilon^2}{D^2} L_3^2, \quad (3.5.2)$$

with the corresponding eigenvectors

$$E_{1,6} = \begin{pmatrix} 1 \\ \pm\sqrt{2} \\ -\frac{\varepsilon}{2} \\ \mp\frac{1}{2}\sqrt{2} \\ -\frac{1}{D^2}\frac{\varepsilon}{2} \\ \mp\frac{1}{2}\sqrt{2}\frac{1}{D} \end{pmatrix}, \quad E_{2,5} = \begin{pmatrix} -\frac{\alpha}{2}\varepsilon^2 \\ \mathcal{O}(\varepsilon^3) \\ 1 \\ \pm L_2 \\ \mathcal{O}(\varepsilon) \\ \mathcal{O}(\varepsilon) \end{pmatrix}, \quad E_{3,4} = \begin{pmatrix} -\frac{\beta}{2}\varepsilon^2 \\ \mathcal{O}(\varepsilon^3) \\ \mathcal{O}(\varepsilon) \\ \mathcal{O}(\varepsilon) \\ 1 \\ \pm L_3 \end{pmatrix}. \quad (3.5.3)$$

Unlike the case $\tau, \theta = \mathcal{O}(1)$, the ordering of the small eigenvalues $\Lambda_{2,5}$ and $\Lambda_{3,4}$ depends on $\hat{\lambda}$, in fact $\Lambda_{2,5}^2 = \Lambda_{3,4}^2$ if $\hat{\lambda} = -\frac{D^2-1}{D^2\hat{\tau}-\hat{\theta}}$. *A priori*, this may seem to be problematic since the construction and the decomposition of the Evans function $\mathcal{D}(\lambda)$ is based on the assumption

$$\Re(\Lambda_1) > \Re(\Lambda_2) > \Re(\Lambda_3) > 0 > \Re(\Lambda_4) > \Re(\Lambda_5) > \Re(\Lambda_6). \quad (3.5.4)$$

However, since the associated eigenvectors $E_{2,5}$ and $E_{3,4}$ remain independent as $\Lambda_{2,5}^2$ crosses through $\Lambda_{3,4}^2$, it is easy to check that neither the construction nor the decomposition of $\mathcal{D}(\lambda)$ is affected by this (one can just interchange the roles of

Λ_2 and Λ_3 and of Λ_4 and Λ_5).

In contrast to the case $\tau, \theta = \mathcal{O}(1)$, we cannot exactly compute the eigenvalues of the stability problem. However, our methods do yield an explicit relation that determines the eigenvalues.

Theorem 3.5.1. *Let $\tau, \theta = \mathcal{O}(\varepsilon^{-2})$, and let $(\alpha, \beta, \gamma, D, \varepsilon)$ be such that there exist homoclinic 1-pulse solutions (Theorem 3.2.1). Then, the eigenvalues $\hat{\lambda}_j^\pm$, $j = 1, 2$, associated to the stability of the 1-pulse solution, are determined by*

$$\begin{aligned} \frac{1}{3}\sqrt{2}\hat{\lambda} = & -\alpha \left(\frac{1}{L_2} - 1 + A^2 \right) - \frac{\beta}{D} \left(\frac{1}{L_3} - 1 + A^{2/D} \right) \\ & \pm \left(\frac{\alpha}{L_2} A^{2L_2} + \frac{\beta}{DL_3} A^{2L_3/D} \right), \end{aligned} \quad (3.5.5)$$

where $L_{2,3} = L_{2,3}(\hat{\lambda})$ are defined in (3.5.2), and A is determined in Theorem 3.2.1. The normalized fast u -components of the associated eigenfunctions are given by

$$\Psi_j^{\pm, u}(\xi) = \begin{cases} \psi^-(\xi) & \text{in } I_j^-, \\ \mp \psi^+(\xi) & \text{in } I_j^+, \end{cases}$$

with $\psi^\pm(\xi)$ as defined in (3.2.13). Note that $\Psi_j^+(\xi)$ are odd functions, while $\Psi_j^-(\xi)$ are even functions.

In the special case $\hat{\tau} = \hat{\theta} = 0$, equation (3.5.5) has two zeroes $\hat{\lambda}_1^\pm$, and they coincide with the eigenvalues $\hat{\lambda}^\pm$ given by (3.4.20). This is consistent with the previous section, since $\hat{\tau} = \hat{\theta} = 0$ to leading order corresponds to $\tau, \theta \ll \varepsilon^{-2}$.

The translation invariant eigenvalue $\lambda = 0$ coincides with the solution $\hat{\lambda}_1^+ = 0$ of the + equation in (3.5.5). Moreover, at $\hat{\tau}(\hat{\theta}) = \hat{\tau}_{tp}(\hat{\theta})$ (3.2.26), the zero eigenvalue $\hat{\lambda}_1^+$ is not a simple solution of the + equation of (3.5.5). To observe this, we differentiate the + equation with respect to $\hat{\lambda}$, and substitute $\hat{\lambda} = 0$ (note that $L_{2,3}(0) = 1$)

$$\frac{1}{3}\sqrt{2} = \frac{1}{2}\alpha\hat{\tau}(1 - A^2 + A^2 \log(A^2)) + \frac{1}{2}\frac{\beta\hat{\theta}}{D} \left(1 - A^{\frac{2}{D}} + A^{\frac{2}{D}} \log\left(A^{\frac{2}{D}}\right) \right),$$

which yields (3.2.26), *i.e.*,

$$\hat{\tau}(\hat{\theta}) = \hat{\tau}_{tp}(\hat{\theta}) = \frac{\frac{2}{3}\sqrt{2} - \frac{\beta\hat{\theta}}{D} \left(1 - A^{\frac{2}{D}} + A^{\frac{2}{D}} \log\left(A^{\frac{2}{D}}\right) \right)}{\alpha(1 - A^2 + A^2 \log(A^2))}. \quad (3.5.6)$$

Thus, the + equation of (3.5.5) has a double eigenvalue at zero at $\hat{\tau} = \hat{\tau}_{tp}$. Hence, as $\hat{\tau}$ passes through $\hat{\tau}_{tp}$, a real eigenvalue crosses the imaginary axis. Moreover, the bifurcation into a traveling pulse solution, obtained in the existence analysis of the previous chapter, is confirmed by the stability analysis. In Sections 3.5.3

and 3.5.4, we will investigate whether the bifurcating traveling pulse solutions are stable, and whether this bifurcation is subcritical or supercritical.

First, we will prove Theorem 3.5.1, and in the next section, the evolution of the eigenvalues $\hat{\lambda}_j^\pm$ as function of the parameters will be studied. Note that unlike the case $\tau, \theta = \mathcal{O}(1)$, the number of small eigenvalues, that is, the number of solutions to (3.5.5), can be more than two. It will be shown that eigenvalues may ‘pop out’ of the essential spectrum and possibly merge to form a pair of complex conjugate eigenvalues which crosses the imaginary axis. So, the standing pulse solution can also destabilize through a Hopf bifurcation.

Proof of Theorem 3.5.1. As we know from the previous section(s), a solution $\phi(\xi)$ to the eigenvalue problem (3.5.1) – written as a 6-dimensional dynamical system – can be built from the basis $\{\phi_2(\xi), \phi_3(\xi)\}$ with $\phi_{2,3}(\xi)$ as given by (3.4.13) and (3.4.14), see also Figure 3.4.

To facilitate the analysis and to obtain insight directly into the eigenfunctions, we consider the general function $\phi(\xi) = \mu_2\phi_2(\xi) + \mu_3\phi_3(\xi)$ instead of working with the basis functions $\phi_{2,3}(\xi)$ themselves, as in Section 3.4.2, see also the final paragraph of Section 3.4.3. By calculations similar to those in Section 3.4.3, we find for the \tilde{v} - and \tilde{w} -components of $\phi(\xi)$

$$\phi^{\tilde{v}}(\xi) = \begin{cases} \mu_2 e^{\varepsilon L_2(\xi+\xi_*)} & \text{in } I_s^-, \\ \left(\mu_2 - \frac{C^-}{L_2}\right) e^{\varepsilon L_2(\xi+\xi_*)} + \frac{C^-}{L_2} e^{-\varepsilon L_2(\xi+\xi_*)} & \text{in } I_s^0, \\ \left(\frac{C^+}{L_2} + \left(\mu_2 - \frac{C^-}{L_2}\right) e^{2\varepsilon L_2 \xi_*}\right) e^{\varepsilon L_2(\xi-\xi_*)} \\ + \left(\frac{C^-}{L_2} e^{-2\varepsilon L_2 \xi_*} - \frac{C^+}{L_2}\right) e^{-\varepsilon L_2(\xi-\xi_*)} \\ + \left(\frac{C^+}{DL_3} + \left(\mu_3 - \frac{C^-}{DL_3}\right) e^{2\frac{\varepsilon}{D} L_3 \xi_*}\right) E_3^{\tilde{v}} e^{\frac{\varepsilon}{D} L_3(\xi-\xi_*)} \\ + \frac{1}{DL_3} (C^- e^{-2\frac{\varepsilon}{D} L_3 \xi_*} - C^+) E_4^{\tilde{v}} e^{-\frac{\varepsilon}{D} L_3(\xi-\xi_*)} & \text{in } I_s^+, \end{cases} \quad (3.5.7)$$

and

$$\phi^{\tilde{w}}(\xi) = \begin{cases} \mu_3 e^{\frac{\varepsilon}{D} L_3(\xi+\xi_*)} & \text{in } I_s^-, \\ \left(\mu_3 - \frac{C^-}{DL_3}\right) e^{\frac{\varepsilon}{D} L_3(\xi+\xi_*)} + \frac{C^-}{DL_3} e^{-\frac{\varepsilon}{D} L_3(\xi+\xi_*)} & \text{in } I_s^0, \\ \left(\frac{C^+}{DL_3} + \left(\mu_3 - \frac{C^-}{DL_3}\right) e^{2\frac{\varepsilon}{D} L_3 \xi_*}\right) e^{\frac{\varepsilon}{D} L_3(\xi-\xi_*)} \\ + \frac{1}{DL_3} (C^- e^{-2\frac{\varepsilon}{D} L_3 \xi_*} - C^+) e^{-\frac{\varepsilon}{D} L_3(\xi-\xi_*)} \\ + \left(\frac{C^+}{L_2} + \left(\mu_2 - \frac{C^-}{L_2}\right) e^{2\varepsilon L_2 \xi_*}\right) E_2^{\tilde{w}} e^{\varepsilon L_2(\xi-\xi_*)} \\ + \left(\frac{C^-}{L_2} e^{-2\varepsilon L_2 \xi_*} - \frac{C^+}{L_2}\right) E_5^{\tilde{w}} e^{-\varepsilon L_2(\xi-\xi_*)} & \text{in } I_s^+, \end{cases} \quad (3.5.8)$$

where $L_{2,3}$ are defined in (3.5.2), and $C^\pm \in \mathbb{R}$ are the as yet unknown factors in front of the leading order behavior of the u -components of $\phi(\xi)$, that is,

$\phi^u(\xi) = u_0^\pm(\xi) + \mathcal{O}(\varepsilon) = \mp C^\pm \psi^\pm(\xi) + \mathcal{O}(\varepsilon)$. Note that C^\pm relate to $C_{2,3}^\pm$ in Section 3.4.3 through $C^\pm = \mu_2 C_2^\pm + \mu_3 C_3^\pm$. Observe that we have not neglected all of the $\mathcal{O}(\varepsilon)$ terms in (3.5.7) or (3.5.8) in the region I_s^+ , since the ordering of $\Lambda_{2,5}^2$ and $\Lambda_{3,4}^2$ may change as $\hat{\lambda}$ is varied (see Remark 3.4.1: all $\mathcal{O}(\varepsilon)$ terms with $E_{3,4}^{\tilde{v}}$ and $E_{2,5}^{\tilde{w}}$ may have a dominant effect as $\xi \rightarrow \infty$).

The slow growth for $\xi \rightarrow \infty$ of $\phi(\xi)$ is determined by the slow-fast transmission functions $t_{2,3}(\hat{\lambda})$,

$$\begin{aligned} t_2(\hat{\lambda}) &:= \mu_2 t_{22}(\hat{\lambda}) + \mu_3 t_{32}(\hat{\lambda}) = \frac{C^+}{L_2} + \left(\mu_2 - \frac{C^-}{L_2} \right) e^{2\varepsilon L_2 \xi_*}, \\ t_3(\hat{\lambda}) &:= \mu_2 t_{23}(\hat{\lambda}) + \mu_3 t_{33}(\hat{\lambda}) = \frac{C^+}{DL_3} + \left(\mu_3 - \frac{C^-}{DL_3} \right) e^{2\frac{\varepsilon}{D} L_3 \xi_*}. \end{aligned} \quad (3.5.9)$$

The slow-fast transmission functions $t_{2,3}$ have a similar meaning as the transmission function t_1 , see Lemma 3.3.5. The product of $t_{2,3}$ with $e^{\Lambda_{2,3}\xi}$ (3.5.2) determines the growth rate of $\phi(\xi)$ for $\xi \rightarrow \infty$ in the direction of the eigenvector $E_{2,3}$ (3.5.3). Therefore, the solution $\phi(\xi)$ is an eigenfunction if $t_2 = t_3 = 0$, *i.e.*, if

$$\begin{pmatrix} t_{22} & t_{32} \\ t_{23} & t_{33} \end{pmatrix} \begin{pmatrix} \mu_2 \\ \mu_3 \end{pmatrix} = \begin{pmatrix} 0 \\ 0 \end{pmatrix}, \quad (3.5.10)$$

for some $(\mu_2, \mu_3) \neq (0, 0)$, which implies that $t_{22}t_{33} - t_{23}t_{32} = 0$. This reconfirms the factorization of the Evans function $\mathcal{D}(\hat{\lambda})$ (Corollary 3.3.7). Here, we proceed with a direct calculation of the eigenvalues, which is somewhat more straightforward than that of Section 3.4.3 and has the advantage that it simultaneously gives information on the associated eigenfunctions. Equations (3.5.9) and (3.5.10) imply that

$$\mu_2 = \frac{C^-}{L_2} - \frac{C^+}{L_2} e^{-2\varepsilon L_2 \xi_*}, \quad \mu_3 = \frac{C^-}{DL_3} - \frac{C^+}{DL_3} e^{-2\frac{\varepsilon}{D} L_3 \xi_*}.$$

This yields that the leading order behavior of \tilde{v}, \tilde{w} -components in the fast fields I_f^\pm is given by

$$\begin{aligned} \phi^{\tilde{v}}(-\xi_*) &= \frac{C^-}{L_2} - \frac{C^+}{L_2} e^{-2\varepsilon L_2 \xi_*}, & \phi^{\tilde{v}}(\xi_*) &= \frac{C^-}{L_2} e^{-2\varepsilon L_2 \xi_*} - \frac{C^+}{L_2}, \\ \phi^{\tilde{w}}(-\xi_*) &= \frac{C^-}{DL_3} - \frac{C^+}{DL_3} e^{-2\frac{\varepsilon}{D} L_3 \xi_*}, & \phi^{\tilde{w}}(\xi_*) &= \frac{C^-}{DL_3} e^{-2\frac{\varepsilon}{D} L_3 \xi_*} - \frac{C^+}{DL_3}. \end{aligned}$$

Next, we examine the first equation in system (3.5.1), and we expand $u_h(\xi)$ and $u(\xi)$ in the fast fields in the usual way. The leading order term and the $\mathcal{O}(\varepsilon)$ term satisfy the solvability condition by construction. However, at the $\mathcal{O}(\varepsilon^2)$ level, we find

$$\begin{aligned} \mathcal{L}^- u_2^- &= \hat{\lambda} u_0^- + \alpha \frac{C^-}{L_2} - \alpha \frac{C^+}{L_2} e^{-2\varepsilon L_2 \xi_*} + \beta \frac{C^-}{DL_3} - \beta \frac{C^+}{DL_3} e^{-2\frac{\varepsilon}{D} L_3 \xi_*} \\ &\quad + 6u_{h,0}^- u_{h,2}^- u_0^-, \\ \mathcal{L}^+ u_2^+ &= \hat{\lambda} u_0^+ + \alpha \frac{C^-}{L_2} e^{-2\varepsilon L_2 \xi_*} - \alpha \frac{C^+}{L_2} + \beta \frac{C^-}{DL_3} e^{-2\frac{\varepsilon}{D} L_3 \xi_*} - \beta \frac{C^+}{DL_3} \\ &\quad + 6u_{h,0}^+ u_{h,2}^+ u_0^+. \end{aligned} \quad (3.5.11)$$

Applying the solvability condition and implementing the integral relations (3.2.18), which are still valid since their derivation was independent of the magnitude of τ and θ , we find

$$\begin{pmatrix} \frac{1}{3}\sqrt{2}\hat{\lambda} + H_1(\hat{\lambda}) & -H_2(\hat{\lambda}) \\ H_2(\hat{\lambda}) & -\frac{1}{3}\sqrt{2}\hat{\lambda} - H_1(\hat{\lambda}) \end{pmatrix} \begin{pmatrix} C^- \\ C^+ \end{pmatrix} = \begin{pmatrix} 0 \\ 0 \end{pmatrix}, \quad (3.5.12)$$

with

$$\begin{aligned} H_1(\hat{\lambda}) &:= \alpha \left(\frac{1}{L_2} - 1 + A^2 \right) + \frac{\beta}{D} \left(\frac{1}{L_3} - 1 + A^{2/D} \right), \\ H_2(\hat{\lambda}) &:= \frac{\alpha}{L_2} A^{2L_2} + \frac{\beta}{DL_3} A^{2L_3/D}, \end{aligned} \quad (3.5.13)$$

where A is defined as in Theorem 3.2.1. Note that both quantities $H_{1,2}(\hat{\lambda})$ explicitly depend on $\hat{\lambda}$ through $L_{2,3}$. There are nontrivial solutions $\hat{\lambda}$ of (3.5.12) if

$$\frac{1}{3}\sqrt{2}\hat{\lambda} + H_1(\hat{\lambda}) = \pm H_2(\hat{\lambda}) \quad \text{and} \quad C^- = \pm C^+, \quad (3.5.14)$$

which is equivalent to (3.5.5). The structure and parity of the u -components of the eigenfunctions $\Psi_j^\pm(\xi)$ follow from the relations between C^+ and C^- (3.5.14). \square

3.5.2 Bifurcations for $\tau = \mathcal{O}(\varepsilon^{-2})$ and $\theta = 1$

A complete analysis of equations (3.5.5) is involved and cumbersome. Therefore, we restrict the analysis to the case where only τ is large and θ is just $\mathcal{O}(1)$. Note that this restriction has also been imposed in Chapter 2 and in [53, 70, 71]. So, we put $\hat{\tau} = \varepsilon^2\tau$ and $\hat{\theta} = 0$. Since $L_3 = 1$, the equations for the eigenvalues (3.5.5) become

$$\begin{aligned} \frac{1}{3}\sqrt{2}\hat{\lambda} &= \alpha(1 - A^2) - \frac{\alpha}{L_2}(1 - A^{2L_2}) && =: f^+(\hat{\lambda}), \\ \frac{1}{3}\sqrt{2}\hat{\lambda} &= \alpha(1 - A^2) - \frac{\alpha}{L_2}(1 + A^{2L_2}) - 2\frac{\beta}{D}A^{2/D} && =: f^-(\hat{\lambda}). \end{aligned} \quad (3.5.15)$$

To investigate these equations we introduce $T := \hat{\tau}\hat{\lambda}$, such that the functions f^\pm become functions of T , and do not depend on $\hat{\tau}$, see (3.5.2). Increasing $\hat{\tau}$ now influences the slope of the left hand side of (3.5.15), i.e., $\frac{1}{3}\sqrt{2}\hat{\lambda}$ is now replaced by $\frac{1}{3}\sqrt{2}\frac{T}{\hat{\tau}} =: l(T; \hat{\tau})$. The essential spectrum is after this rescaling to leading order given by the half plane $\Sigma_1 := \{T : \Re(T) < -1\}$, see Lemma 3.3.2. It immediately follows that the sign of α has a significant impact on the possible occurrence of bifurcations.

Corollary 3.5.2. *Let $\tau = \frac{\hat{\tau}}{\varepsilon^2} = \mathcal{O}(\varepsilon^{-2})$ and $\theta = \mathcal{O}(1)$, and let $(\alpha, \beta, \gamma, D, \varepsilon)$ be such that there exist homoclinic 1-pulse solutions (Theorem 3.2.1). If $\alpha < 0$, then the 1-pulse solution does not bifurcate, its stability does not change as function of τ or $\hat{\tau}$ (and is thus determined by Theorem 3.4.1).*

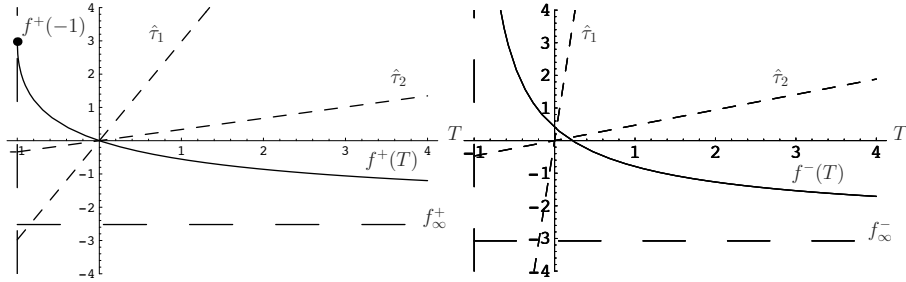


Figure 3.6: In the left frame we plotted $f^+(T)$ for $(\alpha, \beta, \gamma, D, A) = (-3, 2, 0.906, 5, 0.4)$, and in the right frame we plotted $f^-(T)$ for the same parameters. The dashed lines represent $l(T; \hat{\tau})$ for $\hat{\tau}_1 < \hat{\tau}_2$. Note that $f^-(0) > 0$ and $f_\infty^- = \lim_{T \rightarrow \infty} f^-(T) < 0$, so that $\hat{\lambda}_1^-(\hat{\tau}) \rightarrow 0$ as $\hat{\tau} \rightarrow \infty$.

Proof. This result is based on the observation that $(f^\pm)'(T) < 0$ and $(f^\pm)''(T) > 0$ if $\alpha < 0$, which can be checked by straightforward calculus. This implies that both $f^\pm(T)$ have a unique intersection with the line $l(T; \hat{\tau})$; for $f^+(T)$ this intersection takes place at $\hat{\lambda}_1^+(\hat{\tau}) \equiv 0$, for $f^-(T)$ the sign of $\hat{\lambda}_1^-(\hat{\tau})$ is determined by the sign of $f^-(0) = -2\left(\alpha A^2 + \frac{\beta}{D} A^{2/D}\right)$, the quantity that also determines the stability of the 1-pulse solution if $\tau = \mathcal{O}(1)$ (Theorem 3.4.1). See Figure 3.6 for two typical cases. \square

Corollary 3.5.3. Let $\tau = \frac{\hat{\tau}}{\varepsilon^2} = \mathcal{O}(\varepsilon^{-2})$ and $\theta = \mathcal{O}(1)$, and let $(\alpha, \beta, \gamma, D, \varepsilon)$ be such that there exist homoclinic 1-pulse solutions (Theorem 3.2.1). If $\alpha > 0$, two new eigenvalues bifurcate out of the essential spectrum σ_{ess} as τ increases, the first one, $\hat{\lambda}_2^-(\hat{\tau})$, at $\tau = \tau_{e,1} \ll \mathcal{O}(\varepsilon^{-2})$, i.e., at $\hat{\tau} \ll 1$, the second one, $\hat{\lambda}_2^+(\hat{\tau})$, at $\hat{\tau} = \hat{\tau}_{e,2} := -\frac{1}{3}\sqrt{2}(\alpha(1 - A^2 + \log A^2))^{-1}$. If the 1-pulse solution is unstable for $\tau = \mathcal{O}(1)$, then it remains unstable for $\tau \gg 1$. If it is stable then $\hat{\lambda}_{1,2}^-$ merge at $\hat{\tau} = \hat{\tau}_c$ to form a pair of complex conjugate eigenvalues and we distinguish between two cases. We define f_∞^- by $f_\infty^- := \alpha(1 - A^2) - 2\frac{\beta}{D}A^{2/D}$. Then

- (i) If $f_\infty^- < 0$, then the 1-pulse solution is destabilized by $\hat{\lambda}_2^+(\hat{\tau})$ and it bifurcates into a traveling 1-pulse solution at $\hat{\tau} = \hat{\tau}_{tp} = \frac{2}{3}\sqrt{2}(\alpha(1 - A^2 + A^2 \log A^2))^{-1} > \hat{\tau}_{e,2}$.
- (ii) If $f_\infty^- > 0$, then depending on the parameter values the 1-pulse solution either is destabilized by $\hat{\lambda}_2^+(\hat{\tau})$ at $\hat{\tau} = \hat{\tau}_{tp}$ and it bifurcates into a traveling 1-pulse solution, or it is destabilized by the complex pair $\hat{\lambda}_{1,2}^-(\hat{\tau})$ at $\hat{\tau} = \hat{\tau}_H$ and it undergoes a Hopf bifurcation.

Moreover, if $\hat{\lambda}_{1,2}^-$ cross the imaginary axis, they will merge again at $\hat{\tau} = \hat{\tau}_r$ and appear as a pair of real, but positive, eigenvalues. The bifurcation values $\hat{\tau}_c$ and

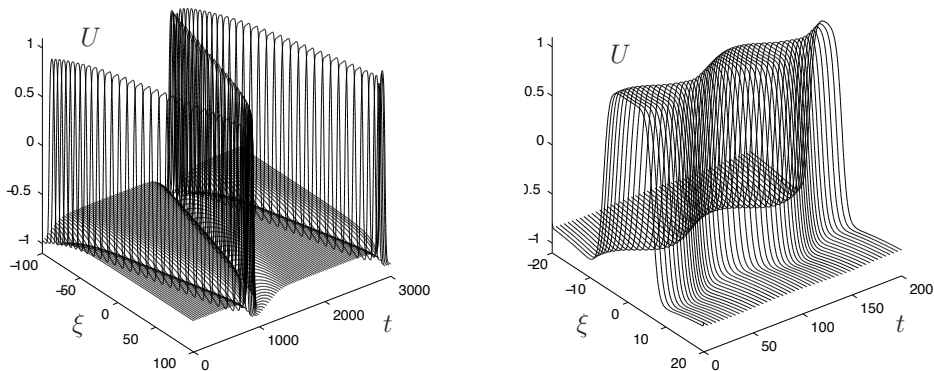


Figure 3.7: In the left frame, a numerically obtained stable traveling pulse solution for $(\alpha, \beta, \gamma, D, \tau, \theta, \varepsilon) = (6, 3, 4, 2, 110, 1, 0.1)$ is depicted. The theoretically predicted values for $\hat{\tau}_{tp}$ and $\hat{\tau}_H$ for these parameter values are to leading order $\hat{\tau}_{tp} = 0.588$ and $\hat{\tau}_H = 0.907$. In the right frame, a stable breathing pulse solution exists for $(\alpha, \beta, \gamma, D, \tau, \theta, \varepsilon) = (6, 3, 4, 10, 49.7, 1, 0.1)$ is plotted. Here, the predicted bifurcation points are to leading order $\hat{\tau}_{tp} = 0.369$ and $\hat{\tau}_H = 0.243$. Therefore, the observed patterns are in line with the theory.

$\hat{\tau}_r$ are determined by a tangency condition

$$\frac{1}{3}\sqrt{2}\hat{\lambda} = f^-(\hat{\lambda}; \hat{\tau}_{c,r}) \quad \text{and} \quad \frac{1}{3}\sqrt{2} = \frac{d}{d\hat{\lambda}}f^-(\hat{\lambda}; \hat{\tau}_{c,r}) \quad \text{with} \quad \hat{\lambda} \in \mathbb{R}.$$

The value of $\hat{\tau}_H$ is (implicitly) given by

$$\frac{1}{3}\sqrt{2}\hat{\lambda}i = f^-(i\hat{\lambda}; \hat{\tau}_H) \quad \text{with} \quad \hat{\lambda} \in \mathbb{R}. \quad (3.5.16)$$

The edge bifurcation $\tau_{e,1}$ can be determined explicitly by studying $\mathcal{D}(\lambda)$ near the tip of σ_{ess} for $\tau \ll \frac{1}{\varepsilon^2}$, see [14].

In Figure 3.7 an example is given of a traveling pulse solution and of a breathing pulse solution, obtained by numerical simulation of (3.1.1).

Proof. The proof is based on a careful analysis of the graphs of $f^\pm(T)$ and their intersections with the line $l(T; \hat{\tau})$, parametrized by $\hat{\tau}$ – see Figures 3.8 and 3.9 for two typical cases. We state, without proof, several properties of $f^\pm(T)$ for

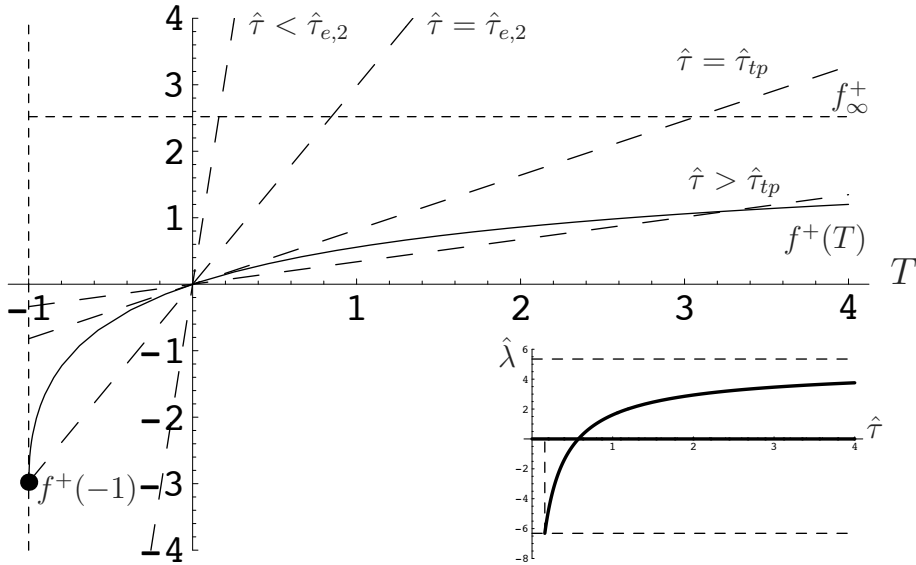


Figure 3.8: The functions $f^+(T)$ and $l(T; \hat{\tau})$ for $(\alpha, \beta, \gamma, D, A) = (3, 2, 1.87, 5, 0.4)$ and various values of $\hat{\tau}$. There are two bifurcations: an edge bifurcation at $\hat{\tau} = \hat{\tau}_e$ and a bifurcation to a traveling pulse solution at $\hat{\tau} = \hat{\tau}_{tp}$. The evolution of the two eigenvalues $\hat{\lambda}_{1,2}^+$ as functions of $\hat{\tau}$ is plotted in the lower right corner.

$\alpha > 0$:

$$\begin{aligned}
 f^+(-1) &= \alpha(1 - A^2 + \log A^2) < 0, \quad f^-(-1) = -\infty, \quad f^+(0) = 0, \\
 f^-(0) &= -2 \left(\alpha A^2 + \frac{\beta}{D} A^{2/D} \right), \quad (f^\pm)'(T) > 0, \quad (f^\pm)''(T) < 0, \\
 \lim_{T \rightarrow \infty} f^+(T) &:= f_\infty^+ = \alpha(1 - A^2) > 0, \\
 \lim_{T \rightarrow \infty} f^-(T) &:= f_\infty^- = \alpha(1 - A^2) - 2 \frac{\beta}{D} A^{2/D}.
 \end{aligned} \tag{3.5.17}$$

We first consider $f^+(T)$. We observe that for $\hat{\tau}$ small, that is, $\hat{\tau} < \frac{1}{3}\sqrt{2} \frac{1}{f^+(-1)} = \hat{\tau}_{e,2}$, $f^+(T)$ intersects $l(T; \hat{\tau})$ only in $T = 0$: $\hat{\lambda}_1^+(\hat{\tau}) \equiv 0$. However, at $\hat{\tau}_{e,2}$ a second eigenvalue $\hat{\lambda}_2^+ = -\frac{1}{\hat{\tau}_{e,2}} < 0$ ($T = -1$) is created from the essential spectrum by an edge bifurcation. For increasing $\hat{\tau}$, this second eigenvalue $\hat{\lambda}_2^+(\hat{\tau})$ increases. At $\hat{\tau} = \hat{\tau}_{tp}$ the two eigenvalues $\hat{\lambda}_{1,2}^+(\hat{\tau})$ merge in zero, where $\hat{\tau}_{tp}$ can be deduced from (3.5.6), see Figure 3.8.

Since $f^-(T) \rightarrow -\infty$ as $T \downarrow -1$, we conclude that $f^-(T) \cap l(T; \hat{\tau})$ consists of two points if $\hat{\tau}$ is small enough, one determined by $\hat{\lambda}_1^-$, that corresponds with $\hat{\lambda}^-$ as given by (3.4.20), the other by $\hat{\lambda}_2^-$ close to the tip of σ_{ess} . Since $\hat{\lambda}_2^-$ does

not exist for $\tau = \mathcal{O}(1)$, we conclude that it must have appeared from σ_{ess} at $\tau_{e,1} \ll \mathcal{O}(\varepsilon^{-2})$. If $f^-(0) > 0$, *i.e.*, if the 1-pulse solution is unstable for $\tau = \mathcal{O}(1)$ (Theorem 3.4.1), we observe that $\hat{\lambda}_1^-(\hat{\tau}) > 0$, and $\hat{\lambda}_2^-(\hat{\tau}) < 0$ for all $\hat{\tau}$, *i.e.*, the pulse solution remains unstable. If $f^-(0) < 0$, *i.e.*, if the 1-pulse solution is stable, the negative eigenvalues $\hat{\lambda}_{1,2}^-(\hat{\tau})$ merge at $\hat{\tau} = \hat{\tau}_c$, here $f^-(T)$ and $l(T; \hat{\tau})$ are tangent, see Figure 3.9. If $f_\infty^- > 0$, *i.e.*, if we are in case (ii), there is a second tangency at $\hat{\tau}_r > \hat{\tau}_c$ for $T > 0$ and $\hat{\lambda}_{1,2}^-$ reappear as positive real eigenvalues. Thus, the complex pair $\hat{\lambda}_{1,2}^-$ travels through the imaginary axis and $\Re(\hat{\lambda}_{1,2}^-)$ changes sign at $\hat{\tau}_H \in (\hat{\tau}_c, \hat{\tau}_r)$, see Figure 3.9. If $f_\infty^- < 0$, case (i), $\hat{\lambda}_{1,2}^-$ remain complex conjugates. A somewhat more elaborate analysis shows that $\Re(\hat{\lambda}_{1,2}^-) < 0$ for all $\hat{\tau}$, and that $\hat{\lambda}_{1,2}^- \rightarrow \frac{3}{2}\sqrt{2}f_\infty^- < 0$ as $\hat{\tau} \rightarrow \infty$, *i.e.*, $\hat{\lambda}_{1,2}^-$ approach σ_{ess} from two sides as $\hat{\tau} \rightarrow \infty$. It thus follows that the pulse is destabilized by $\hat{\lambda}_2^+(\hat{\tau})$ in case (i). In case (ii), it depends on the exact values of the parameters whether $\hat{\lambda}_2^+(\hat{\tau})$ or $\hat{\lambda}_{1,2}^+(\hat{\tau})$ is the first to cross through the imaginary axis as $\hat{\tau}$ increases, see Figure 3.10. \square

Although we do have explicit expressions for $\hat{\tau}_{tp}$ and $\hat{\tau}_H$, it is in general not possible to obtain explicit analytic control of the relative magnitude of $\hat{\tau}_{tp}$ and $\hat{\tau}_H$ (in case (ii) of Corollary 3.5.3). Therefore, we plotted in Figure 3.10 the evolution of $\hat{\tau}_{tp}$ and $\hat{\tau}_H$ as function of α for several values of D (with $\beta = 3, \gamma = 4$ fixed). We observe that by changing the parameters we have control over the order the bifurcation points $\hat{\tau}_{tp}$ and $\hat{\tau}_H$. Moreover, the bifurcation points may coincide and the three eigenvalues $\hat{\lambda}_{1,2}^-$ and $\hat{\lambda}_2^+$ may cross the imaginary axis simultaneously in the co-dimension 2 bifurcation point $(\alpha_{tp,H}, \hat{\tau}_{tp,H})$.

Remark 3.5.1. Some analytical insight in the value of the co-dimension two bifurcation point $\hat{\tau}_{tp,H}$ can be obtained by considering the limit $D \rightarrow \infty$. This case may be seen as a two-component system limit of (3.1.1), see Remark 3.1.3. As a consequence, A^2 in (3.2.6) approaches $\frac{(\gamma-\beta)}{\alpha}$ (since the constant term in the U -equation of (3.1.1) is replaced by $\gamma - \beta$), and the 1-pulse solution is stable if $\alpha > \gamma - \beta > 0$, see Remark 3.4.3. If we define $X \in (0, 1)$ by $\frac{(\gamma-\beta)}{\alpha}$, then $\hat{\tau}_{tp}$ is given by $\frac{\mathcal{F}(X)}{\alpha}$, where $\mathcal{F}(X) = \frac{2}{3}\sqrt{2}(1 - X + X \log X)^{-1}$. It follows from (3.5.16) that $\hat{\tau}_{tp,H}$ is now determined by the solution of

$$\frac{1}{\sqrt{1 + i\mathcal{C}_2\mathcal{F}(X)}} \left(X\sqrt{1 + iY\mathcal{F}(X)} + 1 \right) + \frac{1}{3}\sqrt{2}iY + X - 1 = 0,$$

where $Y = \frac{\lambda_1^-}{\alpha}$. It follows (by a numerical solver) that $X = 0.885\dots$ and $Y = 0.367\dots$, which implies that, for $D \rightarrow \infty$, $(\alpha_{tp,H}, \hat{\tau}_{tp,H}) = \left(\frac{\gamma-\beta}{0.885}, \frac{122}{\gamma-\beta} \right)$. This agrees very well with the values obtained in Figure 3.10.

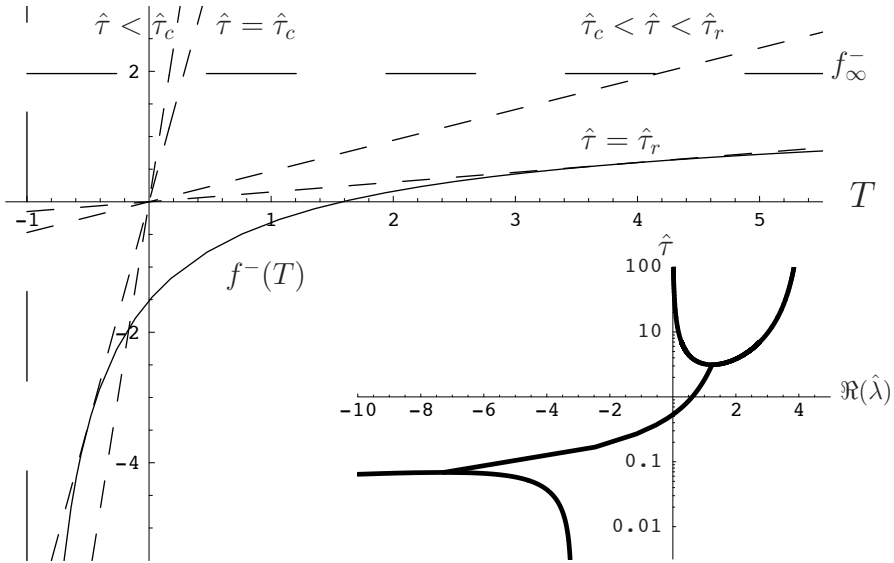


Figure 3.9: The functions $f^-(T)$ and $l(T; \hat{\tau})$ for $(\alpha, \beta, \gamma, D, A) = (3, 2, 1.86, 5, 0.4)$. At $\hat{\tau} = \hat{\tau}_c = 0.0686$ two eigenvalues merge and form a complex pair of eigenvalues with negative real part. At $\hat{\tau} = \hat{\tau}_H = 0.532$ this complex pair crosses through the imaginary axis, and we observe a Hopf bifurcation. At $\hat{\tau} = \hat{\tau}_r = 3.13$ the complex pair merge again to form two real positive eigenvalues. The evolution of the real part of the eigenvalues $\hat{\lambda}_{1,2}^-$ as functions of $\hat{\tau}$ is plotted in the lower right corner (note that the axes are interchanged and that the $\hat{\tau}$ -axis is plotted logarithmically).

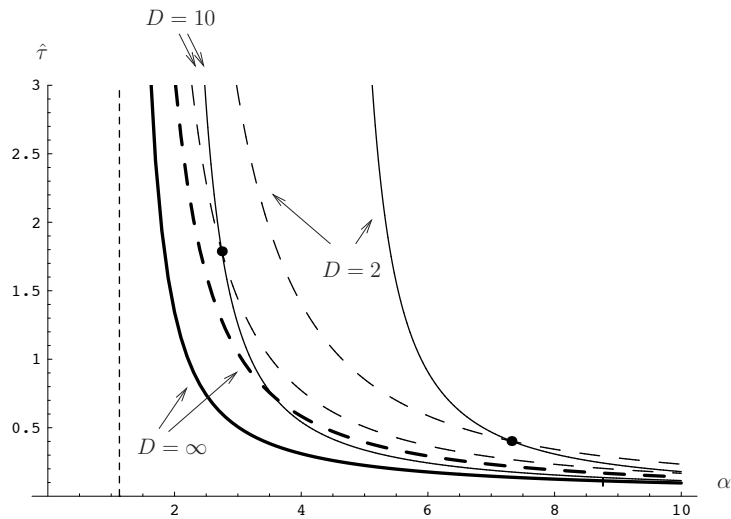


Figure 3.10: The Hopf bifurcation (solid line) and the bifurcation to a traveling pulse (dashed line) as functions of α for various values of D with $\beta = 3$, and $\gamma = 4$ fixed. Observe that for larger D the α -region where the Hopf bifurcation occurs, that is, $\hat{\tau}_H < \hat{\tau}_{tp}$, grows. The lines intersect at a co-dimension 2 bifurcation. For $D = 2$ we have $(\alpha_{tp,H}, \hat{\tau}_{tp,H}) = (7.32, 0.40)$. For $D = 10$ we have $(\alpha_{tp,H}, \hat{\tau}_{tp,H}) = (2.75, 1.79)$, and for $D = \infty$ (see Remark 3.5.1) we have $(\alpha_{tp,H}, \hat{\tau}_{tp,H}) = (1.13, 122)$, *i.e.*, a point outside the frame indicated by the dashed vertical line. Note that, by changing the values of β and γ , it is also possible that for larger D the α -region where the Hopf bifurcation occurs shrinks.

3.5.3 Stability of the traveling 1-pulse solution

In this section, we determine the stability of the traveling pulse solutions. Recall from Theorem 3.2.2 that we explicitly need large τ and/or θ for the existence of a traveling pulse solution. As in the previous sections, we put $\hat{\tau} = \varepsilon^2\tau$ and $\hat{\theta} = \varepsilon^2\theta$. In the traveling coordinate $\xi_m = \xi - \varepsilon ct$, the linearized stability problem associated to the pulse solution $(u_{tp}(\xi), v_{tp}(\xi), w_{tp}(\xi))$, see Theorem 3.2.2, reads

$$\begin{cases} u_{\xi\xi} + \left(1 - 3(u_{tp})^2\right)u &= -\varepsilon cu_{\xi} + \varepsilon^2 \left(\hat{\lambda}u + \alpha\tilde{v} + \beta\tilde{w}\right), \\ \tilde{v}_{\xi\xi} &= -\varepsilon(u + c\hat{\tau}\tilde{v}_{\xi}) + \varepsilon^2\tilde{v} \left(\hat{\tau}\hat{\lambda} + 1\right), \\ \tilde{w}_{\xi\xi} &= -\frac{\varepsilon}{D^2}(u + c\hat{\theta}\tilde{w}_{\xi}) + \frac{\varepsilon^2}{D^2}\tilde{w} \left(\hat{\theta}\hat{\lambda} + 1\right), \end{cases} \quad (3.5.18)$$

where we once again scaled $v(\xi) = \varepsilon\tilde{v}(\xi)$, $w(\xi) = \varepsilon\tilde{w}(\xi)$, $\lambda = \varepsilon^2\hat{\lambda}$, and removed the subscript m from ξ_m . Note that for the justification of the scaling of λ we use Lemma 3.2.3. Since the essential spectrum is still bounded away from the imaginary axis (Lemma 3.3.3), the nonlinear stability of a solution is still completely determined by the eigenvalues of the stability problem (3.5.18) (Remark 3.3.1).

We write system (3.5.18) as a linear system in \mathbb{C}^6

$$\begin{aligned} \phi_{\xi}(\xi) &= \mathcal{M}^{tp}(\xi; \lambda, \varepsilon)\phi(\xi) \quad \text{with} \\ \phi(\xi) &= (u(\xi), p(\xi), \tilde{v}(\xi), q(\xi), \tilde{w}(\xi), r(\xi))^t, \end{aligned} \quad (3.5.19)$$

where $p(\xi) = u_{\xi}(\xi)$, $q(\xi) = \frac{1}{\varepsilon}\tilde{v}_{\xi}(\xi)$, and $r = \frac{D}{\varepsilon}\tilde{w}_{\xi}(\xi)$. Observe that the trace of the matrix \mathcal{M}^{tp} is no longer zero. The eigenvalues of $\mathcal{M}_{\infty}^{tp} := \lim_{\xi \rightarrow \pm\infty} \mathcal{M}^{tp}$ are given by

$$\Lambda_{1,6} = \pm\sqrt{2}, \quad \Lambda_{2,5} = \varepsilon\Gamma^{\pm}, \quad \Lambda_{3,4} = \frac{\varepsilon}{D}\Theta^{\pm},$$

where Γ^{\pm} and Θ^{\pm} are defined by

$$\begin{aligned} \Gamma^{\pm} &:= \frac{1}{2}(-c\hat{\tau} \pm \sqrt{G_v}) \quad \text{with } G_v := c^2\hat{\tau}^2 + 4(\hat{\lambda}\hat{\tau} + 1), \\ \Theta^{\pm} &:= \frac{1}{2}\left(-c\frac{\hat{\theta}}{D} \pm \sqrt{G_w}\right) \quad \text{with } G_w := c^2\frac{\hat{\theta}^2}{D^2} + 4(\hat{\lambda}\hat{\theta} + 1). \end{aligned} \quad (3.5.20)$$

Note that $\Re(\Lambda_{2,5})$ and $\Re(\Lambda_{3,4})$ can change order, but, as in Section 3.5.1, this has no influence on the analysis since the eigenvectors $E_{2,5}$ and $E_{3,4}$ remain independent,

$$E_{1,6} = \begin{pmatrix} 1 \\ \pm\sqrt{2} \\ -\frac{\varepsilon}{2} \\ \mp\frac{1}{2}\sqrt{2} \\ -\frac{\varepsilon}{2D^2} \\ \mp\frac{1}{2D}\sqrt{2} \end{pmatrix}, \quad E_{2,5} = \begin{pmatrix} -\frac{\alpha}{2}\varepsilon^2 \\ \mathcal{O}(\varepsilon^3) \\ 1 \\ \Gamma^{\pm} \\ \mathcal{O}(\varepsilon) \\ \mathcal{O}(\varepsilon) \end{pmatrix}, \quad E_{3,4} = \begin{pmatrix} -\frac{\beta}{2}\varepsilon^2 \\ \mathcal{O}(\varepsilon^3) \\ \mathcal{O}(\varepsilon) \\ \mathcal{O}(\varepsilon) \\ 1 \\ \Theta^{\pm} \end{pmatrix}. \quad (3.5.21)$$

Following the same procedure used in the previous sections, we can determine the \tilde{v}, \tilde{w} -components of a slow function $\phi(\xi)$, and, after imposing that the two slow-fast transmission functions $t_{2,3}$ should be zero, we obtain

$$\phi_{tp}^{\tilde{v}}(\xi) = \begin{cases} \frac{2C^-}{\sqrt{G_v}} e^{\varepsilon\Gamma^+(\xi+\xi_*)} - \frac{2C^+}{\sqrt{G_v}} e^{\varepsilon\Gamma^+(\xi-\xi_*)} & \text{in } I_s^-, \\ \frac{2C^-}{\sqrt{G_v}} e^{\varepsilon\Gamma^-(\xi+\xi_*)} - \frac{2C^+}{\sqrt{G_v}} e^{\varepsilon\Gamma^+(\xi-\xi_*)} & \text{in } I_s^0, \\ \frac{2C^-}{\sqrt{G_v}} e^{\varepsilon\Gamma^-(\xi+\xi_*)} - \frac{2C^+}{\sqrt{G_v}} e^{\varepsilon\Gamma^-(\xi-\xi_*)} & \text{in } I_s^+, \\ + \frac{1}{D} E_4^{\tilde{v}} \left(\frac{2C^-}{\sqrt{G_w}} e^{\frac{\varepsilon}{D}\Theta^-(\xi+\xi_*)} - \frac{2C^+}{\sqrt{G_w}} e^{\frac{\varepsilon}{D}\Theta^-(\xi-\xi_*)} \right) & \text{in } I_s^+, \end{cases} \quad (3.5.22)$$

$$\phi_{tp}^{\tilde{w}}(\xi) = \begin{cases} \frac{1}{D} \left(\frac{2C^-}{\sqrt{G_w}} e^{\frac{\varepsilon}{D}\Theta^+(\xi+\xi_*)} - \frac{2C^+}{\sqrt{G_w}} e^{\frac{\varepsilon}{D}\Theta^+(\xi-\xi_*)} \right) & \text{in } I_s^-, \\ \frac{1}{D} \left(\frac{2C^-}{\sqrt{G_w}} e^{\frac{\varepsilon}{D}\Theta^-(\xi+\xi_*)} - \frac{2C^+}{\sqrt{G_w}} e^{\frac{\varepsilon}{D}\Theta^+(\xi-\xi_*)} \right) & \text{in } I_s^0, \\ \frac{1}{D} \left(\frac{2C^-}{\sqrt{G_w}} e^{\frac{\varepsilon}{D}\Theta^-(\xi+\xi_*)} - \frac{2C^+}{\sqrt{G_w}} e^{\frac{\varepsilon}{D}\Theta^-(\xi-\xi_*)} \right) & \text{in } I_s^+, \\ + E_5^{\tilde{w}} \left(\frac{2C^-}{\sqrt{G_v}} e^{\varepsilon\Gamma^-(\xi+\xi_*)} - \frac{2C^+}{\sqrt{G_v}} e^{\varepsilon\Gamma^-(\xi-\xi_*)} \right) & \text{in } I_s^+. \end{cases} \quad (3.5.23)$$

In principle, we could now analyze the u -equation in the fast fields by expanding $\phi^u(\xi)$, $u_{tp}(\xi)$, and c in orders of ε , and then impose the solvability condition. This would lead to an implicit expression for $\hat{\lambda}$ similar to, but more complicated than, (3.5.5) (in the limit $c = 0$ it reduces to (3.5.5)). However, we refrain from doing so here.

3.5.4 Small speed c : the weakly nonlinear analysis

Although we do not derive a stability result for a pulse solution with general speed c , we are interested in the stability of a traveling pulse solution just after the bifurcation. Therefore, we put $c = \delta$, where $0 < \varepsilon \ll \delta \ll 1$. Moreover, for computational convenience we once again assume that only τ is large, that is, $\tau = \varepsilon^{-2}(\hat{\tau}_{tp} + \mathcal{O}(\varepsilon, \delta))$, and that $\hat{\theta} = 0$. We know from Lemma 2.4.1, which is in essence a corollary of Theorem 3.2.2, that such traveling pulse solutions exist for $\hat{\tau} = \hat{\tau}_{tp} + \delta^2 \hat{\tau}_2 + \mathcal{O}(\delta^3)$ and

$$\hat{\tau}_2 = \frac{3}{32} \sqrt{2\alpha} \hat{\tau}_{tp}^4 \left[1 - A_0^2 + A_0^2 \log A_0^2 - \frac{1}{3} A_0^2 \log^3 A_0^2 + \frac{\alpha A_0^4 \log^2 A_0^2 (\log A_0^2 - 1)}{\alpha A_0^2 + \frac{\beta}{D} A_0^{2/D}} \right], \quad (3.5.24)$$

where A_0 is a solution of $\alpha A^2 + \beta A^{2/D} = \gamma$, *i.e.*, A_0 is the leading order approximation of a solution A of (3.2.6), such that $\alpha A_0^2 + \frac{\beta}{D} A_0^{2/D} > 0$. This implies that the traveling pulse solution bifurcated from a stationary 1-pulse solution that is stable for $\tau = \mathcal{O}(1)$. Since we are interested in the possible bifurcation of stable traveling pulse solutions, we also assume that this stationary 1-pulse solution is stable up to $\hat{\tau} = \hat{\tau}_{tp} + \mathcal{O}(\varepsilon, \delta)$, *i.e.*, $\alpha > 0$, and the 1-pulse solution is not destabilized by a Hopf bifurcation (see Corollary 3.5.3).

Lemma 3.5.4. *Under the above assumptions, the dominant eigenvalue of the bifurcating traveling pulse solution is given by*

$$\hat{\lambda}_2^+ = -\delta^2 C(A_0, \alpha) \hat{\tau}_2 + \mathcal{O}(\delta^3, \varepsilon), \quad (3.5.25)$$

where $\hat{\tau}_2$ is given in (3.5.24), and $C(A_0, \alpha) = \frac{4}{3} \sqrt{2} \frac{1}{\hat{\tau}_{tp}^3} \frac{1}{\frac{1}{2} \sqrt{2} - \frac{1}{4} \alpha A_0^2 \hat{\tau}_{tp} \log^2 A_0^2} > 0$.

The second order correction term $\hat{\tau}_2$ can be positive, as well as negative. Therefore, this lemma confirms the expectation that a subcritical bifurcation ($\hat{\tau}_2 < 0$) yields an unstable traveling pulse solution, while a supercritical bifurcation ($\hat{\tau}_2 > 0$) yields a stable traveling pulse solution.

Proof. This proof is an elaborate exercise. We only present the main arguments. By assumption, the stability of the bifurcating traveling pulse solution is determined by the sign of $\hat{\lambda}_2^+$. In order to determine this sign, we expand the two small eigenvalues in powers of δ , $\hat{\lambda}_i^+ = \hat{\lambda}_{i,0}^+ + \delta \hat{\lambda}_{i,1}^+ + \delta^2 \hat{\lambda}_{i,2}^+ + \delta^3 \hat{\lambda}_{i,3}^+ + \delta^4 \hat{\lambda}_{i,4}^+ + \mathcal{O}(\delta^5)$. Similarly, we expand the other quantities in powers of δ . From Chapter 2, we recall that $\xi_* = \xi_{*,0} + \delta^2 \xi_{*,2} + \delta^4 \xi_{*,4} + \mathcal{O}(\delta^5)$, with $A_0 = e^{-\varepsilon \xi_{*,0}}$, and

$$\xi_{*,2} = \frac{1}{16} \frac{1}{\varepsilon} \frac{\alpha A_0^2 \hat{\tau}_{tp}^2 \log A_0^2 (\log A_0^2 - 1)}{\alpha A_0^2 + \frac{\beta}{D} A_0^{2/D}}.$$

By using the solvability condition, one can show that the u -components in the fast fields I_f^\pm , $u_1^\pm(\xi)$ and $u_{tp,1}^\pm(\xi)$, are of order δ , and by Lemma 3.2.3 that $u_{tp,1}^\pm(\xi)$ is even. Moreover, by linearity of the differential operator \mathcal{L}^\pm it follows that

$$u_{1,j}^\pm = C^\pm \left((u_{tp,1,j}^\pm)_\xi + K_j^\pm \psi^\pm \right), \quad K_j^\pm \in \mathbb{R}, \quad (3.5.26)$$

where the first index in the underscore of $u_{1,j}^\pm(\xi)$ states the order of ε , while the second index states the order of δ . Looking to the leading order behavior of the u -components in the fast fields, implementing the behavior of the \tilde{v} , \tilde{w} -components, imposing the solvability conditions, and recalling that we assumed to be close to the bifurcation, we find

$$\hat{\lambda}_{i,0}^+ = 0 \quad \text{and} \quad C^+ = C^-(1 + \delta C_1^+ + \delta^2 C_2^+ + \delta^3 C_3^+ + \delta^4 C_4^+) + \mathcal{O}(\delta^5).$$

Analyzing the $\mathcal{O}(\delta)$ term and the $\mathcal{O}(\delta^2)$ term we obtain

$$C_1^+ = C_2^+ = 0 \quad \text{and} \quad \hat{\lambda}_{i,1}^+ = 0.$$

The $\mathcal{O}(\delta^3)$ term induces twice the following relation between C_3^+ and $\hat{\lambda}_{i,2}^+$:

$$0 = -2C_3^+ \left(\alpha A_0^2 + \frac{\beta}{D} A_0^{\frac{2}{D}} \right) + \frac{1}{2} \alpha \hat{\lambda}_{i,2}^+ A_0^2 (\hat{\tau}_{tp})^2 \log A_0^2 (\log A_0^2 - 1).$$

This gives a 1-parameter family of solutions, C_3^+ as function of $\hat{\lambda}_{i,2}^+$. Thus, we must examine the $\mathcal{O}(\delta^4)$ term. We find, together with a relation between C_4^+ and $\hat{\lambda}_{i,3}^+$, another relation between C_3^+ and $\hat{\lambda}_{i,2}^+$,

$$0 = \frac{1}{2}\sqrt{2}(\hat{\lambda}_{i,2}^+)^2\hat{\tau}_{tp} + \frac{1}{4}\sqrt{2}\hat{\lambda}_{i,2}^+\hat{\tau}_{tp}^2 - \frac{2}{3}\sqrt{2}\hat{\lambda}_{i,2}^+\frac{\hat{\tau}_2}{\hat{\tau}_{tp}} + C_3^+\alpha A_0^2\hat{\tau}_{tp}\log A_0^2 \\ - \frac{1}{4}\alpha(\hat{\lambda}_{i,2}^+)^2A_0^2\hat{\tau}_{tp}^2\log^2 A_0^2 - \frac{1}{8}\alpha\hat{\lambda}_{i,2}^+A_0^2\hat{\tau}_{tp}^3\log^3 A_0^2 + 2\alpha\hat{\lambda}_{i,2}^+A_0^2\hat{\tau}_{tp}\varepsilon\xi_{*,2}\log A_0^2.$$

Combining these two last equalities, together with the expressions for $\hat{\tau}_{tp}$, $\hat{\tau}_2$, $\xi_{*,0}$ and $\xi_{*,2}$, we find, besides the translation invariance eigenvalue $\hat{\lambda}_{1,2}^+ = 0$ and $C_3^+ = 0$, the second small eigenvalue

$$\hat{\lambda}_{2,2}^+ = -\frac{4}{3}\sqrt{2}\frac{1}{(\hat{\tau}_{tp})^3}\frac{1}{\frac{1}{2}\sqrt{2}-\frac{1}{4}\alpha A_0^2\hat{\tau}_{tp}\log^2 A_0^2}\hat{\tau}_2,$$

which is in the original scaling equal to (3.5.25). The proof is completed by noting that the denominator is always positive. \square

3.5.5 (In)stability of traveling pulse solutions for asymptotically large $\hat{\tau}$

The complexity of the expressions in the stability calculations reduces significantly for asymptotically large values of $\hat{\tau}$. It can be shown that in this limit the stability of the traveling pulse solutions is determined by the sign of β .

Lemma 3.5.5. *Let $\hat{\tau}$ be asymptotically large, that is, $\hat{\tau} = \delta^{-1}$ with $0 < \varepsilon \ll \delta \ll 1$, and let $\hat{\theta} = 0$, then the traveling pulse solutions are stable if and only if $\beta > 0$.*

Note that this lemma is in agreement with Corollary 3.5.3, since $\beta < 0$ corresponds to case (ii) of that corollary. Thus, the traveling pulse solution may undergo another bifurcation for increasing $\hat{\tau}$, most probably of Hopf type (which would generate a traveling breather).

The results of the local analysis near $\hat{\tau} = \hat{\tau}_{tp}$ and the analysis for $\hat{\tau}$ large are combined in Figure 3.11, where the position of the curves in the $(\hat{\tau}, |c|)$ -plane is based on (3.2.20) – note that the speed of the traveling pulse solution for asymptotically large $\hat{\tau}$ is given by $\frac{3}{2}\sqrt{2}(\alpha - \gamma)$ (2.3.15). The parameters are chosen such that, in the right frame, the bifurcating traveling wave is stable at the supercritical bifurcation (Lemma 3.5.4) and stable for $\hat{\tau} \gg 1$ (Lemma 3.5.5). In the left frame, the bifurcation is subcritical, the bifurcating traveling pulse is unstable (Lemma 3.5.4); it must undergo a stabilizing saddle-node bifurcation at a certain critical value $\hat{\tau}_{sn} < \hat{\tau}_{tp}$ (see also Chapter 2), that is followed by a third, destabilizing (Hopf?) bifurcation (Lemma 3.5.5). In principle, more bifurcations are possible. Note that the existence of the bifurcation points at which the stability of the pulses change are deduced from Lemmas 3.5.4 and 3.5.5, in combination with the existence analysis of the previous chapter. Thus, the position of the

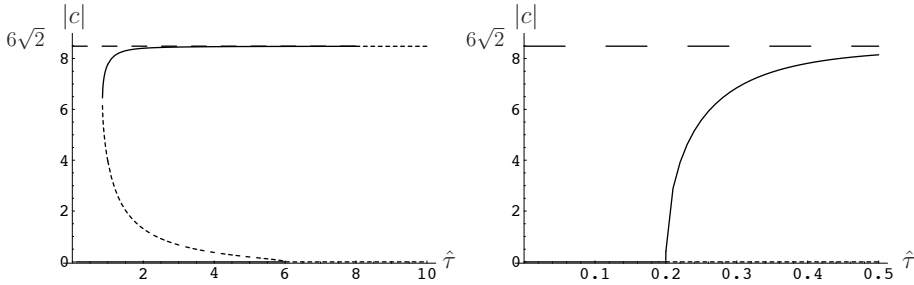


Figure 3.11: Bifurcation curves of the stationary and traveling pulse solutions for $(\alpha, \gamma, D, \theta, \varepsilon) = (5, 1, 4, 1, 0.01)$; $\beta = -3$ in the left frame, so that the traveling pulse bifurcates subcritically from the stationary pulse (Lemma 3.5.4) and becomes unstable for large $\hat{\tau}$ (Lemma 3.5.5); $\beta = 3$ in the right frame: the traveling pulse bifurcates supercritically (Lemma 3.5.4) and remains stable for large $\hat{\tau}$ (Lemma 3.5.5).

third bifurcation in the left frame of Figure 3.11 is only sketched; it has not been obtained from a full stability analysis of the traveling pulse solution.

Proof of Lemma 3.5.5. Since the calculations are straightforward, we only give a sketch of the proof. A detailed analysis of the u -component of the stability problem (3.5.18) yields, besides (3.4.7), that $u_{1,0}^\pm = C^\pm ((u_{tp,1,0}^\pm)_\xi + K_0^\pm \psi^\pm)$ (where we used the notation from the previous section, see (3.5.26)). By applying the solvability condition to the second order correction term (with respect to ε) of the u -component and by using (3.2.28), we obtain

$$\mp \frac{1}{3} \sqrt{2} C^\pm \hat{\lambda} + \alpha \tilde{v}(\pm \xi^*) + \beta \tilde{w}(\pm \xi^*) - \frac{1}{\varepsilon} \alpha C^\pm (v_{tp})_\xi(\pm \xi^*) - \frac{1}{\varepsilon} \beta C^\pm (w_{tp})_\xi(\pm \xi^*) = 0.$$

Now, we compute the leading order behavior of $\tilde{v}(\pm \xi^*)$, $\tilde{w}(\pm \xi^*)$, $(v_{tp})_\xi(\pm \xi^*)$, and $(w_{tp})_\xi(\pm \xi^*)$ with respect to δ . It is not hard to see that the $\tilde{v}(\pm \xi^*)$ and $(v_{tp})_\xi(\pm \xi^*)$ are zero to leading order, and because $\hat{\theta} = 0$, the leading order behavior of $\tilde{w}(\pm \xi^*)$ and $(w_{tp})_\xi(\pm \xi^*)$ is the same as in the case of standing pulse solutions. Hence, it follows that $\hat{\lambda}^+ = 0$ and $\hat{\lambda}_1 = -3\sqrt{2} \frac{\beta}{D} A^{2/D}$ (3.4.20), so that the sign of β determines the stability of the traveling pulse solution for asymptotically large $\hat{\tau}$. \square

3.6 Standing 2-pulse solutions

In this section, we investigate the stability of standing 2-pulse solutions as constructed in Chapter 2 and as reviewed here in Section 3.2.3. The main result

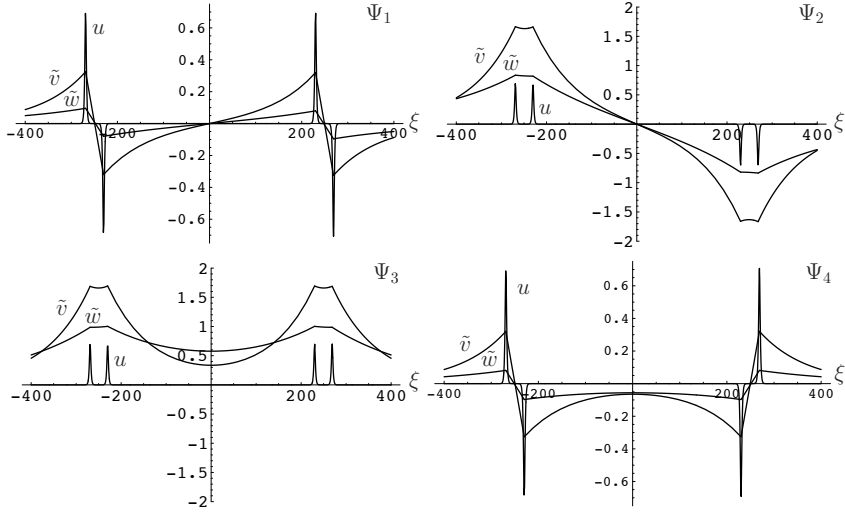


Figure 3.12: The eigenfunctions $\Psi_j(\xi)$ associated to the symmetric standing 2-pulse solution with $\alpha = 3$, $\beta = -1$, $\gamma = 1.22$, $D = 2$, and $\varepsilon = 0.01$. Observe that $\Psi_{1,2}(\xi)$ are odd eigenfunctions, while $\Psi_{3,4}(\xi)$ are even eigenfunctions.

reads

Theorem 3.6.1. *Let $(\alpha, \beta, \gamma, D, \varepsilon)$ be such that there exist K 2-pulse solutions (Theorem 3.2.4). Assume that $\tau, \theta = \mathcal{O}(1)$, then the stability of the 2-pulse solution is governed by four small eigenvalues $\lambda_j = \varepsilon^2 \hat{\lambda}_j$ that are given by*

$$\begin{aligned} \hat{\lambda}_1 &= 0, \quad \hat{\lambda}_2 = 3\sqrt{2}\mathcal{E}, \\ \hat{\lambda}_{3,4} &= -\frac{3}{2}\sqrt{2} \left(\mathcal{A} + \mathcal{D} - \mathcal{E} \pm \sqrt{(\mathcal{A} - \mathcal{D})^2 + (\mathcal{B} + \mathcal{C})^2} \right), \end{aligned} \quad (3.6.1)$$

where $\mathcal{A}, \mathcal{B}, \mathcal{C}, \mathcal{D}$, and \mathcal{E} are defined by

$$\begin{aligned} \mathcal{A} &:= \alpha A_1^2 + \frac{\beta}{D} A_1^{2/D}, & \mathcal{B} &:= \alpha A_1 A_2 + \frac{\beta}{D} A_1^{1/D} A_2^{1/D}, \\ \mathcal{C} &:= \alpha A_1 A_2^{-1} + \frac{\beta}{D} A_1^{1/D} A_2^{-1/D}, & \mathcal{D} &:= \alpha A_2^2 + \frac{\beta}{D} A_2^{2/D}, & \mathcal{E} &:= \mathcal{B} - \mathcal{C}, \end{aligned}$$

in which $A_{1,2}$ are determined by (3.2.30).

As in the previous sections, we can also determine the associated eigenfunctions $\Psi_j(\xi)$, $j = 1, \dots, 4$, explicitly. In fact, if C_i^j is the amplitude of the fast u -component of $\Psi_j(\xi)$ in the fast field I_i^j , $i \in \{2, 4, 6, 8\}$ (3.2.29), i.e., $\Psi_j^u(\xi) =$

$(-1)^{\frac{i}{2}+1}C_i^j\psi_i(\xi)$ with $\psi_i(\xi)$ as in (3.2.34), then we have

$$\begin{aligned}
\Psi_1(\xi) &: C_2^1 = C_4^1 = C_6^1 = C_8^1, \\
\Psi_2(\xi) &: C_2^2 = -C_4^2 = -C_6^2 = C_8^2, \\
\Psi_3(\xi) &: C_2^3 = \frac{B+C}{A-D-\sqrt{(A-D)^2+(B+C)^2}}C_4^3 \\
&= -\frac{B+C}{A-D-\sqrt{(A-D)^2+(B+C)^2}}C_6^3 = -C_8^3, \\
\Psi_4(\xi) &: C_2^4 = \frac{B+C}{A-D+\sqrt{(A-D)^2+(B+C)^2}}C_4^4 \\
&= -\frac{B+C}{A-D+\sqrt{(A-D)^2+(B+C)^2}}C_6^4 = -C_8^4.
\end{aligned} \tag{3.6.2}$$

The eigenfunctions $\Psi_{1,2}(\xi)$ are odd, while $\Psi_{3,4}(\xi)$ are even. In Figure 3.12, we plotted all four eigenfunctions for a certain parameter combination.

In Section 3.6.1, we sketch the proof of Theorem 3.6.1. Then, since the formulas (3.6.1) for $\hat{\lambda}_{2,3,4}$ are complicated, we further investigate these small eigenvalues in Section 3.6.2, showing that there are regions in parameter space in which the 2-pulse solutions are stable, and showing that for asymptotically large values of D the 2-pulse solutions are unstable.

3.6.1 Proof of Theorem 3.6.1

The main difference between the construction and the stability analysis of a 1-pulse solution and a 2-pulse solution is the number of fast and slow intervals. For a 2-pulse solution, we have four fast and five slow intervals (3.2.29) instead of two fast and three slow intervals as is the case for 1-pulse solutions. For the construction of the Evans function, we therefore first assume that there is one large intermediate regime that consists of $I_f^2 \cup I_s^3 \cup I_f^4 \cup I_s^5 \cup I_f^6 \cup I_s^7 \cup I_f^8$. Essentially, the construction of the Evans functions goes exactly as in Section 3.3.4. Similar arguments as in Section 3.4.2 show that the slow basis functions $\phi(\xi)$ do not have a fast growing component in each of the intermediate slow regimes, so that we can define (and determine) the intermediate transmission functions $s_{ij}^{2k+1}(\hat{\lambda})$ in each of the slow regions I_s^{2k+1} ($i = 2, 3, j = 2, 3, 4, 5$, and $k = 1, 2, 3$).

The stability analysis is analogous to that of Section 3.4. For example, the essential spectrum is given in Lemma 3.3.1, we need the same rescalings for λ , $v(\xi)$, and $w(\xi)$, the eigenvalues of \mathcal{M}_∞^{2p} are still given by (3.4.11), and its associated eigenvectors by (3.4.12). The only real difference is that we have to impose (many!) more matching conditions. After a tedious calculation, we find that the \tilde{v}, \tilde{w} -

components of the slow basis function $\phi(\xi)$ are given by

$$\phi_{2p}^{\tilde{v}}(\xi) = \begin{cases} C_2 e^{\varepsilon(\xi+\xi_*^1)} - C_4 e^{\varepsilon(\xi+\xi_*^2)} + C_6 e^{\varepsilon(\xi-\xi_*^2)} - C_8 e^{\varepsilon(\xi-\xi_*^1)} & \text{in } I_s^1, \\ C_2 e^{-\varepsilon(\xi+\xi_*^1)} - C_4 e^{\varepsilon(\xi+\xi_*^2)} + C_6 e^{\varepsilon(\xi-\xi_*^2)} - C_8 e^{\varepsilon(\xi-\xi_*^1)} & \text{in } I_s^3, \\ C_2 e^{-\varepsilon(\xi+\xi_*^1)} - C_4 e^{-\varepsilon(\xi+\xi_*^2)} + C_6 e^{\varepsilon(\xi-\xi_*^2)} - C_8 e^{\varepsilon(\xi-\xi_*^1)} & \text{in } I_s^5, \\ C_2 e^{-\varepsilon(\xi+\xi_*^1)} - C_4 e^{-\varepsilon(\xi+\xi_*^2)} + C_6 e^{-\varepsilon(\xi-\xi_*^2)} - C_8 e^{\varepsilon(\xi-\xi_*^1)} & \text{in } I_s^7, \\ -C_8 e^{-\varepsilon(\xi-\xi_*^1)} + \frac{1}{D} E_4^{\tilde{v}} \left(C_2 e^{-\frac{\varepsilon}{D}(\xi+\xi_*^1)} - C_4 e^{-\frac{\varepsilon}{D}(\xi+\xi_*^2)} \right. \\ \left. + C_6 e^{-\frac{\varepsilon}{D}(\xi-\xi_*^2)} - C_8 e^{-\frac{\varepsilon}{D}(\xi-\xi_*^1)} \right) & \text{in } I_s^9, \end{cases} \quad (3.6.3)$$

and

$$\phi_{2p}^{\tilde{w}}(\xi) = \begin{cases} \frac{1}{D} \left(C_2 e^{\frac{\varepsilon}{D}(\xi+\xi_*^1)} - C_4 e^{\frac{\varepsilon}{D}(\xi+\xi_*^2)} + C_6 e^{\frac{\varepsilon}{D}(\xi-\xi_*^2)} \right. \\ \left. - C_8 e^{\frac{\varepsilon}{D}(\xi-\xi_*^1)} \right) & \text{in } I_s^1, \\ \frac{1}{D} \left(C_2 e^{-\frac{\varepsilon}{D}(\xi+\xi_*^1)} - C_4 e^{\frac{\varepsilon}{D}(\xi+\xi_*^2)} + C_6 e^{\frac{\varepsilon}{D}(\xi-\xi_*^2)} \right. \\ \left. - C_8 e^{\frac{\varepsilon}{D}(\xi-\xi_*^1)} \right) & \text{in } I_s^3, \\ \frac{1}{D} \left(C_2 e^{-\frac{\varepsilon}{D}(\xi+\xi_*^1)} - C_4 e^{-\frac{\varepsilon}{D}(\xi+\xi_*^2)} + C_6 e^{\frac{\varepsilon}{D}(\xi-\xi_*^2)} \right. \\ \left. - C_8 e^{\frac{\varepsilon}{D}(\xi-\xi_*^1)} \right) & \text{in } I_s^5, \\ \frac{1}{D} \left(C_2 e^{-\frac{\varepsilon}{D}(\xi+\xi_*^1)} - C_4 e^{-\frac{\varepsilon}{D}(\xi+\xi_*^2)} + C_6 e^{-\frac{\varepsilon}{D}(\xi-\xi_*^2)} \right. \\ \left. - C_8 e^{\frac{\varepsilon}{D}(\xi-\xi_*^1)} \right) & \text{in } I_s^7, \\ \frac{1}{D} \left(C_2 e^{-\frac{\varepsilon}{D}(\xi+\xi_*^1)} - C_4 e^{-\frac{\varepsilon}{D}(\xi+\xi_*^2)} + C_6 e^{-\frac{\varepsilon}{D}(\xi-\xi_*^2)} \right. \\ \left. - C_8 e^{-\frac{\varepsilon}{D}(\xi-\xi_*^1)} \right) & \text{in } I_s^9. \end{cases} \quad (3.6.4)$$

See Remark 3.4.1, and recall that $\pm\xi_*^{1,2}$ are to leading order the centers of the fast fields. Moreover, note that we again constructed the basis function $\phi(\xi)$ in such a fashion that $t_{2,3} = 0$ (3.5.9). Thus, we follow the approach of Section 3.5.1 (note the similarities between (3.6.3), (3.6.4) and (3.5.22), (3.5.23)), rather than that of Section 3.4.3.

Substituting the values for the \tilde{v}, \tilde{w} -components into the u -equation in the fast fields yields four ODEs for the u -component similar to (3.4.31), (3.4.32), and (3.5.11). In combination with the solvability conditions (3.2.35), the second order correction term of the u -component in the fast fields gives all the information about the eigenvalues. Specifically, the eigenvalues $\hat{\lambda}_{1,2,3,4}$ are the nontrivial solutions of the matrix equation

$$M_2 \begin{pmatrix} C_2 \\ C_4 \\ C_6 \\ C_8 \end{pmatrix} = \begin{pmatrix} 0 \\ 0 \\ 0 \\ 0 \end{pmatrix}, \quad (3.6.5)$$

where M_2 is a 4×4 -matrix given by

$$M_2 := \begin{pmatrix} \frac{1}{3}\sqrt{2}\hat{\lambda} + \mathcal{A} - \mathcal{E} & -\mathcal{C} & \mathcal{B} & -\mathcal{A} \\ \mathcal{C} & -\frac{1}{3}\sqrt{2}\hat{\lambda} - \mathcal{D} + \mathcal{E} & \mathcal{D} & -\mathcal{B} \\ \mathcal{B} & -\mathcal{D} & \frac{1}{3}\sqrt{2}\hat{\lambda} + \mathcal{D} - \mathcal{E} & -\mathcal{C} \\ \mathcal{A} & -\mathcal{B} & \mathcal{C} & -\frac{1}{3}\sqrt{2}\hat{\lambda} - \mathcal{A} + \mathcal{E} \end{pmatrix},$$

and $\mathcal{A}, \mathcal{B}, \mathcal{C}, \mathcal{D}$, and \mathcal{E} are defined in Theorem 3.6.1. The condition that the determinant of this matrix M_2 vanishes yields the four eigenvalues

$$\hat{\lambda}_1 = 0, \quad \hat{\lambda}_2 = 3\sqrt{2}\mathcal{E}, \quad \hat{\lambda}_{3,4} = -\frac{3}{2}\sqrt{2} \left(\mathcal{A} + \mathcal{D} - \mathcal{E} \pm \sqrt{(\mathcal{A} - \mathcal{D})^2 + (\mathcal{B} + \mathcal{C})^2} \right).$$

This completes the proof. \square

Note that by construction $\hat{\lambda}_4 \geq \hat{\lambda}_3$. However, the signs of the eigenvalues $\hat{\lambda}_{2,4}$ are not immediately clear from (3.6.1). Therefore, in order to obtain more explicit statements about stability and instability of the 2-pulse solutions from formulas (3.6.1), we investigate these formulas in the next section.

3.6.2 The small eigenvalues

The main results of this section are that there exist open regions in parameter space in which the 2-pulse solutions are stable (see Lemma 3.6.2), while in the regime with D asymptotically large the 2-pulse solutions are unstable (see Lemma 3.6.3).

Lemma 3.6.2. *Let $(\alpha, \beta, \gamma, D, \varepsilon, \tau, \theta)$ be as in Theorem 3.6.1, and suppose that $\alpha > 0$ and $0 > \beta > -h^*(D)\alpha$, where $h^*(D)$ is the unique positive solution of*

$$\kappa(h, D) := -h^{\frac{D}{D-1}} D^{-2\frac{D}{D-1}} (D-1) + 1 - \frac{h}{D} = 0. \quad (3.6.6)$$

Then, there exists an open interval of γ -values such that the standing 2-pulse solution is stable.

In Figure 3.13, we plotted the three small eigenvalues $\hat{\lambda}_{2,3,4}$ as functions of A_2 for four different combinations of α and β , while the other parameters are kept fixed. We observe that only in the first frame (upper left) do we find a stable standing 2-pulse solution, and this is indeed the only frame for which the parameters α and β fulfill the conditions of Lemma 3.6.2.

Note that for $D = 2$ equation (3.6.6) can be solved explicitly, and the unique solution reads $h^*(2) = 4(\sqrt{2} - 1)$. Moreover, for D large, $\kappa(h, D)$ is given to leading order by $1 - \frac{2h}{D}$, and hence $h^*(D) \rightarrow \frac{D}{2}$ as $D \gg 1$. Moreover, in the other limit, $D \rightarrow 1$, the solution is given by $h^*(1) = 1$.

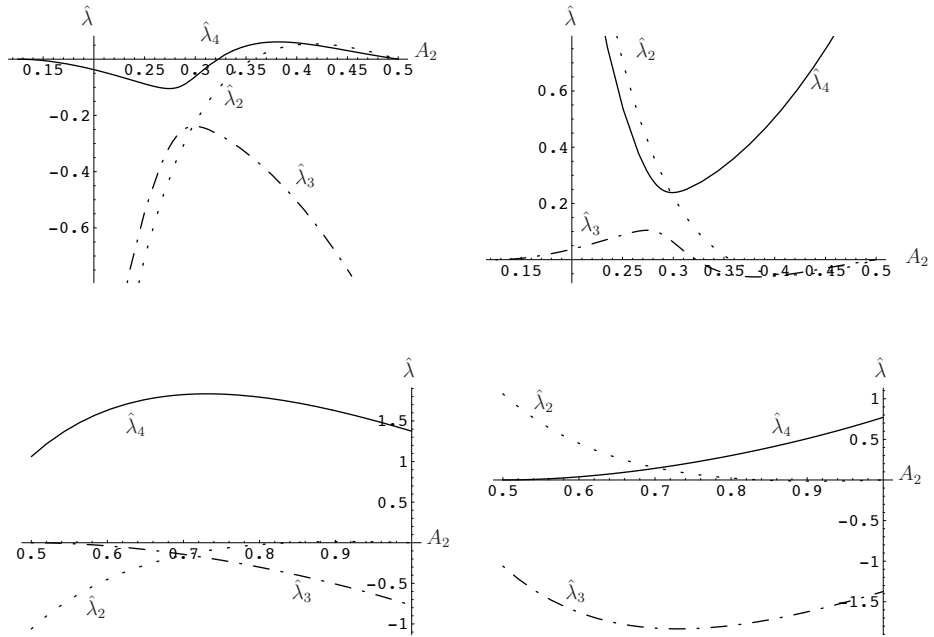


Figure 3.13: The small eigenvalues $\hat{\lambda}_2$ (dotted line), $\hat{\lambda}_3$ (dashed-dotted line), and $\hat{\lambda}_4$ (solid line) as function of A_2 , where $D = 2$ and $(\alpha, \beta) = \{(2, -1), (-2, 1), (1, -2), (-1, 2)\}$, respectively. Note that only for $(\alpha, \beta) = (2, -1)$ does there exist a regime in which the 2-pulse solutions are stable. This is also the only parameter combination of the four for which the hypotheses of Lemma 3.6.2 are satisfied.

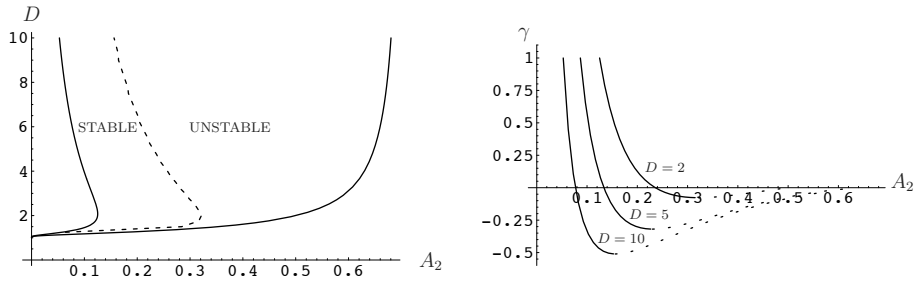


Figure 3.14: In the left frame, we plotted the existence and stability regimes for a given parameter combination fulfilling the assumptions of Lemma 3.6.2 as functions of A_2 and D ($(\alpha, \beta) = (2, -1)$), see (3.6.7). In the right frame, we plotted γ as a function of A_2 for three different values of $D = 2, 5, 10$. The solid line represents a stable 2-pulse solution, while the dotted line represents an unstable 2-pulse solution. We observe a saddle-node bifurcation of 2-pulse solutions, that is, for decreasing γ a stable and an unstable standing 2-pulse solution merge and disappear.

The proof of the above lemma is partly based on solving equations (3.2.30). We observe that the first equation of (3.2.30) is independent of γ . Therefore, for given A_2 , the first equation yields A_1 , and the second equation yields a uniquely determined γ . However, there is a restriction in the choice of A_2 , since it has to lie between A_1 and 1. From the previous chapter we know that this restriction yields (for general D)

$$\left(-\frac{\alpha D^2}{\beta}\right)^{-\frac{1}{2} \frac{D}{D-1}} < A_2 < \min \left\{ \left(-\frac{\alpha}{\beta}\right)^{-\frac{1}{2} \frac{D}{D-1}}, 1 \right\}. \quad (3.6.7)$$

In the left frame of Figure 3.14, we plotted (3.6.7) as function of D with α, β fixed such that the conditions of Lemma 3.6.2 are fulfilled. We also included the curve where the stability of a 2-pulse solution changes. We indeed observe that the stability regime for D asymptotically large shrinks to zero, see Lemma 3.6.3. In the right frame, we plotted γ as function of A_2 for several values of D .

Proof of Lemma 3.6.2. The proof is obtained by choosing γ in a special region such that $\mathcal{A}, \mathcal{B}, \mathcal{C}$, and \mathcal{D} can be determined explicitly by an asymptotic procedure. We introduce $\tilde{\beta} := -\frac{\beta}{\alpha} > 0$ (by assumption), and we choose γ in such a fashion that A_2 is close to its lower boundary, *i.e.*, $A_2 = D^{-\frac{D}{D-1}} \tilde{\beta}^{\frac{1}{2} \frac{D}{D-1}} + \delta =: A_2^l + \delta$, with $0 < \varepsilon \ll \delta \ll 1$, see (3.6.7). Solving the first equation of (3.2.30) yields that $A_1 = A_2^l - \delta + \mathcal{O}(\delta^2)$. Now, we can also determine $\mathcal{A}, \mathcal{B}, \mathcal{C}$, and \mathcal{D} in terms of the

small parameter δ

$$\begin{aligned}\frac{A}{\alpha} &= (1-D)(A_2^l)^2 + 2\frac{D-1}{D}\delta^2 + \mathcal{O}(\delta^3), \\ \frac{B}{\alpha} &= (1-D)(A_2^l)^2 + \mathcal{O}(\delta^3), \\ \frac{C}{\alpha} &= \left(1 - \frac{\tilde{\beta}}{D}\right) - 2\left((D^2 - \tilde{\beta})D^{\frac{2-D}{D-1}}\tilde{\beta}^{\frac{1}{2}}\delta^{\frac{D}{1-D}}\right)\delta + \mathcal{O}(\delta^2), \\ \frac{D}{\alpha} &= (1-D)(A_2^l)^2 + 2\frac{D-1}{D}\delta^2 + \mathcal{O}(\delta^3).\end{aligned}$$

Hence, we find that the four eigenvalues $\hat{\lambda}_{1,2,3,4}$ are

$$\begin{aligned}\hat{\lambda}_1 &= 0, \hat{\lambda}_2 = -3\sqrt{2}\alpha\left(1 - \frac{\tilde{\beta}}{D} + (D-1)(A_2^l)^2\right) + \mathcal{O}(\delta), \\ \hat{\lambda}_3 &= \begin{cases} -3\sqrt{2}\alpha\left(\kappa(\tilde{\beta}, D)\right) + \mathcal{O}(\delta) & \text{for } \kappa(\tilde{\beta}, D) > 0, \\ -6\sqrt{2}\frac{D-1}{D}\alpha\delta^2 + \mathcal{O}(\delta^3) & \text{for } \kappa(\tilde{\beta}, D) < 0, \end{cases} \\ \hat{\lambda}_4 &= \begin{cases} -6\sqrt{2}\frac{D-1}{D}\alpha\delta^2 + \mathcal{O}(\delta^3) & \text{for } \kappa(\tilde{\beta}, D) > 0, \\ -3\sqrt{2}\alpha\left(\kappa(\tilde{\beta}, D)\right) + \mathcal{O}(\delta) & \text{for } \kappa(\tilde{\beta}, D) < 0. \end{cases}\end{aligned}$$

with $\kappa(\tilde{\beta}, D)$ as defined in (3.6.6). We note that equation (3.6.6) indeed has a unique positive solution, since $\kappa(h, D)$ is, as a function of h , monotonically decreasing, $\kappa(0, D) = 1$, and $\kappa(\infty, D) < -\infty$. Moreover, since $\kappa(D^2, D) = 2(1-D) < 0$, we deduce from the monotonicity that $D^2 > h^*(D)$, so that $\tilde{\beta} < h^*(D) < D^2$ by assumption. Hence, we have that $\left(1 - \frac{\tilde{\beta}}{D} + (D-1)(A_2^l)^2\right) > 0$, which implies that $\hat{\lambda}_2 < 0$ for $\alpha > 0$. Moreover, it follows that $\hat{\lambda}_4 < 0$ for $\tilde{\beta} < h^*(D)$. Since $\hat{\lambda}_3 \leq \hat{\lambda}_4$, we have shown that a 2-pulse solution is stable if $0 < \beta < -h^*(D)\alpha$ for γ such that A_2 is close to A_2^l . \square

Observe that we did not yet obtain a result on the instability of the 2-pulse solutions if the parameters do not satisfy the conditions of Lemma 3.6.2. Such results can be obtained, but we refrain from going into the details here. However, we will prove that 2-pulse solutions are always unstable for large D (see Figure 3.14).

Lemma 3.6.3. *Let $\frac{1}{D}$ be asymptotically small, then the 2-pulse solution is unstable for values of $A_2 \in \left(0, \sqrt{-\frac{\beta}{\alpha}}\right)$ that are strictly $\mathcal{O}(1)$ with respect to $\frac{1}{D}$.*

Proof. From Chapter 2, we know that for $\frac{1}{D}$ asymptotically small, $A_1 = \left(1 - \sqrt{-\frac{\beta}{\alpha}}A_2\right)^D$ to leading order. In the case that $\text{sgn}(\beta) = -1$, we now show that the second small eigenvalue $\hat{\lambda}_2$ (3.6.1) is positive. In fact,

$$\begin{aligned}\mathcal{B} - \mathcal{C} &= \alpha A_1(A_2 - A_2^{-1}) + \frac{\beta}{D}A_1^{1/D}(A_2^{1/D} - A_2^{-1/D}) \\ &= \frac{2\beta}{D^2}\left(1 - \sqrt{-\frac{\beta}{\alpha}}A_2\right)\log A_2 + \mathcal{O}(D^{-3}) > 0.\end{aligned}$$

Therefore, $\hat{\lambda}_2 > 0$, and the 2-pulse solution is thus unstable.

In the case that $\text{sgn}(\alpha) = -1$, we show that the fourth small eigenvalue, $\hat{\lambda}_4$, in (3.6.1) is positive. It is enough to show that $\mathcal{A} - \mathcal{B} + \mathcal{C} + \mathcal{D} < 0$.

$$\begin{aligned} \mathcal{A} - \mathcal{B} + \mathcal{C} + \mathcal{D} &= \alpha \left((A_2 - A_1)^2 + A_1 A_2 + A_1 A_2^{-1} \right) \\ &\quad + \frac{\beta}{D} \left(\left(A_2^{1/D} - A_1^{1/D} \right)^2 + A_1^{1/D} A_2^{1/D} + A_1^{1/D} A_2^{-1/D} \right) \\ &= \alpha A_2^2 + \mathcal{O}(D^{-1}) < 0. \end{aligned}$$

Thus, $\hat{\lambda}_4 > 0$, and the 2-pulse solution is also unstable in this case. \square

Chapter 4

Interactions

4.1 Introduction

Patterns are ubiquitous in science and engineering. They form when key physical quantities—for example the concentrations of chemical species—exhibit nontrivial spatial and/or temporal dependence. Stripes, hexagons, spots, fronts, pulses, spirals, targets, sand ripples, and roll cells, are all examples of patterns, to name a few.

Patterns may be classified as being near-equilibrium or far-from-equilibrium. In the former case, the amplitudes of the key physical quantities are close to their equilibrium values everywhere in the domain. Such patterns arise, for example, when stable homogeneous (or equilibrium) states are destabilized by diffusion, as in the classical Turing bifurcation. By contrast, in far-from-equilibrium patterns, the key physical quantities exhibit large excursions away from equilibrium. Often, such patterns have a localized character, *i.e.*, they are close to equilibrium on large parts of the domain and far from equilibrium on relatively small or narrow subdomains. Examples include fronts, which connect two different equilibria, pulses that may be the concatenations of two fronts, spots, and other more-complicated spatially-localized structures.

In the last decade, the three-component reaction-diffusion equation introduced in [60] has become a paradigm model to investigate the rich variety of front, pulse, and spot dynamics. As shown numerically and experimentally in [5, 32, 50, 51, 53, 54, 60, 65, 71], these localized structures can undergo repulsion, annihilation, attraction, breathing, collision, scattering, self-replication, and spontaneous generation. This three-component model consists of a well-studied bistable equation for the activator component, and linear equations for the two inhibitor components, with bidirectional linear coupling. Hence, it may be interpreted as a

FitzHugh-Nagumo type equation augmented with a second inhibitor component. It has become a paradigm problem, among other reasons, because it is simultaneously complex enough to support the rich dynamics of these localized structures and simple enough to permit extensive analysis, as has been shown in one space dimension in the previous chapters.

A scaled version of this paradigm model in 1-D is, see also Chapter 2,

$$\begin{cases} U_t = U_{\xi\xi} + U - U^3 - \varepsilon(\alpha V + \beta W + \gamma), \\ \tau V_t = \frac{1}{\varepsilon^2} V_{\xi\xi} + U - V, \\ \theta W_t = \frac{D^2}{\varepsilon^2} W_{\xi\xi} + U - W, \end{cases} \quad (4.1.1)$$

where $0 < \varepsilon \ll 1$, $D > 1$, $\tau, \theta > 0$, $\alpha, \beta, \gamma \in \mathbb{R}$ and $\mathcal{O}(1)$ with respect to ε , and $(\xi, t) \in \mathbb{R} \times \mathbb{R}^+$. Here, U represents the activator concentration, and V and W represent the concentrations of the inhibitors. This partial differential equation (PDE) has homogeneous steady states $\mathcal{O}(\varepsilon)$ close to $(U, V, W) = (\pm 1, \pm 1, \pm 1)$ and to $(0, 0, 0)$, with the former being stable and the latter unstable. Fronts are solutions that are close to the stable homogeneous steady state near $(-1, -1, -1)$ on a certain interval and then jump to the other stable homogeneous state near $(1, 1, 1)$. Backs are the opposites of fronts, and they are related to fronts via the symmetry $(U, V, W, \gamma) \rightarrow (-U, -V, -W, -\gamma)$ of (4.1.1), so that one may simply refer to both as fronts. Finally, pulses, which are the concatenation of a front and a back, are biasymptotic to either the homogeneous state near $(-1, -1, -1)$ or to that near $(1, 1, 1)$. By symmetry, any result about the former pulse solution also holds for the latter type, and *vice versa*. Hence, one may focus on the former type, without loss of generality.

The third component W was introduced in [60] to stabilize traveling spot solutions in 2-D. In the previous chapters, the relation between the three-component model and its two-component limit has been investigated in detail (in one spatial dimension). We have shown that the third component significantly increases the richness of the dynamics generated by the model. For instance, stationary 2-pulse (4-front) solutions cannot exist in the two-component limit, see Section 2.6. In the current chapter, we will also establish that uniformly traveling 3-front solutions can only exist in the three-component model, see Lemma 4.4.8.

The existence and stability of traveling 1-pulse solutions and standing 1-pulse and 2-pulse solutions was proved in the previous chapters. We used and extended classical methods from geometric singular perturbation theory and from Evans function theory. Moreover, we note that it was critical for the application of these methods that the localized structures were either constant in time or fixed in a co-moving frame.

The current chapter may be viewed as the next natural step in the analysis of the

three-component model (4.1.1). We study dynamically-evolving solutions consisting of N fronts. It is not clear how to use the classical techniques to rigorously establish the existence of these solutions or their stability, since there is not a single, global co-moving frame in which all N fronts are constant. Indeed, any two adjacent fronts may move in opposite directions and/or with different speeds, see Figures 4.1 and 4.2.

Our objectives in this chapter are to derive and to analyze the system of N coupled ordinary differential equations (ODEs) that governs the velocities of the fronts in an N -front solution in the parameter regime $\tau, \theta = \mathcal{O}(1)$ – see Remark 4.1.1. The derivation is readily carried out formally using matched asymptotic expansions. However, a rigorous justification of the validity of these ODEs —*i.e.*, of the validity of reducing the three PDEs in (4.1.1) to a system of N ODEs for the front velocities— requires significant new analysis. This justification is the primary result of this chapter. It will be achieved modifying the renormalization group (RG) method to consider the stability in a bounded variation (BV)-type norm. The second main result is an analysis of the reduced ODEs. In particular, we classify the different possible front dynamics for these N -front solutions, as well as how interacting fronts may pair up into (interacting) pulses.

As a preparatory result, we will show that 1-front solutions travel with velocity $\dot{\Gamma}(t) = \frac{3}{2}\sqrt{2}\varepsilon\gamma$, where $\xi = \Gamma(t)$ denotes the position of the fronts at time t . Moreover, we show that they are stable (see Lemma 4.2.1). The first substantial case involves 2-front solutions. We will show that the front velocities are given by

$$\dot{\Gamma}_1 = \frac{3}{2}\sqrt{2}\varepsilon \left(\gamma - \alpha e^{-\varepsilon(\Gamma_2 - \Gamma_1)} - \beta e^{-\frac{\varepsilon}{B}(\Gamma_2 - \Gamma_1)} \right), \quad \dot{\Gamma}_2 = -\dot{\Gamma}_1,$$

to leading order. Analysis of these ODEs reveals that a 2-front solution asymptotes to a standing 1-pulse solution if and only if this 1-pulse solution is stable and there are no unstable 1-pulse solutions between it and the initial fronts. Otherwise, the fronts may asymptote to $\pm\infty$ or annihilate.

The dynamics exhibited by 3-front and 4-front solutions is more varied. We show, among other things, that 3-front solutions and 4-front solutions for which one (or more) of the outer fronts travels to $\pm\infty$ can be stable. Also, the 4-front solutions can asymptote to a ground state, a stable 1-pulse solution, or a stable 2-pulse solution.

For general $N \geq 1$, we will show that the velocities of the fronts are given to leading order by (4.2.1). Analyzing these ODEs in the generic case when $\gamma \neq 0$, we show that uniformly traveling solutions are possible when the number of fronts is odd, but not when the number of fronts is even. Similarly, in the generic case, we find that stationary N -front solutions can exist when N is even, but not when N is odd. See Lemma 4.4.2.

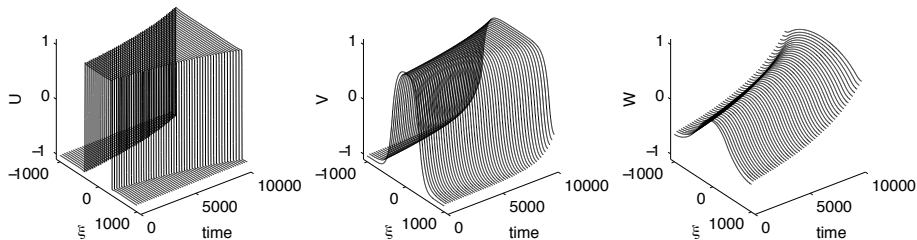


Figure 4.1: These frames show the evolution of respectively the U, V, W -component for a certain approximate 2-front initial condition with system parameters $(\alpha, \beta, \gamma, D, \tau, \theta, \varepsilon) = (6, -5, -2, 5, 1, 1, 0.01)$. The fronts of the 2-front solution repel each other and diverge to $\pm\infty$. Note that the V, W -components interact strongly, while the U -component interacts weakly.

In proving the existence and stability of the dynamically-evolving N -front solutions, we focus exclusively on the case $N = 2$, in order to keep the analysis of the RG method as transparent as possible. Nevertheless, the ideas and arguments in the proof also suffice to rigorously justify the ODE reduction for N -front solutions for general N . There are N eigenvalues near zero, and the spectral splitting holds uniformly for the N -front solutions as follows from the analysis in Chapter 3. See also [47] for a detailed study of the stability of N -pulse solutions using the RG method.

The validity of the ODE system (4.2.1) will be established using an RG method. Indeed, the method will simultaneously give the existence and stability of the N -front solutions, as long as no two adjacent fronts get too close. One begins with the manifold of approximate N -front solutions obtained from a formal derivation. Initial data $\Phi_N(\xi, t = 0) = (U_N(\xi, 0), V_N(\xi, 0), W_N(\xi, 0))$ for the PDE (4.1.1) that lies close to a point on this manifold may be decomposed into the sum of an approximating ‘skeleton’ N -front solution on the manifold and a remainder which lies in the directions transverse to the manifold and whose norm is of the size of the distance to the manifold. Based on leading order matched asymptotic expansions, one expects that $\Phi_N(\xi, t)$ will remain close to the skeleton solution as it evolves on that manifold, *i.e.*, that the remainder remains small. However, proving that this is indeed the case requires a stability analysis about the time-dependent solution on the manifold. With the RG method, we show that there exists a sequence of times $\{t_i^*\}_{i=0}^\infty$, with $t_0^* = 0$, at which one may freeze the skele-

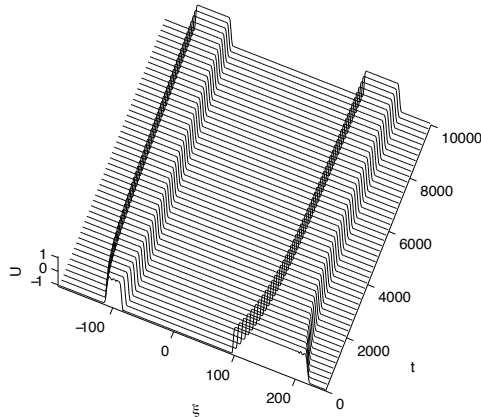


Figure 4.2: In this frame, we show the evolution of the U -component for a certain approximate 4-front initial condition with system parameters $(\alpha, \beta, \gamma, D, \tau, \theta, \varepsilon) = (4, -3, -0.5, 10, 1, 1, 0.01)$. The four fronts asymptote to a stable stationary 2-pulse solution. Note that the back and the front of a pulse do not necessarily move with the same speed and/or in the same direction.

ton solution on the manifold and linearize about this frozen solution in order to approximate the linearization about $\Phi_N(\xi, t)$ on the interval $[t_i^*, t_{i+1}^*]$. Then, at the end of each time interval, one renormalizes the skeleton solution by taking an appropriate point on the manifold, and repeats the above procedure. Projection of the solutions onto the eigenspace associated with the N small $\mathcal{O}(\varepsilon)$ eigenvalues of the linearized operator leads to the ODEs for the positions of the fronts, and projection onto the complementary eigenspace leads to the bounds on the resolvent and semi-group, and hence also to the bounds on the remainder.

There are several competing factors, akin to normal hyperbolicity, which determine whether or not the RG method approach succeeds. On the one hand, the lengths of the intervals, $t_{i+1}^* - t_i^*$, must be sufficiently long so that the contraction estimates obtained from the semi-group estimates are sufficient. On the other hand, the lengths of these intervals must be sufficiently short so that the secular errors which accumulate in making the frozen linearization approximation do not become too big.

Front and pulse interactions have been studied using RG methods in [16, 31, 47, 55]. The underlying strategy in applying the method here is similar to that used in these other studies. The main challenge we face applying the RG method

to the three-component model (4.1.1) is that we cannot use variants of an H^1 -norm, such as used in [16]. These norms are singular when comparing functions with small differences in their asymptotic states at spatial infinity. To overcome this, we define the χ -norm, see (4.3.1), which can be seen as a variant of the usual BV norm.

We observe that the interactions between the fronts and pulses that we study is classified as semi-strong, see [15, 16, 38, 47, 62]. Semi-strong interaction of two adjacent fronts means that the interaction is driven essentially by the component(s) that are not near equilibrium in the intervals between the fronts. In the case of (4.1.1), the front interactions are driven by V and W , see Figure 4.1. Hence, the semi-strong interaction of fronts and pulses in (4.1.1) stems from the separation of length scales in the PDEs, *i.e.*, from their singularly perturbed nature. The interaction in the semi-strong regimes is stronger, and hence the observed front interactions are richer, than that in the weak interaction regime, [19, 20, 55, 59]. In the weak regime, the pulses are assumed to be ‘sufficiently far apart’, so that the pulses can be considered as ‘particles’ to leading order. Semi-strong interacting localized structures change shape and the interaction may even cause ‘bifurcations’. On the other hand, semi-strong interactions are weaker than strong interactions, which occur, for example, when fronts collide or when a pulse self-replicates. For the three-component model (4.1.1), numerical simulations suggest that when two fronts enter the strong interaction regime, where $\Gamma_{i+1}(t) - \Gamma_i(t) \ll \varepsilon^{-1}$ for some i , the fronts collide and disappear, see Figures 4.7 and 4.10. It is a future challenge to analyze strong interactions and to apply the RG method to strongly interacting fronts.

This chapter is organized as follows. In Section 4.2, we present the formal derivation of the ODE (4.2.1). The RG method that rigorously justifies the derivation of this ODE is presented in Section 4.3. Then, a detailed analysis of the ODEs for the cases $N = 1, 2, 3, 4$ is presented in Section 4.4. Moreover, we present some results for general odd or even N .

Remark 4.1.1. The fact that the parameters τ and θ are $\mathcal{O}(1)$ is a key assumption in this chapter. For these values of τ and θ , the terms involving c are to leading order absent in the slow fields, see Chapter 2 and 3. This is crucial, since $c = c(t)$ is not even well-defined in the slow fields. It is a fundamental challenge to adapt the methods used in this chapter for problems where the speeds of the fronts do have a leading order influence in the slow fields. Here, this occurs if τ, θ are $\mathcal{O}(\varepsilon^{-2})$ large, see also the previous chapters. In this parameter regime, traveling 1-pulse solutions and breathing 1-pulse solutions exist and bifurcate from stationary 1-pulse solutions. The proof of Section 4.3 breaks down in this regime, since the essential spectrum asymptotes to the origin in the limit $\varepsilon \rightarrow 0$.

4.2 Formal derivation of N -front dynamics

In this section, we formally derive an N -component ODE describing the dynamics of the N different fronts of an N -front solution. *A priori*, the fronts of an N -front solution all travel with different speeds. Therefore, it is not possible to introduce one co-moving frame which travels along with every front. We formally overcome this problem by introducing N co-moving frames, such that every frame travels along with one of the fronts. This way we obtain N different independent ‘fast’ ODEs. To leading order, we then solve each of these ODEs by singular perturbation techniques and obtain N jump conditions (4.2.4). Since the speeds of the fronts have no leading order influence on any of the intermediate slow fields, we can formally ‘glue’ the N different fast solutions together in the slow fields. Formally, we then obtain an N -component ODE (4.2.1) describing the evolution of the N fronts. The key underlying assumption in this construction is that the speeds of the various fronts appear at higher order in the slow fields, see Remark 4.1.1. The perturbation analysis can be summarized as follows:

Assume that all parameters of (4.1.1) are $\mathcal{O}(1)$ with respect to ε and let ε be small enough. Moreover, assume that the speeds of the fronts of an N -front solution $\Phi_N(\xi, t)$ to (4.1.1) are all $\mathcal{O}(\varepsilon)$. Then, to leading order, the i -th front Γ_i of this N -front solution formally evolves as

$$\begin{aligned} \dot{\Gamma}_i(t) = & (-1)^{i+1} \frac{3}{2} \sqrt{2} \varepsilon [\gamma + \alpha (-e^{\varepsilon(\Gamma_1 - \Gamma_i)} + \dots + (-1)^{i-1} e^{\varepsilon(\Gamma_{i-1} - \Gamma_i)} \\ & + (-1)^i e^{\varepsilon(\Gamma_i - \Gamma_{i+1})} + \dots + (-1)^{N-1} e^{\varepsilon(\Gamma_i - \Gamma_N)}) + \beta (-e^{\frac{\varepsilon}{D}(\Gamma_1 - \Gamma_i)} \\ & + \dots + (-1)^{i-1} e^{\frac{\varepsilon}{D}(\Gamma_{i-1} - \Gamma_i)} + (-1)^i e^{\frac{\varepsilon}{D}(\Gamma_i - \Gamma_{i+1})} + \dots \\ & + (-1)^{N-1} e^{\frac{\varepsilon}{D}(\Gamma_i - \Gamma_N)}] \quad \text{for } i = 1 \dots N. \end{aligned} \quad (4.2.1)$$

Here, Γ_i is the ξ -coordinate of the i -th time the U -component crosses zero and $\dot{\Gamma}$ is the time-derivative of Γ .

Note that $\Gamma_i < \Gamma_j$ if $i < j$, and therefore all the exponentials in (4.2.1) have a negative exponent. Moreover, since we use the fast scaling, the distance between two fronts is of $\mathcal{O}(\varepsilon^{-1})$. Thus, the interactions between the fronts are not exponentially small, as in the case of weak interaction. Also observe that the influence of the i -th front on the j -th front is independent of the number of fronts in between.

This formal result is derived as follows. Since the i -th front of an N -front solution is located at Γ_i , and it moves with speed εc_i , we have that

$$\Gamma_i(t) = \Gamma_i(0) + \varepsilon \int_0^t c_i(s) ds \quad \Rightarrow \quad \dot{\Gamma}_i(t) = \varepsilon c_i(t). \quad (4.2.2)$$

Since the various speeds εc_i of the fronts have no leading order influence on the slow equations, the PDE (4.1.1) to leading order reduces to the following ODE

system:

$$\begin{cases} u_\xi &= p, \\ p_\xi &= -u + u^3 + \varepsilon(\alpha v + \beta w + \gamma - c_i p), \\ v_\xi &= \varepsilon q, \\ q_\xi &= \varepsilon(v - u) + \mathcal{O}(\varepsilon^3), \\ w_\xi &= \frac{\varepsilon}{D} r, \\ r_\xi &= \frac{\varepsilon}{D}(w - u) + \mathcal{O}(\varepsilon^3). \end{cases} \quad (4.2.3)$$

In the N fast fields, the regions around the fronts, the solution is governed by the first two ODEs with different speeds εc_i and with different fixed v, w -components, that is, $(v, w) = (v_i, w_i)$. In the fast fields, the U -component to leading order jumps from a locally invariant manifold $\mathcal{M}_\varepsilon^\pm$ to the other $\mathcal{M}_\varepsilon^\mp$, where $\mathcal{M}_\varepsilon^\pm = \{u = \pm 1 - \frac{1}{2}\varepsilon(\alpha v + \beta w + \gamma) + \mathcal{O}(\varepsilon^2), p = \mathcal{O}(\varepsilon^2)\}$. Therefore, the solution has to lie in the intersection of their unstable and stable manifold, *i.e.*, it has to lie in $W^u(\mathcal{M}_\varepsilon^\pm) \cap W^s(\mathcal{M}_\varepsilon^\mp)$. The distance between those two manifolds, which has to be zero to leading order, is measured by a Melnikov integral, see Chapter 2 and [57]. This integral yields N conditions

$$\varepsilon(\alpha v_i + \beta w_i + \gamma) \int_{-\infty}^{\infty} p_0(\xi) d\xi + (-1)^i c_i \int_{-\infty}^{\infty} p_0(\xi)^2 d\xi = \mathcal{O}(\varepsilon\sqrt{\varepsilon}), \quad i = 1, \dots, N,$$

with $p_0(\xi)$ the derivative of the leading order integrable flow, that is, $p_0(\xi)$ is the p -solution of the (u, p) -system of (4.2.3) with $\varepsilon = 0$. In particular, $p_0(\xi) = \frac{1}{2}\sqrt{2}\operatorname{sech}^2(\frac{1}{2}\sqrt{2}\xi)$. Integrating gives N jump conditions

$$\alpha v_i + \beta w_i + \gamma = (-1)^{i+1} \frac{1}{3} \sqrt{2} c_i \quad \text{for } i = 1, \dots, N. \quad (4.2.4)$$

In the $N+1$ slow fields, the regions in between the fronts, the solution is governed by the last four ODEs of (4.2.3) with u fixed at either $+1$ or -1 . To leading order, these ODEs can be solved explicitly

$$\begin{aligned} v(\xi) &= A_j e^{\varepsilon\xi} + B_j e^{-\varepsilon\xi} + (-1)^j, \\ w(\xi) &= C_j e^{\frac{\varepsilon}{D}\xi} + D_j e^{-\frac{\varepsilon}{D}\xi} + (-1)^j, \quad j = 1, \dots, N+1 \end{aligned} \quad (4.2.5)$$

Note that $v(\xi)$ and $w(\xi)$ would not change in leading order if $|\xi| \ll \varepsilon^{-1}$ during the passage of a slow manifold. Since they clearly should change, we assume that $\Delta\Gamma_i = \Gamma_{i+1} - \Gamma_i = \mathcal{O}(\varepsilon^{-1})$, see Remark 4.3.1.

To determine the constants A_j, B_j, C_j, D_j, v_i and w_i as function of the front locations Γ_i , we implement the boundary conditions and match the slow solutions (4.2.5) and their derivatives, in the fast regions. This yields

$$\begin{aligned} v_i &= -e^{\varepsilon(\Gamma_1 - \Gamma_i)} + \dots + (-1)^{i-1} e^{\varepsilon(\Gamma_{i-1} - \Gamma_i)} \\ &\quad + (-1)^i e^{\varepsilon(\Gamma_i - \Gamma_{i+1})} + \dots + (-1)^{N-1} e^{\varepsilon(\Gamma_i - \Gamma_N)}, \\ w_i &= -e^{\frac{\varepsilon}{D}(\Gamma_1 - \Gamma_i)} + \dots + (-1)^{i-1} e^{\frac{\varepsilon}{D}(\Gamma_{i-1} - \Gamma_i)} \\ &\quad + (-1)^i e^{\frac{\varepsilon}{D}(\Gamma_i - \Gamma_{i+1})} + \dots + (-1)^{N-1} e^{\frac{\varepsilon}{D}(\Gamma_i - \Gamma_N)}. \end{aligned} \quad (4.2.6)$$

Combining (4.2.6) with the jump conditions (4.2.4) and using (4.2.2) gives (4.2.1).

Lemma 4.2.1. *Assume that all conditions of the formal construction are met. Moreover, assume that $N = 1$, that is, we look at 1-front solutions. Then these 1-front solutions travel with speed*

$$\dot{\Gamma}(t) = \varepsilon c = \frac{3}{2}\sqrt{2}\varepsilon\gamma. \quad (4.2.7)$$

Moreover, these 1-front solutions are stable.

Proof. Equation (4.2.7) is a direct consequence of (4.2.1) with $N = 1$. However, since we only have to introduce one co-moving frame, this result can also be made rigorous by the method used in Chapter 2. Likewise, the stability of these 1-front solutions directly follows from the pulse-stability analysis in Chapter 3: the 1-front solutions can only have one small eigenvalue, the translational eigenvalue at $\lambda = 0$. \square

4.3 A renormalization group method

We reformulate the results of the previous section in a rigorous manner, see Theorem 4.3.2 in Section 4.3.2, and use the RG method developed in [16, 55] to rigorously prove this theorem. In order to focus on the essence of the method, and avoid technical details, we only consider the case $N = 2$ of (4.2.1) in full detail. The proof of the general case runs along the same lines modulo certain technicalities, such as the uniform spectral compatibility, see (4.3.7). In order to formulate the theorem, we first need to introduce a suitable norm.

4.3.1 The χ -norm

We define the χ -norm by

$$\|(U, V, W)\|_{\chi} := \|U\|_{\chi} + \|V\|_{\chi} + \|W\|_{\chi}, \text{ with } \|\cdot\|_{\chi} := \|\chi \cdot\|_{L^1} + \|\partial_{\xi} \cdot\|_{L^1}, \quad (4.3.1)$$

where $\chi(\xi)$ is a positive function with mass 1, that is, $\bar{\chi} = \int_{-\infty}^{\infty} \chi(\xi) d\xi = 1$, and it is exponentially decaying with an $\mathcal{O}(1)$ parameter with respect to ε (for example, $\chi(\xi) = \frac{1}{2}e^{-|\xi|}$). It is straightforward to check that the χ -norm is indeed a norm; and, in essence, it is a weighted $W^{1,1}$ -norm. We also define the normed space X

$$X := \{(U, V, W) \mid \|(U, V, W)\|_{\chi} < \infty\}. \quad (4.3.2)$$

The reason for using this particular norm, instead of a more usual one such as the scaled variant of the H^1 -norm used in [16], is that this χ -norm is well behaved with respect to differences in asymptotic behavior at spatial infinity. The need for this is explained as follows. An N -front solution to (4.1.1) only asymptotes to leading order to $(-1, -1, -1)$ at $\xi = -\infty$, see Chapter 2. However, the skeleton

solution which we use to approximate an N -front solution (see (4.3.6)), asymptotes exactly to $(-1, -1, -1)$ at $-\infty$. Therefore, although the error is only of $\mathcal{O}(\varepsilon)$ -size at spatial infinity, the H^1 -norm of this error is unbounded. Since the tails of the N -front solution and the skeleton solution are exponentially flat, the seminorm $\|\partial_\xi \cdot\|_{L^1}$ (all constants have norm zero) does not yield an unbounded error. To make this seminorm $\|\partial_\xi \cdot\|_{L^1}$ into a norm, we add the component $\|\chi \cdot\|_{L^1}$, which, by the third assumption on χ , also does not penalize errors at infinity. The first two properties we impose on the weight χ , positivity and mass one, make sure that the χ -norm uniformly dominates the L^∞ -norm.

Lemma 4.3.1. *Let u, v be integrable functions such that $\|u\|_\chi, \|v\|_\chi < \infty$. Then, the χ -norm has the following three properties:*

$$\|u\|_{L^\infty} \leq \|u\|_\chi, \quad (4.3.3)$$

$$\|G * u\|_\chi \leq 2\|G\|_{L^1}\|u\|_\chi, \quad (4.3.4)$$

$$\|uv\|_\chi \leq 2\|u\|_\chi\|v\|_\chi. \quad (4.3.5)$$

where G in (4.3.4) is an L^1 -function (in this chapter typically a Green's function), and $*$ the usual convolution.

Proof. The first property, (4.3.3), is established via the following inequalities:

$$u(x) - u(y) = \int_y^x u_\xi d\xi \implies |u(x)| \leq \int_{-\infty}^\infty |u_\xi| d\xi + |u(y)|.$$

Multiplying by $\chi(y)$, integrating over all y in $(-\infty, \infty)$, and recalling that χ is positive and has mass one, we find that

$$|u(x)| \leq \|u_\xi\|_{L^1} + \int_{-\infty}^\infty |\chi(y)u(y)| dy \implies \|u\|_{L^\infty} \leq \|u\|_\chi.$$

The proofs of the second and third properties, (4.3.4) and (4.3.5), heavily rely on the first property. To prove the second property (4.3.4), we use Hölder's inequality, the fact that $(G * u)_\xi = G * u_\xi$ [36], the inequality $\|G * u\|_{L^p} \leq \|G\|_{L^1}\|u\|_{L^p}$ for $1 \leq p \leq \infty$ [36], and finally the above result (4.3.3),

$$\begin{aligned} \|G * u\|_\chi &= \|\chi(G * u)\|_{L^1} + \|(G * u)_\xi\|_{L^1} \\ &\leq \|\chi\|_{L^1}\|G * u\|_{L^\infty} + \|G * u_\xi\|_{L^1} \\ &\leq \|G\|_{L^1}\|u\|_{L^\infty} + \|G\|_{L^1}\|u_\xi\|_{L^1} \\ &\leq 2\|G\|_{L^1}\|u\|_\chi. \end{aligned}$$

To prove the third property (4.3.5) observe that

$$\begin{aligned} \|uv\|_\chi &\leq \|u\chi v\|_{L^1} + \|uv_\xi\|_{L^1} + \|v\chi u\|_{L^1} + \|vu_\xi\|_{L^1} \\ &\leq \|u\|_{L^\infty}\|v\|_\chi + \|v\|_{L^\infty}\|u\|_\chi \\ &\leq 2\|u\|_\chi\|v\|_\chi. \end{aligned}$$

This completes the proof. \square

4.3.2 The main result

In order to give an accurate formulation of the main result of this chapter, *i.e.*, that the dynamics of an N -front solution of (4.1.1) is indeed determined by the formally derived equations (4.2.1), we first need to introduce some more notation. We define the stationary skeleton N -front solution $\Phi_\Gamma(\xi)$ by

$$\Phi_\Gamma(\xi) = \begin{pmatrix} \Phi_1(\xi) \\ \Phi_2(\xi) \\ \Phi_3(\xi) \end{pmatrix} = \begin{pmatrix} U_0(\xi; \Gamma) \\ G_V * U_0(\xi; \Gamma) \\ G_W * U_0(\xi; \Gamma) \end{pmatrix}, \quad (4.3.6)$$

in which $U_0(\xi, \Gamma)$ is the leading order approximation of the U -component of a stationary N -front solution of (4.1.1),

$$U_0(\xi, \Gamma) = -1 + \sum_{i=1}^N (-1)^{i-1} \tanh\left(\frac{1}{2}\sqrt{2}(\xi - \Gamma_i)\right). \quad (4.3.7)$$

Here, Γ_i determines the location of the i -th front, more precisely, $U_0(\xi)$ has its i -th sign change at $\xi = \Gamma_i$. By definition, we have that $\Gamma_i < \Gamma_{i+1}$, and since the interaction of the fronts is semi-strong, we may assume that $\Delta\Gamma_i = \Gamma_{i+1} - \Gamma_i = \mathcal{O}(\varepsilon^{-1})$, see Remark 4.3.1. The functions $G_{V,W}(\xi)$ are the Green's functions associated to the stationary V and W -equations of (4.1.1) with $U(\xi, t) = U_0(\xi)$. For example, $G_V * U_0$ is the (exact!) solution of

$$0 = \frac{1}{\varepsilon^2} V_{\xi\xi} + U_0 - V. \quad (4.3.8)$$

Straightforward computations yield that

$$G_V = -\frac{1}{2}\varepsilon e^{-\varepsilon|\xi|}, \quad \text{and} \quad G_W = -\frac{1}{2}\frac{\varepsilon}{D} e^{-\frac{\varepsilon}{D}|\xi|}, \quad (4.3.9)$$

which are both L^1 -functions with norm 1.

The graph of the functions $\Phi_\Gamma(\xi)$ forms an N -dimensional manifold $\mathcal{M}_{N,0}$. Note that $\mathcal{M}_{N,0}$ has a boundary $\partial\mathcal{M}_{N,0}$ consisting of $N-1$ co-dimension 1 hyperplanes at which $\Gamma_i = \Gamma_{i+1}$ ($i = 1, \dots, N-1$). The evolution within $\mathcal{M}_{N,0}$ is (to leading order) determined by (4.2.1). The dynamical skeleton N -front solution $\Phi_{\Gamma(t)}(\xi)$ is defined to be an N -front solution (4.3.6) whose fronts $\Gamma_i(t)$ evolve according to the ODE (4.2.1).

This ODE has been obtained under the assumptions that $\Gamma_i < \Gamma_{i+1}$ and $\Delta\Gamma_i = \mathcal{O}(\varepsilon^{-1})$ (Remark 4.3.1). However, these properties are not necessarily conserved by the flow generated by (4.2.1): two components $\Gamma_i(t)$ and $\Gamma_{i+1}(t)$ of a solution of (4.2.1) may in principle cross and thus change order. See Section 4.4, in which the dynamics generated by (4.2.1) is studied. In other words, the evolution of

(4.2.1) may drive a solution towards the boundary $\partial\mathcal{M}_{N,0}$. Our methods – and in fact all methods considered in the literature – break down in the strong interaction regime, *i.e.*, for solutions of the PDE (4.1.1) that have two fronts $\Gamma_i(t)$ and $\Gamma_{i+1}(t)$ that become too close. In fact, we will see in the simulations presented in Section 4.4 that these fronts will in general annihilate each other in the PDE, while their approximating counterparts will survive the collision and move through each other in the ODE simulations – something that is impossible in the PDE. Therefore, we define $t_m = t_m(\Gamma(0))$ of a solution $\Gamma(t)$ of (4.2.1) as the maximal time for which $\min_i \Delta\Gamma_i(t) > \varepsilon^{-1/2}$ for all time $0 \leq t < t_m$. Thus, $\Gamma(t_m)$ is $\mathcal{O}(\varepsilon^{-1/2})$ close to $\partial\mathcal{M}_{N,0}$ and $t_m = \mathcal{O}(\varepsilon^{-2})$ since $\Delta\Gamma_i(0) = \mathcal{O}(\varepsilon^{-1})$ by definition and $\dot{\Gamma}_i(t) = \mathcal{O}(\varepsilon)$ for all i . Note that our methods in principle allow us to extend our results into regions in which $\Delta\Gamma_i(t) = \mathcal{O}(\varepsilon^{-\sigma})$ for any $\sigma \in (0, 1)$, see Remark 4.3.1. In that sense the choice for the critical distance, $\sigma = \frac{1}{2}$, is somewhat arbitrary. However, it does provide us with a unique definition of $t_m(\Gamma(0))$, and none of the other possible choices for σ appear to give more insight than the present one. Note also that the fronts do not necessarily collide. In fact, $\Gamma(t)$ remains bounded away from $\partial\mathcal{M}_{N,0}$ for many choices of $\Gamma(0)$. In other words, $t_m(\Gamma(0)) = \infty$ for large sets of initial conditions – see Section 4.4.

We can now formulate the main result.

Theorem 4.3.2. *Let $\varepsilon > 0$ be sufficiently small and assume that all parameters of (4.1.1) are $\mathcal{O}(1)$ with respect to ε . Let $\Phi_N(\xi, t) = (U_N(\xi, t), V_N(\xi, t), W_N(\xi, t))$ be a solution of (4.1.1) which is $\mathcal{O}(\varepsilon)$ close to the N -front manifold $\mathcal{M}_{N,0}$ at $t = 0$, *i.e.*, there is a $\Gamma(0)$ such that $\Delta\Gamma_i(0) = \mathcal{O}(\varepsilon^{-1})$ and*

$$\|\Phi_N(\cdot, 0) - \Phi_{\Gamma(0)}\|_X < \tilde{C}\varepsilon,$$

for some $\tilde{C} > 0$. Then, $\Phi_N(\xi, t)$ remains $\mathcal{O}(\varepsilon)$ close to $\mathcal{M}_{N,0}$ for $0 \leq t < t_m$ and its evolution is governed by (4.2.1), the leading order dynamics of the fronts of $\Phi_{\Gamma(t)}(\xi)$. In particular, $\Phi_N(\xi, t)$ can be decomposed into

$$\Phi_N(\xi, t) = \Phi_{\Gamma(t)}(\xi) + Z(\xi, t) \quad (4.3.10)$$

with

$$\|Z(\cdot, t)\|_X \leq C\varepsilon \quad \text{for all } 0 \leq t < t_m. \quad (4.3.11)$$

This theorem establishes the validity of the N -front dynamics formally obtained in Section 4.2.

By using an improved skeleton solution $\tilde{\Phi}_\Gamma(\xi)$ and the same RG procedure as in this section, it is possible to improve on this result. For instance, we can prove the existence of an attracting manifold $\mathcal{M}_{N,1}$ with the property that a solution $\tilde{\Phi}_N(\xi, t)$ with initial conditions $\tilde{\Phi}_N(\xi, 0)$ starting only $\mathcal{O}(\sqrt{\varepsilon})$ close to $\mathcal{M}_{N,1}$, will

eventually be $\mathcal{O}(\varepsilon^2)$ close to it. This manifold $\mathcal{M}_{N,1}$ is an $\mathcal{O}(\varepsilon)$ correction to the manifold $\mathcal{M}_{N,0}$. To determine the improved skeleton solution $\tilde{\Phi}_\Gamma(\xi)$ we need the results of this section (with the normal skeleton solution $\Phi_\Gamma(\xi)$ (4.3.6)). Therefore, this section can be seen as a first step in an iteration procedure to obtain an attracting N -dimensional set $\mathcal{M}_{N,\varepsilon}$ with boundary $\partial\mathcal{M}_{N,\varepsilon}$ in the solution space associated to (4.1.1). Away from $\partial\mathcal{M}_{N,\varepsilon}$ the dynamics on $\mathcal{M}_{N,\varepsilon}$ is to leading order governed by (4.2.1). Note that this analysis is somewhat subtle, for instance since the speed of the fronts influences the corrections to the shape of the front solutions in the higher order approximations (and *vice versa*). Nevertheless, this iteration procedure can be performed by embedding the geometrical approach of [15, 16] into the higher order RG method analysis – see [16], where the speed of the interacting pulses determines the amplitude of the pulses at leading order. We refrain from going into the details here. It should be observed that an iterated refinement of the theorem does not yet necessarily establish whether or not $\mathcal{M}_{N,\varepsilon}$ is actually a manifold. See also [2, 72].

We emphasize that the dynamics of the skeleton solution $\Phi_\Gamma(\xi)$ is only to leading order determined by (4.2.1). Because of accumulation of error, the predicted front position could diverge by an $\mathcal{O}(1)$ for nonstationary solutions $\Phi_N(\xi, t)$ after $\mathcal{O}(\varepsilon^{-1})$ time. However, at all points on the manifold the front dynamics are given to leading order by (4.2.1), particularly for the configuration of steady states and traveling waves.

The remainder of this section is devoted to the proof of Theorem 4.3.2, using the RG method, as developed in [16, 55]. As was already stated, we only consider the case $N = 2$ in full detail. For clarity, we note that (4.2.1) reduces to

$$\begin{aligned} \dot{\Gamma}_1 &= \frac{3}{2}\sqrt{2\varepsilon} \left(\gamma - \alpha e^{-\varepsilon(\Gamma_2 - \Gamma_1)} - \beta e^{-\frac{\varepsilon}{B}(\Gamma_2 - \Gamma_1)} \right), \\ \dot{\Gamma}_2 &= -\frac{3}{2}\sqrt{2\varepsilon} \left(\gamma - \alpha e^{-\varepsilon(\Gamma_2 - \Gamma_1)} - \beta e^{-\frac{\varepsilon}{B}(\Gamma_2 - \Gamma_1)} \right), \end{aligned} \quad (4.3.12)$$

in this case.

Substituting the decomposition (4.3.10) into the PDE (4.1.1), we find

$$Z_t + \frac{\partial\Phi_\Gamma}{\partial\Gamma}\dot{\Gamma} = R(\Phi_\Gamma) + L_\Gamma Z + N(Z). \quad (4.3.13)$$

The residual $R(\Phi_\Gamma)$ is defined as the error made by the skeleton solution (4.3.6) and is determined by plugging (4.3.6) into the right hand side of (4.1.1). Since, by construction, $\Phi_{2,3}(\xi)$ solve the second and third components of the right hand side of (4.1.1) exactly for given $\Phi_1(\xi) = U_0(\xi, \Gamma)$ (4.3.8), the second and third components of the residual are zero. However, the first component $R_1 \neq 0$:

$$R(\Phi_\Gamma) = \begin{pmatrix} (U_0)_{\xi\xi} + U_0 - (U_0)^3 - \varepsilon(\alpha(G_V * U_0) + \beta(G_W * U_0) + \gamma) \\ 0 \\ 0 \end{pmatrix}. \quad (4.3.14)$$

The linear operator reads

$$L_\Gamma = \begin{pmatrix} \partial_\xi^2 + 1 - 3\Phi_1^2 & -\varepsilon\alpha & -\varepsilon\beta \\ \frac{1}{\tau} & \frac{1}{\tau} \left(\frac{1}{\varepsilon^2} \partial_\xi^2 - 1 \right) & 0 \\ \frac{1}{\theta} & 0 & \frac{1}{\theta} \left(\frac{D^2}{\varepsilon^2} \partial_\xi^2 - 1 \right) \end{pmatrix}, \quad (4.3.15)$$

Finally, the nonlinear term is given by

$$N(Z) = \left(-3\Phi_1 Z_1^2 - Z_1^3, \quad 0, \quad 0 \right)^t. \quad (4.3.16)$$

The proof of the theorem now consists of several steps, which are all essential to the RG method used [16, 31, 47, 55].

- Step 1: First, we bound the nonlinear growth term $N(Z)$ (4.3.16), see Lemma 4.3.4, and the residual $R(\Phi_{\Gamma(t)})$ (4.3.14), see Lemma 4.3.5, that occur in the PDE (4.3.13). See Section 4.3.3.
- Step 2: In Section 4.3.4, we analyze the linear operator L_Γ in Lemmas 4.3.6 – 4.3.9. We determine that L_Γ has two small eigenvalues and that the rest of its spectrum is well into the left-half complex plane. Moreover, we obtain a bound on the χ -norm of functions which do not have a contribution in the direction of the eigenvectors Ψ_\pm belonging to the small eigenvalues λ_\pm associated to L_Γ .
- Step 3: Next, we start the RG method. We freeze a basepoint $\Gamma^0 := (\Gamma_1^0, \Gamma_2^0)$, that is, we fix the front location, and we rewrite (4.3.13) once more, see Section 4.3.5. Then, we project onto the eigenspace of the small eigenvalues λ_\pm , to obtain the motion of the fronts $\Gamma_{1,2}$ (4.3.45), see Section 4.3.6. In Section 4.3.7, we project onto the eigenspace X_{Γ^0} , the space perpendicular to the eigenspace of the small eigenvalues λ_\pm . The analysis of these projected equations gives a bound on the size of the remainder $Z(\xi, t)$ in some time interval $[0, t^*]$, see Lemma 4.3.11.
- Step 4: At time $t = t^*$, we renormalize by choosing a new basepoint $\Gamma^1 := (\Gamma_1^1, \Gamma_2^1)$, and we show that the χ -norm of the remainder $Z(\xi, t)$ has the same asymptotic magnitude as before renormalization, see Lemma 4.3.15. Moreover, we show that the new basepoint Γ^1 is near the location of the fronts from the previous step at time t^* , $\Gamma(t^*)$. A repetition of Step 3 and the above observation then bounds the remainder $Z(\xi, t)$ for all time (4.3.11). See Section 4.3.8.
- Step 5: With this estimate on the remainder $Z(\xi, t)$, we further investigate the evolution of the two fronts $\Gamma_{1,2}$ (4.3.45), see Section 4.3.9. This validates (4.3.12) and completes the proof.

Remark 4.3.1. The results established in this chapter are valid under assumption that the fronts Γ_{i+1} and Γ_i do not interact strongly. To leading order, this translates into $\Delta\Gamma_i = \mathcal{O}(\varepsilon^{-1})$, the assumption that has been imposed throughout this chapter. However, the interaction between two neighboring fronts remains semi-strong as long as $\Delta\Gamma_i = \mathcal{O}(\varepsilon^{-\sigma})$, for some $\sigma > 0$. All results remain valid under this somewhat weaker assumption. The proofs for the more general results may become slightly more technical, though, since it may be necessary to incorporate (straightforward) higher order calculations. Therefore, we refrain from going into the details here.

Since the notation $\mathcal{O}(\varepsilon^{-\sigma})$, $\sigma > 0$, plays a crucial role in this chapter, we recall its definition. A quantity $Q(\varepsilon)$ is of $\mathcal{O}(\varepsilon^{-\sigma})$ for some $\sigma > 0$, if there exists a $C > 0$, independent of ε , and an $\varepsilon_0 > 0$, such that $\varepsilon^\sigma |Q(\varepsilon)| > C$ for all $0 < \varepsilon < \varepsilon_0$.

4.3.3 Nonlinearity and residual

In the section, we bound the norms of the nonlinear term N and the residual R , but before we do so we compute bounds on Φ_1 , the first component of Φ_Γ (4.3.6), in several norms.

Lemma 4.3.3. $\|\Phi_1\|_\chi = \mathcal{O}(1)$.

Proof. To compute the L^1 -norm of $(\Phi_1)_\xi$, observe that

$$(\Phi_1)_\xi = \frac{1}{2}\sqrt{2} \left(\operatorname{sech}^2 \left(\frac{1}{2}\sqrt{2}(\xi - \Gamma_1) \right) - \operatorname{sech}^2 \left(\frac{1}{2}\sqrt{2}(\xi - \Gamma_2) \right) \right).$$

Since $|\Gamma_1 - \Gamma_2| \geq C\varepsilon^{-\sigma}$ for some $\sigma > 0$, we obtain that

$$\|(\Phi_1)_\xi\|_{L^1} = \left\| \sqrt{2}\operatorname{sech}^2 \left(\frac{1}{2}\sqrt{2}\xi \right) \right\|_{L^1} + \text{exp. small} = \mathcal{O}(1).$$

By the assumptions on $\chi(\xi)$, we observe that also $\|\chi\Phi_1\|_{L^1} = \mathcal{O}(1)$. \square

Now, we establish the following bound on the χ -norm of $N(Z)$:

Lemma 4.3.4. $\|N(Z)\|_\chi \leq C \{ \|Z_1\|_\chi^2 + \|Z_1\|_\chi^3 \}$, where C is an $\mathcal{O}(1)$ -constant.

Proof. This follows immediately from (4.3.16), (4.3.5), and Lemma 4.3.3. \square

Next, we bound the residual R .

Lemma 4.3.5. $\|R\|_{L^\infty} = \mathcal{O}(\varepsilon)$, and $\|R\|_\chi = \mathcal{O}(\varepsilon)$.

Proof. We only need to prove the second bound on R , since the first bound then follows from (4.3.3). Moreover, since $R_{2,3} = 0$, we only need to consider the

χ -norm of R_1 . A short calculation shows that

$$(U_0)_{\xi\xi} + U_0 - (U_0)^3 = \frac{3}{2} \left(e^{\sqrt{2}(\Gamma_1 - \Gamma_2)} - 1 \right) \operatorname{sech}^2\left(\frac{1}{2}\sqrt{2}(\xi - \Gamma_1)\right) \operatorname{sech}^2\left(\frac{1}{2}\sqrt{2}(\xi - \Gamma_2)\right),$$

which is exponentially small. Therefore, the leading order behavior of R_1 is given by

$$R_1(\Phi_\Gamma) = -\varepsilon (\alpha(G_V * U_0) + \beta(G_W * U_0) + \gamma). \quad (4.3.17)$$

Now, by (4.3.4), the fact that $\|G_{V,W}\|_{L^1} = 1$, and Lemma 4.3.3, we obtain the following bound for the leading order terms in R_1 :

$$\begin{aligned} \|R_1\|_\chi &= \varepsilon \|\alpha(G_V * U_0) + \beta(G_W * U_0) + \gamma\|_\chi \\ &\leq \varepsilon (2|\alpha| \|G_V\|_{L^1} \|U_0\|_\chi + 2|\beta| \|G_W\|_{L^1} \|U_0\|_\chi + |\gamma|) \\ &\leq \varepsilon (2(|\alpha| + |\beta|) \|U_0\|_\chi + |\gamma|) = \mathcal{O}(\varepsilon). \end{aligned}$$

□

4.3.4 Resolvent

In this section, we analyze the linear operator L_Γ (4.3.15), with Γ fixed. We start by computing its spectrum $\sigma(L_\Gamma)$. The spectrum $\sigma(L_\Gamma)$ can be split in essential spectrum $\sigma_{\text{ess}}(L_\Gamma)$ and point spectrum $\sigma_{\text{p}}(L_\Gamma)$. The following lemma gives, to leading order, the location of both parts:

Lemma 4.3.6. *The essential spectrum $\sigma_{\text{ess}}(L_\Gamma)$ of the linear operator is contained in the left half plane and bounded away from zero in an $\mathcal{O}(1)$ -fashion. More precisely, to leading order,*

$$\Re(\sigma_{\text{ess}}(L_\Gamma)) \leq \max \left\{ -\frac{1}{\tau}, -\frac{1}{\theta}, -2 \right\}, \quad (4.3.18)$$

where the inequality is understood pointwise. The point spectrum $\sigma_{\text{p}}(L_\Gamma)$ of the operator has, besides two negative $\mathcal{O}(1)$ -eigenvalues in the vicinity of $-\frac{3}{2}$ (which may be contained in the essential spectrum), two small eigenvalues λ_\pm . The eigenvalue λ_- is to leading order given by $\lambda_- = -3\sqrt{2}\varepsilon^2(\alpha A^2 + \frac{\beta}{D}A^{\frac{2}{D}})$, where A solves $\alpha A^2 + \beta A^{\frac{2}{D}} = \gamma$. The eigenvalue $\lambda_+ = \mathcal{O}(\varepsilon^\mu)$, with $\mu > 2$. The associated ‘small’ eigenvectors Ψ_\pm are

$$\Psi_\pm = \begin{pmatrix} \psi_1 \mp \psi_2 \\ 0 \\ 0 \end{pmatrix} + \varepsilon \begin{pmatrix} \mathcal{R}_1 \\ \mathcal{R}_2 \\ \mathcal{R}_3 \end{pmatrix}, \quad (4.3.19)$$

with

$$\psi_{1,2}(\xi; \Gamma_{1,2}) = \left| \frac{\partial U_0}{\partial \Gamma_{1,2}} \right| = \frac{1}{2} \sqrt{2} \operatorname{sech}^2\left(\frac{1}{2}\sqrt{2}(\xi - \Gamma_{1,2})\right), \quad (4.3.20)$$

and where a straightforward computation yields that $\|\mathcal{R}_i\|_{L^\infty} = \mathcal{O}(1)$, $\|\mathcal{R}_1\|_{L^1}$, $\|\mathcal{R}_1\|_{L^2} = \mathcal{O}(1)$, and $\|\mathcal{R}_{2,3}\|_{L^1}$, $\|\mathcal{R}_{2,3}\|_{L^2}^2 = \mathcal{O}(\varepsilon^{-1})$.

Proof. The operator L_Γ is, to leading order, the same as the linear operator associated to a stationary 2-front solution as studied in Section 3.4. Hence, its spectrum and its eigenfunctions are to leading order the same. Therefore, only the statements about the error terms $\mathcal{R}_i(\xi)$ do not follow immediately from the previous chapter. Nevertheless, these estimates follow also directly from the structure of the linear operator L_Γ and its eigenfunctions Ψ_\pm .

Clearly, all the \mathcal{R}_i 's must be bounded and integrable (since Ψ_\pm is an eigenfunction). The structure of \mathcal{R}_1 is determined by L_1 , the operator at the (1,1) entry of L_Γ . Thus \mathcal{R}_1 must decay exponentially with a $\mathcal{O}(1)$ rate, which implies that $\|\mathcal{R}_1\|_{L^{\infty,1,2}} = \mathcal{O}(1)$.

Since $\mathcal{R}_{2,3}$ are determined by $L_{2,3}$, the second and third diagonal entries of L_Γ , respectively, they will decay slowly with an exponential rate of $\mathcal{O}(\varepsilon)$. Therefore, both $\|\mathcal{R}_{2,3}\|_{L^1}$ and $\|\mathcal{R}_{2,3}\|_{L^2}^2$ are $\mathcal{O}(\varepsilon^{-1})$, while $\|\mathcal{R}_{2,3}\|_{L^\infty} = \mathcal{O}(1)$. \square

Note that $\psi_{1,2}(\xi)$ are strongly localized functions around $\xi = \Gamma_{1,2}$. Moreover, $\|\psi_{1,2}\|_{L^1} = 2$, see Lemma 4.3.3, and $\|\psi_{1,2}\|_{L^2}^2 = \frac{2}{3}\sqrt{2}$. Also observe that in the previous chapter, $\mu = \infty$, which corresponds to the translation invariant eigenvalue $\lambda^+ \equiv 0$.

Lemma 4.3.7. *The adjoint operator L_Γ^\dagger of L_Γ has the same two small eigenvalues λ_\pm as L_Γ . Moreover, the small adjoint eigenvectors Ψ_\pm^\dagger associated to these small eigenvalues λ_\pm are to leading order the same as the small eigenvectors Ψ_\pm (4.3.19). Although the correction terms to the small adjoint eigenvectors, \mathcal{R}_i^\dagger , may differ from (4.3.19), their norms are of the same order.*

Proof. The adjoint operator of L_Γ is given by $L_\Gamma^\dagger = L_\Gamma^t$, so that L_Γ^\dagger has the same spectrum as L_Γ . The associated eigenfunctions can be computed by the variation of constants formula, combined with the observation that the eigenvalues λ_\pm are small. \square

With these small (adjoint) eigenvectors at hand we split the normed space X (4.3.2) into the eigenspace X_Γ^C and its spectral complement X_Γ , where the eigenspace X_Γ^C is spanned by the two small eigenvectors Ψ_\pm (4.3.19). To project on these two spaces, we introduce the spectral projection π_Γ , which, in terms of the small (adjoint) eigenfunctions Ψ_\pm , Ψ_\pm^\dagger , is given by

$$\pi_\Gamma \Phi = \frac{(\Phi, \Psi_-^\dagger)}{(\Psi_-, \Psi_-^\dagger)} \Psi_- + \frac{(\Phi, \Psi_+^\dagger)}{(\Psi_+, \Psi_+^\dagger)} \Psi_+, \quad (4.3.21)$$

where (\cdot, \cdot) denotes the standard L^2 -inner product. Note that we have, by Lemmas 4.3.6 and 4.3.7,

$$\begin{aligned} (\Psi_{\pm}, \Psi_{\pm}^{\dagger}) &= \left(\begin{pmatrix} \psi_1 \mp \psi_2 \\ 0 \\ 0 \end{pmatrix} + \varepsilon \begin{pmatrix} \mathcal{R}_1 \\ \mathcal{R}_2 \\ \mathcal{R}_3 \end{pmatrix}, \begin{pmatrix} \psi_1 \mp \psi_2 \\ 0 \\ 0 \end{pmatrix} + \varepsilon \begin{pmatrix} \mathcal{R}_1^{\dagger} \\ \mathcal{R}_2^{\dagger} \\ \mathcal{R}_3^{\dagger} \end{pmatrix} \right) \\ &= (\psi_1 \mp \psi_2, \psi_1 \mp \psi_2) + \varepsilon (\psi_1 \mp \psi_2, \mathcal{R}_1^{\dagger}) + \varepsilon (\mathcal{R}_1, \psi_1 \mp \psi_2) \\ &\quad + \varepsilon^2 \sum_{i=1}^3 (\mathcal{R}_i, \mathcal{R}_i^{\dagger}) \\ &= (\psi_1 \mp \psi_2, \psi_1 \mp \psi_2) + \mathcal{O}(\varepsilon). \end{aligned}$$

The complementary projection is defined by $\tilde{\pi}_{\Gamma} = I - \pi_{\Gamma}$. The spaces X_{Γ} and X_{Γ}^C are thus determined by

$$X_{\Gamma} = \{\Phi \in X \mid \pi_{\Gamma}\Phi = 0\} \quad \text{and} \quad X_{\Gamma}^C = \{\Phi \in X \mid \tilde{\pi}_{\Gamma}\Phi = 0\}. \quad (4.3.22)$$

Since L_{Γ} is an analytic operator we can generate its semigroup by the Laplace transform of the resolvent. We define the contour \mathcal{C}

$$\mathcal{C}(t) := \{t - i \mid t \in (-\infty, -\nu)\} \cup \{-\nu + \frac{t}{\nu}i \mid t \in (-\nu, \nu)\} \cup \{-t + i \mid t \in (\nu, \infty)\}, \quad (4.3.23)$$

with $\nu := \frac{1}{2} \min\{\tau^{-1}, \theta^{-1}, \frac{3}{2}\}$. The contour \mathcal{C} splits the complex plane into two pieces, one containing the small eigenvalues λ_{\pm} , while the other piece contains the rest of the spectrum of L_{Γ} and is bounded away from the origin in an $\mathcal{O}(1)$ -fashion. Moreover, the spectrum $\sigma(L_{\Gamma})$ is an $\mathcal{O}(1)$ distance away from contour \mathcal{C} (Lemma 4.3.6 and Chapter 3). See Figure 4.3. Thus, we generate the semigroup S associated to L_{Γ} restricted to the space X_{Γ} (4.3.22) by the contour integral

$$S(t)F = \frac{1}{2\pi i} \int_{\mathcal{C}} e^{\lambda t} (\lambda - L_{\Gamma})^{-1} F d\lambda, \quad (4.3.24)$$

where we assume that $F \in X_{\Gamma}$.

Lemma 4.3.8. *Assume that $F \in X_{\Gamma}$, then $\Phi = S(t)F$ satisfies*

$$\|\Phi\|_{\mathcal{X}} \leq C e^{-\nu t} \|F\|_{\mathcal{X}}, \quad (4.3.25)$$

To prove this semigroup estimate, we first need to prove an intermediate lemma on the resolvent:

Lemma 4.3.9. *There exists a constant $C > 0$ such that for all λ an $\mathcal{O}(1)$ distance from $\sigma(L_{\Gamma})$, and for all $F \in X_{\Gamma}$ (4.3.22), the solutions G to the inhomogeneous problem $(L_{\Gamma} - \lambda)G = F$ satisfy $\|G\|_{\mathcal{X}} \leq C\|F\|_{\mathcal{X}}$.*

Proof. First, we observe by (4.3.4) and (4.3.9) that the solution \tilde{g}_i to the inhomogeneous problem $(L_i - \lambda)\tilde{g}_i = \tilde{f}_i$, where L_i is the operator in the i -th element of the diagonal of (4.3.15), obeys

$$\|\tilde{g}_i\|_{\mathcal{X}} \leq C\|\tilde{f}_i\|_{\mathcal{X}}, \quad (4.3.26)$$

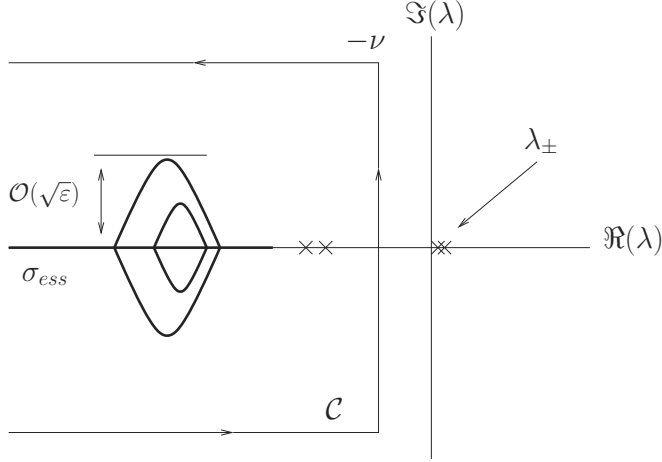


Figure 4.3: The contour \mathcal{C} splits the complex plane into two pieces, one containing the small eigenvalues λ_{\pm} , while the other piece contains the rest of the spectrum of L_{Γ} . Moreover, the spectrum $\sigma(L_{\Gamma})$ is an $\mathcal{O}(1)$ distance away from contour \mathcal{C} . See Section 3.3.2 for more details on the structure of σ_{ess} .

as long as λ is at an $\mathcal{O}(1)$ distance from the spectrum $\sigma(L_i)$ of L_i . Note that this is automatically satisfied for λ which are $\mathcal{O}(1)$ distance away from $\sigma(L_{\Gamma})$.

Next, we write $G = (g_1, g_2, g_3)^t$ and $F = (f_1, f_2, f_3)^t$. Then,

$$g_2 = (L_2 - \lambda)^{-1} \left(f_2 - \frac{g_1}{\tau} \right), \quad g_3 = (L_3 - \lambda)^{-1} \left(f_3 - \frac{g_1}{\theta} \right).$$

By the above result (4.3.26), we know

$$\|g_{2,3}\|_{\mathcal{X}} \leq C (\|f_{2,3}\|_{\mathcal{X}} + \|g_1\|_{\mathcal{X}}). \tag{4.3.27}$$

Next, we define

$$h(\xi) := f_1 + \varepsilon\alpha(L_2 - \lambda)^{-1}f_2 + \varepsilon\beta(L_3 - \lambda)^{-1}f_3.$$

So that g_1 is implicitly determined by

$$g_1 = (L_1 - \lambda)^{-1} \left(h - \frac{\varepsilon\alpha}{\tau}(L_2 - \lambda)^{-1}g_1 - \frac{\varepsilon\beta}{\theta}(L_3 - \lambda)^{-1}g_1 \right).$$

Hence, solving for g_1

$$g_1 = \left(I + \frac{\varepsilon\alpha}{\tau}(L_1 - \lambda)^{-1}(L_2 - \lambda)^{-1} + \frac{\varepsilon\beta}{\theta}(L_1 - \lambda)^{-1}(L_3 - \lambda)^{-1} \right)^{-1} (L_1 - \lambda)^{-1}h.$$

From (4.3.26) we obtain

$$\|(L_1 - \lambda)^{-1}(L_{2,3} - \lambda)^{-1}\|_{\mathcal{X} \rightarrow \mathcal{X}} = \mathcal{O}(1).$$

From the Neumann expansion of the inverse we have

$$\left\| \left(I + \frac{\varepsilon\alpha}{\tau}(L_1 - \lambda)^{-1}(L_2 - \lambda)^{-1} + \frac{\varepsilon\beta}{\theta}(L_1 - \lambda)^{-1}(L_3 - \lambda)^{-1} \right)^{-1} \right\|_{\mathcal{X} \rightarrow \mathcal{X}} = \mathcal{O}(1).$$

Thus, we find, again by (4.3.26)

$$\|g_1\|_{\mathcal{X}} \leq C \|(L_1 - \lambda)^{-1}h\|_{\mathcal{X}} \leq C (\|f_1\|_{\mathcal{X}} + \varepsilon\|f_2\|_{\mathcal{X}} + \varepsilon\|f_3\|_{\mathcal{X}}). \quad (4.3.28)$$

The proof of the lemma follows from the combination of (4.3.27) and (4.3.28). \square

Proof of Lemma 4.3.8. The contour \mathcal{C} divides the complex plane into two pieces, and the spectrum $\sigma(L_\Gamma) \setminus \lambda_\pm$ is completely contained in one of these pieces. Moreover, the spectrum is an $\mathcal{O}(1)$ distance away from the contour \mathcal{C} . Since by assumption $F \in X_\Gamma$, the result follows from Lemma 4.3.9. \square

Remark 4.3.2. Because of the specific χ -norm we use, it is possible that we get extra point spectrum at the tip of the essential spectrum (compared to the previous chapter). However, the essential spectrum is in the left half plane and an $\mathcal{O}(1)$ distance away from the imaginary axis (4.3.18). Therefore, this ‘new’ point spectrum does not generate instabilities, and we can neglect it.

4.3.5 Initializing the renormalization group method

We use the RG method developed in [55], and adapted to singularly perturbed problems in [16, 31, 47]. We assume that the initial condition $\Phi_2(\xi, 0) = (U_2(\xi, 0), V_2(\xi, 0), W_2(\xi, 0))$ is close to the skeleton solution $\Phi_{\Gamma^*}(\xi)$,

$$\|Z_0^*\|_{\mathcal{X}} := \|\Phi_2(\cdot, 0) - \Phi_{\Gamma^*}\|_{\mathcal{X}} < \delta, \quad (4.3.29)$$

for some Γ^* , see (4.3.6), and some $\delta > 0$. Then, the following lemma holds:

Lemma 4.3.10. *Let $0 < \varepsilon \leq \delta \ll 1$ be sufficiently small and let $\Phi_2(\xi, t)$ and $\Phi_{\Gamma^*}(\xi)$ satisfy (4.3.29).*

- a) *There exists a unique smooth operator $\mathcal{H} : X \rightarrow \mathbb{R}^2$ such that the function $\Phi_{\Gamma^0}(\xi)$ with $\Gamma^0 := \Gamma^* + \mathcal{H}(Z_0^*)$ satisfies $Z_0^0(\xi) := \Phi_2(\xi, 0) - \Phi_{\Gamma^0}(\xi) \in X_{\Gamma^0}$. Moreover, $\|Z_0^0\|_{\mathcal{X}} = \mathcal{O}(\delta)$.*
- b) *If $Z_0^*(\xi) \in X_{\tilde{\Gamma}}$, for a $\Phi_{\tilde{\Gamma}}(\xi)$ of the form (4.3.6), then there exists a $C > 0$ such that*

$$|\Gamma^0 - \Gamma^*| \leq C \|Z_0^*\|_{\mathcal{X}} |\Gamma^* - \tilde{\Gamma}| \leq C\delta |\Gamma^* - \tilde{\Gamma}|. \quad (4.3.30)$$

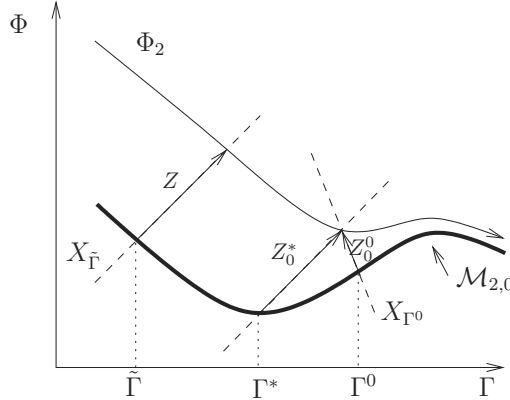


Figure 4.4: Schematic plot of the geometry of a curve of the 2-front solutions with initial condition Φ_2 in the (Γ, Φ) -plane. It gives a geometrical interpretation of the spaces $X_{\tilde{\Gamma}}$ and X_{Γ^0} , and the perturbations Z_0^* and Z_0^0 analyzed in Lemma 4.3.10. Moreover, it also illustrates the manifold $\mathcal{M}_{2,0}$. The first part of the lemma states that $Z_0^0 \in X_{\Gamma^0}$ is small as long as Z_0^* is small. According to the second part, if Z^* belongs to a $X_{\tilde{\Gamma}}$, then the distance between Γ^0 and Γ^* is of the asymptotic magnitude of the distance between Γ^0 and $\tilde{\Gamma}$ times the asymptotic magnitude of Z_0^* .

The first part of the lemma states that if the initial condition Φ_2 is close to a function Φ_{Γ^*} of the form (4.3.6), then there exists a basepoint $\Gamma^0 = (\Gamma_1^0, \Gamma_2^0)$ such that $\Phi_2 - \Phi_{\Gamma^0}$ is also small, and it is perpendicular to the space spanned by the small eigenvalues associated to L_{Γ^0} . Moreover, the mapping $(\Phi_2, \Gamma^*) \rightarrow \Gamma^0$ given by $\Gamma^0 := \Gamma^* + \mathcal{H}(Z_0^*)$ is smooth. The second part of the lemma concerns situations in which one wants to shift from one basepoint to another: if the initial perturbation is already perpendicular to the small eigenvalue space associated to a $L_{\tilde{\Gamma}}$, then the distance $|\Gamma^0 - \Gamma^*|$ between the new basepoint Γ^0 and Γ^* is small compared to the distance $|\Gamma^* - \tilde{\Gamma}|$ between the old basepoint $\tilde{\Gamma}$ and Γ^* , see Figure 4.4.

Proof. Consider a Γ^0 such that $\Phi_2(\xi, 0) = \Phi_{\Gamma^*}(\xi) + Z_0^*(\xi) = \Phi_{\Gamma^0}(\xi) + Z_0^0(\xi)$. The condition $Z_0^0(\xi) \in X_{\Gamma^0}$ is equivalent to

$$\pi_{\Gamma^0}(Z_0^0) = \pi_{\Gamma^0}(Z_0^* + \Phi_{\Gamma^*} - \Phi_{\Gamma^0}) = 0. \tag{4.3.31}$$

By (4.3.19) and Lemma 4.3.7, this is equivalent up to $\mathcal{O}(\varepsilon)$ to

$$\begin{aligned} \Lambda_1(\Gamma^0, Z_0^*) &:= \left([Z_0^* + \Phi_{\Gamma^*} - \Phi_{\Gamma^0}]_1, \psi_1(\Gamma_1^0) \right) = 0, \\ \Lambda_2(\Gamma^0, Z_0^*) &:= \left([Z_0^* + \Phi_{\Gamma^*} - \Phi_{\Gamma^0}]_1, \psi_2(\Gamma_2^0) \right) = 0, \end{aligned} \tag{4.3.32}$$

where $\psi_{1,2}$ are defined by (4.3.20) with $\Gamma_{1,2} = \Gamma_{1,2}^0$, respectively. Note that, since the adjoint eigenvectors are zero to leading order in the second and third components (4.3.19), we do not need to consider the second and third components of (4.3.31).

Observe that $\Lambda_i(\Gamma^*, 0) = 0$. The gradient of the map $\Lambda = (\Lambda_1, \Lambda_2)$ with respect to Γ^0 at $(\Gamma^*, 0)$ is given by

$$\nabla_{\Gamma^0} \Lambda|_{(\Gamma^0=\Gamma^*, Z_0^*=0)} = \begin{pmatrix} \|\psi_1\|_{L^2}^2 & 0 \\ 0 & -\|\psi_2\|_{L^2}^2 \end{pmatrix} + \mathcal{O}(\varepsilon), \quad (4.3.33)$$

where we have used that $\frac{\partial}{\partial \Gamma_i^0} [\Phi_{\Gamma^0}]_1 = \mp \psi_i$ to leading order, see (4.3.20). Thus, the map Γ is uniformly invertible near $(\Gamma^*, 0)$. Hence, for δ sufficiently small, the implicit function theorem guarantees the existence of a unique smooth function $\mathcal{H}(Z_0^*)$ such that Φ_{Γ^0} with $\Gamma^0 := \Gamma^* + \mathcal{H}(Z_0^*)$ satisfies (4.3.32), *i.e.*, $Z_0^0 \in X_{\Gamma^0}$, as introduced in the lemma.

To prove the second part of *a*), we observe that the implicit function theorem also guarantees that $\mathcal{H}(Z_0^*)$ is uniformly $\mathcal{O}(1)$ -Lipschitz and that $\mathcal{H}(0) = 0$. This yields

$$\begin{aligned} \|Z_0^0\|_{\mathcal{X}} &= \|Z_0^* + \Phi_{\Gamma^*} - \Phi_{\Gamma^0}\|_{\mathcal{X}} \leq \|Z_0^*\|_{\mathcal{X}} + \|\Phi_{\Gamma^*} - \Phi_{\Gamma^0}\|_{\mathcal{X}} \leq \delta + C|\Gamma^* - \Gamma^0| \\ &\leq \delta + C|\mathcal{H}(Z_0^*)| \leq \delta + C|\mathcal{H}(Z_0^*) - \mathcal{H}(0)| \leq C\delta. \end{aligned}$$

For part *b*), we observe that if $Z_0^* \in X_{\tilde{\Gamma}}$ then $([Z_0^*]_1, \psi_i(\tilde{\Gamma}_i)) = \mathcal{O}(\varepsilon)$. Since $\delta \geq \varepsilon$, substitution of this into (4.3.32) yields to leading order

$$\begin{aligned} \left| \left([\Phi_{\Gamma^0} - \Phi_{\Gamma^*}]_1, \psi_i(\tilde{\Gamma}_i) \right) \right| &= \left| ([Z_0^*]_1, \psi_i(\Gamma_i^0)) \right| \\ &\leq M \left| \left([Z_0^*]_1, \left(\psi_i(\tilde{\Gamma}_i) - \psi_i(\Gamma_i^0) \right) \right) \right|. \end{aligned} \quad (4.3.34)$$

Next, we use the mean value theorem and (4.3.20) to obtain

$$\left| \left([\Phi_{\Gamma^0} - \Phi_{\Gamma^*}]_1, \psi_i(\Gamma_i^0) \right) \right| = \left| \left(\psi_i(\Gamma_i^{mvt}), \psi_i(\Gamma_i^0) \right) \right| |\Gamma^0 - \Gamma^*| \quad (4.3.35)$$

where $\Gamma_i^{mvt} \in (\Gamma_i^0, \Gamma_i^*)$. From part *a*) we know that $|\Gamma_i^0 - \Gamma_i^*| = \mathcal{O}(\delta)$, so that to leading order in δ

$$\left| \left(\psi_i(\Gamma_i^{mvt}), \psi_i(\Gamma_i^0) \right) \right| = \|\psi_i\|_{L^2}^2 = \mathcal{O}(1). \quad (4.3.36)$$

Combining (4.3.35) with (4.3.36), we find that the left hand side of (4.3.34) is proportional to $|\Gamma^0 - \Gamma^*|$. To bound the right hand side of (4.3.34), we use property (4.3.3)

$$\begin{aligned} \left| \left([Z_0^*]_1, \left(\psi_i(\tilde{\Gamma}_i) - \psi_i(\Gamma_i^0) \right) \right) \right| &\leq \| [Z_0^*]_1 \|_{L^\infty} \|\psi_i(\tilde{\Gamma}_i) - \psi_i(\Gamma_i^0)\|_{L^1} \\ &\leq \|Z_0^*\|_{\mathcal{X}} \|\psi_i(\tilde{\Gamma}_i) - \psi_i(\Gamma_i^0)\|_{L^1}. \end{aligned}$$

In order to control this L^1 -norm, we distinguish between two cases. First, assume that $|\tilde{\Gamma} - \Gamma^0| > 4$, then

$$\|\psi_i(\tilde{\Gamma}_i) - \psi_i(\Gamma_i^0)\|_{L^1} \leq 2 \int_{-\infty}^{\infty} |\psi_i| d\xi = 4 \leq |\tilde{\Gamma} - \Gamma^0|.$$

If $|\tilde{\Gamma} - \Gamma^0| < 4$, then we once more use the mean value theorem

$$\|\psi_i(\tilde{\Gamma}_i) - \psi_i(\Gamma_i^0)\|_{L^1} \leq |\tilde{\Gamma} - \Gamma^0| \int_{-\infty}^{\infty} |\psi_i(\Gamma_i^{mvt}(\xi))| d\xi = C|\tilde{\Gamma} - \Gamma^0|.$$

Thus, the right hand side of (4.3.34) is bounded by $C\|Z_0^*\|_{\mathcal{X}}|\tilde{\Gamma} - \Gamma^0|$. Using the triangle inequality on $|\tilde{\Gamma} - \Gamma^0|$, we obtain the desired result. \square

Before we can initialize the first iteration step of the RG method, we need an *a priori* bound on its time step. Let t_l^* be the upperbound on the time step such that the remainder Z stays smaller than $\sqrt{\varepsilon}$, that is,

$$t_l^* := \inf \left\{ t \mid \|Z(\cdot, t)\|_{\mathcal{X}} > \sqrt{\varepsilon} \right\}. \quad (4.3.37)$$

This time step bound is well defined, and it is positive, by continuity of the remainder and by the assumption that the remainder is $\mathcal{O}(\varepsilon)$ small at $t = 0$, see Theorem 4.3.2 and Lemma 4.3.10 a) with $\delta = \varepsilon$. So, by construction the remainder $Z(\xi, t)$ stays $\mathcal{O}(\sqrt{\varepsilon})$ small for all $0 \leq t \leq t_l^*$. A very rough estimate shows that t_l^* is at least $\mathcal{O}(\varepsilon^{-\frac{1}{2}})$. The second time step bound, t_u^* , is

$$t_u^* := \frac{1}{4\nu} |\log \varepsilon|, \quad (4.3.38)$$

where we recall the definition of ν from the line under (4.3.23). This second bound arises naturally from the forthcoming analysis, see Lemma 4.3.11. The actual time step bound, t^* , is now defined as the minimum of the above two time step bounds

$$t^* := \min \{t_l^*, t_u^*\}. \quad (4.3.39)$$

We will show that $t_u^* < t_l^*$, so that $t^* = t_u^*$, see Lemma 4.3.11.

With this definition of the time step bound, we begin the first iteration of the RG method. We freeze the basepoint $\Gamma = (\Gamma_1, \Gamma_2) = (\Gamma_1^0, \Gamma_2^0) = \Gamma^0$ with $\Gamma_1^0 < \Gamma_2^0$ and $|\Gamma_2^0 - \Gamma_1^0| \leq \mathcal{O}(\varepsilon^{-1})$, and we decompose the actual solution Φ_2 into

$$\Phi_2(\xi, t) = \Phi_{\Gamma(t)}(\xi) + Z^0(\xi, t), \text{ such that } Z^0(\xi, t) \in X_{\Gamma^0} \text{ for all } t \leq t^*, \quad (4.3.40)$$

which can be done by Lemma 4.3.10 a). This decomposition transforms the nonlinear PDE (4.3.13) into

$$\begin{aligned} Z_t^0 + \frac{\partial \Phi_{\Gamma}}{\partial \Gamma} \dot{\Gamma} &= R + L_{\Gamma^0} Z^0 + \Delta L Z^0 + N(Z^0), \\ Z^0(\xi, 0) &= Z_0^0, \end{aligned} \quad (4.3.41)$$

where $\Delta L := L_{\Gamma} - L_{\Gamma^0}$, the secular term which measures the growth of the remainder Z^0 while Γ slides away from Γ^0 , and $Z_0^0 = Z_0^* - \Phi_{\Gamma^*} - \Phi_{\Gamma^0}$ (see Lemma 4.3.10).

4.3.6 Projecting onto the small eigenspace $X_{\Gamma^0}^C$

In the next section, we project equation (4.3.41) onto the space X_{Γ^0} to derive estimates on the remainder $Z^0(\xi, t)$. Here, we project onto the eigenspace $X_{\Gamma^0}^C$, the space spanned by the small eigenvectors of the operator L_{Γ^0} , to derive a rough version of the equation of the motion of the two fronts $\Gamma_{1,2}$. Since $Z^0(\xi, t) \in X_{\Gamma^0}$ for all $t \leq t^*$ (4.3.40) and since the projection π_{Γ^0} commutes with the operator L_{Γ^0} , we have that $\pi_{\Gamma^0} L_{\Gamma^0} Z^0 = L_{\Gamma^0} \pi_{\Gamma^0} Z^0 = 0$. We obtain the projected equation

$$\pi_{\Gamma^0} \left(\frac{\partial \Phi_{\Gamma}}{\partial \Gamma} \dot{\Gamma} \right) = \pi_{\Gamma^0} (R + \Delta LZ^0 + N(Z^0)) .$$

By definition of π_{Γ^0} (4.3.21), this is equivalent to

$$\left(\frac{\partial \Phi_{\Gamma}}{\partial \Gamma} \dot{\Gamma}, \Psi_{\pm}^{\dagger} \right) = \left(R + \Delta LZ^0 + N(Z^0), \Psi_{\pm}^{\dagger} \right) . \quad (4.3.42)$$

Observe by (4.3.6), (4.3.7), and (4.3.20) that

$$\begin{aligned} \frac{\partial \Phi_{\Gamma}}{\partial \Gamma} \dot{\Gamma} &= \begin{pmatrix} \frac{\partial \Phi_1}{\partial \Gamma_1} & \frac{\partial \Phi_1}{\partial \Gamma_2} \\ \frac{\partial \Phi_2}{\partial \Gamma_1} & \frac{\partial \Phi_2}{\partial \Gamma_2} \\ \frac{\partial \Phi_3}{\partial \Gamma_1} & \frac{\partial \Phi_3}{\partial \Gamma_2} \end{pmatrix} \begin{pmatrix} \dot{\Gamma}_1 \\ \dot{\Gamma}_2 \end{pmatrix} \\ &= \begin{pmatrix} -\psi_1 \dot{\Gamma}_1 + \psi_2 \dot{\Gamma}_2 \\ -(G_V * \psi_1) \dot{\Gamma}_1 + (G_V * \psi_2) \dot{\Gamma}_2 \\ -(G_W * \psi_1) \dot{\Gamma}_1 + (G_W * \psi_2) \dot{\Gamma}_2 \end{pmatrix} . \end{aligned} \quad (4.3.43)$$

On the other hand

$$\begin{aligned} (\psi_1, \psi_2) &= \text{exp. small}, \quad (\psi_i, \mathcal{R}_i^{\dagger}) = \mathcal{O}(1), \quad \text{and} \\ \left(G_{V,W} * \psi_i, \mathcal{R}_{2,3}^{\dagger} \right) &\leq \|G_{V,W} * \psi_i\|_{L^{\infty}} \|\mathcal{R}_{2,3}^{\dagger}\|_{L^1} = \mathcal{O}(\varepsilon) \mathcal{O}(\varepsilon^{-1}) = \mathcal{O}(1), \end{aligned} \quad (4.3.44)$$

where $\mathcal{R}_{2,3}^{\dagger}$ are defined in the proof of Lemma 4.3.7. Therefore, (4.3.42) reduces to leading order to

$$\begin{pmatrix} -\|\psi_1\|_{L^2}^2 & -\|\psi_2\|_{L^2}^2 \\ -\|\psi_1\|_{L^2}^2 & \|\psi_2\|_{L^2}^2 \end{pmatrix} \begin{pmatrix} \dot{\Gamma}_1 \\ \dot{\Gamma}_2 \end{pmatrix} = \begin{pmatrix} \left(R + \Delta LZ^0 + N(Z^0), \Psi_+^{\dagger} \right) \\ \left(R + \Delta LZ^0 + N(Z^0), \Psi_-^{\dagger} \right) \end{pmatrix} .$$

Note that the second and third components of $R + \Delta LZ + N(Z)$ are identically zero. Therefore, inverting the matrix of the left hand side, we obtain

$$\begin{aligned} \dot{\Gamma}_1 &= - \frac{1}{\|\psi_1\|_{L^2}^2} (R_1 + [\Delta LZ^0]_1 + [N(Z^0)]_1, \psi_1) (1 + \mathcal{O}(\varepsilon)), \\ \dot{\Gamma}_2 &= \frac{1}{\|\psi_2\|_{L^2}^2} (R_1 + [\Delta LZ^0]_1 + [N(Z^0)]_1, \psi_2) (1 + \mathcal{O}(\varepsilon)). \end{aligned} \quad (4.3.45)$$

In Section 4.3.9, we will further investigate these two ODEs and we will validate (4.3.12). However, to do so, we first need a better bound on the remainder $Z^0(\xi, t)$. This bound is obtained by projecting (4.3.41) onto X_{Γ^0} .

4.3.7 Projecting onto X_{Γ^0}

Projection of (4.3.41) onto X_{Γ^0} yields

$$\begin{aligned} Z_t^0 &= \tilde{R} + L_{\Gamma^0} Z^0 + \tilde{\pi}_{\Gamma^0} (\Delta L Z^0 + N(Z^0)) \\ Z^0(\xi, 0) &= Z_0^0, \end{aligned} \quad (4.3.46)$$

with $\tilde{R} = \tilde{\pi}_{\Gamma^0} \left(R - \frac{\partial \Phi_{\Gamma}}{\partial \Gamma} \dot{\Gamma} \right)$. The variation of constants formula applied to (4.3.46) yields

$$Z^0(\xi, t) = S(t) Z_0^0 + \int_0^t S(t-s) (\tilde{R} + \tilde{\pi}_{\Gamma^0} (\Delta L Z^0 + N(Z^0))) ds, \quad (4.3.47)$$

where S is the semigroup generated by L_{Γ^0} , see (4.3.24). The main result of this section reads

Lemma 4.3.11. *There exists a constant $C > 0$, independent of ε , such that the remainder $Z^0(\xi, t)$ stays $\mathcal{O}(\varepsilon)$ small during one time step $t^* = t_u^* = \frac{1}{4\nu} |\log \varepsilon|$. More precisely,*

$$\|Z^0(\cdot, t)\|_{\chi} \leq C (e^{-\nu t} \|Z_0^0\|_{\chi} + \varepsilon) \leq \varepsilon C \quad \text{for } t \in [0, t^*]. \quad (4.3.48)$$

Before we can prove this lemma, we need some intermediate results, Lemmas 4.3.12–4.3.14. As a preliminary step we define two useful quantities

$$T_0(t) := \sup_{0 \leq s \leq t} e^{\nu s} \|Z^0(\cdot, s)\|_{\chi}. \quad (4.3.49)$$

$$T_1(t) := \sup_{0 \leq s \leq t} |\Gamma(s) - \Gamma^0|. \quad (4.3.50)$$

The first quantity measures the growth of the remainder Z^0 in the weighted χ -norm, and the latter measures the maximal distance a 2-front solution Φ_{Γ} has travelled from its basepoint Γ^0 . Observe that, by the assumptions on the time step t^* , $T_0(t) = \mathcal{O}(\varepsilon^{1/4})$. The fact that we have an *a priori* upperbound on T_0 is one of the reasons for imposing the special bounds (4.3.37) and (4.3.38). To bound $T_1(t)$ in terms of $T_0(t)$, we need estimates on the nonlinear term $N(Z^0)$ and the secular term $\Delta L Z^0$.

Lemma 4.3.12. *There exists a constant $C > 0$ such that $\|N(Z^0)\|_{\chi} \leq C \|Z^0\|_{\chi}^2$, and $\|\Delta L Z^0\|_{\chi} \leq C |\Gamma - \Gamma^0| \|Z^0\|_{\chi}$ for $t \leq t^*$.*

Proof. The nonlinear term $N(Z^0)$ has already been analyzed in Lemma 4.3.4. However, we now have an extra assumption on the magnitude of the remainder (4.3.37) and (4.3.39). Therefore, the bound on $N(Z^0)$ can be sharpened

$$\|N(Z^0)\|_{\chi} \leq C \left(\|[Z^0]_1\|_{\chi}^2 + \|[Z^0]_1\|_{\chi}^3 \right) \leq C \|Z^0\|_{\chi}^2 \quad \text{for } t \leq t^*. \quad (4.3.51)$$

The bound on the secular term ΔLZ^0 follows from

$$\begin{aligned}
\|\Delta LZ^0\|_{\mathcal{X}} &= \|3(\Phi_1^2(\Gamma) - \Phi_1^2(\Gamma^0)) [Z^0]_1\|_{\mathcal{X}} \\
&= \|3(\Phi_1^2(\Gamma) - \Phi_1^2(\Gamma^0)) \chi [Z^0]_1\|_{L^1} + \|3(\Phi_1^2(\Gamma) - \Phi_1^2(\Gamma^0)) \\
&\quad ([Z^0]_1)_\xi\|_{L^1} + \|3(\Phi_1^2(\Gamma) - \Phi_1^2(\Gamma^0))_\xi [Z^0]_1\|_{L^1} \\
&\leq C \left\{ \|\Phi_1^2(\Gamma) - \Phi_1^2(\Gamma^0)\|_{L^\infty} \|[Z^0]_1\|_{\mathcal{X}} + \|(\Phi_1^2(\Gamma) \right. \\
&\quad \left. - \Phi_1^2(\Gamma^0))_\xi [Z^0]_1\|_{L^1} \right\} \tag{4.3.52} \\
&\leq C \left\{ |\Gamma - \Gamma^0| \|Z^0\|_{\mathcal{X}} + \|(\Phi_1^2(\Gamma) - \Phi_1^2(\Gamma^0))_\xi\|_{L^1} \|[Z^0]_1\|_{L^\infty} \right\} \\
&\leq C |\Gamma - \Gamma^0| \|Z^0\|_{\mathcal{X}},
\end{aligned}$$

where we used (4.3.3) and the Lipschitz continuity of Φ_1^2 and $(\Phi_1^2)_\xi$. \square

Using (4.3.45), we can estimate $T_1(t)$

Lemma 4.3.13. $T_1(t) \leq C(\varepsilon t + T_0(t)^2)$ for $t \in [0, t^*]$.

Note that this implies that $T_1(t)$ is at most $\mathcal{O}(\sqrt{\varepsilon})$.

Proof.

$$\begin{aligned}
T_1(t) &= \sup_{0 \leq s \leq t} \left| \int_0^s \Gamma_s ds \right| \leq \int_0^t |\Gamma_s| ds \\
&\leq C \left\{ \int_0^t \sum_{i=1}^2 (|(R_1, \psi_i)| + |([\Delta LZ^0]_1, \psi_i)| + |(N(Z^0))_1, \psi_i|) ds \right\} \\
&\leq C \left\{ \int_0^t \|\psi_i\|_{L^1} (\|R_1\|_{L^\infty} + \|\Delta LZ^0\|_{\mathcal{X}} + \|N(Z^0)\|_{\mathcal{X}}) ds \right\} \\
&\leq C \{ \varepsilon t + T_1 T_0 + T_0^2 \},
\end{aligned}$$

where, besides (4.3.51) and (4.3.52), we used the fact that $\psi_{1,2} \in L^1$, (4.3.3), and Lemma 4.3.5. By assumption, $T_0(t)$ is at most $\mathcal{O}(\varepsilon^{1/4})$, this completes the proof. \square .

For a sharper bound on T_0 , we need estimates on the terms of the integrand of (4.3.47).

Lemma 4.3.14. *The terms of the integrand of (4.3.47) can be estimated by*

$$\begin{aligned}
\|S(t-s) \tilde{\pi}_{\Gamma^0}(\Delta LZ^0)\|_{\mathcal{X}} &\leq C e^{-\nu(t-s)} T_1 \|Z^0\|_{\mathcal{X}}, \\
\|S(t-s) \tilde{\pi}_{\Gamma^0}(N(Z^0))\|_{\mathcal{X}} &\leq C e^{-\nu(t-s)} \|Z^0\|_{\mathcal{X}}^2, \\
\|S(t-s) \tilde{R}\|_{\mathcal{X}} &\leq \varepsilon C e^{-\nu(t-s)}, \quad \text{for } t \in [0, t^*].
\end{aligned} \tag{4.3.53}$$

Proof. The first two inequalities of (4.3.53) immediately follow from Lemma 4.3.12 combined with the semigroup estimate (4.3.25) and the observation that projections are bounded in the χ -norm. To prove the last bound, we need to show that the asymptotic magnitude of \tilde{R} is $\mathcal{O}(\varepsilon)$. To do so, we observe that (4.3.45) combined with (4.3.3) gives

$$\dot{\Gamma}_{1,2} \leq C (\|R_1\|_\chi + \|\Delta LZ^0\|_\chi + \|N(Z^0)\|_\chi) .$$

By Lemmas 4.3.5, 4.3.12 and 4.3.13, all three of the above norms are $\mathcal{O}(\varepsilon)$ for $t \in [0, t^*]$. Therefore, $\dot{\Gamma}_{1,2} \leq \varepsilon C$. Now, the second and third component of $R - \frac{\partial \Phi_\Gamma}{\partial \Gamma} \dot{\Gamma}$ can be estimated using the above observation together with (4.3.43) and (4.3.44)

$$\begin{aligned} \left\| - \left(\frac{\partial \Phi_{2,3}}{\partial \Gamma_1} \dot{\Gamma}_1 + \frac{\partial \Phi_{2,3}}{\partial \Gamma_2} \dot{\Gamma}_2 \right) \right\|_\chi &= \left\| -(G_{V,W} * \psi_1) \dot{\Gamma}_1 + (G_{V,W} * \psi_2) \dot{\Gamma}_2 \right\|_\chi \\ &\leq \varepsilon C \|G_{V,W} * (\psi_1 + \psi_2)\|_\chi \\ &\leq \varepsilon C . \end{aligned}$$

It is now obvious that the χ -norms of the components $\tilde{R}_{2,3}$ are $\mathcal{O}(\varepsilon)$. The first component of \tilde{R} will also be $\mathcal{O}(\varepsilon)$. To see this, observe that, up to exponentially small terms,

$$\tilde{\pi}_{\Gamma^0} \left(-\frac{\partial \Phi_1}{\partial \Gamma_1} \dot{\Gamma}_1 - \frac{\partial \Phi_1}{\partial \Gamma_2} \dot{\Gamma}_2 \right) = \dot{\Gamma}_1 \left[\frac{(\psi_1^t, \psi_1^0)}{\|\psi_1^0\|_{L^2}^2} \psi_1^0 - \psi_1^t \right] + \dot{\Gamma}_2 \left[\psi_2^t - \frac{(\psi_2^t, \psi_2^0)}{\|\psi_2^0\|_{L^2}^2} \psi_2^0 \right] , \quad (4.3.54)$$

where $\psi_i^0 = \psi_i(\xi; \Gamma_i^0)$, while $\psi_i^t = \psi_i(\xi; \Gamma_i(t))$. Since the functions $\psi_i(\xi)$ are Lipschitz continuous and in L^1 , we can bound the χ -norm of (4.3.54) by

$$\left\| \tilde{\pi}_{\Gamma^0} \left(-\frac{\partial \Phi_1}{\partial \Gamma_1} \dot{\Gamma}_1 - \frac{\partial \Phi_1}{\partial \Gamma_2} \dot{\Gamma}_2 \right) \right\|_\chi \leq C \varepsilon \sqrt{\varepsilon} ,$$

where we again used that $\dot{\Gamma}_{1,2} \leq \varepsilon C$ and lemma 4.3.13. The χ -norm of $\tilde{\pi}_{\Gamma^0} R_1$ is not larger than the χ -norm of R_1 , and from Lemma 4.3.5 we recall that $\|R_1\|_\chi = \mathcal{O}(\varepsilon)$. Therefore, $\|\tilde{R}\|_\chi = \mathcal{O}(\varepsilon)$ for $t \in [0, t^*]$. \square

With the above three lemmas, we can now prove Lemma 4.3.11.

Proof of Lemma 4.3.11. Taking the χ -norm of $Z^0(\xi, t')$ (4.3.47) at $t = t' \in [0, t^*]$, we find

$$\begin{aligned} \|Z^0(\cdot, t')\|_\chi &\leq C \left\{ e^{-\nu t'} \|Z_0^0\|_\chi + \int_0^{t'} e^{-\nu(t'-s)} (\varepsilon + T_1(s) \|Z^0(\cdot, s)\|_\chi \right. \\ &\quad \left. + \|Z^0(\cdot, s)\|_\chi^2) ds \right\} . \end{aligned}$$

Multiplying the above inequality by $e^{\nu t'}$ and taking the supremum over $t' \in (0, t)$, we find

$$\begin{aligned} T_0(t) &\leq C \left\{ T_0(0) + \varepsilon \int_0^t e^{\nu s} ds + T_1(t) T_0(t) \int_0^t ds + (T_0(t))^2 \int_0^t e^{-\nu s} ds \right\} \implies \\ T_0(t) &\leq C \left\{ T_0(0) + \varepsilon e^{\nu t} + T_1(t) T_0(t) t + (T_0(t))^2 \right\} . \end{aligned}$$

Next, we eliminate $T_1(t)$ from the above inequality by using Lemma 4.3.13,

$$T_0(t) (1 - \varepsilon C t^2) \leq C \{T_0(0) + \varepsilon e^{\nu t} + t(T_0(t))^3 + (T_0(t))^2\}. \quad (4.3.55)$$

Since the time step $t^* \ll \min\{(T_0(t))^{-1}, \varepsilon^{-1/2}\}$, we can incorporate the cubic term into the quadratic term, and we can conservatively underestimate the left hand side by $\frac{T_0(t)}{2}$. Thus, we obtain a simple quadratic inequality

$$T_0(t) \leq C \{T_0(0) + \varepsilon e^{\nu t} + (T_0(t))^2\}. \quad (4.3.56)$$

Plainly, if (4.3.56) is satisfied, then so is (4.3.55). To study the inequality (4.3.56), we look at the related quadratic equation in $T_0(t)$,

$$(T_0(t))^2 - \frac{1}{C}T_0(t) + T_0(0) + \varepsilon e^{\nu t} = 0.$$

Since $T_0(0) + \varepsilon e^{\nu t} \leq \mathcal{O}(\varepsilon^{3/4}) \ll 1$, both roots of the quadratic, $r_{1,2}$, are real and positive. To leading order, they have the form

$$r_1 = 2C (T_0(0) + \varepsilon e^{\nu t}) \quad \text{and} \quad r_2 = \frac{1}{2C}.$$

Thus, the values of $T_0(t)$ satisfying (4.3.56) lie in the domain $0 < T_0(t) < r_1$ and $T_0(t) > r_2$. Moreover, since $T_0(0) < r_1$ and $T_0(t)$ is continuous, we know that

$$T_0(t) \leq r_1 = 2C (T_0(0) + \varepsilon e^{\nu t}) \quad (4.3.57)$$

for all $t \leq t^*$. Using the definition of $T_0(t)$ (4.3.49) we have completed the proof. \square

4.3.8 Iteration

In Sections 4.3.5–4.3.7, we performed one step of the RG procedure. We found that in the time interval $[0, t^*]$ the remainder $Z^0(\xi, t)$ with respect to the decomposition (4.3.40) stays $\mathcal{O}(\varepsilon)$ small. The next step of the RG procedure is to choose at time $t = t^*$ a different basepoint, $\Gamma^1 := (\Gamma_1^1, \Gamma_2^1)$, and to decompose the 2-front solution Φ_2 with respect to this new basepoint, as follows:

$$\Phi_2(\xi, t) = \Phi_{\Gamma(t)}(\xi) + Z^1(\xi, t), \quad \text{where } Z^1(\xi, t) \in X_{\Gamma^1} \text{ for all } t \in [t^*, 2t^*], \quad (4.3.58)$$

see Figure 4.4 (with, in notation of this section, $\tilde{\Gamma} \rightarrow \Gamma^0, \Gamma^* \rightarrow \Gamma(t^*), \Gamma^0 \rightarrow \Gamma^1, Z \rightarrow Z_0^0, Z_0^* \rightarrow Z_0^0(t^*),$ and $Z_0^0 \rightarrow Z_0^1$). The idea of the RG method is now to restart the procedure of Sections 4.3.5–4.3.7 with the same PDE (4.3.41), however, with the new basepoint Γ^1 and the new initial condition Z_0^1 , and to show that the remainder $Z^1(\xi, t)$ stays $\mathcal{O}(\varepsilon)$ small in the interval $[t^*, 2t^*]$. Of course, one first has to prove that this new basepoint Γ^1 is not too far away from the location of the front at the end of the first time step $\Gamma(t^*)$, more precisely,

that the renormalization has no leading order influence on the dynamics of the fronts, and that the new initial condition $Z_0^1(\xi) := Z^1(\xi, t^*)$ is of order $\mathcal{O}(\varepsilon)$. This first step will be proved in Lemma 4.3.15. Then, to show that $Z^1(\xi, t)$ stays $\mathcal{O}(\varepsilon)$ on the time interval $[t^*, 2t^*]$, we note that the analysis on $[0, t^*]$ presented in Sections 4.3.5–4.3.7 depended only on the asymptotic magnitude of the initial condition and on the length of the time interval. Hence, because these quantities are of the same size for this second time interval, the analysis of those sections may be repeated to directly yield that $Z^1(\xi, t)$ stays $\mathcal{O}(\varepsilon)$ small on $[t^*, 2t^*]$.

Lemma 4.3.15. *Let $Z_0^1(\xi)$ denote the initial condition of (4.3.41) on the second interval $[t^*, 2t^*]$, (4.3.58). Then,*

$$|\Gamma^1 - \Gamma(t^*)| = \mathcal{O}(\varepsilon^2 |\log \varepsilon|) \quad \text{and} \quad \|Z_0^1\|_{\mathcal{X}} = \mathcal{O}(\varepsilon).$$

Proof. Since $Z^0(\xi, t) \in X_{\Gamma^0}$ for all $t \leq t^*$ (4.3.40), (4.3.30) in Lemma 4.3.10 yields

$$|\Gamma^1 - \Gamma(t^*)| \leq C |\Gamma(t^*) - \Gamma^0| \|Z^0(\cdot, t^*)\|_{\mathcal{X}}.$$

We use the definition (4.3.49) of T_1 , and Lemma 4.3.13, together with Lemma 4.3.11, to further estimate the right hand side of the above inequality

$$\begin{aligned} |\Gamma^1 - \Gamma(t^*)| &\leq C |\Gamma(t^*) - \Gamma^0| \|Z^0(\cdot, t^*)\|_{\mathcal{X}} \\ &\leq C (\varepsilon |\log \varepsilon| + T_0^2) \|Z^0(\cdot, t^*)\|_{\mathcal{X}} \\ &\leq C \left(\varepsilon |\log \varepsilon| + (\|Z_0^0\|_{\mathcal{X}} + \varepsilon^{3/4})^2 \right) \|Z^0(\cdot, t^*)\|_{\mathcal{X}} \\ &\leq C \left(\varepsilon |\log \varepsilon| + (\varepsilon + \varepsilon^{3/4})^2 \right) \varepsilon \\ &\leq C \varepsilon^2 |\log \varepsilon|. \end{aligned}$$

By continuity of $\Phi_2(\xi, t)$ in $t = t^*$ and Lipschitz continuity of $\Phi_{\Gamma(t)}(\xi)$, we can now estimate $\|Z_0^1\|_{\mathcal{X}}$

$$\begin{aligned} \|Z_0^1\|_{\mathcal{X}} &\leq \|Z_0^1 - Z^0(\cdot, t^*)\|_{\mathcal{X}} + \|Z^0(\cdot, t^*)\|_{\mathcal{X}} \\ &\leq \|\Phi_2(\xi, t^*) - \Phi_{\Gamma(t^*)}(\xi) - \Phi_2(\xi, t^*) + \Phi_{\Gamma^1}(\xi)\|_{\mathcal{X}} + \|Z^0(\cdot, t^*)\|_{\mathcal{X}} \\ &\leq C |\Gamma^1 - \Gamma(t^*)| + \|Z^0(\cdot, t^*)\|_{\mathcal{X}} \\ &\leq C (\varepsilon^2 |\log \varepsilon| + \varepsilon) \leq \varepsilon C. \end{aligned}$$

This proves the lemma. □

4.3.9 Completion of the proof of Theorem 4.3.2

In this section, we finish the proof of Theorem 4.3.2. In the previous section, we established that the remainder $Z(\xi, t)$ also stays $\mathcal{O}(\varepsilon)$ small in the second time interval. Repeating the same arguments, we can show that by choosing a

new basepoint Γ^2 at $2t^*$ the remainder $Z^2(\xi, t)$ also stays small in the interval $[2t^*, 3t^*]$. By this iterative procedure, and since $t^* \gg 1$, we can now conclude that the remainder $Z(\xi, t)$ stays $\mathcal{O}(\varepsilon)$ small up till t^m , that is, up to the moment we approach the boundary $\partial\mathcal{M}_{2,0}$. Here, the analysis of the previous sections breaks down since the fronts approach the strong interaction regime, so that the inner product (ψ_1, ψ_2) is no longer exponentially small, *i.e.*, the fast fronts are no longer strongly localized. For instance, the derivation of (4.3.45) heavily relies on this fact. This proves (4.3.11).

To prove (4.3.12), we further analyze the expressions for $\dot{\Gamma}_{1,2}$ (4.3.45). Since we know that the χ -norm of the remainder $Z(\xi, t)$ is $\mathcal{O}(\varepsilon)$ small for all time up to t^m , we conclude from (4.3.52) and (4.3.51) that

$$([\Delta LZ]_{1, \psi_{1,2}}) = \mathcal{O}(\varepsilon^2 |\log \varepsilon|), \quad ([N(Z)]_{1, \psi_{1,2}}) = \mathcal{O}(\varepsilon^2).$$

Now, the inner product involving R_1 is $\mathcal{O}(\varepsilon)$. Therefore, the above terms are of higher order, and we can neglect them in (4.3.45). After neglecting exponentially small terms, the residual R_1 is given by, see (4.3.17),

$$R_1(\Phi_\Gamma) = -\varepsilon(\alpha(G_V * U_0) + \beta(G_W * U_0) + \gamma).$$

The projections of $G_{V,W} * U_0$ can be explicitly computed using (4.3.7), (4.3.9), and (4.3.20) – see also the Melnikov integrals of Chapter 2. To leading order, we obtain

$$(R_1, \psi_{1,2}) = -2\varepsilon \left(\gamma - \alpha e^{-\varepsilon(\Gamma_2 - \Gamma_1)} - \beta e^{-\frac{\varepsilon}{D}(\Gamma_2 - \Gamma_1)} \right).$$

Finally, since $\|\psi_i\|_{L^2}^2 = \frac{2}{3}\sqrt{2}$, the evolution of $\Gamma_{1,2}$ is to leading order indeed given by (4.3.12). This completes the proof of Theorem 4.3.2. \square

4.4 The dynamics of N -front solutions

In this section, we analyze the dynamics of the fronts of N -front solutions. The system of ODEs describing the evolution of these fronts was formally derived in Section 4.2, and this derivation was made rigorous in the previous section, see Theorem 4.3.2. In Section 4.4.2, we classify the dynamics of all possible 2-front solutions, showing that the two fronts move toward a stable 1-pulse solution if and only if the system parameters are such that the 1-pulse solution is stable (for these parameters) and such that there is no unstable 1-pulse solution in between the initial data and the attractor. In Sections 4.4.3 and 4.4.4, we prove similar results for 3-front and 4-front solutions, respectively. For example, we determine the stability of front-solutions for which one or more of the fronts travel to infinity. To prove all the statements of these three sections, it is useful first to prove a statement for general N -front solutions. That is, N -front solutions for N odd are

not stationary, while N -front solutions for N even do not travel with a uniform $\mathcal{O}(\varepsilon)$ speed. This will be proved in the first section.

Note that Theorem 4.3.2 states that the derivation is valid up to time t_m , which can be $+\infty$. After t_m , the fronts enter the strong interaction regime. Here, the system of ODEs no longer describes the dynamics of the fronts. For example, two components of the system of ODEs can cross, while this is not possible in the PDE case. The following conjecture is backed up by the numerical simulations, see Figures 4.7 and 4.10.

Conjecture 4.4.1. *A pair of colliding fronts of the PDE (4.1.1) disappears for $\mathcal{O}(1)$ parameters with respect to ε .*

This yields that after collision between two of the fronts in the ODE description, these two fronts should be removed from the system. Therefore, the N -dimensional system of ODEs reduces to an $N-2$ -dimensional system.

Remark 4.4.1. The trivial dynamics of a 1-front solution is completely captured by Lemma 4.2.1.

4.4.1 N -front solutions with N even and N odd

In this section, we investigate the differences between odd and even N -front solutions. By studying the total movement of the N fronts, we can prove the following lemma:

Lemma 4.4.2. *Let $0 < \varepsilon \ll 1$ be sufficiently small, and assume that all other parameters in (4.1.1) are $\mathcal{O}(1)$ with respect to ε . Moreover, assume that $\gamma \neq 0$. Then, for N odd, there exist no stationary N -front solutions to (4.1.1), and for N even there exist no uniformly traveling N -front solutions with $\mathcal{O}(\varepsilon)$ velocity.*

Proof. We begin with the case of N odd. The speed of the i -th front is given by (4.2.1). Summing these front velocities over all N and noting the pairwise cancellations of terms for adjacent fronts, we find that for N odd,

$$\sum_{i=1}^N \dot{\Gamma}_i(t) = \frac{3}{2} \sqrt{2\varepsilon} \gamma. \quad (4.4.1)$$

Thus, there must be a net movement of the fronts in the direction given by the sign of γ . The assumption that $\gamma \neq 0$ now proves the first part of the lemma.

For N even, the sum of N components is to leading order zero, see again (4.2.1). This yields that, there can be no net movement of the N fronts. Therefore, it is not possible to have a uniformly traveling N -front solution with an $\mathcal{O}(\varepsilon)$ speed. \square

Corollary 4.4.3. *For N odd, at least one of the fronts of an N -front solution has to travel to $\pm\infty$, where the sign is determined by the sign of γ . If N is even and one of the fronts of an N -front solution travels to $\pm\infty$, then at least one of the other fronts has to travel in the opposite direction, i.e., to $\mp\infty$.*

It is of interest to observe that the dynamics of an N -front solution for which one of the fronts is far away from all of the others can be completely understood from the dynamics of an $(N-1)$ -front solution and those of a single front, independently. In this case, to leading order, the system of ODEs for the N -front solution breaks up into the ODE (4.2.7) for a 1-front solution and a system of ODEs (4.2.1) for an $(N-1)$ -front solution. Since for N odd always at least one of the fronts travels to $\pm\infty$, this yields that, when looking at a fixed interval, an N -front solution with N odd will eventually behave like an M -front solution, with $M < N$ even.

Remark 4.4.2. In the nongeneric case where $\gamma = 0$ there do exist stationary odd N -front solutions.

4.4.2 The 2-front solutions

The dynamics of the fronts of a 2-front solution can be deduced in a straightforward fashion from (4.3.12). Observe that the fronts travel with opposite velocities. Therefore, we can rewrite the system of ODEs for the front dynamics as one ODE for the dynamics of the distance, $\Delta\Gamma := \Gamma_2 - \Gamma_1$,

$$\dot{\Delta\Gamma} = 3\sqrt{2}\varepsilon \left(\alpha e^{-\varepsilon\Delta\Gamma} + \beta e^{-\frac{\varepsilon}{D}\Delta\Gamma} - \gamma \right). \quad (4.4.2)$$

The fixed points $\Delta\Gamma_*^i, i \in \mathbb{N}$, of this ODE coincide with the solutions of the existence condition for standing 1-pulse solutions as derived in Chapter 2. In particular, there are either zero, one, or two solutions, depending on the signs of α, β , and on the size of $\alpha + \beta$ relative to γ , see Lemma 2.2.2 in Chapter 2. The stability of these particular standing 1-pulse solutions is determined by the sign of the small eigenvalue $\lambda_1 := -3\sqrt{2}\varepsilon^2 \left(\alpha e^{-\varepsilon\Delta\Gamma_*^i} + \frac{\beta}{D} e^{-\frac{\varepsilon}{D}\Delta\Gamma_*^i} \right)$, see Chapter 3. On a case-by-case basis, we draw the following conclusions about solutions $\Delta\Gamma(t)$: If (4.4.2) has no roots, then $\Delta\Gamma(t)$ tends to ∞ for all initial data $\Delta\Gamma(t)$ if and only if $\gamma < 0$, otherwise it tends to 0. If (4.4.2) has one root $\Delta\Gamma_*^1$, then if it is stable $\Delta\Gamma(t)$ tends to $\Delta\Gamma_*^1$, whereas if it is unstable $\Delta\Gamma(t)$ tends to 0 or to ∞ , depending on the sign of $\Delta\Gamma(0) - \Delta\Gamma_*^1$. Finally, if (4.4.2) has two roots, one stable $\Delta\Gamma_*^1$ and the other unstable $\Delta\Gamma_*^2$, then we distinguish two cases: Firstly, if $\Delta\Gamma_*^1 > \Delta\Gamma_*^2$ then initial conditions larger than the unstable root, that is, $\Delta\Gamma(0) > \Delta\Gamma_*^2$ tend to $\Delta\Gamma_*^1$, while smaller initial conditions tend to 0. Secondly, if $\Delta\Gamma_*^1 < \Delta\Gamma_*^2$ then initial conditions smaller than the unstable root, that is, $\Delta\Gamma(0) < \Delta\Gamma_*^2$ tend to $\Delta\Gamma_*^1$, while larger initial conditions tend to ∞ . This yields the following lemma:

Lemma 4.4.4. *The fronts of a 2-front solution $\Delta\Gamma(t)$ asymptote to a standing 1-pulse solution with width $\Delta\Gamma = \Delta\Gamma_*^1$ if and only if this 1-pulse solution is*

stable and there is no unstable standing 1-pulse solution determined by $\Delta\Gamma_*^2$ with $\Delta\Gamma(0) < \Delta\Gamma_*^2 < \Delta\Gamma_*^1$ or $\Delta\Gamma(0) > \Delta\Gamma_*^2 > \Delta\Gamma_*^1$.

Proof of Lemma 4.4.4. Equation (4.4.2) has at most two fixed points $\Delta\Gamma_*^{1,2}$ for a given parameter combination (Lemma 2.2.2). The stability of these fixed points is determined by

$$\lambda_1 = \frac{\partial\dot{\Delta\Gamma}}{\partial\Delta\Gamma}. \quad (4.4.3)$$

Since (4.4.2) is a 1-dimensional, autonomous ODE, this proves the lemma. \square

See also Figure 4.5, where we plotted $\dot{\Delta\Gamma}$ as function of $\Delta\Gamma$, as well as the solutions of the ODE (4.4.2) and the PDE (4.1.1) for two different initial conditions.

Due to the symmetry of the PDE (4.1.1), we immediately obtain a result on ‘2-back solutions’, that is, solutions that asymptote to $(+1, +1, +1)$ at $-\infty$. These 2-back solutions turn out to be relevant for understanding the dynamics of 3- and 4-front solutions, see the next two sections.

Lemma 4.4.5. *The ODE*

$$\dot{\Delta\Gamma} = 3\sqrt{2}\varepsilon (\alpha e^{-\varepsilon\Delta\Gamma} + \beta e^{-\frac{\varepsilon}{D}\Delta\Gamma} + \gamma). \quad (4.4.4)$$

describes the evolution of the distance between the fronts of a 2-back solution $\Delta\Gamma(t)$. The fronts approach a standing 1-pulse solution (which asymptotes to $(+1, +1, +1)$) with width $\Delta\Gamma = \Delta\Gamma_^1$ if and only if this 1-pulse solution is stable and there is no unstable standing 1-pulse solution (which asymptotes to $(+1, +1, +1)$) determined by $\Delta\Gamma_*^2$ with $\Delta\Gamma(0) < \Delta\Gamma_*^2 < \Delta\Gamma_*^1$ or $\Delta\Gamma(0) > \Delta\Gamma_*^2 > \Delta\Gamma_*^1$.*

Finally, it is worth noting that for $\Delta\Gamma \gg \varepsilon^{-1}$, (4.4.2) reduces, to leading order, to $\dot{\Delta\Gamma} = -3\sqrt{2}\varepsilon\gamma$, and the dynamics is, just as in the case of 1-front solutions, completely determined by the sign of γ . More specifically, the two fronts have a weak tail-tail interaction ($\Delta\Gamma \gg \varepsilon^{-1}$), and they can be interpreted as two single 1-front solutions, see Lemma 4.2.1.

4.4.3 The 3-front solutions

The dynamics of the fronts in 3-front solutions is quite rich. We deduce conditions under which 3-front solutions for which one of the outer fronts travels to $\pm\infty$ are stable, see Corollary 4.4.6 and 4.4.7. Moreover, we prove the existence of uniformly traveling 3-front solutions, see Lemma 4.4.8. The presence of the second inhibitor component W is necessary for the validity of this lemma, *i.e.*, Lemma 4.4.8 does not hold for a two-component version of (4.1.1).

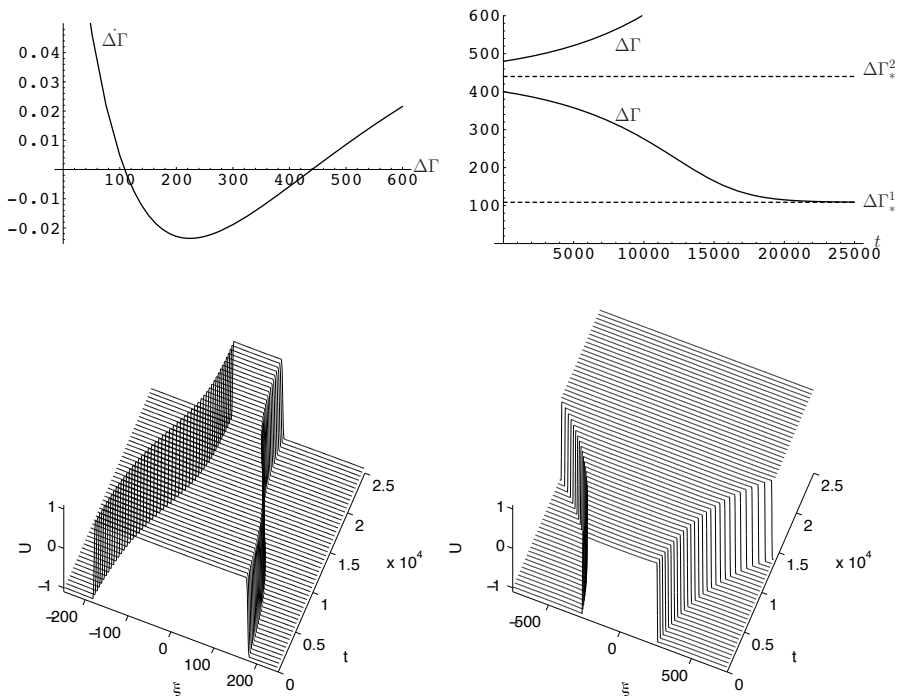


Figure 4.5: In these frames the parameters are $(\alpha, \beta, \gamma, D, \tau, \theta, \varepsilon) = (6, -5, -2, 5, 1, 1, 0.01)$. In the upper left frame, we plotted $\Delta\dot{\Gamma}$ (4.4.2) as a function of $\Delta\Gamma$. Observe that $\Delta\dot{\Gamma}$ has two zeroes $\Delta\Gamma_*^{1,2}$. The first zero is $\Delta\Gamma_*^1 \approx 109$, and the associated eigenvalue is $\lambda_1(\Delta\Gamma_*^1) < 0$. The second zero is $\Delta\Gamma_*^2 \approx 440$, and the associated eigenvalue is $\lambda_1(\Delta\Gamma_*^2) > 0$. Therefore, the 1-pulse solution with width $\Delta\Gamma_*^1$ is stable, while the 1-pulse solution with width $\Delta\Gamma_*^2$ is unstable. In the upper right frame, we plotted the evolution of the pulse distance $\Delta\Gamma$ according to the ODE (4.4.2) for two different initial conditions, one just below the unstable stationary width $\Delta\Gamma_*^2$, and one just above this value. In the lower two frames, we plotted the evolution of the U -component of the PDE (4.1.1) for (approximately) the same two initial conditions. These plots are obtained from numerical simulations of (4.1.1). We observe that the dynamics of the two fronts $\Gamma_{1,2}$ agrees to within the error of the asymptotic approximation with the dynamics of the derived ODE (4.4.2). More specifically, in the lower left frame the distance between the two fronts, $\Delta\Gamma$, approaches 115, which is to leading order the same as $\Delta\Gamma_*^1 \approx 109$ (since $115 = 1.09\varepsilon^{-1} + \mathcal{O}(1)$ for $\varepsilon = 0.01$). In the lower right frame the two fronts diverge, as described by Lemma 4.4.4.

The system of ODEs describing the leading order behavior of the dynamics of these three fronts, up to collision, reads

$$\begin{aligned}
\dot{\Gamma}_1 &= \frac{3}{2}\sqrt{2}\varepsilon \left(\gamma + \alpha \left(-e^{\varepsilon(\Gamma_1-\Gamma_2)} + e^{\varepsilon(\Gamma_1-\Gamma_3)} \right) \right. \\
&\quad \left. + \beta \left(-e^{\frac{\varepsilon}{D}(\Gamma_1-\Gamma_2)} + e^{\frac{\varepsilon}{D}(\Gamma_1-\Gamma_3)} \right) \right), \\
\dot{\Gamma}_2 &= -\frac{3}{2}\sqrt{2}\varepsilon \left(\gamma + \alpha \left(-e^{\varepsilon(\Gamma_1-\Gamma_2)} + e^{\varepsilon(\Gamma_2-\Gamma_3)} \right) \right. \\
&\quad \left. + \beta \left(-e^{\frac{\varepsilon}{D}(\Gamma_1-\Gamma_2)} + e^{\frac{\varepsilon}{D}(\Gamma_2-\Gamma_3)} \right) \right), \\
\dot{\Gamma}_3 &= \frac{3}{2}\sqrt{2}\varepsilon \left(\gamma + \alpha \left(-e^{\varepsilon(\Gamma_1-\Gamma_3)} + e^{\varepsilon(\Gamma_2-\Gamma_3)} \right) \right. \\
&\quad \left. + \beta \left(-e^{\frac{\varepsilon}{D}(\Gamma_1-\Gamma_3)} + e^{\frac{\varepsilon}{D}(\Gamma_2-\Gamma_3)} \right) \right).
\end{aligned} \tag{4.4.5}$$

By Lemma 4.4.2 and Corollary 4.4.3, we know that there are no stationary 3-front solutions, and that at least one front has to travel to $\pm\infty$.

To get additional insight in the dynamics of a 3-front solution, we first assume that (at least) the third front travels to $+\infty$. Another case, in which Γ_3 does not go to $+\infty$ and in which the leftmost pulse travels to $-\infty$, will be discussed later on. We introduce four new coordinates

$$B_i = e^{-\frac{\varepsilon}{D}\Gamma_i} \quad \text{for } i = 1, 2, 3 \quad \text{and} \quad t' = \frac{3}{2}\sqrt{2}\frac{\varepsilon^2}{D}t. \tag{4.4.6}$$

The rescaling of time absorbs the terms in front of the parentheses of (4.4.5) into the time-variable. The transformations of Γ_i are such that the fronts traveling to $+\infty$ now travel to 0, while fronts which previously travel to $-\infty$ now travel to $+\infty$. In the new coordinate system, the assumption $\Gamma_1 < \Gamma_2 < \Gamma_3$ reads $B_3 < B_2 < B_1$, and the system of ODEs (4.4.5) transforms into

$$\begin{aligned}
\dot{B}_1 &= -B_1 \left(\gamma + \alpha \left(-\frac{B_2^D}{B_1^D} + \frac{B_3^D}{B_1^D} \right) + \beta \left(-\frac{B_2}{B_1} + \frac{B_3}{B_1} \right) \right), \\
\dot{B}_2 &= B_2 \left(\gamma + \alpha \left(-\frac{B_2^D}{B_1^D} + \frac{B_3^D}{B_2^D} \right) + \beta \left(-\frac{B_2}{B_1} + \frac{B_3}{B_2} \right) \right), \\
\dot{B}_3 &= -B_3 \left(\gamma + \alpha \left(-\frac{B_3^D}{B_1^D} + \frac{B_3^D}{B_2^D} \right) + \beta \left(-\frac{B_3}{B_1} + \frac{B_3}{B_2} \right) \right).
\end{aligned} \tag{4.4.7}$$

This system of ODEs possesses the line(s) of fixed points $(B_1, B_2, B_3) = (B_1, B_*B_1, 0)$, where B_* solves

$$\alpha B_*^D + \beta B_* = \gamma. \tag{4.4.8}$$

We note that this condition is the same as the existence condition of a standing 1-pulse solution of Chapter 2, as well as that of the fixed points of (4.4.2) after the coordinate transformation. Hence, equation (4.4.8) has, depending on the parameters, 0, 1 or 2 solutions. Recall that $B_3 = 0$ corresponds with the third front Γ_3 traveling to infinity. Therefore, this coordinate transformation (4.4.6) enables us to study fixed points at infinity [46].

Under the assumption that there exists at least one line of fixed points, that is, that there exists at least one B_* solving (4.4.8), we determine the stability of one of these fixed points, which we call $B_f = B_f(B_1; B_*)$. The linearization around B_f yields

$$\begin{pmatrix} -(\alpha DB_*^D + \beta B_*) & \alpha DB_*^{D-1} + \beta & -\beta \\ \alpha DB_*^{D+1} + \beta B_*^2 & -(\alpha DB_*^D + \beta B_*) & \beta \\ 0 & 0 & -\gamma \end{pmatrix}.$$

This matrix has three eigenvalues: $\lambda_1 = 0$, $\lambda_2 = -2(\alpha DB_*^D + \beta B_*)$, and $\lambda_3 = -\gamma$. The third eigenvalue λ_3 implies that the fixed point B_f is stable only if $\gamma > 0$, which is consistent with the fact that $\gamma < 0$ implies a net movement to $-\infty$, see (4.4.1). The sign of the second eigenvalue λ_2 is the same as the sign of the small eigenvalue of a standing 1-pulse solution, see (4.4.3) and Chapter 3. Therefore, this fixed point B_f is only stable if $\gamma > 0$ and the corresponding standing 1-pulse solution is stable. In this case, the line of fixed points is normally attracting.

The eigenvectors belonging to the eigenvalues read

$$e_1 = \begin{pmatrix} 1 \\ B_* \\ 0 \end{pmatrix}, e_2 = \begin{pmatrix} 1 \\ -B_* \\ 0 \end{pmatrix}, e_3 = \begin{pmatrix} K_1 \\ K_2 \\ 1 \end{pmatrix},$$

where $K_{1,2}$ are some computable constants. We observe that the eigenspace belonging to the neutral eigenvalue λ_1 is, as expected, exactly the line of fixed points belonging to B_f . Therefore, this eigenvalue can be seen as a translation invariant eigenvalue, *i.e.*, only the distance between Γ_1 and Γ_2 (or the ratio of B_1 and B_2) is important and not the actual location. Therefore, λ_1 generates no instabilities, and we have shown that a fixed point B_f is stable if and only if $\gamma > 0$ and $\alpha DB_*^D + \beta B_* > 0$, where B_* solves (4.4.8). Transforming back to the original coordinates, we have proved the following corollary:

Corollary 4.4.6. *Let B_* solve (4.4.8). Then, the 3-front solution for which the third front Γ_3 travels to $+\infty$ and the other two fronts $\Gamma_{1,2}$ asymptote to a 1-pulse solution with width $-\frac{D}{\varepsilon} \log B_*$ is attracting if and only if $\gamma > 0$ and $\alpha DB_*^D + \beta B_* > 0$.*

See also frame III of Figures 4.6 and 4.7 for a plot of the system of ODEs in the original coordinates and a plot of a numerical simulation of the PDE (4.1.1), with system parameters satisfying the above corollary.

A similar analysis can be performed for the dynamics of fronts traveling to $-\infty$. However, we now have to use a slightly different coordinate transformation

$$C_i = e^{\frac{\varepsilon}{D}\Gamma_i} \quad \text{for } i = 1, 2, 3 \quad \text{and} \quad t' = \frac{3}{2}\sqrt{2}\frac{\varepsilon^2}{D}t. \quad (4.4.9)$$

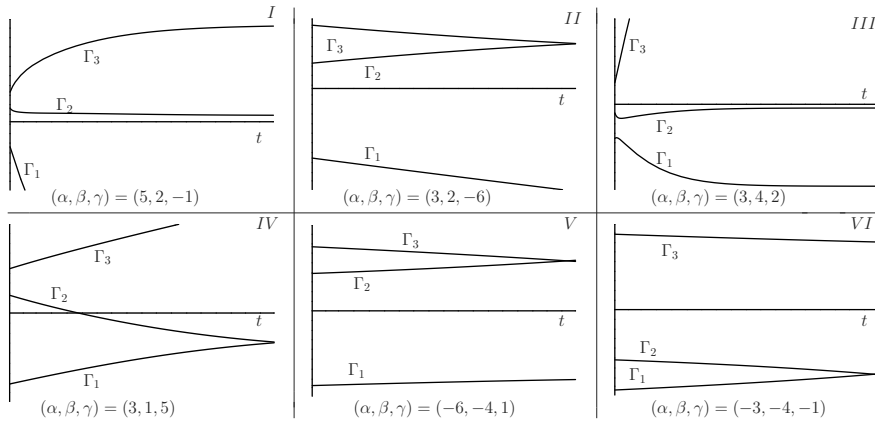


Figure 4.6: In these six frames, we plotted 6 different types of behavior of the fronts of a 3-front solution with $\text{sgn}(\alpha) = \text{sgn}(\beta)$. The values of (α, β, γ) vary from frame to frame, (D, ε) are fixed at $(5, 0.01)$. In the first and third frames the 3-front solution evolves to a stable 1-pulse solution combined with a front traveling to $\pm\infty$. In the other four cases, two of the fronts collide, and the system of ODEs (4.4.5) no longer describes the dynamics of the fronts of a 3-front solution to the PDE (4.1.1) after the collision. Compare this figure also with Figure 4.7, which shows the front locations in the corresponding PDE simulations.

In these new coordinates, the system of ODEs has the line(s) of fixed points $(C_1, C_2, C_3) = (0, C_* C_3, C_3)$, where C_* solves

$$\alpha C_*^D + \beta C_* = -\gamma, \tag{4.4.10}$$

which is the existence condition for a standing 1-pulse solution with $(U, V, W)(\pm\infty) = (1, 1, 1) + \mathcal{O}(\varepsilon)$, as well as the condition to have fixed points of (4.4.4), see also Chapter 2. A linear stability analysis comparable to that of previous paragraph yields the following corollary:

Corollary 4.4.7. *Let C_* solve (4.4.10). Then, the 3-front solution for which the first front Γ_1 travels to $-\infty$ and the other two fronts $\Gamma_{2,3}$ asymptote to a 1-pulse solution with width $-\frac{D}{\varepsilon} \log C_*$ is attracting if and only if $\gamma < 0$ and $\alpha D C_*^D + \beta C_* > 0$.*

From lemma 4.4.2, we know that uniformly traveling 3-front solutions may exist. It turns out from the next lemma that a necessary condition for this type of solution to exist is that the parameters α and β have different signs. Thus, the third component of the PDE (4.1.1) is strictly necessary for the system to support traveling 3-front solutions; the two-component limit of the PDE, *i.e.*, the system

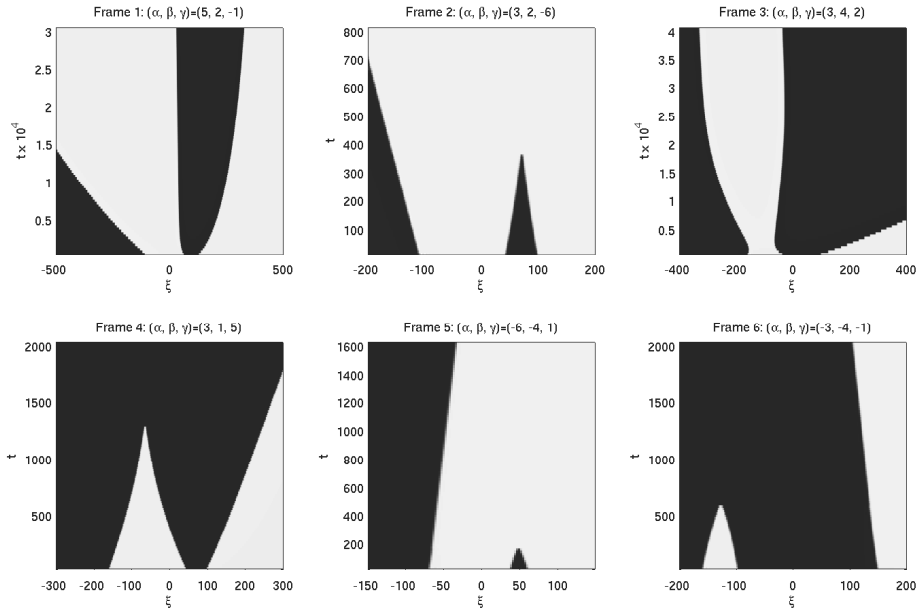


Figure 4.7: In these six frames, we show simulations of the PDE (4.1.1) for the same parameter values and the same initial conditions as in Figure 4.6. Thus, the values of (α, β, γ) vary from frame to frame, while the other parameters ($D, \varepsilon, \tau, \theta$) are kept fixed at $(5, 0.01, 1, 1)$. The black regions indicates that the value of $U = -1$, while white indicates $U = 1$. In all the six frames, one of the outer fronts travel to $\pm\infty$, depending on the sign of γ , see Corollary 4.4.3. In frames 1 and 3, the two other fronts form a stable 1-pulse solution. In frames 2, 4, 5 and 6, the other two fronts collide and disappear, see Conjecture 4.4.1. The dynamics of the remaining fronts after these collisions is described by (4.2.7). Note that in all six cases the actual spatial domain of the simulation was $[-1000, 1000]$. So, we have zoomed in on the spatial domain where the interesting dynamics takes place.

of PDEs without the third component and with $\beta = 0$, see the previous chapters, does not support uniformly traveling 3-front solutions.

Lemma 4.4.8. *If the sign of α and β are the same, then there exist no 3-front solutions traveling with uniform $\mathcal{O}(\varepsilon)$ speed to $\pm\infty$. However, when the assumption is dropped, there exist parameter combinations for which (4.1.1) supports uniformly traveling 3-front solutions.*

Proof. By (4.4.1) each of the fronts of a uniformly traveling 3-front solution has to travel with speed $\frac{1}{2}\sqrt{2}\varepsilon\gamma$. Plugging this into (4.4.5), we find

$$\begin{aligned} -2\gamma &= 3\left(\alpha\left(-e^{\varepsilon(\Gamma_1-\Gamma_2)} + e^{\varepsilon(\Gamma_1-\Gamma_3)}\right) + \beta\left(-e^{\frac{\varepsilon}{D}(\Gamma_1-\Gamma_2)} + e^{\frac{\varepsilon}{D}(\Gamma_1-\Gamma_3)}\right)\right), \\ -4\gamma &= 3\left(\alpha\left(-e^{\varepsilon(\Gamma_1-\Gamma_2)} + e^{\varepsilon(\Gamma_2-\Gamma_3)}\right) + \beta\left(-e^{\frac{\varepsilon}{D}(\Gamma_1-\Gamma_2)} + e^{\frac{\varepsilon}{D}(\Gamma_2-\Gamma_3)}\right)\right), \\ -2\gamma &= 3\left(\alpha\left(-e^{\varepsilon(\Gamma_1-\Gamma_3)} + e^{\varepsilon(\Gamma_2-\Gamma_3)}\right) + \beta\left(-e^{\frac{\varepsilon}{D}(\Gamma_1-\Gamma_3)} + e^{\frac{\varepsilon}{D}(\Gamma_2-\Gamma_3)}\right)\right). \end{aligned} \quad (4.4.11)$$

The third equation is a linear combination of the first two equations. Therefore, we can neglect the third equation and solve the system of the first two equations. Moreover, since only the distances between the fronts are important, there are only two unknowns, $\Gamma_1 - \Gamma_2$ and $\Gamma_2 - \Gamma_3$. So, *a priori*, system (4.4.11) is solvable. Rewriting the first two equations, we find the equality

$$\frac{1}{2}\alpha\left(e^{\varepsilon(\Gamma_1-\Gamma_2)} + e^{\varepsilon(\Gamma_2-\Gamma_3)}\right) + \frac{1}{2}\beta\left(e^{\frac{\varepsilon}{D}(\Gamma_1-\Gamma_2)} + e^{\frac{\varepsilon}{D}(\Gamma_2-\Gamma_3)}\right) = \alpha e^{\varepsilon(\Gamma_1-\Gamma_3)} + \beta e^{\frac{\varepsilon}{D}(\Gamma_1-\Gamma_3)}. \quad (4.4.12)$$

By construction $\Gamma_1 < \Gamma_2 < \Gamma_3$, therefore the following two inequalities hold:

$$e^{\varepsilon(\Gamma_1-\Gamma_3)} < e^{\varepsilon(\Gamma_2-\Gamma_3)}, \quad e^{\varepsilon(\Gamma_1-\Gamma_3)} < e^{\varepsilon(\Gamma_1-\Gamma_2)}. \quad (4.4.13)$$

This yields that equality (4.4.12) cannot be fulfilled if $\text{sgn}(\alpha) = \text{sgn}(\beta)$. Therefore, there cannot be uniformly traveling 3-front solutions if α and β have the same sign.

To show that there are parameter combinations for which (4.4.12) holds if $\text{sgn}(\alpha) \neq \text{sgn}(\beta)$, we prescribe the parameters $\alpha \neq 0, D, \varepsilon$ and the front positions $\Gamma_1, \Gamma_2, \Gamma_3$, and choose β as solution of (4.4.12), *i.e.*,

$$\beta = -\alpha \frac{\frac{1}{2}\left(e^{\varepsilon(\Gamma_1-\Gamma_2)} + e^{\varepsilon(\Gamma_2-\Gamma_3)}\right) - e^{\varepsilon(\Gamma_1-\Gamma_3)}}{\frac{1}{2}\left(e^{\frac{\varepsilon}{D}(\Gamma_1-\Gamma_2)} + e^{\frac{\varepsilon}{D}(\Gamma_2-\Gamma_3)}\right) - e^{\frac{\varepsilon}{D}(\Gamma_1-\Gamma_3)}}.$$

By (4.4.13) the numerator, as well as the denominator, are positive, and therefore β is well-defined, nonzero (and $\text{sgn}(\alpha) \neq \text{sgn}(\beta)$). The first equality of (4.4.11) now determines a value of the last free parameter γ for which (4.4.11) is solved and a uniformly traveling 3-front solution thus exists. Note that this construction works for all given initial parameter combinations $(\alpha, D, \varepsilon, \Gamma_1, \Gamma_2, \Gamma_3)$. \square

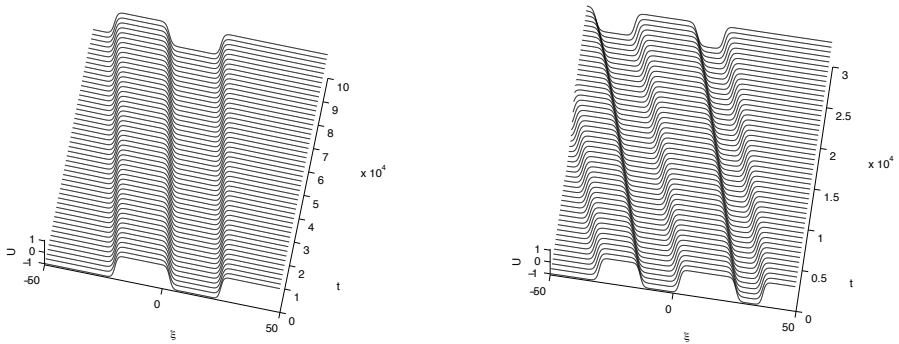


Figure 4.8: In the left frame, we plotted a uniformly traveling 3-front solution. The system parameters read $(\alpha, \beta, \gamma, D, \tau, \theta, \varepsilon) = (1, -0.430454, -0.00266715, 2, 1, 1, 0.1)$. Note that β and γ are constructed by the method described in the proof of Lemma 4.4.8 with $(\Gamma_1, \Gamma_2, \Gamma_3) = (-20, 3, 25)$. In the right frame, we plotted a uniformly traveling 5-front solution. Here the system parameters read $(\alpha, \beta, \gamma, D, \tau, \theta, \varepsilon) = (1, -0.650548, -0.0230866, 2, 1, 1, 0.1)$.

See Figure 4.8 for a uniformly traveling 3-front solution. In the same figure a uniformly traveling 5-front solution is shown, the existence of this type of solutions can be proved by similar (but more involved) arguments. This gives rise to the following conjecture:

Conjecture 4.4.9. *For every N odd there exist uniformly traveling N -front solutions. For every N even there exist stationary N -front solutions.*

We refer to the previous chapters for the proof of this conjecture for $N = 2, 4$.

4.4.4 The 4-front solutions

As N increases, the dynamics of the N fronts naturally becomes more and more complex. A 4-front solution may, for example, evolve toward one of three types of stationary patterns, the ground state, a 1-pulse solution, or a 2-pulse solution, see Figures 4.9 and 4.10. The system of ODEs describing the evolution of the

four fronts, up to collision, is obtained from (4.2.1) with $N = 4$,

$$\begin{aligned}
 \dot{\Gamma}_1 &= \frac{3}{2}\sqrt{2}\varepsilon \left(\gamma + \alpha \left(-e^{\varepsilon(\Gamma_1-\Gamma_2)} + e^{\varepsilon(\Gamma_1-\Gamma_3)} - e^{\varepsilon(\Gamma_1-\Gamma_4)} \right) \right. \\
 &\quad \left. + \beta \left(-e^{\frac{\varepsilon}{D}(\Gamma_1-\Gamma_2)} + e^{\frac{\varepsilon}{D}(\Gamma_1-\Gamma_3)} - e^{\frac{\varepsilon}{D}(\Gamma_1-\Gamma_4)} \right) \right), \\
 \dot{\Gamma}_2 &= -\frac{3}{2}\sqrt{2}\varepsilon \left(\gamma + \alpha \left(-e^{\varepsilon(\Gamma_1-\Gamma_2)} + e^{\varepsilon(\Gamma_2-\Gamma_3)} - e^{\varepsilon(\Gamma_2-\Gamma_4)} \right) \right. \\
 &\quad \left. + \beta \left(-e^{\frac{\varepsilon}{D}(\Gamma_1-\Gamma_2)} + e^{\frac{\varepsilon}{D}(\Gamma_2-\Gamma_3)} - e^{\frac{\varepsilon}{D}(\Gamma_2-\Gamma_4)} \right) \right), \\
 \dot{\Gamma}_3 &= \frac{3}{2}\sqrt{2}\varepsilon \left(\gamma + \alpha \left(-e^{\varepsilon(\Gamma_1-\Gamma_3)} + e^{\varepsilon(\Gamma_2-\Gamma_3)} - e^{\varepsilon(\Gamma_3-\Gamma_4)} \right) \right. \\
 &\quad \left. + \beta \left(-e^{\frac{\varepsilon}{D}(\Gamma_1-\Gamma_3)} + e^{\frac{\varepsilon}{D}(\Gamma_2-\Gamma_3)} - e^{\frac{\varepsilon}{D}(\Gamma_3-\Gamma_4)} \right) \right), \\
 \dot{\Gamma}_4 &= -\frac{3}{2}\sqrt{2}\varepsilon \left(\gamma + \alpha \left(-e^{\varepsilon(\Gamma_1-\Gamma_4)} + e^{\varepsilon(\Gamma_2-\Gamma_4)} - e^{\varepsilon(\Gamma_3-\Gamma_4)} \right) \right. \\
 &\quad \left. + \beta \left(-e^{\frac{\varepsilon}{D}(\Gamma_1-\Gamma_4)} + e^{\frac{\varepsilon}{D}(\Gamma_2-\Gamma_4)} - e^{\frac{\varepsilon}{D}(\Gamma_3-\Gamma_4)} \right) \right).
 \end{aligned} \tag{4.4.14}$$

Of course (4.4.14) has quite some structure, for instance $\sum_{i=1}^4 \dot{\Gamma}_i = 0$. In fact, the system has a 2-dimensional invariant manifold

$$\mathcal{M}_0 := \{(\Gamma_1(t), \Gamma_2(t), \Gamma_3(t), \Gamma_4(t)) \mid \Gamma_4(t) = -\Gamma_1(t), \Gamma_3(t) = -\Gamma_2(t)\}. \tag{4.4.15}$$

The manifold \mathcal{M}_0 can be interpreted as representing the dynamics of symmetric 2-pulse solutions within the larger family of 4-front interactions. Hence, if \mathcal{M}_0 is attracting then the fronts will organize into two pairs of pulses, *i.e.*, the front dynamics evolve into pulse dynamics.

Moreover, the fixed points of \mathcal{M}_0 can be determined by solving $\dot{\Gamma}_{1,2}(t) = 0$. These equations yield

$$\begin{cases} 0 = \gamma + \alpha \left(-e^{\varepsilon(\Gamma_1-\Gamma_2)} + e^{\varepsilon(\Gamma_1+\Gamma_2)} - e^{2\varepsilon\Gamma_1} \right) \\ \quad + \beta \left(-e^{\frac{\varepsilon}{D}(\Gamma_1-\Gamma_2)} + e^{\frac{\varepsilon}{D}(\Gamma_1+\Gamma_2)} - e^{2\frac{\varepsilon}{D}\Gamma_1} \right), \\ 0 = \gamma + \alpha \left(-e^{\varepsilon(\Gamma_1-\Gamma_2)} - e^{\varepsilon(\Gamma_1+\Gamma_2)} + e^{2\varepsilon\Gamma_2} \right) \\ \quad + \beta \left(-e^{\frac{\varepsilon}{D}(\Gamma_1-\Gamma_2)} - e^{\frac{\varepsilon}{D}(\Gamma_1+\Gamma_2)} + e^{2\frac{\varepsilon}{D}\Gamma_2} \right), \end{cases}$$

which coincides with the existence condition of stationary 2-pulse solutions constructed in Theorem 2.5.1 of Chapter 2. The analysis of the previous chapter establishes the (in)stability of the fixed points of \mathcal{M}_0 , *i.e.*, of the symmetric stationary 2-pulse solutions.

Lemma 4.4.10. *If $\alpha > 0$ and $\beta > 0$, then the manifold \mathcal{M}_0 (4.4.15) is normally attracting (linearly stable), while it is normally repelling if $\alpha < 0$ and $\beta < 0$.*

Proof. We linearize about points on \mathcal{M}_0 . After a suitable rescaling of the time, we obtain that the linear evolution of the perturbation v is given by the matrix equation

$$\begin{pmatrix} \dot{v}_1 \\ \dot{v}_2 \\ \dot{v}_3 \\ \dot{v}_4 \end{pmatrix} = \begin{pmatrix} \mathcal{A} & \mathcal{C} & -\mathcal{D} & \mathcal{E} \\ \mathcal{C} & \mathcal{B} & \mathcal{F} & -\mathcal{D} \\ -\mathcal{D} & \mathcal{F} & \mathcal{B} & \mathcal{C} \\ \mathcal{E} & -\mathcal{D} & \mathcal{C} & \mathcal{A} \end{pmatrix} \begin{pmatrix} v_1 \\ v_2 \\ v_3 \\ v_4 \end{pmatrix},$$

where

$$\begin{aligned} \mathcal{A} &= -\mathcal{C} + \mathcal{D} - \mathcal{E}, \mathcal{B} = -\mathcal{C} + \mathcal{D} - \mathcal{F}, \mathcal{C} = \alpha A_1 A_2^{-1} + \beta A_1^{\frac{1}{b}} A_2^{-\frac{1}{b}}, \\ \mathcal{D} &= \alpha A_1 A_2 + \beta A_1^{\frac{1}{b}} A_2^{\frac{1}{b}}, \mathcal{E} = \alpha A_1^2 + \beta A_1^{\frac{2}{b}}, \mathcal{F} = \alpha A_2^2 + \beta A_2^{\frac{2}{b}}, \text{ and } A_i = e^{\varepsilon \Gamma_i}. \end{aligned}$$

Note that this matrix is singular since adding all the rows yields $(0, 0, 0, 0)$, and that it is symmetric across both diagonals. The eigenvalues and eigenvectors of the matrix read

$$\begin{aligned} \lambda_1 &= 0, & e_1 &= [1 \quad 1 \quad 1 \quad 1]^t, \\ \lambda_2 &= -2(\mathcal{C} - \mathcal{D}), & e_2 &= [1 \quad -1 \quad -1 \quad 1]^t, \\ \lambda_3 &= K_3, & e_3 &= [1 \quad L_3 \quad -L_3 \quad -1]^t, \\ \lambda_4 &= K_4, & e_4 &= [1 \quad L_4 \quad -L_4 \quad -1]^t, \end{aligned} \tag{4.4.16}$$

where K_i and L_i are known constants. The eigenvalue-eigenvector pair λ_1 and e_1 correspond to uniform translations of the 4-front solution. Small perturbations in the direction of e_1 cause the positions of the four fronts to shift by the same constant small amount. Hence, the relative distances between pulses stay the same, and such perturbations do not destabilize the 4-front solution, since linear stability is only up to translates. Then, in order to study perturbations in the directions of the other three eigenvectors, we may mod out the translation invariance and assume, without loss of generality, that the components of these perturbations sum to zero. The third and fourth eigenvalues, $\lambda_{3,4}$ have eigenvectors $e_{3,4}$ along the direction of \mathcal{M}_0 . Therefore, these eigenvalues are not important for the stability result. Thus, the second eigenvalue λ_2 , whose eigenvector e_2 is perpendicular to \mathcal{M}_0 , yields the stability result. It is given by

$$\lambda_2 = -2(\mathcal{C} - \mathcal{D}) = 2\alpha A_1(A_2 - A_2^{-1}) + 2\beta A_1^{\frac{1}{b}} \left(A_2^{\frac{1}{b}} - A_2^{-\frac{1}{b}} \right).$$

Note that the eigenvalue λ_2 explicitly depends on time via $A_{1,2}$. By construction $\Gamma_1 < \Gamma_2 < 0$, hence $0 < A_1 < A_2 < 1$. This yields that $\lambda_2(t) < 0$ for all time t if $\alpha > 0$ and $\beta > 0$, while $\lambda_2(t) > 0$ for all time t if $\alpha < 0$ and $\beta < 0$. Thus, \mathcal{M}_0 is normally attracting if $\alpha, \beta > 0$ and normally repelling if $\alpha, \beta < 0$ [9]. \square

Recall from Corollary 4.4.3 that if one front escapes to $+\infty$ there is always another front traveling to $-\infty$. For a stability analysis of the fixed points at infinity, we therefore have to combine the coordinate transformations (4.4.6) and (4.4.9) of the last section. We introduce the new coordinates

$$C_i = e^{\frac{\varepsilon}{b}\Gamma_i} \text{ for } i = 1, 2, \quad B_i = e^{-\frac{\varepsilon}{b}\Gamma_i} \text{ for } i = 3, 4 \text{ and } t' = \frac{3}{2}\sqrt{2}\frac{\varepsilon^2}{D}t. \tag{4.4.17}$$

In these new coordinates, the system of ODEs (4.4.14) reads

$$\begin{aligned}
\dot{C}_1 &= C_1 \left(\gamma + \alpha \left(-\frac{C_1^D}{C_2^D} + C_1^D B_3^D - C_1^D B_4^D \right) \right. \\
&\quad \left. + \beta \left(-\frac{C_1}{C_2} + C_1 B_3 - C_1 B_4 \right) \right), \\
\dot{C}_2 &= -C_2 \left(\gamma + \alpha \left(-\frac{C_1^D}{C_2^D} + C_2^D B_3^D - C_2^D B_4^D \right) \right. \\
&\quad \left. + \beta \left(-\frac{C_1}{C_2} + C_2 B_3 - C_2 B_4 \right) \right), \\
\dot{B}_3 &= -B_3 \left(\gamma + \alpha \left(-C_1^D B_3^D + C_2^D B_3^D - \frac{B_4^D}{B_3^D} \right) \right. \\
&\quad \left. + \beta \left(-C_1 B_3 + C_2 B_3 - \frac{B_4}{B_3} \right) \right), \\
\dot{B}_4 &= B_4 \left(\gamma + \alpha \left(-C_1^D B_4^D + C_2^D B_4^D - \frac{B_4^D}{B_3^D} \right) \right. \\
&\quad \left. + \beta \left(-C_1 B_4 + C_2 B_4 - \frac{B_4}{B_3} \right) \right).
\end{aligned} \tag{4.4.18}$$

This system has the line(s) of fixed points $(C_1, C_2, B_3, B_4) = (0, C_2, \frac{K_*}{C_2}, 0)$, where K_* solves

$$\alpha K_*^D + \beta K_* = -\gamma, \tag{4.4.19}$$

see (4.4.10). To determine the linear stability of one of these fixed points $K_f = K_f(C_2; K_*)$, we linearize around this point. This yields the matrix

$$\begin{pmatrix}
\gamma & 0 & 0 & 0 \\
\beta & -(\alpha D K_*^D + \beta K_*) & -(\alpha D K_*^{D-1} C_2^2 + \beta C_2^2) & \beta C_2^2 \\
\beta \frac{K_*^2}{C_2^2} & -(\alpha D \frac{K_*^{D+1}}{C_2^2} + \beta \frac{K_*^2}{C_2^2}) & -(\alpha D K_*^D + \beta K_*) & \beta \\
0 & 0 & 0 & \gamma
\end{pmatrix}.$$

The four eigenvalues of this matrix read $\lambda_1 = 0$, $\lambda_2 = -2(\alpha D K_*^D + \beta K_*)$, $\lambda_3 = \gamma$, and $\lambda_4 = \gamma$. The third and fourth eigenvalues are stable if $\gamma < 0$. The eigenvector belonging to the neutral eigenvalue λ_1 points in the direction of the line of fixed points generated by K_f , so it yields no instabilities. The second eigenvalue is stable as long as $\alpha D K_*^D + \beta K_* > 0$, which is the same condition as for 3-front solutions (Corollary 4.4.7) and 1-pulse solutions (to $(U, V, W)(\pm\infty) = (-1, -1, -1) + \mathcal{O}(\varepsilon)$, see the previous chapters). This proves the following corollary:

Corollary 4.4.11. *A 4-front solution for which the outer two fronts $\Gamma_{1,4}$ travel to $\pm\infty$, respectively, and for which the other two fronts $\Gamma_{2,3}$ asymptote to a 1-pulse solution with width $-\frac{D}{\varepsilon} \log K_*$ is stable if and only if $\gamma < 0$ and $\alpha D K_*^D + \beta K_* > 0$, where K_* solves (4.4.19).*

See also Figure 4.9 frames *IV* and *V*, and Figure 4.10 frame 8.

There is another fixed point at infinity, namely the fixed point where both two left fronts, $\Gamma_{1,2}$, travel to $-\infty$, while the other two fronts, $\Gamma_{3,4}$, travel to $+\infty$. To determine the stability of these fixed points we again need a transformation. First of all, we define $K_1, (K_4)$ as the distance between Γ_1 and $\Gamma_2, (\Gamma_3$ and $\Gamma_4)$. This way, we get a system of ODEs with the variables $\Gamma_{1,4}, K_1$ and K_4 . Next, we use a transformation similar to (4.4.17)

$$C_1 = e^{\frac{\varepsilon}{D}\Gamma_1}, B_4 = e^{-\frac{\varepsilon}{D}\Gamma_4}, L_{1,4} = e^{\frac{\varepsilon}{D}K_{1,4}} \quad \text{and} \quad t' = \frac{3}{2}\sqrt{2}\frac{\varepsilon^2}{D}t,$$

to obtain a system of ODEs with the variables $C_1, B_4, L_{1,4}$. Analyzing the fixed points of this system yields the following corollary:

Corollary 4.4.12. *A 4-front solution for which the two left fronts $\Gamma_{1,2}$ travel to $-\infty$ with a fixed width $-\frac{D}{\varepsilon}\log L_1^*$ and for which the two right fronts $\Gamma_{3,4}$ travel to $+\infty$ with a fixed width $-\frac{D}{\varepsilon}\log L_4^*$ is stable if and only if $L_1^* = L_4^*$ and $\alpha D(L_1^*)^{-D} + \beta(L_1^*)^{-1} > 0$, where L_1^* solves (4.4.19).*

See also Figure 4.9 frame III, and Figure 4.10 frame 7.

Remark 4.4.3. System (4.4.14) actually possesses a 1-parameter family of invariant manifolds by translation invariance of the underlying PDE.

$$\mathcal{M}_K := \{(\Gamma_1(t), \Gamma_2(t), \Gamma_3(t), \Gamma_4(t)) \mid \Gamma_4(t) = -\Gamma_1(t) + K, \Gamma_3(t) = -\Gamma_2(t) + K\},$$

where $K \gg 2\Gamma_2$. Each of these manifolds is normally attracting if $\alpha > 0$ and $\beta > 0$, while they are normally repelling if $\alpha < 0$ and $\beta < 0$.

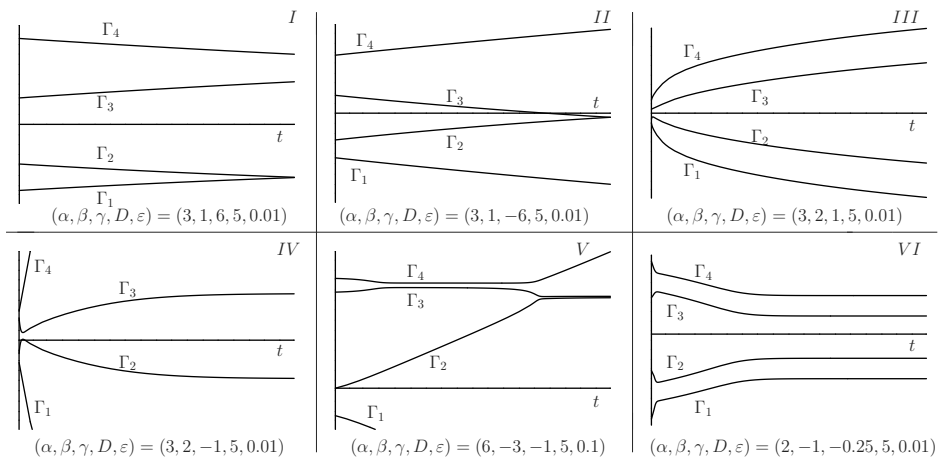


Figure 4.9: In these frames, we plotted five different types behaviors of the fronts of a 4-front solution according to the ODEs (4.4.14). After collision between two of the fronts, see frame *I* and *II*, the ODE description of a 4-front solution is no longer valid, and it should be replaced by the ODE description of a 2-front solution (4.4.2). After collision there are therefore three scenarios possible, the two remaining fronts merge, they form a stable 1-pulse solution, or they tend to $\pm\infty$. See also frames 1, 2 and 3 of Figure 4.10. In the third frame, two 1-pulse solutions simultaneously travel very slowly to $\pm\infty$. In the fourth and fifth frames, the solutions asymptote to a stable 1-pulse solution homoclinic to $(U, V, W) = (1, 1, 1) + O(\varepsilon)$, while the other two fronts travel to $\pm\infty$. In the sixth frame, we see a stable 2-pulse solution, see also Sections 2.5 and 3.6.

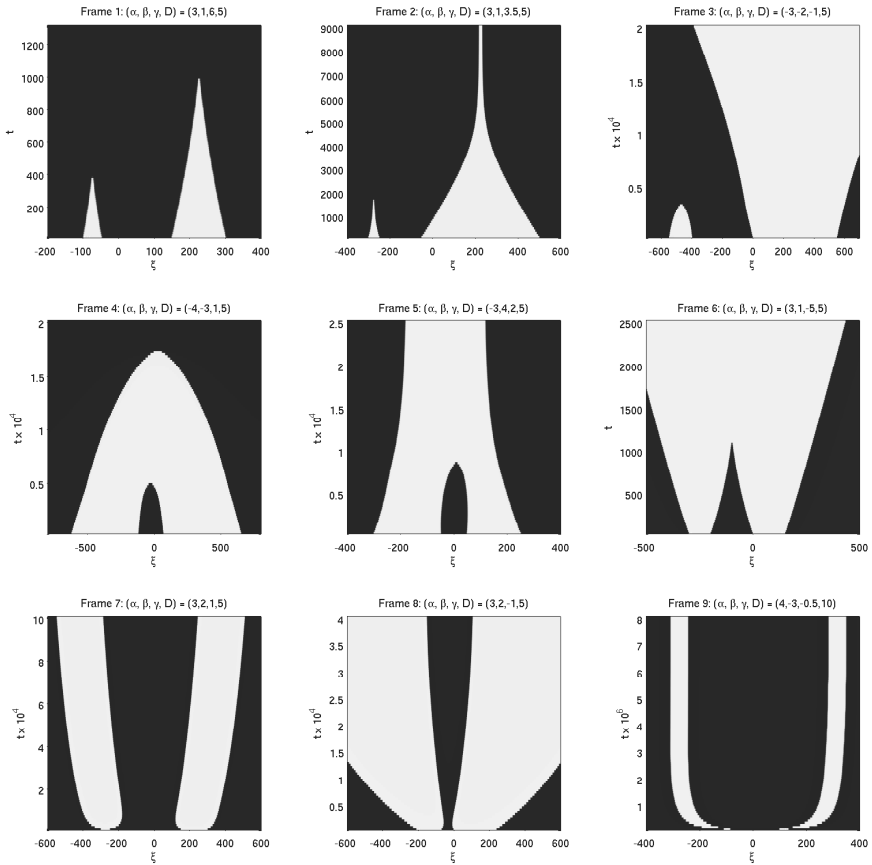


Figure 4.10: In these frames, we plot the possible behaviors of a 4-front solution as seen in numerical simulations of the PDE (4.1.1). The black color indicates that $U = -1$, while white indicates $U = 1$. The first three frames, the upper row, correspond to the first frame of Figure 4.9. Two of the outer fronts collide and disappear. The two remaining fronts now behave in three possible ways, they collide and disappear (Frame 1), they form a stable 1-pulse solution (Frame 2), or they diverge (Frame 3), see also Lemma 4.4.4 and Figure 4.5. The next three frames, the middle row, correspond to the second frame of Figure 4.9. Here, the inner two fronts collide and disappear, and the remaining two fronts disappear (Frame 4), stabilize (Frame 5), or diverge (Frame 6), see again Lemma 4.4.4 and Figure 4.5. The last three frames, the lower row, correspond to *III*, *IV*, and *VI*, respectively. None of the fronts collide, and we obtain two slowly diverging 1-pulse solutions (Frame 7), the outer fronts diverging while the inner fronts form a stable 1-pulse solution (Frame 8), or a stable 2-pulse solution (Frame 9). Note that for all the nine simulations the actual spatial domain was $\xi \in [-1000, 1000]$, $\tau = \theta = 1$ and $\varepsilon = 0.01$.

Bibliography

- [1] J.C. Alexander, R.A. Gardner, C.K.R.T. Jones [1990]. A topological invariant arising in the stability analysis of travelling waves, *J. Reine Angew. Math.* **410**, 167–212.
- [2] P.W. Bates, K. Lu, C. Zeng [2008]. Approximately invariant manifolds and global dynamics of spike states, *Invent. Math.* **174**(2), 355–433.
- [3] D.R. Bes, J. Kurchan [1990]. *The treatment of collective coordinates in many-body systems: an application of the BRST invariance*, Lecture Notes in Phys. **34**, World Scientific, Singapore.
- [4] J.G. Blom, P.A. Zegeling [1994]. Algorithm 731: A Moving-Grid Interface for Systems of One-Dimensional Time-Dependent Partial Differential Equations, *ACM Transactions in Mathematical Software* **20**, 194–214.
- [5] M. Bode, A.W. Liehr, C.P. Schenk, H.-G. Purwins [2002]. Interaction of dissipative solitons: particle-like behaviour of localized structures in a three-component reaction-diffusion system, *Physica D* **161**, 45–66.
- [6] J. Bricmont, A. Kupiainen, G. Lin [1994]. Renormalization group and asymptotics of solutions of nonlinear parabolic equations. *Comm. Pure Appl. Math.* **47**(6), 893–922.
- [7] L.-Y. Chen, N. Goldenfeld, Y. Oono [1996]. Renormalization group and singular perturbations: multiple-scales, boundary layers, and reductive perturbation theory, *Phys. Rev. E* **54**(1), 376–394.
- [8] E.A. Coddington, N. Levinson [1955]. *Theory of ordinary differential equations*. McGraw-Hill Book Company, New-York.
- [9] W. A. Coppel [1978]. *Dichotomies in stability theory*. Lecture Notes in Math. **629**, Springer-Verlag, Berlin-New York.
- [10] R.E.L. DeVille, A. Harkin, M. Holzer, K. Josi, T.J. Kaper [2008]. Analysis of a renormalization group method and normal form theory for perturbed ordinary differential equations, *Physica D* **237**(8), 1029–1052.

- [11] A. Doelman, R.A. Gardner, T.J. Kaper [1998]. Stability analysis of singular patterns in the 1D Gray-Scott model: a matched asymptotics approach, *Physica D* **122**, 1–36.
- [12] A. Doelman, R.A. Gardner, T.J. Kaper [2001]. Large stable pulse solutions in reaction-diffusion equations, *Ind. Univ. Math. J.* **50**(1), 443–507.
- [13] A. Doelman, R.A. Gardner, T.J. Kaper [2002]. A Stability Index Analysis of 1-D patterns of the Gray-Scott Model, *Memoirs of the AMS* **155**(737).
- [14] A. Doelman, D. Iron, Y. Nishiura [2004]. Destabilization of fronts in a class of bi-stable systems, *SIAM Math. J. An.* **35**(6), 1420–1450.
- [15] A. Doelman, T.J. Kaper [2003]. Semistrong pulse interactions in a class of coupled reaction-diffusion equations, *SIAM J. Appl. Dyn. Sys.* **2**(1), 53–96.
- [16] A. Doelman, T.J. Kaper, K. Promislow [2007]. Nonlinear asymptotic stability of the semistrong pulse dynamics in a regularized Gierer-Meinhardt model, *SIAM J. Math. Anal.* **38**(6), 1760–1787.
- [17] A. Doelman, T.J. Kaper, H. van der Ploeg [2001]. Spatially periodic and aperiodic multi-pulse patterns in the one-dimensional Gierer-Meinhardt equation, *Meth. Appl. An.* **8**(3), 387–414.
- [18] J.-P. Eckm, G. Schneider [2002]. Non-linear stability of modulated fronts for the Swift-Hohenberg equation, *Comm. Math. Phys.* **225**(2), 361–397.
- [19] S.-I. Ei [2002]. The motion of weakly interacting pulses in reaction-diffusion systems, *J. Dyn. Diff. Eq.* **14**(1), 85–137.
- [20] S.-I. Ei, M. Mimura, M. Nagayama [2002]. Pulse-pulse interactions in reaction-diffusion systems, *Physica D* **165**, 176–198.
- [21] J.W. Evans [1971]. Nerve axon equations. I. Linear approximations, *Ind. Univ. Math. J* **21**, 877–885.
- [22] J.W. Evans [1972]. Nerve axon equations. II. Stability at rest, *Ind. Univ. Math. J* **22**, 75–90.
- [23] J.W. Evans [1972]. Nerve axon equations. III. Stability of the nerve impulse, *Ind. Univ. Math. J* **22**, 577–593.
- [24] J.W. Evans [1975]. Nerve axon equations. IV. The stable and the unstable impulse, *Ind. Univ. Math. J* **24**, 1169–1190.
- [25] J.W. Evans, N. Fenichel, J.A. Feroe [1982]. Double impulse solutions in nerve axon equations, *SIAM J. Appl. Math.* **42**, 219–234.

- [26] R.A. Fisher [1937]. The wave of advance of advantageous genes, *An. of Eugenics* **7**, 355–369.
- [27] N. Fenichel [1971]. Persistence and smoothness of invariant manifolds for flows, *Ind. Univ. Math. J.* **21**, 193–226.
- [28] N. Fenichel [1979]. Geometric singular perturbation theory for ordinary differential equations, *J. Diff. Eq.* **31**, 53–98.
- [29] R.A. Gardner, C.K.R.T. Jones [1990]. Traveling waves of a perturbed diffusion equation arising in a phase field model, *Ind. Univ. Math. J.* **39**(4), 1197–1222.
- [30] R.A. Gardner, C.K.R.T. Jones [1991]. Stability of travelling wave solutions of diffusive predator-prey systems, *Trans. AMS* **327**(2), 465–524.
- [31] M. Guha, K. Promislow [2009]. Front propagation in a noisy, nonsmooth excitable media, *Disc. Cont. Dyn. Sys.* **23**(3), 617–638.
- [32] S.V. Gurevich, Sh. Amiranashvili, H.-G. Purwins [2006]. Breathing dissipative solitons in three-component reaction-diffusion system, *Phys. Rev. E* **74**(6), 066201.
- [33] G. Hek [2000]. *Bifurcations of homoclinic orbits in singularly perturbed flows*, ISBN: 90-393-2370-0, Univ. Utrecht, the Netherlands.
- [34] S. Hastings [1982]. Single and multiple pulse waves for the FitzHugh-Nagumo equations, *SIAM J. Appl. Math.* **42**, 247–260.
- [35] D. Henry [1981]. *Geometric theory of semilinear parabolic equations*. Lecture Notes in Math. **840**, Springer-Verlag, Berlin.
- [36] L. Hörmander [1983]. *The analysis of linear partial differential operators. I. Distribution theory and Fourier analysis*. Grundlehren der Mathematischen Wissenschaften **256**, Springer-Verlag, Berlin.
- [37] R.B. Hoyle [2006]. *Pattern formation. An introduction to methods*. Cambridge University Press, Cambridge.
- [38] D. Iron, M.J. Ward [2002]. The dynamics of multispikes solutions to the one-dimensional Gierer-Meinhardt model, *SIAM J. Appl. Math.* **62**(6), 1924–1951.
- [39] C.K.R.T. Jones [1995]. Geometric singular perturbation theory, in *Dynamical systems, Montecatini Terme, 1994*, Lecture Notes in Math. **1609**, R. Johnson (ed.), Springer-Verlag.
- [40] C.K.R.T. Jones, N. Kopell [1994]. Tracking invariant manifolds with differential forms in singularly perturbed systems, *J. Diff. Eq.* **108**(1), 64–88.

- [41] C.K.R.T. Jones, T.J. Kaper, N. Kopell [1996]. Tracking invariant manifolds up to exponentially small errors, *SIAM J. Math. An.* **27**(2) 558–577.
- [42] L.P. Kadanoff [1966]. Scaling laws for ising models near TC, *Physics* **2**, 263–272.
- [43] T.J. Kaper [1999]. An introduction to geometric methods and dynamical systems theory for singular perturbation problems, *Proc. of Symposia in Appl. Math.* **56**, 85–131.
- [44] C.A. Klausmeier [1999]. Regular and irregular patterns in semiarid vegetation, *Science* **284**, 1826–1828.
- [45] A.N. Kolmogorov, I.G. Petrowskii, N. Piscounov [1937]. Etude de l'équation de la diffusion avec croissance de la quantité de matière et son application à un problème biologique, *Moscow Univ. Math. Bulletin* **1**, 1–25.
- [46] S. Lefschetz [1977]. *Differential equations: geometric theory*. Dover, New York.
- [47] R.O. Moore, K. Promislow [2008]. The semistrong limit of multipulse interaction in a thermally driven optical system, *J. Diff. Eq.* **245**(6), 1616–1655.
- [48] P.M. Morse, H. Feshbach [1953]. *Methods of theoretical physics*. McGraw-Hill Book Company, New York.
- [49] Y. Nishiura [2002]. *Far-from-equilibrium dynamics*. Translations of Math. Monographs **209**, AMS, Providence.
- [50] Y. Nishiura, Y. Oyama, K.-I. Ueda [2007]. Dynamics of traveling pulses in heterogeneous media of jump type, *Hokkaido Math. J.* **36**(1), 207–242.
- [51] Y. Nishiura, T. Teramoto, K.-I. Ueda [2003]. Scattering and separators in dissipative systems, *Phys. Rev. E* **67**, 056210.
- [52] Y. Nishiura, T. Teramoto, K.-I. Ueda [2005]. Scattering of traveling spots in dissipative systems, *CHAOS* **15**(4), 047509.
- [53] Y. Nishiura, T. Teramoto, X. Yuan, K.-I. Ueda [2007]. Dynamics of traveling pulses in heterogeneous media, *CHAOS* **17**(3), 037104.
- [54] M. Or-Guil, M. Bode, C.P. Schenk, H.-G. Purwins [1998]. Spot bifurcations in three-component reaction-diffusion systems: The onset of propagation, *Phys. Rev. E* **57**, 6432–6437.
- [55] K. Promislow [2002]. A renormalization method for modulational stability of quasi-steady patterns in dispersive systems, *SIAM J. Math. Anal.* **33**(6), 1455–1482.

- [56] A.P. Rasker [2005]. *Pulses in a bi-stable reaction-diffusion system*, MA thesis, KdV Inst., Univ. Amsterdam, the Netherlands.
- [57] C. Robinson [1983]. Sustained resonance for a nonlinear system with slowly-varying coefficients, *SIAM J. Math. An.* **14**, 847–860.
- [58] J. Rubin, C.K.R.T. Jones [1998]. Existence of standing pulse solutions to an inhomogeneous reaction-diffusion system, *J. Dyn. Diff. Eq.* **10**, 1–35.
- [59] B. Sandstede [2002]. Stability of travelling waves, *Handbook of Dyn. Sys.* **2**, 983–1055, B. Fiedler (ed.), North-Holland, Amsterdam, the Netherlands.
- [60] C.P. Schenk, M. Or-Guil, M Bode, H.-G. Purwins [1997]. Interacting pulses in three-component reaction-diffusion systems on two-dimensional domains, *PRL* **78**(19), 3781–3784.
- [61] E.C.G. Stueckelberg, A. Petermann [1953]. La normalisation des constantes dans la theorie des quanta, *Helv. Phys. Acta* **26**, 499–520.
- [62] W. Sun, M.J. Ward, R. Russell [2005]. The slow dynamics of two-spike solutions for the Gray-Scott and Gierer-Meinhardt systems: competition and oscillatory instabilities, *SIAM J. Appl. Dyn. Sys.* **4**(4), 904–953.
- [63] N. Valkhoff [2006]. *Stabilization by competing instability mechanisms*, ISBN: 90-9021311-2, Amsterdam, the Netherlands.
- [64] P. van Heijster [2005]. *Dynamics of two-front solutions in a bi-stable reaction-diffusion equation*, MA thesis, KdV Inst., Univ. Amsterdam, the Netherlands.
- [65] V.K. Vanag, I.R. Epstein [2007]. Localized patterns in reaction-diffusion systems, *CHAOS* **17**(3), 037110.
- [66] K.G. Wilson [1971]. Renormalization group and critical phenomena. I. renormalization group and the Kadanoff scaling picture, *Phys. Rev. B* **4**, 3174 - 3183.
- [67] K.G. Wilson [1971]. Renormalization group and critical phenomena. II. phase-space cell analysis of critical behavior, *Phys. Rev. B* **4**, 3184 - 3205.
- [68] S.L. Woodruff [1993]. The use of an invariance condition in the solution of multi-scale singular perturbation problems: ordinary differential equations, *Stud. Appl. Math.* **90**(3), 225–248.
- [69] S.L. Woodruff [1995]. A uniformly-valid asymptotic solution to a matrix system of ordinary differential equations and a proof of its validity, *Stud. Appl. Math.* **94**(4), 393–413.

-
- [70] L. Yang, A.M. Zhabotinsky, I.R. Epstein [2006]. Jumping solitary waves in an autonomous reaction-diffusion system with subcritical wave instability, *Phys. Chem. Chem. Phys.* **8**, 4647–4651.
- [71] X. Yuan, T. Teramoto, Y. Nishiura [2007]. Heterogeneity-induced defect bifurcation and pulse dynamics for a three-component reaction-diffusion system, *Phys. Rev. E* **75**(3), 036220.
- [72] S. Zelik, A. Mielke [2008]. Multi-pulse evolution and space-time chaos in dissipative systems, *Memoirs of the AMS*, to appear.
- [73] <http://www.animalspapper.com/wallpaper/Zebra-1>
- [74] <http://www.uni-muenster.de/Physik.AP/Purwins/Gruppe/Purwins-en.html>

Summary

Pattern formation is a very lively field of research within the nonlinear sciences, where the traditional disciplines of mathematics, physics, chemistry, and biology merge, interact, and exchange ideas. *Reaction-diffusion equations* serve as relevant, often simplified models within several branches of these fields. Therefore, *reaction-diffusion equations* can be considered as the key prototype models in which one can begin to develop a fundamental understanding of complex patterns. From a mathematical perspective, *reaction-diffusion equations* are arguably the most simple *nonlinear partial differential equations* that exhibit complex patterns.

Localized structures form a special class of solutions to these *reaction-diffusion equations*. These structures are solutions remaining close to a trivial background state (inactive), except in one or more localized spatial regions where the solutions are active. Think for example about a heart. It is not beating constantly (active): a beat is followed by a period of inactivity before it beats again. Another example is a stern wave of a boat in still water. At the bow of the boat two stern waves (active) propagate through the water, while the rest of the water remains still (inactive).

In recent years, significant progress has been made in our mathematical understanding of the simplest localized structures. These being fronts and pulses that are stationary, so not moving in time, or that are uniformly traveling, so move with a constant speed, through a one-dimensional domain. In general, the behavior of localized structures is less well-ordered: those structures interact with each other and thus also move with different velocities. At present, there is a well-developed theory that describes the interaction of fronts and pulses in the *weak* interaction regime. In this regime these fronts or pulses are ‘far away’ from each other, meaning, all components of the structure interact only through their trivial background states mentioned above. However, there is no mathematical theory that explains the interaction of fronts and pulses in the *strong* interaction regime, where all the components of the fronts and pulses are close to each other. In that regime, interesting behavior such as collision, repulsion, annihilation, and self-replication of fronts and pulses can be observed. In between the weak and strong interaction regimes lies a third regime, the *semi-strong* interaction regime, where

certain components of the fronts or pulses interact via the background state, while the remaining components interact strongly with each other. Understanding this regime is a fundamental next step in furthering our understanding of how simple one-dimensional localized structures interact.

In this thesis, we study the *semi-strong* interaction of simple localized structures. We do this by studying a three-component *reaction-diffusion equation*. A scaled version of this equation, which is of *activator-inhibitor-inhibitor*-type, has been introduced in the mid-nineties to describe the phenomena observed by gas-discharge experiments. From a mathematical point of view this equation is particularly interesting because of the rich dynamics it exhibits and its relative simplicity. The equation is *singularly perturbed*, and therefore it has a *slow-fast* nature. The fast component is a well-known and well-studied bistable equation, which is only weakly coupled to two linear slow equations. In conclusion, this equation has only one nonlinear term. Localized structures of singularly perturbed problems typically interact with each other in a semi-strong fashion.

Before we can thoroughly study the interaction between multi-fronts and multi-pulses, we first need to prove that those structures exist. This is shown in the second chapter. We formally construct stationary one-pulses and two-pulses (also called two-fronts and four-fronts) using *geometric singular perturbation theory*. This construction is made rigorous by a geometric argument, which heavily relies on the intersection of hyper-surfaces in a six-dimensional space. This way, we show how the width of a one-pulse depends on the system parameters. We also prove that for the existence of stationary two-pulses it is necessary that the *reaction-diffusion equation* has a third component, the second *inhibitor*. Moreover, we show that the equation possesses uniformly traveling one-pulses. After that, we analyze several bifurcations, for example the subcritical bifurcation of a stationary one-pulse to a uniform traveling pulse, but also the saddle-node bifurcation of stationary one-pulses. Finally, we show several numerical simulations. On the one hand these simulations back up the theoretical results, on the other hand they give examples of the complex dynamics the *reaction-diffusion equation* possesses.

We would like to point out that the methods used in this chapter, as well as the methods used in the next chapter, are all general applicable. Therefore they can also be used to construct more exotic localized structures of more complex *reaction-diffusion equations*. However, in most cases this construction will not lead to such explicit results as we have seen for the *reaction-diffusion equation* at hand here. This is one of the reasons that makes this equation amenable to a rigorous mathematical analysis.

In the third chapter, we analyze the stability of the localized structures constructed in the previous chapter. However, since the present *Evans function*

theory is restricted to two-component *slow-fast* systems, we need to extend it in such a way that it is also applicable for general *slow-fast* systems. With this new theory we then determine the stability of the earlier constructed localized structures. For instance, the stability of the stationary one-pulses is determined by its width and a few of the system parameters. Finally, we analyze the stability of the various types of bifurcations. This way we prove that there is a region in *parameter space* where the stationary one-pulse as well as the uniformly traveling one-pulse are stable. Thus, we have a region where we have coexistence of stationary stable one-pulses and uniformly traveling stable one-pulses. Note that in this chapter we have to analyze a *linear nonautonomous ordinary differential equation*, whereas we had to analyze a *nonlinear autonomous ordinary differential equation* in the previous chapter.

In the last chapter, we study the semi-strong interaction regime. Using a *renormalization group method*, we derive a system of *ordinary differential equations* describing the motion of the various fronts of a multi-front. Note that details of this reduction method strongly depend on the problem at hand. In the final part of this chapter, we analyze the system of *ordinary differential equations*. For instance, we show that stationary multi-fronts only exist if they have an even number of fronts. Likewise, we prove that uniformly traveling multi-fronts do not exist in the case the solutions have an even number of fronts. Finally, we study the multi-front dynamics in more detail for solutions with not too many fronts. For example, we identify several, possibly *attracting manifolds*. We then construct a uniformly traveling three-front, and we determine the stability type of *fixed points at infinity*.

Samenvatting: Frontinteractie in een driecomponenten systeem

Patroonvorming is een interdisciplinair onderzoeksgebied in de niet-lineaire wetenschappen, waar de traditionele wetenschappen zoals natuurkunde, wiskunde, scheikunde en biologie samenkomen en ideeën uitwisselen. Patroonvorming wordt vaak aan de hand van (over)gesimplificeerde *reactie-diffusie vergelijkingen* bestudeerd. Deze vergelijkingen kunnen dan ook als de bouwstenen van patroonvorming worden gezien. Puur wiskundig bekeken zijn *reactie-diffusie vergelijkingen* misschien wel de makkelijkste *niet-lineaire partiële differentiaalvergelijkingen* die complexe patronen vertonen.

Gelocaliseerde structuren vormen een speciale klasse van oplossingen van *reactie-diffusie vergelijkingen*. Dit zijn oplossingen die inactief, ook wel in rust, zijn behalve in een of meer gelocaliseerde intervallen waar de oplossingen actief zijn. Denk bijvoorbeeld aan een hart. Dit klopt niet constant, het geeft een klop (actief) en is dan een periode inactief voordat het weer klopt. Een ander voorbeeld is de boeg golf die een boot maakt als hij door vlak water vaart. Achter de boot zien we twee boeggolven (actief) zich door het water voortbewegen (in twee gelocaliseerde intervallen), terwijl de rest van het water gewoon vlak is (inactief).

De afgelopen decennia is er veel progressie geboekt in het wiskundig begrijpen van de simpelste gelocaliseerde structuren, welteverstaan de stationaire en de uniformlopende fronten en pulsen in één ruimtelijke dimensie. Dit zijn dus oplossingen die niet variëren in de tijd (stationair) en oplossingen die zich met een constante snelheid voortbewegen (uniformlopend). Er is echter nog vrijwel niets bekend over de interactie tussen dit soort simpele gelocaliseerde structuren, waarbij de verschillende gelocaliseerde structuren zich dus met verschillende snelheden kunnen voortbewegen. Alleen wanneer de structuren ver uit elkaar liggen en alle componenten van de structuur elkaar zodoende slechts *zwak* beïnvloeden is er een sluitende wiskundige theorie. De interessante gevallen waarbij de verschillende

structuren dicht bij elkaar liggen en al de componenten elkaar zodoende *sterk* beïnvloeden, denk bijvoorbeeld aan de botsing tussen twee pulsen, zijn wiskundig nog grotendeels niet begrepen. Er is echter nog een derde vorm van interactie, de zogenaamde *semi-sterke* interactie, hierbij beïnvloeden sommige componenten van de structuren elkaar op een *zwakke* manier, terwijl de andere componenten elkaar op een *sterke* manier beïnvloeden. De *semi-sterke* interactie ligt dan ook tussen *zwakke* en *sterke* interactie. Daarom kan het begrijpen van deze vorm van interactie ook beschouwd worden als de volgende noodzakelijke stap richting een wiskundige theorie over de interactie van simpele, eendimensionale, gelokaliseerde structuren.

In dit proefschrift bestuderen wij de *semi-sterke* interactie van simpele gelokaliseerde structuren. Dit doen wij aan de hand van een driecomponenten *reactie-diffusie vergelijking* (vandaar de titel: Frontinteracties in een driecomponenten systeem). Een variant van deze vergelijking is midden jaren negentig geïntroduceerd om de fenomenen waargenomen bij gasontladingen te beschrijven, en zij is van de vorm *activator-inhibitor-inhibitor*. Wiskundig gezien is deze vergelijking vooral interessant vanwege haar rijke dynamica en relatieve eenvoud. De vergelijking is *singulier* gestoord, en wordt daarom ook wel een *langzaam-snel* vergelijking genoemd. De *snelle* component is een bekende *bistabiele* vergelijking, en zij is slechts zwak gekoppeld aan twee lineaire *langzame* vergelijkingen. Al met al heeft de vergelijking maar één niet-lineaire term. Aangezien de vergelijking *singulier* gestoord is beïnvloeden gelokaliseerde multifronten en multipulsen elkaar meestal op een *semi-sterke* manier.

Voordat de interactie tussen gelokaliseerde multifronten en multipulsen bestudeerd kan worden moeten wij (natuurlijk) eerst bewijzen dat deze gelokaliseerde structuren op zichzelf bestaan. Dit doen wij in het tweede hoofdstuk. Met behulp van *geometrische singuliere storingsrekening* construeren wij formeel stationaire eenpulsen en tweepulsen (ook wel tweefronten en vierfronten). Wij maken deze constructie rigoreus met behulp van een geometrisch argument. Dit argument berust grotendeels op het doorsnijden van *hypervlakken* in een zesdimensionale ruimte. Zo leiden wij bijvoorbeeld af hoe de breedte van een puls afhangt van de parameters van de vergelijking. Ook bewijzen we dat voor het bestaan van stationaire tweepulsen het strikt noodzakelijk is dat de vergelijking een derde component heeft. Daarnaast laten wij zien dat de vergelijking ook uniform-lopende eenpulsen ondersteunt. Hierna analyseren wij verschillende soorten bifurcaties, bijvoorbeeld de *subkritische* bifurcatie van de stationaire eenpuls naar de uniform-lopende eenpuls, maar ook de *zadel-knoop* bifurcatie van stationaire eenpulsen. We eindigen dit hoofdstuk met een aantal numerieke simulaties, enerzijds om de bovengenoemde resultaten te staven, anderzijds om enkele voorbeelden te geven van de complexe dynamica die de vergelijking bezit.

Merk op dat de in dit hoofdstuk gebruikte methodes, alsmede de gebruikte metho-

des van het aankomende hoofdstuk, allemaal algemeen toepasbaar zijn. Zij kunnen daarom dus ook gebruikt worden om meer exotische gelocaliseerde structuren van complexere *reactie-diffusie vergelijkingen* te construeren. Echter, in vele gevallen zal deze constructie niet zulke expliciete resultaten opleveren als voor de vergelijking die hier bestudeerd wordt. Dit maakt deze vergelijking dan ook zo geschikt voor een grondige wiskundige analyse.

In het derde hoofdstuk onderzoeken wij vervolgens de stabiliteit van de zojuist geconstrueerde stationaire en uniform-lopende pulsen. Aangezien de bestaande *Evans functie theorie* voor *langzaam-snel* vergelijkingen zich beperkt tot tweecomponenten vergelijkingen, breiden wij deze theorie eerst uit zodat zij ook geschikt is voor algemenere *langzaam-snel* vergelijkingen. Met deze theorie leiden wij vervolgens voor elk soort geconstrueerde puls een stabiliteitsconditie af. De stabiliteit van een stationaire eenpuls wordt bijvoorbeeld bepaald door de breedte van de eenpuls en door enkele parameters van de vergelijking. Hierna bestuderen wij ook nog de stabiliteit van de verscheidene bifurcaties en bewijzen bijvoorbeeld dat er een interval in *parameterruimte* is waarin zowel de stationaire eenpuls als de uniform-lopende eenpuls stabiel zijn. Er is dus een interval waarin er sprake is van *coëxistentie* van stabiele stationaire en stabiele uniform-lopende eenpulsen. Merk op dat waar we in het vorige hoofdstuk nog een *niet-lineaire autonome gewone differentiaalvergelijking* oplossen, we in dit hoofdstuk een *lineaire niet-autonome gewone differentiaalvergelijking* bestuderen.

In het laatste hoofdstuk bestuderen wij de *semi-sterke* frontinteractie. Gebruikmakend van een *renormalisatie groep methode* bewijzen wij dat de verandering van de positie van een front dat in interactie is met andere fronten beschreven kan worden aan de hand van een *gewone differentiaalvergelijking*. De frontdynamica van een N -front kan op deze manier dus beschreven worden met een N -dimensionaal systeem van *gewone differentiaalvergelijkingen*. Merk op dat de exacte details van deze reductiemethode sterk afhangen van de vergelijking die je bestudeert. In het laatste gedeelte van dit hoofdstuk analyseren we het afgeleide N -dimensionale systeem van *gewone differentiaalvergelijkingen*. Zo laten we bijvoorbeeld zien dat stationaire N -fronten alleen kunnen bestaan voor N even, terwijl uniform-lopende N -fronten juist niet bestaan voor N even. Uiteindelijk bestuderen we in detail de N -frontdynamica voor N niet te groot, dat is, voor $N < 5$. Wij identificeren enkele eventueel *aantrekkende invariante variëteiten*, bekijken *vaste punten op oneindig* en construeren een uniform-lopende driefront.

Dankwoord

Het komt niet vaak voor dat je de gelegenheid krijgt om de mensen die jou de afgelopen tijd hebben geholpen zo expliciet kunt bedanken als in een proefschrift. Hier wil ik dan ook graag gebruik van maken. Ik zal beginnen met alle mensen te bedanken die ik hieronder vergeten ben te noemen maar die desondanks een positieve bijdrage aan mijn proefschrift hebben geleverd.

De persoon die het meest heeft bijgedragen aan dit proefschrift (na mij natuurlijk) is Arjen. Arjen, je was echter ook buiten de wiskunde een grote steun. De vele gesprekken die wij hebben gevoerd over van alles en nog wat heb ik altijd zeer gewaardeerd, met als hoogtepunt natuurlijk onze zeven uur durende autotrip naar Oberwolfach (en terug). Ik had mij geen betere begeleider, mentor, motivator en raadgever kunnen wensen! Arjen, vanuit het diepste van mijn hart, bedankt!

Naast Arjen was er natuurlijk mijn co-auteur (en begeleider) Tasso. De duizenden emails die wij hebben uitgewisseld waarin jij mij miljoenen keren hebt moeten corrigeren, en niet op de laatste plaats voor mijn houtjetouwtje-Engels, waren zeer waardevol. Daarnaast heb ik zeer genoten van de vele voetbalgesprekken die wij hebben gehad tijdens onze twee kortstondige bezoekerperiodes, naast de uren wiskunde natuurlijk. Bedankt, jij en Arjen samen vormden de perfecte begeleiding.

I also would like to thank Professor K. Promislow and Professor Y. Nishiura. During my visits to Michigan and Sapporo you both gave me a warm welcome. Moreover, you helped me a lot in the development of my mathematical understanding of, respectively, the renormalization group method and heterogeneous media. Thank you!

Voor de numerieke code die ik heb gebruikt wil ik graag Paul Zegeling bedanken. Paul bedankt dat je jouw code aanpaste zodat ik hem kon gebruiken, dit heeft mij zeker veel tijd en geklungel bespaard.

Ook bedank ik al mijn collega's van het CWI en de UvA. Mede door jullie ging ik de afgelopen vier jaar elke dag fluitend naar mijn kantoor. Sommigen van jullie

dienen natuurlijk bij naam genoemd te worden: Nada, Susanne, Bernard, Jens, Janis, Jeroen, Alexander, Michel, Sjors, Vivi en Geertje, bedankt!

Of course three important people are missing from the list above, namely Svetlana, Maciej, and Antonios. My two beloved office mates and my 'master'. In the last couple of years, the three of you became so much more than just colleagues. Sveta, thank you for all those lovely tennis matches (one day you will win!) and your patience in the early mornings with me! Maciej, thank you for all the good advice about you know what and introducing me to the better restaurants of Amsterdam. Antonios, thank you for everything. You have been a kind of big brother to me, not only for functional analysis but also for life in general. I especially liked our two weeks of 'marriage' in the small hotel room in Berlin.

Ook wil ik de UvA bedanken. Bedankt dat ik voor jullie college mocht geven en eerstejaars studenten mocht begeleiden. Het was een leerzame en aangename onderbreking van de week, maar vooral erg leuk.

Maar er is natuurlijk een leven naast wiskunde. Het leeuwendeel hiervan bracht ik door op mijn geliefde roeivereniging Skøll, dan wel in de boot, dan wel met een toeter langs het water, dan wel met een biertje aan de bar. Skøll, je was een meer dan welkome afwisseling, bedankt! Veel van mijn huidige vrienden heb ik dan ook op Skøll leren kennen: Rik, Ramon, Aart, Gabriël, Anne-Dienke, Wendy, Marlies en Lisa, ik hou van jullie allemaal ... maar toch net ietsje heel veel meer van Klaske. Liefje, bedankt dat je de laatste paar maanden mijn vriendinnetje wilde zijn, en mij gesteund hebt tijdens de laatste zware loodjes van het schrijven van dit proefschrift.

Michel en Steven, als ik het even had gehad met de grote boze stad, kon ik altijd bij een van jullie terecht in mijn *hometown* Heerhugowaard, en na de vele geweldige vakanties met jullie startte ik altijd weer vrolijk met rekenen. Dit is mijn proefschrift zeker ten goede gekomen, bedankt!

Als laatste bedank ik natuurlijke de belangrijkste mensen in mijn leven, mijn vader, moeder, zus, Mark, Lars, Sven en Tess. Bedankt voor al jullie vertrouwen, steun, aanmoedigingen en opbeurende woorden, zonder jullie had dit proefschrift mij veel meer hoofdpijn bezorgd.

Curriculum Vitae

Peter van Heijster werd op 10 september 1981 geboren in Heerhugowaard. Zijn middelbareschoolopleiding genoot hij aan het Han Fortmann College, waar hij in 1999 met succes zijn eindexamen afrondde. Vervolgens is hij aan de Universiteit van Amsterdam wiskunde gaan studeren. Aan het eind van het eerste jaar haalde hij cum laude zijn propedeuse. Bovendien kreeg hij de aanmoedigingsprijs voor de beste eerste jaars student wiskunde. In April 2005 rondde hij zijn studie wiskunde cum laude af, met als specialisatie richting partiële differentiaalvergelijkingen en dynamische systemen. Direct hierna begon hij aan zijn promotie bij het Centrum Wiskunde & Informatica. Dit mondde uit in het voor u liggende proefschrift, wat bijna vier jaar na het beginnen van het promotietraject zal worden verdedigd.